Oxytocin Receptor-Mediated Signaling in Astrocytes

DISSERTATION ZUR ERLANGUNG DES
DOKTORGRADES DER NATURWISSENSCHAFTEN (DR. RER. NAT.)
DER FAKULTÄT FÜR BIOLOGIE UND VORKLINISCHE MEDIZIN
DER UNIVERSITÄT REGENSBURG

Vorgelegt von
Carl-Philipp Meinung
aus
Meiningen

Im Jahr
2020

Das Promotionsgesuch wurde eingereicht am: 30.04.2020

Die Arbeit wurde angeleitet von: Prof. Dr. Inga Neumann und PD Dr. Barbara Di Benedetto

....

Carl-Philipp Meinung

Oxytocin Receptor-Mediated Signaling in Astrocytes

DISSERTATION ZUR ERLANGUNG DES
DOKTORGRADES DER NATURWISSENSCHAFTEN (DR. RER. NAT.)
DER FAKULTÄT FÜR BIOLOGIE UND VORKLINISCHE MEDIZIN
DER UNIVERSITÄT REGENSBURG

Vorgelegt von
Carl-Philipp Meinung
aus
Meiningen

Im Jahr
2020

DECLARATION

Herewith, I declare that this thesis is my own work and I did not make use of any other sources and auxiliary means besides those listed in the bibliography.

Regensburg, 30.04.2020 ....

Carl-Philipp Meinung

Table of contents

ABSTRACT

Especially in higher vertebrates, astrocytes are an indispensible part of signal processing within the brain. Thus, the mode of action of a neuroactive peptide such as OXT cannot be fully understood without this integral part of the CNS. The effects of OXT on neuronal cells have been well characterized, while its effects on astrocytic cells, specifically on OXTR-coupled signaling and its resulting cellular consequences, are poorly understood and might very well differ. To characterize the effect of OXT on astrocytic gene expression, intracellular signaling, as well as astrocyte-specific proteins, synthetic OXT was either administered *icv* in male Wistar rats or applied to cultured rat primary cortical astrocytes. Due to the results of this analysis implying an acute OXT-induced cytoskeletal remodeling and alterations to gap-junction coupling, I next examined the underlying molecular mechanisms and cellbiological consequences of these alterations. Here I found that OXT led to rapid elongation and formation of astrocytic processes *in vitro* and *in vivo*, while simultaneously impairing astrocytic intercellular connectivity. Mechanistically, both of these effects were OXTR-specific, conveyed via PKC and, to a lesser extent, MEK1/2 signaling. Notably, OXT-induced cytoskeletal remodeling and impairment of gap-junctions were characteristic for OXT, since its closely related sister-peptide AVP did not affect the examined parameters. CLSM and STED-microscopy following *icv* or *ex vivo* administration of OXT furthermore revealed changes to astrocyte-neuron spatial relationships in two brain regions associated with high responsiveness of astrocytic markers to OXT, i.e. PVN and hippocampus. In depth *in vitro* studies identified the previously undescribed Sp1-Gem signaling axis to be at the base of these effects. A combination of knockdown, knockout and overexpression experiments revealed that OXT drives *Gem* expression via the transcription factor Sp1 and that Gem is required and sufficient for the effects of OXT on astrocytes. The Sp1-Gem axis was differentially regulated by OXT in neuronal cells, identifying it as key driver in the cell type-specific response of astroglial cells to OXT. Based on these findings, astrocyte-specific AAV-mediated *Gem* or *Oxtr* shRNA knockdown vectors were established as tools for a targeted manipulation of astrocytic OXTR signaling and future assessment of astrocytic contribution to the physiological and behavioral effects of OXT. To this end, shRNA oligonucleotides were screened for knockdown efficiency *in vitro* and subsequently packaged into viral vectors providing astrocyte-specific expression via transcriptional control of shRNA expression under the *hGFAP* promoter.

1 INTRODUCTION

1.1 The neuropeptide oxytocin

Due to its various physiological and behavioral functions, there has been a growing scientific interest in the nonapeptide oxytocin (OXT) and its cognate receptor over the last decade. However, the research on OXT and its closely related sister-peptide arginine vasopressin (AVP) dates back more than a century. Besides a multitude of physiological functions, this research unraveled a remarkable degree of evolutionary conservedness of the OXT/AVP systems (Acher et al., 1995; Donaldson and Young, 2008; Hoyle, 1999), indicating a high degree of selective pressure acting on both, the genes coding for OXT/AVP homologs, as well as their receptors. As a result of a gene duplication of their common ancestor gene *vasotocin,* which homologs can be traced back to invertebrate phylae like *annelida* or *mollusca,* OXT/AVP-like neuropeptides are found in all vertebrate species. Their evolutionary conservation extends beyond the chemical structures of the peptides and their receptors, as it can also be observed in a similar anatomical distribution of the synthesizing neurons and receptor expression patterns (Grinevich et al., 2016; Vargas-Pinilla et al., 2015). Moreover, striking functional similarities exist, with OXT/AVP homologs regulating osmotic homeostasis and social/sexual behaviors throughout large parts of the animal kingdom (Lema et al., 2015; Soares et al., 2012; Van Kesteren et al., 1995).

In mammals, OXT and AVP are mainly synthesized in magnocellular neurons of the paraventricular nucleus (PVN) and the supraoptic nucleus (SON) of the hypothalamus in a mutually exclusive manner (Mohr et al., 1988; Sofroniew, 1983). A detailed immunohistochemical analysis in rats revealed an additional expression in magnocellular accessory nuclei of the hypothalamus constituting around one-third of OXT/AVP-positive cells (Rhodes et al., 1981). An additional site of OXT synthesis is posed by parvocellular neurons of the PVN, but also scattered extra-hypothalamic neurons (De Vries and Buijs, 1983; Knobloch and Grinevich, 2014). Contrary to magnocellular neurons, these cells do not project to the neurohypophysis, but instead form connections with a) areas in the brain stem and spinal cord, where they are involved in the regulation of autonomic processes and pain perception (Swanson et al., 1980) and b) magnocellular neurons of the SON/PVN to regulate OXT release (Eliava et al., 2016).

OXT synthesizing cells express the *Oxt* gene, which encodes a signal peptide (SP), the nonapeptide and its attached neurophysin (NP). The 4850bp gene contains three exons, two introns (Ivell and Richter, 1984), as well as a promoter region for which binding of various hormone receptors (Adan et al., 1993; Richard and Zingg, 1990; Sladek and Somponpun, 2004) and the transcription factor CREB (Sharma et al., 2012) was identified. The newly synthesized SP-OXT-NP pre-peptide is packaged into neurosecretory large dense-core vesicles (Tooze, 1998) where it undergoes extensive posttranslational modifications (Altstein and Gainer, 1988; Gainer et al., 1977). The magnocellular cells of the PVN and SON send axonal projections to the neurohypophysis, a neuro-hemal organ of neuronal (i.e. ectodermal) origin. OXT-containing vesicles are stored in and released from neuronal terminals into neurohypophysial capillaries, permitting entry into the peripheral blood stream (Hatton, 1990).

Within the brain, OXT neurons project to various mesolimbic and forebrain structures like the bed nucleus of the stria terminalis (BNST), septal nuclei, nucleus accumbens, prefrontal cortex, medial and central amygdala, hippocampus and the anterior olfactory nucleus (Dolen et al., 2013; Grinevich et al., 2016; Sofroniew, 1980). In contrast to peripheral OXT release, intracerebral OXT release seems to occur non-synaptically, as neither presynaptic localization of OXT containing vesicles nor postsynaptic oxytocin receptors (OXTR) could be observed yet (Knobloch et al., 2012; Theodosis, 1985). *Oxt* mRNA has been detected in dendrites (Mohr and Richter, 2003), suggesting local synthesis of OXT and consequent dendritic release (Pow and Morris, 1989). Indeed, Pow and Morris were the first to describe such dendritic release of nonapeptides using electronmicroscopic tools (Morris and Pow, 1991). Instead of being transmitted synaptically, OXT is released axo-dendritically at axonal projection sites, or somato-dendritically within the PVN/SON. These diffusion-like neuropeptide actions led to the view of OXT as neuromodulator, rather than neurotransmitter (Landgraf and Neumann, 2004; Leng and Ludwig, 2008). The anatomical distribution of OXT projections and release sites is summarized in Fig. 1.

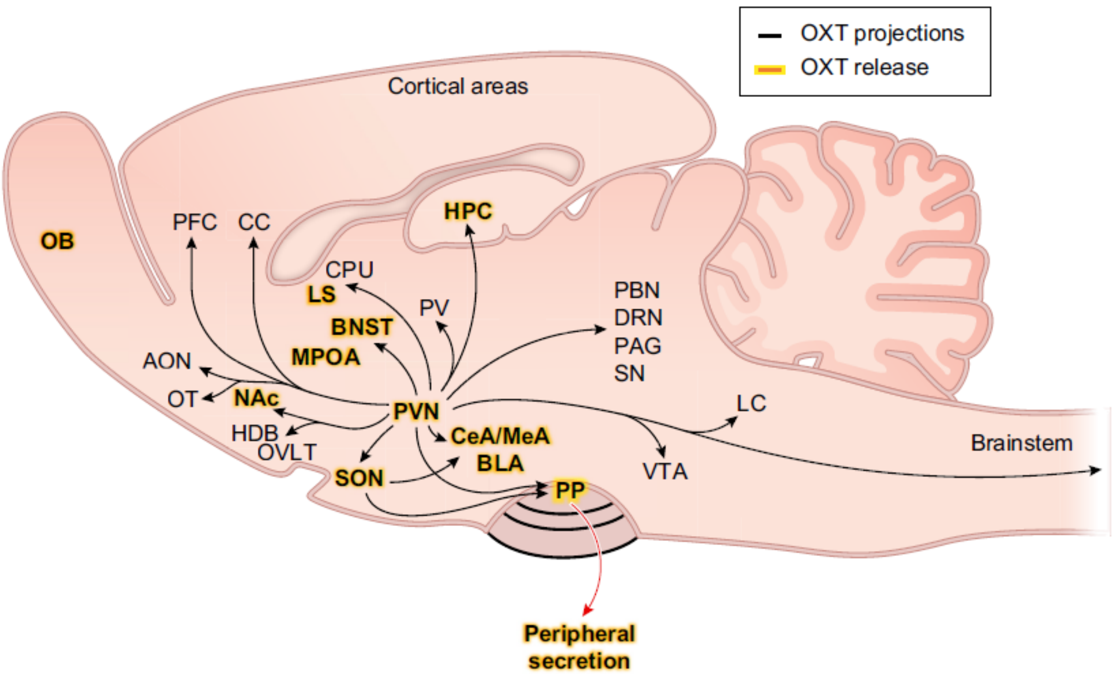

Figure 1. Projections and release sites of the OXT system in an anatomical scheme of the rat brain (sagittal slice).

OXTergic projections originating from the PVN/SON are depicted as black lines, connecting OXTR expressing brain areas. Brain regions where OXT release has directly been shown are highlighted in yellow. AON, anterior olfactory nucleus; OB, olfactory bulb; OT, olfactory tubercle; Nac, nucleus accumbens; OVLT, organum vasculosum laminae terminalis; SON, supraoptic nucleus; PVN, paraventricular nucleus of the hypothalamus; PP, posterior pituitary; PFC, prefrontal cortex; CC, cingulate cortex; MPOA, medial preoptic area; BNST, bed nucleus of the stria terminalis; LS, lateral septum; CPu, caudate putamen;PV, paraventricular nucleus of the thalamus; CeA, central amygdala; MeA, medial amygdala; BLA, basolateral amygdala; VTA, ventral tegmental area; LC, locus coeruleus; PBN, parabrachial nucleus; DRN, dorsal raphe nucleus; PAG, periaqueductal gray; SN, substantia nigra; HPC, hippocampus; HDB, nucleus of the horizontal limb of the diagonal band. Scheme adapted from (Jurek and Neumann, 2018).

Interestingly, peripheral and central release can occur coordinated or independently, increasing the response specificity of the OXT system to external stimuli. Stimuli triggering simultaneous release include parturition, lactation (suckling), physical and emotional stress, as well as osmotic challenge, mating and social interaction (reviewed in Jurek and Neumann, 2018). It should, however, be noted that differences in temporal dynamics of central and peripheral release do still exist for these stimuli. An examples for a stimulus triggering independent central OXT is the anorexic neuropeptide α-melanocyte stimulating hormone (α-MSH). While α-MSH induced OXT release within the SON, it inhibited release into the bloodstream (Sabatier et al., 2003).

Dependent on the stimulus and site of release, OXT drives an adequate physiological or behavioral response, including the modulation of physiological parameters such as pain perception, appetite and HPA axis activity, but also the regulation of complex social behaviors and emotionality. A large body of literature has demonstrated that the endogenous OXT system promotes learning and memory functions, maternal behavior, sexual aggression, social preference and bonding (reviewed in Jurek and Neumann, 2018). Moreover, its robust anxiolytic, anti-stress, and pro-social effects have brought the brain OXT system up for discussion as a potential therapeutic target for psychopathologies such as anxiety disorders (Labuschagne et al., 2010; Landgraf and Neumann, 2004; MacDonald and Feifel, 2014), major depressive disorder or autism spectrum disorder (Bakermans-Kranenburg and van Ijzendoorn, 2014). In this context, a detailed understanding of the mode of action of OXT is of particular relevance and might contribute to the identification of new treatment options.

1.2 The OXTR and its downstream effectors

On a cellular level, OXT mediates its functions mainly via the OXTR. In the periphery, the Oxtr gene displays a widespread expression pattern, including the renal cortex, adrenal medulla, heart, retina, skin, fat tissue, the enteric nervous system, bones and taste buds (Colaianni et al., 2014; Deing et al., 2013; Eckertova et al., 2011; Gutkowska and Jankowski, 2012; Halbach et al., 2015; Ostrowski et al., 1995; Taylor et al., 1989). In the brain, Oxtr expression is found in all above mentioned brain areas (for review, see Jurek and Neumann, 2018) and various non-neuronal cell types (Di Scala-Guenot and Strosser, 1992a; Yuan et al., 2016). OXTR-positive cells display a wide range of properties that in some cases are even co-characteristic. For example, *Oxtr* expressing neurons within the PVN are exclusively glutamatergic, whereas within the BNST OXTR-positive neurons are of GABAergic nature (Dabrowska et al., 2013). The highly conserved 17kb *Oxtr* gene consists of four exons and three introns and codes for a 389 amino acid 7-transmembrane domain (TM) G protein-coupled receptor (GPCR) (Kimura et al., 1992; Rozen et al., 1995). The first three extracellular loops of the OXTR are most critical for OXT binding by interacting with the tertiary structure of the peptide (Postina et al., 1996). OXT does not exclusively bind to OXTRs (K_i =0.79nM), but also to the vasopressin receptors V1a (K_i =120nM), V1b (K_i=1.782nM) and V2 (K_i =1.544nM), although with lower affinity (Akerlund et al., 1999). This fact makes it both difficult and important to validate OXTR specificity in any OXT-dependent effect to be studied.

Oxtr expression is under tight transcriptional and post-transcriptional control, strongly enhancing the regulatory capacity of the OXT-OXTR system. This is reflected by binding sites for various transcription factors/repressors like Sp1, AP1/2, c-Myb, NF-κB, estrogen receptors, C/EBP and Peg3 in the *Oxtr* sequence (Frey et al., 2018; Terzidou et al., 2006 and reviewed in Blanks et al., 2007), as well as additional epigenetic and miRNA-based mechanisms (Beery et al., 2016; Choi et al., 2013). Moreover, the availability of the ligand itself seems to be able to affect OXTR quantities, since both chronic intracerebroventricular (*icv*), as well as repeated intranasal administration reduced *Oxtr* mRNA expression in various brain regions (Huang et al., 2014; Peters et al., 2014). Extracellular signals regulating *Oxtr* expression include labor-induced mechanical stretch and interleukin-β release (Terzidou et al., 2011; Terzidou et al., 2005), as well as estrogen and progesterone (Quinones-Jenab et al., 1997; Schumacher et al., 1990).

Once the receptor is expressed and trafficked to its subcellular localization, the biochemical environment of the plasma membrane and interaction partners within the membrane are able to alter both signal perception, i.e. affinity, and activation patterns of downstream effectors (Busnelli et al., 2016; Gimpl and Fahrenholz, 2001; Reversi et al., 2006; Romero-Fernandez et al., 2013; Wiegand and Gimpl, 2012; Wrzal et al., 2012). Additionally, the coupled signaling cascades will determine the cellular and, later on, network output. Due to its major role in uterine contractions during birth, these cascades were initially mainly studied in myometrial cells.

The first level of signal processing following ligand binding is characterized by the respective subforms of $G_\alpha/G_\beta/G_\gamma$ proteins immediately coupled to the receptor, which can vary dependent on the cell type and physiological state. For example, the OXTR is coupled to the inhibitory G_α protein subforms $G_{\alpha i1\text{-}3}$, $G_{\alpha oA}$ and $G_{\alpha oB}$ in myometrial cells (Busnelli et al., 2012), whereas coupling to the activating $G_{q/11}$ subform and subsequent phospholipase C (PLC) activation was described in myometrial membranes (Ku et al., 1995). Another example is the $G_{q/11}$–mediated increased contractility of myometrial cells of non-pregnant rats vs. the $G_{\beta\gamma}$-dependent decrease of contractility in myometrial cells of pregnant rats (Zhou et al., 2007). As exemplified here, such differential coupling can in consequence lead to a contrary response to the same signal, reflecting the highly context-dependent nature of OXTR signaling.

As a general characteristic of GPCRs, the second level of signal processing is an activation of second messengers by either the activated G proteins or direct interactions. This mechanism provides an enormous amount of amplification, enabling small quantities of a ligand to trigger a significant response. The main second messenger recruited by G proteins is Ca^{2+}, which can be released from internal stores and/or enter cells from the extracellular space. $G_{q/11}$ coupled OXTR signaling activates phospholipase C, which in turn leads to the cleavage of phosphatidylinositol 4,5-bisphosphate to inositol-3-phosphate (IP3) and diacylglycerol (DAG). IP3 binding to IP3 receptors located in the endoplasmatic reticulum subsequently triggers Ca^{2+} release from intracellular stores (for review see Mikoshiba, 2007). In cells of the central nervous system, this has been described for both neuronal (Ayar et al., 2014) and astrocytic cells (Di Scala-Guenot et al., 1994) in the context of OXT. In contrast, OXT led to a decrease of intracellular calcium in lipopolysaccharide-challenged microglial BV-2 cells (Yuan et al., 2016). The full extent of signal amplification additionally requires Ca^{2+} influx from the extracellular space via calcium channels. For OXT, the involvement of various transient receptor potential cation channels (TrpC; specifically TrpC1/TrpC3-6; Chung et al., 2010; Murtazina et al., 2011; Shlykov et al., 2003; Ulloa et al., 2009) and transient receptor potential vannilloid channels (TrpV; specifically TrpV2/TrpV4; van den Burg et al., 2015; Ying et al., 2015), as well as voltage operated channels (Sanborn, 2007) has been reported. That this aspect of OXTR signaling is of critical relevance at the behavioral level was demonstrated in 2015 by van den Burg et al., as pharmacological blockade of TrpV2 within the PVN prevented the acute anxiolytic effect of OXT by inhibiting downstream activation of the mitogen activated protein kinase (MAPK) pathway that had been previously shown to mediate this effect (Blume et al., 2008; Jurek et al., 2012). Other Ca^{2+}-dependent downstream effectors of the OXTR are the calmodulin dependent kinases II/IV (Jurek et al., 2015), calcineurin (Pont et al., 2012) and protein kinase C (PKC; Devost et al., 2008a). We recently found that OXT induces *de novo* protein synthesis in neuronal cells in a PKC-dependent manner by stimulating the translational activator eukaryotic elongation factor 2 (Martinetz et al., 2019). Notably, one of the newly synthesized proteins, neuropeptide Y receptor Y5, was sufficient and necessary for the anxiolytic effect of acute OXT within the PVN. In a broader picture, this demonstrates an intracellular feed-forward mechanism of OXT, supporting its own effect on gene expression (see below) by facilitating the translation of the newly transcribed mRNAs.

The third level of signal transduction is additionally shaped by downstream effectors not dependent on increased cellular Ca^{2+} levels. The transactivation of the epidermal growth factor receptor (EGFR) and subsequent activation of MAPK pathways studied both in myometrial cells and neurons, is a link of OXTR signaling to such effectors (Blume et al., 2008; Lin et al., 2012; Zhong et al., 2003). Although the direct signal transducer is yet unknown, OXTR-coupled signaling triggers the auto-phosphorylation activity of the EGFR tyrosine kinase domains, which subsequently recruits the membrane-bound GTPase Rat sarcoma (Ras). Full MAPK activation is then accomplished by a phosphocascade of [c-Raf-1(Map3k)/Map2k/ERK1/2], although ERK1/2 independent signaling was observed for the Map2k family member MEK1/2 in some cases (Fischmann et al., 2009; Jurek et al., 2015; Jurek et al., 2012; Kim et al., 2015). OXT-induced phosphorylation peaks for c-Raf and ERK1/2 have been described as early as 5min or 10min, respectively (Blume et al., 2008), however the timecourse of ERK1/2 phosphorylation in particular seems to be cell type-dependent (Terzidou et al., 2011). Other members of the MAPK family that have been linked to OXTR signaling in myometrial cells are p38 and ERK5 (Brighton et al., 2011; Devost et al., 2008b; Kim et al., 2017). In general, MAP kinases are involved in the regulation of a wide variety of cellular processes ranging from cell differentiation and migration, apoptosis to regulation of gene expression in response to external stimuli. In the context of OXT, exertion of such transcriptional control has been mainly studied for two distinct transcriptional regulators. First, the transcription factor CREB was found to mediate OXTR/MAPK-induced spatial memory formation during motherhood (Tomizawa et al., 2003), hippocampal long-term potentiation (Lin et al., 2012), as well as *Crf* expression (Jurek et al., 2015). Second, the myocyte enhancer factor 2 (MEF-2) was activated by OXT in myometrial (Devost et al., 2008b) and neuronal cells (Meyer et al., 2018), leading to neurite outgrowth in the latter. In general, OXT seems to have profound effects on the formation and elongation/retraction of cellular processes. While OXT caused less ramification in hippocampal glutamatergic neurons *ex vivo* (Ripamonti et al., 2017), it induced process elongation in human neuroblastoma and glioblastoma cells (Lestanova et al., 2016; Lestanova et al., 2017). The latter effect was accompanied by a variety of changes in the expression of genes associated with cytoskeletal dynamics. In line, OXT was found to increase myometrial contractility via activation of the RhoA/ROCK signaling pathway, most pronounced during late pregnancy (Gogarten et al., 2001; Tahara et al., 2002). The GTPase RhoA and its effector ROCK belong to the major regulators of the cellular cytoskeleton and as such are involved in cellular migration, morphology, adhesion, motility and smooth muscle contraction. (Van Aelst and D'Souza-Schorey, 1997). ROCK targets Ser19 of the myosin light chain (MLC; Totsukawa et al., 2000), while simultaneously inhibiting myosin light chain phosphatase (MYPT) via phosphorylations at threonines 696 and/or 853 (Feng et al., 1999; Kawano et al., 1999) and, in consequence, increases F-actin contractility.

Finally, the desensitization of the OXT-OXTR signaling axis is initiated via OXTR phosphorylation by the G protein-coupled receptor kinase 2 and is already initiated 4s following ligand binding (Hasbi et al., 2004). This phosphorylation enables subsequent binding of β-arrestin2, which in turn uncouples the receptor from its G proteins and simultaneously acts as an adapter for clathrin-mediated endocytosis (Goodman et al., 1996; Smith et al., 2006). The endocytotic vesicles are stored intracellulary, and the receptor is reinserted into the membrane around 4h after the initial internalization (Conti et al., 2009). In addition, β-arrestin provides a negative feedback mechanism by inhibiting insertion of TrpV channels into the plasma membrane (Ying et al., 2015). Interestingly, β-arrestin additionally seems to play a role in the nuclear translocation of the OXTR, a process so far exclusively described in osteoblasts (Di Benedetto et al., 2014). A potential secondary negative feedback mechanism is the prevention of prolonged calcium influx via TrpC3/5 channels by inhibitory phosphorylation of these channels by PKC (Venkatachalam et al., 2003).

Taken together, the high degree of regulatory capacity, from ligand over receptor to the cell type-specific identity of coupled downstream effectors, enable the OXT-OXTR system to bring about physiological and behavioral responses, which are diverse and highly specific at the same time. In the brain, OXT actions are not restricted to neurons, which makes an understanding of these actions on other cell types of the CNS imperative.

1.3 Astrocytes – Maintenance of CNS homeostasis and active participation in neuronal communication

The first description of a neural cell that would later be classified as glia cell dates back to 1851 (Müller, 1851). Heinrich Müller had described cells of the retina, which were later named Müller cells, while six years later Karl Bergmann described radial like cells of the cerebellum (later named Bergmann glia; Bergmann, 1857). Carl Frommann coined the term glia cell (from greek: *γλία, glue*), when describing '*Leim erfüllte Interstitien*' (glue-filled interstitiae; Frommann, 1867). Based on their star-shaped appearance with processes pointing in all directions, Michael von Lenhossék was the first to use the term 'astrocyte' in 1895 (Lenhossék, 1895). This term was later on popularized by Santiago Ramón y Cajal, who developed the first astroglia-specific staining technique based on gold and mercury chloride-sublimate staining (Garcia-Marin et al., 2007). These anatomical studies fostered speculations on the physiological functions of these cells, some of them turning out to be surprisingly correct when examined experimentally later on. Such examinations were enabled by electrophysiological experiments in the late 1950s providing the first evidence of neuron-glia interactions (Hertz, 1965; Hild et al., 1958; Orkand et al., 1966). The establishment of purified cultures by Jean de Villis allowed research to provide insights into astroglial biology on a single-cell level (Morrison and de Vellis, 1981). The findings of the following decades (see below) even led some researchers to call for a shift from a neurocentric to a gliocentric view of the brain. The glia cells that populate the CNS (neuroglia) are characterized by form, function and developmental origin. Neuroglia are subdivided into macro and microglia, with the first including cells of neuroectodermal origin (astrocytes, oligodendrocytes, ependymal cells), while the latter are of mesodermal origin and originate from macrophages invading the brain during early development (Sierra et al., 2014).

Evolutionary, neuro-supportive glial cells could be traced back to higher *Platyhelminthes*, with support of neuronal cells by 'proto-astrocytes' first observed in *Nemathelmintes* (Golubev, 1988; Oikonomou and Shaham, 2011). Neuroglia were then found in all higher taxa including *Arthropoda*, *Mollusca* and *Annelida* (Hartline, 2011), as well as vertebrates with a general trend for increased glia to neuron-ratios throughout the course of evolution (Friede, 1954; Reichenbach, 1989). This increase follows the increase in brain thickness, as well as neuronal energy expenditure and reflects the resulting elevated demand for metabolic support and homeostatic maintenance. Moreover, the complex astrocyte-neuron interplay on the synaptic level (for a more detailed description see 1.4) allowed for a progressive increase in the computational power of the CNS, which is also reflected by large increases in astrocytic size, complexity and signal procession speed particularly seen in humans. This has been remarkably demonstrated by engraftment of human glial progenitor cells (hGPCs) into neonatal mice. Chimeric mice devoloped mature hominid astrocytes, which caused sharp enhancements of LTP, as well as improved learning capabilities in a variety of behavioral tests (Han et al., 2013). Despite significant advances in the identification of astrocytes (see below), their exact abundance, especially in relation to other cell types, is still under debate. In rodents, the glia to neuron ratio is around 0.3 – 0.4, with 10-20% of CNS cells being astrocytes (Sun et al., 2017), whereas the glia-neuron ratio in higher mammals increases to around 1.5-2.0 (Pelvig et al., 2008; Sherwood et al., 2006). However, of these glia cells only ~20-40% where found to be astrocytes, while oligodendrocytes make up ~50% and microglia ~5-10% (Mittelbronn et al., 2001). Verkhratsky and Nedergaard (2018) describe astrocytes throughout the course of evolution as 'highly opportunistic supportive cells that tailor their form and function to match the demands of progressively changing nervous tissue. In this context, the CNS evolved through division of functions between cell types: the neurons become mostly responsible for rapid propagation of signals associated with action potential and chemical synapses, whereas neuroglia assumed the responsibility for homeostasis and defense'. In case of astrocytes, these homeostatic functions are manifold and include ionostasis, pH buffering, H_2O homeostasis and thereby regulation of extracellular space volume, reactive oxygen species homeostasis, neurotransmitter uptake and recycling, neurovascular coupling, clearance of waste products, systemic energy homeostasis, regulation of food intake and nutrient shuttling to neurons. This homeostatic focus is reflected by a broad variety of membrane transporters, ion channels and metabolic enzymes being the most highly expressed astrocytic genes (Cahoy et al., 2008). Hence, astrocytes are indispensable to maintain a stable molecular environment within the CNS and thereby support vital neuronal functions.

Developmentally, astrocytes, in contrast to microglia, originate from neuroepithelium-derived neuronal progenitors (Kriegstein and Alvarez-Buylla, 2009) and differentiate to astrocytes after the neurogenic period of the CNS, in which early neurons populate neuronal layers. In rodents, the subsequent gliogenic switch, characterized by the expression of gliogenic transcription factors like NFIA or Sox9 (Deneen et al., 2006; Freeman, 2010), occurs on embryonic day (E) 12 in the spinal cord and around E16-18 in the cortex. Neurons and astrocytes born in the same region will generally develop together, and by that give rise to regional specificity (Gao et al., 2014; Magavi et al., 2012). However, the described embryonic astrogliogenesis accounts only for a part of adult CNS astrocytes. In rodents, the number of non-neuronal cells increases from 4 million to over 140 million during the second and third postnatal weeks (Bandeira et al., 2009), whereas in cats the astrocyte-to-neuron ratio almost doubles from ~0.8 in young kittens to ~1.48 in adult animals (Brizzee and Jacobs, 1959). An important factor in this postnatal increase is most likely the retained (low) proliferative capacity of astrocytes, which distinguishes them from the majority of neurons (Ge and Jia, 2016).

The identification of astrocyte-specific markers facilitated the understanding of astroglial biology to a great extent. However, even today, specific identification and targeting of astrocytes is not trivial and topic of ongoing debates, since the high degree of morphological and transcriptomic heterogeneity rendered identification of an universal astrocytic marker impossible to the date. Therefore, only a combination of techniques and markers led to a more concise picture. Early on, classical histological techniques based on Cajal's sublimated gold-chloride staining accomplished labeling of astroglial filaments and endfeet. Later, glial fibrillary acidic protein (GFAP) within the CNS was identified to be exclusively expressed in astrocytes and has been the most commonly used astrocytic marker since. GFAP is an intermediate filament of the astrocytic cytoskeleton (Bignami et al., 1972; Hol and Pekny, 2015; Ludwin et al., 1976), which displays a subpopulation and region-specific heterogenic expression *in vivo.* For example, 60% of astrocytes in the adult hippocampus are GFAP positive, while this holds true for only 12% of astrocytes in the mouse entorhinal cortex. GFAP seems to be generally upregulated in reactive astrocytes *in vivo* (Bushong et al., 2002; Nolte et al., 2001; Ogata and Kosaka, 2002; Walz and Lang, 1998), while almost all astrocytes are GFAP positive *in vitro* (Walz, 2000; Yeh et al., 2013). Even though GFAP stains the astrocytic cytoskeleton, its use for this purpose is somewhat limited by its lack of localization to finer and distal processes

(Connor and Berkowitz, 1985). Other proposed markers are the calcium binding protein S100B (Savchenko et al., 2000), the glutamate transporters EAAT1 and EAAT2 (Jungblut et al., 2012), the enzyme glutamine synthetase (Anlauf and Derouiche, 2013), the intermediate filament vimentin (Pekny et al., 1999), the water channel aquaporin 4 (Nielsen et al., 1997), the transcription factor Sox9 (Sun et al., 2017), the foliate metabolism enzyme aldehyde dehydrogenase 1 family member L1 (ALDH1L1; Cahoy et al., 2008) and the gap-junction proteins Cx30/Cx43 (Dermietzel et al., 1991; Nagy et al., 1999). All of these markers provide distinct advantages and disadvantages in terms specificity, inclusiveness and subcellular distribution depending on the specific aim of the study and therefore have to be chosen carefully beforehand (for a concise review see Verkhratsky and Nedergaard, 2018).

Additionally, astrocytes can be visualized by either dye-loading with a patch pipette or expression of a fluorescent protein/calcium indicator, e.g. EGFP, under the promoter of an astrocytic marker gene like *Gfap*. Due to the subcellular distribution of fluorescent dyes or proteins to even fine astrocytic processes, these techniques allow for a more detailed analysis of the morphology of astrocytes and their spatial relationship to neighbouring cells. The application of the above mentioned markers and approaches led to the identification of a variety of astrocytic subpopulations. First, protoplasmic astroglia represent the major population of astrocytes in the grey matter of the brain and spinal cord. These cells possess a small soma (~10µm in diameter) with 5-10 primary processes (~50µm in length) that branch to a dense peripheral arborization underlying their spongiform appearance. A single protoplasmic astrocyte in the rodent cortex may contact 4-8 neurons, surround ~300-600 neuronal dendrites, and interact with 20,000-120,000 synapses residing within its domain (Bushong et al., 2002; Halassa et al., 2007b). Second, fibrous astrocytes populate the white matter of the CNS and are organized in rows between the axonal bundles. Their arborization is less complex than that of protoplasmic astrocytes, and their overlapping processes reflect the absence of domain organization characteristic for protoplasmic cells. The processes of fibrous astrocytes establish several perivascular endfeet and send numerous long (up to 100µm) extensions that contact axons at nodes of Ranvier (Lundgaard et al., 2014).

The morphological heterogeneity of astrocytes seems to be mirrored by a remarkable degree of molecular heterogeneity (Chai et al., 2017), which is believed to play a role in their ability to specifically accompany distinct neuronal circuits despite their high spatial overlap (Martin et al., 2015). Fluorescence activated cell sorting with subsequent RNA sequencing revealed that astrocytes are especially enriched in transcripts of genes involved in cellular metabolism compared to neurons (Lovatt et al., 2007). Later studies showed a strong increase in expression of phagocytotic genes in mature (17-30d) vs. immature (7-8d; Cahoy et al., 2008) astrocytes, further supporting the involvement of astroglia in synaptic pruning (Chung et al., 2013). In conditions of CNS injury and disease, astrocytes switch to a so-called reactive state, which is characterized by alterations in the astrocytic gene expression profile (Zamanian et al., 2012). Specifically, this state is more directed towards interactions with the immune system and cytoskeletal motility. Notably, astrocytes cultured *in vitro* display a similar transcriptome to such a reactive state, stressing the importance to validate *in vitro* findings under non-reactive, more physiological conditions, i.e. *in vivo*. In contrast, astrocytes show very similar electrophysiological properties in all brain regions, a feature for which the above mentioned heterogeneity of astrocytes is not observed (Du et al., 2016). In general, astroglia possess a hyperpolarized resting potential (~80mV) and low input resistance, which is reflected by an almost linear current to voltage relationship (Chvatal et al., 1995; Dallerac et al., 2013; Mishima and Hirase, 2010).

1.4 Astrocytic networks and their regulation

A characteristic feature of astrocytes is their high degree of intercellular connectivity via gap-junctions. In a variety of tissues these specialized subcellular areas allow a tightening of the intercellular cleft to ~2-3nm (Evans and Martin, 2002), and the connexons residing within these areas permit intercellular transport of ions, second messengers, nucleotides, siRNA and metabolites smaller than 1kDa (Harris, 2007; Tabernero et al., 2006; Valiunas et al., 2005). In the grey matter, two neighbouring astrocytes are connected with about 230 gap-junctions on average. Injection of Lucifer yellow or biocytin into a single astrocyte results in staining of ~50–100 adjacent astroglial cells. The concept of a panglial syncytium connecting all macroglia into a single functional network, which has been described in invertebrates (Mugnaini, 1986), does not fully apply to the mammalian CNS. In many brain regions anatomically segregated astroglial networks follow anatomical structures (Giaume et al., 2010; Roux et al., 2011) and even coupling between adjacent astrocytes is not always present, as 15-20% of neighbouring astrocytes were found to be uncoupled (Houades et al., 2006; Meme et al., 2009). Thus, astroglial coupling is not only defined by spatial proximity, and astroglial networks may represent a non-binary second level of information processing parallel to that formed by neurons.

A single gap-junction is composed of two adjacent (homo-or heteromeric) connexons that are assembled from six connexin (Cx) subunits. The *Cx* gene family has 21 members in humans coding for 4-TM proteins with differing molecular mass which also underlies their nomenclature (e.g. Cx26, Cx43) (Dermietzel et al., 1990; Saez et al., 2003). Several hundred connexons form so-called gap-junctional plaques between two coupled cells in a homo-or heterocellular manner (e.g. astrocyte-oligodendrocyte or astrocyte-neuron; Altevogt and Paul, 2004; Alvarez-Maubecin et al., 2000). Homocellular astrocytic gap-junctions are formed by

Cx26,Cx30 and Cx43, with Cx43 being the most abundant, ubiquitously expressed isoform (Giaume et al., 1991; Kunzelmann et al., 1999; Nagy et al., 2004). Cx30 is most prominently found within the thalamus and leptominges, but not in the white matter (Sohl et al., 2004), while Cx26 expression is restricted to subcortical areas like the hypothalamus and subthalamic nuclei (Nagy et al., 2011). The expression of connexins seems to be regulated by neuronal factors, since co-culturing neurons with astrocytes upregulates Cx43 and triggers Cx30 expression. Without exposure to neuronal factors, cultured astrocytes show detectable levels of Cx30 only in a mature state (21d onwards; Koulakoff et al., 2008). The biophysical properties of connexons are regulated by multiple factors including pH, transjunctional or membrane voltage (Herve and Derangeon, 2013), subunit composition, intracellular calcium levels and phosphorylation state, which is controlled by protein kinases A, C, and G, as well as MAPK signaling (Ek-Vitorin et al., 2006). Phosporylation of Cx43 at Ser368 by PKC or at Ser279/Ser282 by MAPK signaling can additionally lead to internalization and possible subsequent degradation of the gap-junction which involves internalization into a specific doublemembrane vacuole termed annular junction or connexosome (Kjenseth et al., 2010). These regulatory mechanisms contribute to the high turnover rate of connexins with a half-life of several hours. In addition, connexons can act as gated pores, known as hemichannels (Esseltine and Laird, 2016), which have been identified in astrocytes *in vitro* and *in vivo* and can be formed by all three types of astrocytic connexons (Giaume et al., 2013). Generally, hemichannels are in a closed state, but their opening can be triggered by low external calcium concentration, substantial depolarization, specific intracellular $Ca2^+$ signals or exposure to proinflammatory agents (Orellana et al., 2012; Orellana et al., 2009). Hemichannels are discussed to be one of the major ways for astroglial secretion of neuroactive substances (see the concept of gliotransmission and the tripartite synapse below).

Notably, recent studies have demonstrated a variety of non-channel functions for astrocytic connexins, including synapse invasion (Pannasch et al., 2014), synaptic glutamate clearance (Pannasch et al., 2019), cellular migration and adhesion (Ghezali et al., 2018). These functions seem to be accomplished by close interactions with other membrane proteins (e.g. glutamate transporters) or adapter proteins like ezrin (Dukic et al., 2017; Pidoux et al., 2014), which connect connexins to the cytoskeleton of its harboring cell and, thereby, form a membrane bound signaling hub capable of integrating signals from different cellular compartments.

1.5 The tripartite synapse

With their perisynaptic astrocytic processes (PAPs), astrocytes are in contact with at least half of all neuronal synapses. PAPs express high levels of glutamate transporters, as well as ezrin and radixin, which anchor them to the astrocytic cytoskeleton and may be at the base of the rapid morphological plasticity that has been described for astrocytic processes (Derouiche and Frotscher, 2001; Hirrlinger et al., 2004; Lavialle et al., 2011). Furthermore, PAPs have an extremely high surface to volume ratio and express a barrage of receptors, ion channels and transporters that couple astrocytic homeostatic functions to neuronal activity (Grosche et al., 2002). Together with the concept of ‘gliotransmission’ describing that astroglia release neuroactive substances (Araque et al., 2014), these observations led to the model of the tripartite synapse (Araque et al., 1999; Halassa et al., 2007a), in which astrocytes are not merely seen as passive housekeeping cells, but are acknowledged as active participants of signal transduction in the brain (Fig.2). At its core this concept is based on a bidirectional communication between synaptic elements and PAPs, by which neuronal activity is sensed by astrocytes and triggers rapid alterations in synaptic coverage, as well as release of neuroactive substances. The first will in turn affect the efficiency of neurotransmitter reuptake and, thus, availability of neurotranmsitters in the synaptic cleft, while the latter directly shapes synaptic communication (Dityatev and Rusakov, 2011). In addition, findings that astrocytes are critical for synapse formation, maturation, maintenance, as well as elimination further stress their important role in shaping neuronal communication. Exemplary, this was demonstrated by a reduction of synaptic density and dendritic spines following disruption of direct astrocyte-neuron contacts (Lippman Bell et al., 2010; Nishida and Okabe, 2007). In consequence, altered spatial relationships between astrocytes and neurons may affect higher cognitive processes, as suggested by Ostroff et al. (2014). Here, rapid retraction of astroglial processes from synapses in the lateral amygdala was found to be a prerequisite for synaptic remodeling associated with memory consolidation during Pavlovian fear conditioning (Ostroff et al., 2014). In general, synaptic coverage by astrocytes is highly dynamic and dependent on the brain status. During sleep, for example, synaptic coverage is decreased, while in wakefulness the opposite is observable (Bellesi et al., 2015).

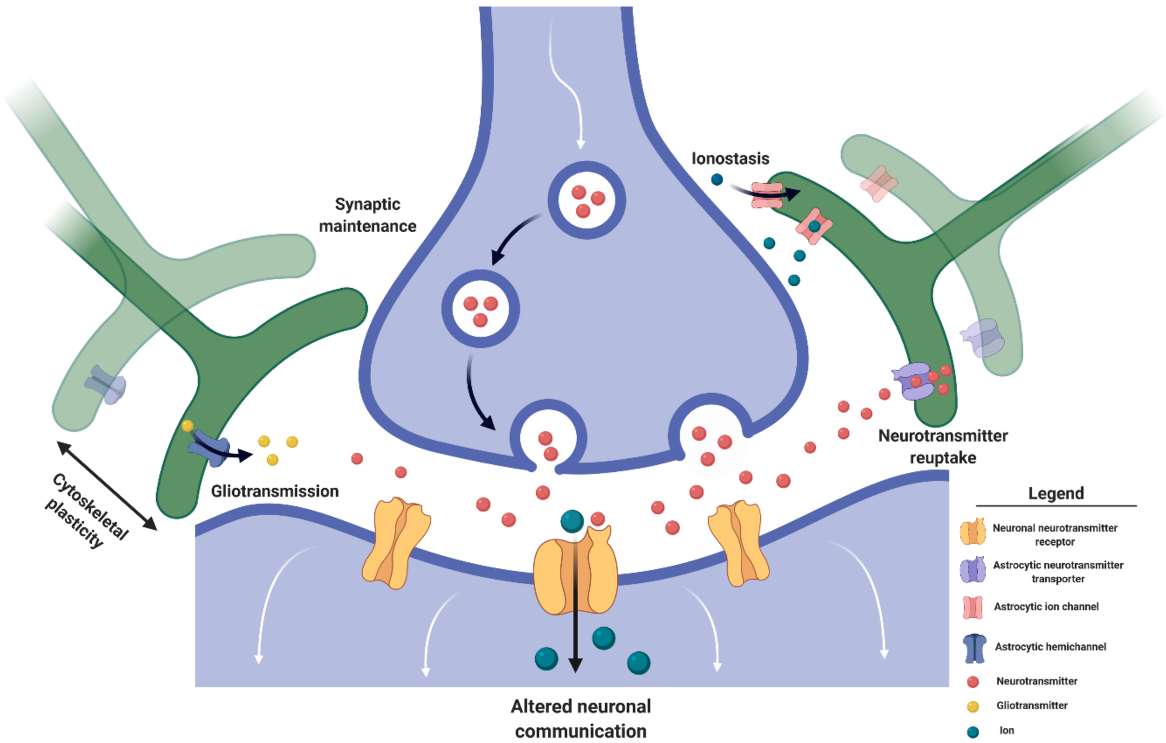

Figure 2. Neuron-astrocyte interactions at the tripartite synapse. At the synaptic cleft, thin terminal structures of highly arborized astrocytic processes form perisynaptic processes (PAPs) and are in close contact with synaptic boutons. PAPs modulate the synaptic environment by uptake of ions and neuroactive substances, whereas gliotransmitters released from PAPs actively alter synaptic communication. In parallel, astrocytes maturate and maintain synapses via contact-dependent mechanisms. The highly plastic spatial relationship between neurons and astrocytes determines the efficiency of all of these functions and is dependent on physiological states and neuronal activity. Illustration created on BioRender.com.

1.6 Neuron-glia interactions in the OXT system

The above described ability of astrocytes to rapidly respond to an altered environment of neuroactive substances is provided by the expression of numerous ionotropic and metabotropic receptors. Astrocytes monitor synaptic transmission by brain regionspecific expression of receptors for almost all neurotransmitters and neuromodulators (Cahoy et al., 2008; Neary et al., 2004; Verkhratsky and Nedergaard, 2018). The hypothalamic SON has emerged as an important model system to study the plasticity of such neuron-glia interactions. Pioneering studies observed a (reversible) reduction in glial coverage of SON OXT neurons during pregnancy and lactation, a physiological condition associated with hyperactivity of the OXT system (Theodosis et al., 1986a). In consequence, the surfaces of ~50% of all OXTergic, but not AVPergic, neurons become directly juxtaposed and, in some cases, form 'shared-synapses' in which two presynaptic boutons were observed to target a single postsynaptic element. A direct involvement of OXT was further suggested by identical observations following administration of chronic OXT *icv* via osmotic minipumps for 6d (Theodosis et al., 1986b). Interestingly, AVP administration had no effect on SON remodeling. Follow-up studies demonstrated that these changes occur only in rats undergoing a prolonged diestrus and are dependent on the concomitant actions of progesterone and estradiol (Montagnese et al., 1990). Mechanistical work in acute SON slices of pregnant rats (PD19) further characterized the effect of OXT (100nM) as OXTR-specific, Ca^{2+}- and GABA-dependent, as well as requiring *de novo* protein synthesis (Langle et al., 2003). The resulting consequences of this neuron-glia remodeling for neuronal communication are increased glutamate availability and release probability (Oliet et al., 2001), as well as an elevated glutamate spillover from uncovered to neighboring synapses (Piet et al., 2004), which in turn leads to a stronger depression of GABAergic transmission via activation of presynaptic mGluRs. Moreover, the gliotransmitter D-serine, an endogenous co-agonist at NMDA receptors and, therefore, critical for the induction of long-term potentiation is less available at synapses lacking glial coverage (Panatier et al., 2006).

On an intracellular level, ERK1/2 has been implicated in OXT-induced retraction of astrocytic processes in acute SON slices of lactating rats, as pre-incubation with the MEK1/2 inhibitor U0126 decreased miniature EPSC frequency and prevented OXT-evoked (10pM) neuronal bursts, as well as neuronal F-actin dynamics. Notably, differential ERK1/2 activation patterns were observed as early as 5min post-application, as OXT increased cytosolic pERK1/2 levels in neurons, whereas it triggered an elevation of nuclear pERK1/2 in astrocytes (Wang and Hatton, 2007). Furthermore, bath application of 10pM, but not 1nM, OXT reduced levels of GFAP in acute SON slices of both lactating female rats and virgin male rats independently from neuronal activity (Wang et al., 2017; Wang and Hatton, 2009).

To this date, it remains unclear, whether the above described findings are due to direct action of OXT on astrocytes. In support of this hypothesis are the findings of Di-Scala Guenot and Strosser (1992a, 1992b, 1994), who demonstrated reversible binding of the radio-iodinated OXTR antagonist [125I]OTA to cultured hypothalamic and hippocampal astrocytes (Di Scala-Guenot and Strosser, 1992a). In contrast to neurons, astrocytes displayed both low and high affinity binding sites. Follow-up studies with synthetic OXT revealed that Mg^{2+}-dependent binding of OXT dose-dependently (starting at 10nM) triggers Ca^{2+} release from astrocytic intracellular stores, with some cells showing Ca^{2+} oscillations (Di Scala-Guenot et al., 1994; Di Scala-Guenot and Strosser, 1992b). Astrocytic *Oxtr* expression seems to be regulated by intercellular interactions, as TGF-β1/2 released from neuronal cells increased *Oxtr* mRNA in cultured astrocytes, whereas direct contact decreased OXTR binding and simultaneously increased *Oxtr* mRNA (Mittaud et al., 2002). However, the exact type of regulation might be exerted by a combination of released and contact-dependent factors, since contact to neuronal membranes alone decreased both [125I]OTA binding, as well as *Oxtr* mRNA (Mittaud et al., 2002). Notably, the *Oxtr* expressed by cultured astrocytes is in fact identical to the transcripts expressed in neuronal and uterine cells (Strosser et al., 2001). In the context of development, prolonged exposure of rat neural progenitor cells to OXT drove them more into a neuronal lineage than into the astrocytic/oligodendrocytic fate (Palanisamy et al., 2018). However, the molecular and physiological consequences of astrocytic OXTR signaling remain largely unknown and might be, at least partially, different from neuronal OXTR signaling due to the cell type-specific gene expression profile and physiological roles of astrocytes.

In addition to effects of OXT on astrocytes, direct actions of astrocytes on OXT neurons have been reported. This was suggested by findings that *icv* administration of the gliotoxin L-aminoadipic acid (L-AAA) suppressed OXT neuronal activity in SON slice preparations and blocked the occurrence of the milk ejection reflex, which essentially depends on OXT secretion into blood (Wang and Hatton, 2009). It should, however, be mentioned that gliotoxins such as L-AAA have recently been criticized for lacking astrocyte specificity and inducing non-physiological effects.

1.7 The small GTPase Gem as a potential mediator of OXT actions on astrocytes

Due to its preferential expression in astrocytes (Piddini et al., 2001; Zhang et al., 2014) and its significant upregulation within the PVN following *icv* administration of OXT for 30min in a RNA microarray study (Martinetz et al., 2019), one such cell type-specific molecular link may be the protein Gem (<u>G</u>TP binding protein over<u>e</u>xpressed in skeletal <u>m</u>uscle). As a member of the RGK (Rad/Rem/Rem2/Gem/Kir) monomeric GTPases, Gem belongs to the Ras-superfamily and hence displays a Ras-like core domain, in which GTPase activity is located (Correll et al., 2008; Splingard et al., 2007). However, unlike most GTPases, RGKs are not predominantly regulated as nucleotide-dependent molecular switches. In most cases, their GTPase activity is below detection level, and GTP binding does not induce conformational changes characteristic for Ras-like GTPases (Cohen et al., 1994; Opatowsky et al., 2006; Sasson et al., 2011). Instead, atypical extensions of both N- and C-terminus provide additional binding and phosphorylation sites for regulatory proteins and downstream effectors. In the periphery, RGKs are widely and differentially found in a variety of tissues, with Gem being predominantly expressed in the gall bladder, urinary bladder, heart, kidney, lung, testes, uterus and adrenal glands (Maguire et al., 1994). The expression of Gem is specifically induced by mitogenic and cytokine stimuli. For example, the PKC activator PMA and, to a greater extent, the acetylcholine analog carbachol both triggered Gem expression in neuroblastoma cells (Leone et al., 2001). In blood T cells, increased quantities of Gem were detected following exposure to either fetal bovine serum (FBS) or PMA (Maguire et al., 1994). Interleukin-1α, TNFα and LPS stimulation of porcine aortic endothelial cells, but not thymus, spleen or lymph cells, yielded similar results (Vanhove et al., 1997). Transcriptional control of the *Gem* gene was so far only studied in blood T cells, in which Gem expression is driven by the transcription factors Tax and CREB (Chevalier et al., 2014).

Functionally, two main roles have been described for Gem. First, the majority of studies demonstrate profound effects on cytoskeleton-dependent processes, like cellular migration, cell division, adhesion and elongation/ramification of cellular extensions. In a variety of cell types, overexpression of Gem induces cellular elongation, cell flattening, loss of stress fibres and focal adhesions, as well as increased migration (Chevalier et al., 2014; Leone et al., 2001; Piddini et al., 2001; Ward et al., 2002). Gem is exerting its effects through direct and indirect interactions with the RhoA/ROCK pathway and actin filaments/microtubules. Binding to its effector Gem interacting protein (Gmip) triggers the Rho GTPase activating protein (RhoGAP) activity of Gmip, which in turn distinctly inhibits RhoA, but not other members of the Rho-GTPase family (Hatzoglou et al., 2007). The Gem-Gmip complex is recruited to the plasma membrane by the active (i.e. phosphorylated) form of the membrane-cytoskeletal linker ezrin. Additionally, inhibition of Gem-binding to its interaction site in ROCK1 alters the substrate specificity of ROCK1 and specifically prevents downstream phosphorylation of the ROCK substrates MLC/MYPT (Ward et al., 2002) independent of RhoA. This not only plays a role in cellular morphology/migration, but was shown to be critical for vesicular transport and exocytosis. JFC1 vesicles are able to recruit Gmip to locally inhibit RhoA and by that transverse cortical actin structures that otherwise inhibit exocytosis (Johnson et al., 2012). Second, Gem inhibits the $Ca_{v1.2}$ subunit of the voltage gated L-type calcium channel (L-VGCC) by sequestering its pore-forming β-subunit in the cytoplasm and immobilizing its voltage sensor (Yang et al., 2012). This inhibition was shown to be critical for Ca^{2+}-dependent growth homone release from neurosecretory cells (Beguin et al., 2001) and activity dependent arborization of mouse neurons (Krey et al., 2013).

A finely balanced posttranslational control involving various phosphorylation sites in the N- and C-terminal domains of Gem, as well as binding of the regulatory proteins CaM and 14-3-3 governs the two main functions of Gem. In its unbound form, Gem is imported into the nucleus via the importin α5, whereas either CaM or 14-3-3 binding localize Gem to the cytoplasm (Mahalakshmi et al., 2007a; Mahalakshmi et al., 2007b) and stabilize the protein (Ward et al., 2004). This cytoplasmatic localization is required for binding of Gem to the β-subunit of the L-VGCC and the subsequent inhibition of the channel. Simultaneously, the cytoskeletal effects of Gem are inhibited by conjunct CaM and 14-3-3 binding through inhibition of its interaction with Gmip and possibly ezrin (Beguin et al., 2005; Hatzoglou et al., 2007). In response to phosphorylations at S289/S261 in its C-terminal domain by PKC and/or cdc42, 14-3-3 binding is prevented which shifts the balance in favor of cytoskeletal regulation through ezrin/Gmip and subsequent RhoA/ROCK inhibition (Ward et al., 2004).

Despite its well-described regulation, only a single study has examined the physiological role of Gem. Gem knockout mice are glucose intolerant and have an impaired glucose-stimulated release of insulin, as well as abnormal pancreatic β-cell Ca^{2+} signaling (Gunton et al., 2012). Given the multitude of cellular effects exerted by Gem, it is likely that its physiological role extends far beyond that. Despite its high expression in astrocytes, the specific role of Gem in the brain is largely unclear.

1.8 Aims and objectives

The neuropeptide OXT exerts manifold regulations of physiological and emotional processes. Its modes of action on neuronal cells have been well characterized. However, its effects on astrocytic cells, specifically on OXTR-coupled signaling cascades and the expression of astrocytic genes, are poorly understood and might very well differ from those on neurons. Astrocytes are increasingly appreciated as indispensable components of the CNS that actively shape information processing. Thus, the biology of a neuroactive signaling peptide like OXT cannot be fully understood without a more holistic and integrative approach to the CNS.

Therefore, the first aim of my thesis was to characterize the effects of OXT on astrocytic signaling cascades and gene expression *in vitro* and to compare the resulting activation pattern to published data of neuronal cells. In this context, I furthermore aimed to examine the acute effect of centrally administered OXT on astrocyte-specific proteins in brain regions associated with actions of the OXT system. To this end, synthetic OXT was either administered *icv* in male Wistar rats or applied to cultured rat primary cortical astrocytes, and the effects on the above mentioned parameters were analyzed by either (phospho-specific) immunoblotting, qPCR or immunostainings.

Based on my findings of rapid OXT-induced alterations of astrocytic cytoskeletal dynamics and gap-junction coupling, the second aim of my thesis was to examine the underlying mechanisms and cellbiological consequences of the observed effects. In this context, I further aimed to examine potential OXT-induced changes in astrocyte-to-neuron spatial relationships in two brain regions, i.e., the PVN and hippocampus, which had shown the highest responsiveness of astrocytic markers to OXT. To achieve this, I applied a combined approach of CLSM/STED-microscopy following *icv* and *ex vivo* administration of OXT, as well as various genetic and pharmacological manipulations *in vitro*.

Based on these findings, the third aim of my thesis was to establish astrocyte-specific AAV-mediated shRNA knockdown vectors as tools for a targeted manipulation of astrocytic OXTR signaling and future assessment of astrocytic contribution to the physiological and behavioral effects of OXT. For this purpose, shRNA nucleotides targeted against candidates identified in the second part of my thesis were screened for knockdown efficiency *in vitro* and subsequently packaged into viral vectors providing astrocyte-specific expression.

Overall, this thesis aims to provide a) a better understanding of the effects and underlying mechanisms of OXT actions on astrocytes and b) a tool to study the involvement of astrocytes in the physiological and behavioral effects of OXT.

2 MATERIALS AND METHODS

2.1 Animals

The examination of the effects of central OXT infusion and astrocyte-specific knockdown of Gem or OXTR was performed in adult male Wistar rats (250-300g; Charles River, Sulzfeld, Germany) housed under standard laboratory conditions. After surgery, rats were single-housed in polycarbonate observation cages five days before biological sample isolation. Experiments were performed in the light phase between 0800 and 1200 hour, in accordance with the Guide for the Care and Use of Laboratory Animals of the Government of Oberpfalz and the guidelines of the NIH.

Due to the advantages of transgenic animals, connexin knockout studies were performed in acute slices derived from adult male C57BL/6 mice (Connexin30 knockout (Cx30KO), Connexin43 knockout (Cx43KO) and wild type C57BL/6; Pannasch et al., 2014) housed under standard laboratory conditions in accordance with the regulations of the guidelines of the European Community Council Directives of January 1st 2013 (2010/63/EU) and of the local animal welfare committee (certificate A751901, Ministère de l'Agriculture et de la Pêche). All efforts were made to reduce the number of animals used, as well as their suffering.

2.2 Cannula Implantations

For implantation of guide cannulas, rats were anesthesized with isoflurane (Isofluran Baxter, Baxter Germany GmbH, Unterschleißheim, Germany) and fixed into a stereotactic frame. For *icv* infusions, unilateral, stainless steel cannulas (21G, 12mm long, Injecta GmbH, Klingenthal, Germany) were implanted 2mm above the right lateral ventricle (Fig.3; AP: -1.0mm bregma, ML: +1.6mm lateral, DV: +1.8mm below the surface of the skull; G Paxinos, 2008). The guide cannula was fixed with two stainless steel screws using dental cement. After surgery, an antibiotic (100µl, 2.5% Baytril®, Bayer Vital GmbH, Klingenthal, Germany) was administered subcutaneously to avoid post-surgical infections. The guide cannula was kept feasible with a dummy cannula, which was cleaned every day during handling. Rats were handled daily for 5 days to reduce non-specific stress responses during experiments.

2.3 Microinfusions

For examination of the effects of central OXT infusion on astrocytes, rats received an *icv* infusion of either vehicle (Veh, sterile Ringer solution, pH 7.4, 5µl) or synthetic OXT (1 nmol/5 µl; Blume et al., 2008). For this, an infusion cannula (30G, 14 mm) connected to a Hamilton syringe via polyethylene tubing was lowered into the guide cannula (Fig.3) and infusions were slowly performed over 1min. Marks on the tubing allowed precise control of the volume administered. Following the infusion, the system was left in place for at least 10s to allow diffusion to occur. After withdrawal of the infusion cannula, the stylette was again inserted into the guide cannula. After termination of the experiment, rats were killed by CO_2-exposure followed by cervical translocation. In order to control for correct for cannula placement, 2µl ink were injected and brains were harvested. Next, coronal sections were prepared using a razorblade and only animals with ink distribution were included in the statistical analysis

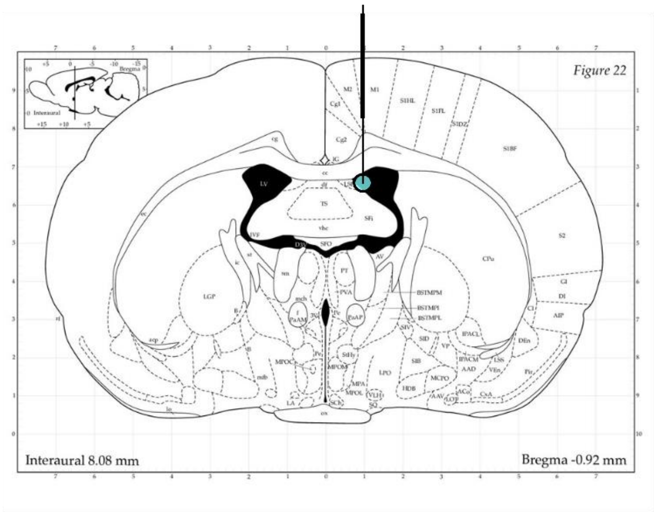

Figure 3. Placement of guide cannula (thick black line) and infusion cannula (thin black line) for *icv* administration of OXT. Coordinates for stereotactic implantation of the guide cannula used were AP: -1.0mm bregma, ML: +1.6mm lateral, DV: +1.8mm. Torquise circle marks point of infusion. Illustration adopted from Paxinos and Watson (2006).

For the establishment of astrocyte-specific knockdown of either *Oxtr* or *Gem* mRNA within the PVN, rats received local bilateral intra-PVN microinfusions of AAV6-GFAP::shRNA constructs or a control vector expressing a scrambled RNA oligonucleotide (Custom designed on www.vectorbuilder.com; Fig.4; all combinations of 70/280/560nl volume and 10^8/10^{10}/10^2 GC/ml were tested; For more detailed information on the used vectors see Appendix 1). The transfected shRNAs were priorly screened *in vitro* for sufficient knockdown efficiency (see 2.5.1, Fig.4 and 3.4). In order to accomplish cell type specificity, first, an AAV6 capsid was selected for viral packaging. Among available adenoviral capsids, AAV6 packaged vectors show the highest tropism for astrocytes compared to other cell types of the CNS (Schober et al., 2016). Second, the shRNA expression is driven by the full-length promoter fragment of the human *GFAP* (*hGFAP)* gene, thereby further increasing cell type specificity. In the applied vectors, the co-expressed mCherry protein was used as a fluorescent reporter. To examine transfection specificity (ratio mCherry+/GFAP+ cells) and perturbance (ratio GFAP+/mCherry+ cells), rats were transcardially perfused three weeks post-transduction to analyze brains immunohistologically (see 2.10). Briefly, rats were anaesthetized by CO_2-exposure to prevent anaesthesia-induced changes to astrocytes (Thrane et al., 2012) and the left ventricle was cannulated. Next, the right atrium was cut to ellow efflux of the perfusate and 0.01M PBS was transcardially perfused for 5min at a rate of 20ml/min by a multi-speed pump. Last, the perfusion solution was changed to 4% Paraformaldehyde (PFA) in 0.01M PBS and perfused for 15min at a rate of 20ml/min. Subsequently, brains were processed as described in 2.10. In order to assess knockdown efficiency, RNA was isolated from PVN micropunches (see 2.6) and quantified by RT-PCR as described in 2.6.1.

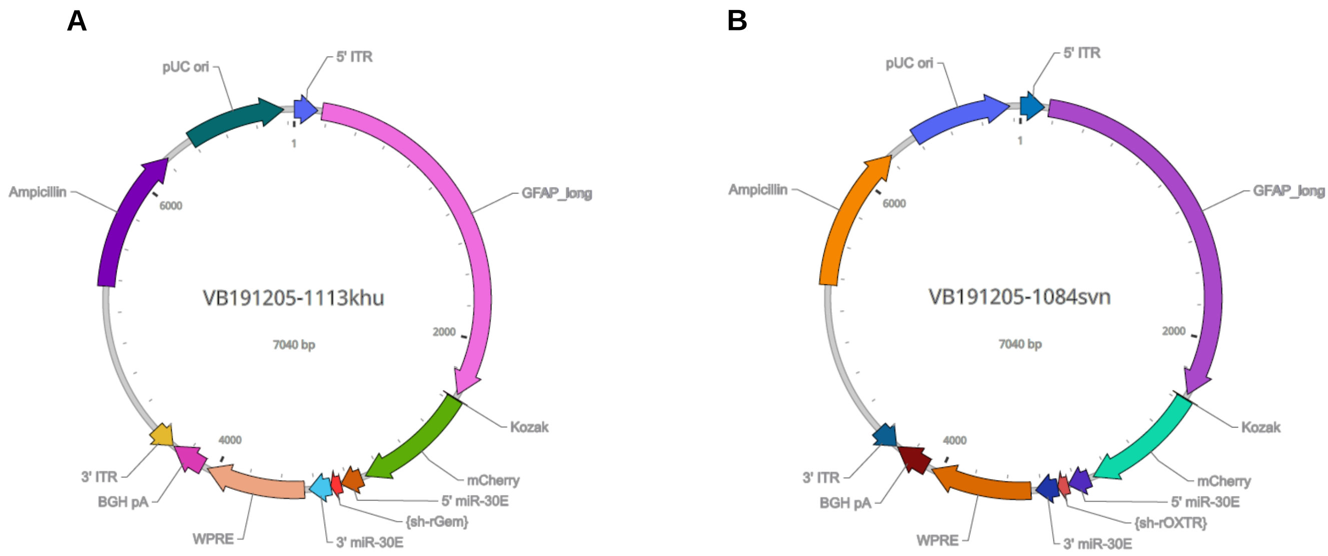

Figure 4. Adenoviral vectors used for astrocyte-specific knockdown of either *Oxtr* or *Gem* mRNA within the rat PVN. In both vectors shRNA, as well as mCherry expression is driven by the long fragment of the *hGFAP* promoter. **A)** Adenoviral vector expressing a shRNA targeted against the rat *Gem* mRNA. **B)** Adenoviral vector expressing a shRNA targeted against the rat *Oxtr* mRNA.

2.4 Preparation of acute hippocampal *ex vivo* slices

Mice were decapitated and both hippocampi were fixed to a small block of agar on which acute slices (350µM) were prepared in a vibratome in oxygenized ACSF. Following bath application of either Veh (ACSF) or OXT (500nM) for 10min, slices were fixed in 4% PFA in PBS for 2h followed by 2h of blocking in PBS containing 2g gelatine/l and 1% Triton-X and stained under the conditions described in 2.10/2.12 for morphological analysis, as well as 3D-reconstruction and determination of astrocyte-synapse spatial relationship.

2.5 Cells

Primary rat cortical astrocytes. Cells isolated from newborn pups (adapted from Schildge et al., 2013 ; post-natal day 1-3) were used for all *in vitro* experiments on astrocytes. For dissection, the pup was decapitated and the scalp was cut by performing a midline incision from caudal to rostral. Next, two diagonal cuts inferior to the cerebellum were performed, and the skull was cut along the *sutura sagittalis* from caudal to rostral. Using this procedure, four brains were harvested with a micro spatula and transferred into a dissection dish containing ice-cold Hanks balanced salt solution (HBSS; Invitrogen, Carlsbad, USA). Here, the cortex hemispheres were separated from the remaining parts of the brain, as well as from the meninges to prevent later contamination of the cultures with meningeal cells. The eight hemispheres were transferred into a second dissection dish containing 3ml ice-cold HBSS, in which they were cut into small pieces with a razorblade. Cortex pieces were transferred into a 50-ml falcon tube containing 20ml of a 0.2% trypsin solution and were subsequently incubated at 37°C for 30min while shaking them thoroughly every 10min. After centrifugation for 5min at 180g, the tissue suspension was aspirated *ad* 15ml and resuspended to obtain a single cell suspension. Subsequently, the suspension was filtrated through a 70-µm cell strainer (Corning, New York, USA; 352350) into a fresh 50-ml tube and centrifuged at 180g for 5min. After resuspending the cell pellet in 10ml of astrocyte growth medium ((Dulbecco's Modified Eagle's Medium – (DMEM, high glucose) Sigma-Aldrich, St. Louis, USA; D6429) containing 10% foetal bovine serum (FBS), 1% Penicillin/Streptomycin (Life Technologies, Darmstadt, Germany), 1% Mem non-essential Amino acid solution (100x, Sigma-Aldrich) and 1% Glutamax (Life Technologies; 35050038), the mixed cortical cells were seeded in a T75 cell culture flask (Sarstedt, Nürnbrecht, Germany) previously coated with 15ml of a poly-D-lysine solution (0.01% poly-D-lysine in H_2O, Sigma Aldrich; P7886). The flasks were incubated at 37°C and 5% CO_2, and the medium was first changed after two days and subsequently every four days. After 7-8 days in culture, when the mixed cultures had reached confluence, the flasks were shaken on an orbital shaker for 30min at 37°C and 180rpm. After aspirating the supernatant containing microglial cells, fresh growth medium was added, and the cells were again shaken for 6h at 240 rpm to remove oligodendrocyte precursor cells. The remaining adherent astrocytic layer was trypsinated and seeded into two new TC75 cell culture flasks. After 7 or 14 days in culture, cells are seeded for experiments and treated as described below.

H32 neuronal cell line. The immortalized foetal rat hypothalamic cell line H32 (Mugele et al., 1993) was cultured at 37 °C and 5% CO2 in DMEM F-12 Ham (Sigma Aldrich; D8437) containing 10% FBS and 1% penicillin/streptomycin.

2.5.1 Transfection of Astrocytes by Electroporation

In order to study the involvement of different proteins of interest in astrocytic OXTR signaling, astrocytes were transfected with various siRNA oligonucleotides (Cx43 (*Gja1*) siRNA, sc-60008, Santa Cruz Biotechnology, Dallas, USA; *Sp1* siRNA, Santa Cruz, sc-61895; *Gem* siRNA, Origene, Rockville, USA, SR507514) or a *Gem* overexpression plasmid (Fig. 5a, VectorBuilder) by electroporation (Neon™ Transfection System, ThermoFisher; MPK5000). In another set of experiments, cells were transfected with a plasmid expressing a shRNA oligonucleotide under control of the long fragment of the *hGFAP* promoter targeted against *Gem* (Fig.5b) or *Oxtr* (Fig.5c) mRNAs to screen for knockdown efficiency *in vitro.* For detailed conditions of electroporation, please see Tab.1. In case of siRNAs, a scrambled oligonucleotide (scrRNA) served as a control transfection, while a plasmid expressing solely the fluorescent reporter protein EGFP (Fig.5d, VectorBuilder) served as a control condition for plasmid transfections. Conditions of EGFP/scrRNA transfections were always identical to the respective transfection of interest. For more detailed information on the used DNA plasmids see Appendix 2.

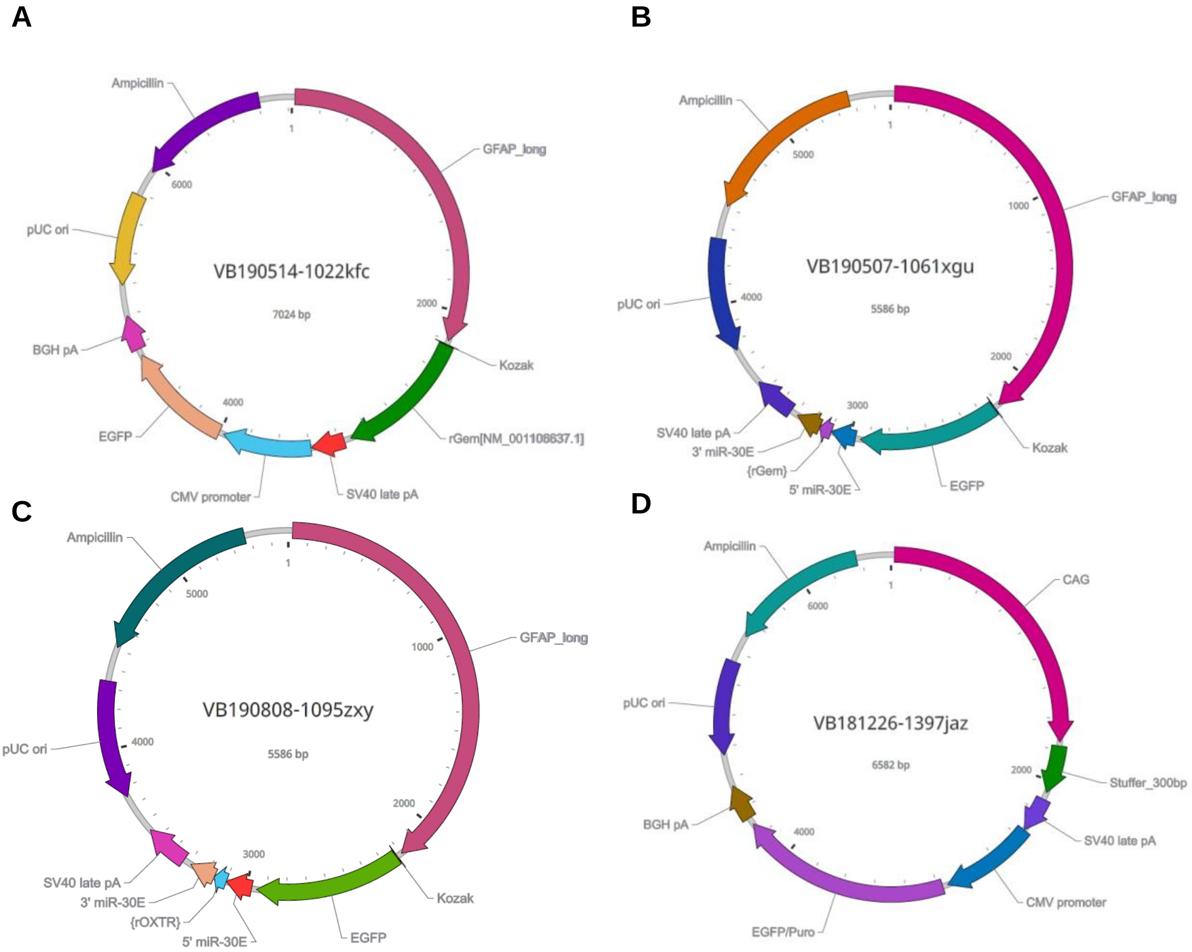

Figure 5. DNA plasmids used for *in vitro* transfections. **A)** *Gem* overexpression plasmid expressing the *Gem* open reading frame (NCBI RefSeq NM_001106637.1) under the control of the long fragment of the *hGFAP* promoter and EGFP under the *CMV* promoter. **B-C)** DNA plasmids expressing a shRNA and EGFP under the control of the long fragment of the *hGFAP* promoter targeted against (B) the rat *Gem* mRNA or (C) the rat *Oxtr* mRNA. **D)** Control vector expressing solely EGFP under the control of the *CMV* promoter.

Table 1. Conditions of electroporation of primary astrocytes for oligonucleotides or plasmids tested during the establishment process. Resulting cell viability was rated on a scale from + to +++, with + representing poor viability and +++ representing viability similar to non-transfected cells. Conditions which were consequently applied in experiments are shown in bold letters, conditions assessed during establishment of transfections are shown in non-bold letters.

Format	**Experiment**	**Coating solution**	**Cell No.**	**DNA (µg)**	**siRNA**	**Neon Tip**	**Vol. plating Medium**	**Time post-transfection**	**Transfection settings**	**Result**
48-well plate	*Gem* Overexpression	PDL	3×10^4	0.5		10 µl	250 µl	72 h	Various settings	**V:1100 1100 1300 ms:20 30 10 #2 1 3 Settings shown above provided best transfection and viability rates**
24-well plate/ 4-chamber object slide	***Gem* Overexpression**	**PDL**	$\mathbf{6\times10^4}$	**0.5**		**10 µl**	**500 µl**	**48 h**	**V:1200 ms:10 #3**	**Viability: +++ Significant overexression**
	***Gem* siRNA**	**PDL**	$\mathbf{7\times10^4}$		**10 nM**	**10 µl**	**500 µl**	**48 h**	**V:1300 ms:20 #2**	**Viability: ++ Significant knockdown**
	***Sp1* siRNA**	**PDL**	$\mathbf{7\times10^4}$		**10 nM**	**10 µl**	**500 µl**	**48 h**	**V:1300 ms:20 #2**	**Viability: ++ Significant knockdown**
	Gem shRNA	PDL	6×10^4	0.5		10 µl	500 µl	24 h	V:1200 ms:10 #3	ICC against GFP revealed +70% transfection rate
	***Oxtr* shRNA**	**PDL**	$\mathbf{6\times10^4}$	**0.5**		**10 µl**	**500 µl**	**80 h**	**V:1200 ms:10 #3**	**Viability: +++ Significant knockdown**
	***Gem* shRNA**	**PDL**	$\mathbf{6\times10^4}$	**0.5**		**10 µl**	**500 µl**	**48 h/1 W**	**V:1200 ms:10 #3**	**Expression increased after 48h and remained unchanged after 7d**
35-mm Petri dish	*Gem* overexpression	PLL	4×10^5	2.5		100 µl	1 ml	12 d	V:1100 ms:20 #2	Viability: +++ Not confluent enough for GJIC
	***Gem* overexpression**	**PLL**	$\mathbf{8\times10^5}$	**2.5**		**100 µl**	**1 ml**	**7 d**	**V:1100 ms:20 #2**	**Viability: +++ Confluency suitable for GJIC**
6-well plate	***Sp1* siRNA**	**PDL**	$\mathbf{8\times10^5}$		**10 nM**	**100 µl**	**3 ml**	**48 h**	**V:1100 ms:20 #2**	**Viability: +++ Significant knockdown**
	***Gem* shRNA**	**PDL**	$\mathbf{8\times10^5}$	**5**		**100 µl**	**3 ml**	**80 h**	**V:1200 ms:10 #3**	**Viability: +++ Significant knockdown**
	***Oxtr* shRNA**	**PDL**	$\mathbf{8\times10^5}$	**5**		**100 µl**	**3 ml**	**80 h**	**V:1200 ms:10 #3**	**Viability: +++ Significant knockdown**

	***Gem* overexpression**	**PDL**	**$8x10^5$**	**5**		**100 µl**	**3 ml**	**48h**	**V:1100 ms:20 #2**	**Viability: +++ Significant overexpression**
	***Gem* overexpression**	**PDL**	**$1.1×10^6$**	**5**		**100 µl**	**10 ml**	**72 h**	**V:1100 ms:20 #2**	**Viability: +++ Significant overexpression**
	***Gem* siRNA**	**PDL**	**$1.5×10^6$**		**10 nM**	**100 µl**	**10 ml**	**48 h**	**V:1300 ms:20 #2**	**Viability: ++ Significant knockdown**
	***Sp1* siRNA**	**PDL**	**$1.5×10^6$**		**10 nM**	**100 µl**	**10 ml**	**48 h**	**V:1300 ms:20 #2**	**Viability: ++ Significant knockdown**
	Cx43 siRNA	PDL	$1.1×10^6$		10 nM	100 µl	10 ml	24 h	V:1100 ms:20 #2	Viability: +++ No knockdown
	Cx43 siRNA	PDL	$1x10^6$		10 nM	100 µl	10 ml	24 h	V:1300 ms:20 #2	Viability: ++ Significant knockdown
60-mm Petri dish	Cx43 siRNA	PDL	$1x10^6$		10 nM	100 µl	10 ml	48 h	V:1300 ms:20 #2	Viability: ++ Significant knockdown
	Cx43 siRNA	PDL	$1x10^6$		20 nM	100 µl	10 ml	48 h	V:1700 ms:20 #1	Viability: +++ No knockdown
	Cx43 siRNA	PDL	$1.5×10^6$		10 nM	100 µl	10 ml	24 h	V:1300 ms:20 #2	Viability: ++ Significant knockdown
	scrRNA	PDL	$1.5×10^6$		10 nM	100 µl	10 ml	24 h	V:1300 ms:20 #2	Viability: ++
	CX43 siRNA	PDL	$1.5×10^6$		10 nM	100 µl	10 ml	24 h	V:1300 ms:20 #2	Viability: ++ Significant knockdown
	scrRNA	**PDL**	**$1.5×10^6$**		**10 nM**	**100 µl**	**10 ml**	**48 h**	**V:1300 ms:20 #2**	**Viability: ++**
	CX43 siRNA	**PDL**	**$1.5×10^6$**		**50 nM**	**100 µl**	**10 ml**	**48 h**	**V:1300 ms:20 #2**	**Viability: ++ Significant knockdown**

2.6 RNA-Isolation

From cells. Cells were trypsinized at ~90% confluency, and pellets were lysed in 1ml of peqGold® TriFast (peqLab, Erlangen, Germany). Keeping the cells on ice during the whole procedure prevented degradation of RNA. RNA was extracted according to the manufacturer's protocol. Briefly, the lysate was mixed with 200µl chloroform and centrifuged for 20min at 17000g and 4°C. Following collection of 500µl of the RNA containing upper aqueous phase in a fresh cup, RNA was precipitated with 466µl isopropanol overnight at -20°C. After centrifugation at 17000g for 30min, the RNA pellet was washed twice with 80% ethanol and air-dried for 10min. To minimize contamination with genomic DNA, a subsequent DNA digestion was performed. To this end, the RNA was resuspended in 7µl RNAse-free sterile H_2O and 2µl DNAseI (ThermoFisher; EN0521), as well as 1µl 10x DNAseI reaction buffer (ThermoFisher; B43). Following incubation at 37°C at 1000rpm for 30min, 1µl of 50mM EDTA solution was added to inhibit DNAse activity. Last, DNAse denaturation was carried out at 65°C at 1000rpm for 10min. RNA quantity and quality were determined at 260/280nm and 230/260nm using a NanoDrop spectrophotometer (Thermo Scientific, Waltham, USA).

From rat brain tissue. Animals were killed as described in 2.3 and brains were rapidly removed. A coronal razor cut was made through the brain rostral to the cerebellum and the cut surfaces were placed on a microtome specimen plate containing Leica Tissue Freezing Medium (Leica, Wetzlar, Germany) and frozen on dry ice. Next, 300-µM thick coronal frozen sections were prepared in a cryostat at -4°C. Sections were placed on chilled slides, placed under a stereomicroscope where micropunches of the PVN were prepared using a stainless steel cannula (diameter 1µM). PVN location was determined according to coordinates of (G Paxinos, 2008), as well as using neuroanatomical landmarks such as the ventricles and midline. Consequently, RNA isolation was performed as described for cultured cells (see above).

2.6.1 Reverse Transcriptase PCR (RT PCR), Endpoint PCR and quantitative PCR (qPCR)

RNA was reverse transcribed into cDNA by adding random primers (3 µg/µl) and dNTPs (final concentration 0.5mM; Life Technologies) to 1µg of total RNA. The mix was filled *ad* 15µl with RNAse-free sterile H_2O and incubated for 5min at 65 °C for primer annealing. To initiate reverse transcription, 5xFirstStrandBuffer, Dithioerythritol (DTT; final concentration 5mM), 1µl RNase OUT (40U/µl) and the reverse transcriptase Super Script IV (200U/µl; Life Technologies) were added to a final volume of 21µl. Before addition of the reverse transcriptase, 3µl of each reaction mix were transferred into a fresh cup. These samples served as a negative control (-RT) in endpoint or qPCRs to control for contamination with genomic DNA. cDNA synthesis was performed in a Mastercycler® nexus X2 (Eppendorf, Wesseling-Berzdorf, Germany) at 42°C for 50min and consequently stopped by degradation of the enzyme at 70°C for 15min.

For endpoint PCR, 1µl cDNA, 2pmol of each forward and reverse primers (Metabion, Germany; for a list of PCR-Primers used in this thesis, please see Table 2) and RNAse-free sterile H_2O were added to DreamTaq™ Master Mix (Thermo Scientific), containing dNTPs (final concentration 0.2mM each) and DreamTaq™ polymerase, to a final reaction volume of 25µl. Negative controls consisted of respective –RTs or H_2O. The PCR was run for 40 amplification cycles with an initiating denaturation step at 95°C for 5min, while primer-annealing was performed at 60°C for 15s followed by elongation at 72°C for 30s. The PCR cycler was programmed to run a final elongation at 72°C for 10 additional min. The PCR-products were then loaded onto a 1.5% agarose gel run at 140V for 45min. After electrophoresis, cDNA was detected with Roti®-Gel Stain (Carl Roth GmbH, Karlsruhe, Germany) and visualized at UV-light with a ChemiDoc XRS+ Imager (Bio-Rad).

qPCR was performed with the QuantStudio 3 and QuantStudio 5 Real Time PCR Systems (ThermoFisher). One reaction mixture contained 5µl PowerUp™ SYBR® Green Master Mix (ThermoFisher; A25743), 9µl RNAse-free DEPC-treated H_2O and 2µl of both forward and reverse primers (4pmol, Tab.2), as well as 2µl cDNA reverse transcribed from 1µg RNA and diluted 1:2 in RNAse-free H_2O. To reduce pipetting errors, each sample was pipetted in triplicates and the mean Ct values were used in the final analysis. In a first step, the Uracil-DNA-Glycosylase is activated at 50°C for 2min, followed by the hot-start activation of the Dual-Lock DNA polymerase at 95°C for 2min. Next, a denaturation (95°C, 3s) and annealing/extension (60°C 30s) step are repeated for 40 cycles. The detection dye SYBR® Green binds to double stranded DNA while emitting a fluorescence signal at 522nm proportional to the amount of PCR amplicons during the elongation step of the PCR . Following amplification, a melting curve of the PCR product is calculated by gradually heating the sample from 60°C to 95°C, while constantly measuring SYBR® Green fluorescence. The temperature at which fluorescence is not detectable anymore marks the melting point of the double stranded DNA. Detection of multiple melting points indicates the amplification of non-specific byproducts, which was additionally verified in an agarose gel electrophoresis. The housekeeping genes *Gapdh* and *Rpl* were used as internal reference controls and RNA expression was quantified by comparative $_{\Delta\Delta}$Ct-method .

Table 2. Primers with their respective PCR product size used in PCR and qPCR experiments

Target	Forward primer (5'-3')	Reverse primer (5'-3')	Product size (bp)
Gem (pair1)	ACAGCCTTAGACTGCGGAAC	GGCGCATGGTGACGTTATTC	145
Gem (pair2)	ACCGAGTGGTGCTTATTGGG	CAAGCTCTCCCTTCTGACACA	400
Gem (pair3)	TGTGTCAGAAGGGAGAGCTTG	CAAGGGGACATCTGGACGAC	315
Gem (pair4)	GTGTCTGTGTCAGAAGGGAGA	GCCGCGTCTTAACAATGCTT	394
Gem (pair5)	GAATAACGTCACCATGCGCC	GAGCCATTCATTCTCCCCCTTA	415
Gem (pair6)	CACTCCACTGCTCCCGATG	CTCCCTTCTGACACAGACACTTC	485
Oxtr	CTGGAGTGTCGAGTT GGACC	AGCCAGGAACAGAAT GAGGC	136
Gja1	TTCATTGGGGGAAAGGCGTG	CTGGGCACCTCTCTTTCACTT	173
Gjb6	TTCCAGTTCACCTCACACGG	GGCAGTGGGAATGTCACCTTT	99
Gjb2	GGAACGAGACTCAGGAGCGT	CGGGGAAGAAGTGGTCGTAG	236
Slc1a2	GTGGACTGGCTGCTGGATAG	AGTTGTGTGCGGCATAGACA	223
Slc1a3	GGTGTGGACAAACGCATCAC	TCGGAGGCGGTCCCTTATTG	162
Sp1	AAACACCCCAGGTGATCATGG	CATGAATGGCCTCTCCCCTG	307
Dao	AGGCCCCTTGGATAAAGCAC	GCCAGTGAGTTCACCCATGA	227
Gapdh	TGATGACATCAAGAA GGTGG	CATTGTCATACCAGG AAA TGAG	185
Rpl	ACAAGAAAAAGCGGA TGGTG	TTCCGGTAATGGATC TTTGC	172
Amigo2	TAGACCGACGGCTGGCTAAG	GCCTCCCACCAATCTGGTAA	382
Gfap	GCGAAGAAAACCGCATCACC	TTTGGTGTCCAGGCTGGTTT	77
Gat1	CTATTAGGCCGCAAAGCTGC	GAGAGGAACACCCGCAAAGA	385
Gat3	ATCTGTGCGGGCATCTTCAT	TTAACGGTCACCATCCGTGG	263

2.7 Protein Extraction

Proteins were either isolated from fresh brain tissue punches prepared identically as described under 2.6 (from PVN, whole amygdala and whole Hippocampus) or cell culture. Pellets/punches were resuspended in RIPA lysis buffer (Sigma Aldrich) and incubated on ice for 45min under regular vortexing. Following centrifugation (13200g, 4°C), the supernatant containing the protein lysate was transferred into a fresh cup. Next, protein concentration was measured with a colorimetric BCA protein assay kit (Pierce ™ BCA Protein Assay Kit, Thermo Scientific) according to the manufacturer's guidelines. Briefly, 10µl of seven different solutions containing a defined protein concentration (2µg - 0.025µg Albumin) are mixed with 200µl of BCA solution to obtain a standard curve. In parallel, 2µl of protein lysate are treated identically. After 30min of incubation at 37°C, the resulting luminescent reaction was quantified using an optical density reader (FLUOstar OPTIMA, BMG Labtech, Ortenberg, Germany). To reduce pipetting errors, each sample was pipetted in duplicates and the mean values were used for concentration calculations.

2.8 SDS-PAGE and Western Blot Analysis

For determination of protein expression and phosphorylation levels, 20-30 µg of proteins were mixed with 4xLaemmliBuffer (see Appendix 3) and denatured at 95°C for 5min. Next, separation by molecular weight was performed on a 12.5% Criterion™ TGX Stain-Free™ Gel (Bio-Rad) for 20min at 70V followed by 2h at 100V. After crosslinking the trihalo components of the gel with tryptophan residues of the separated proteins in an UV-induced reaction, the proteins were then transferred to a nitrocellulose membrane (Bio-Rad) for 5-30min (for detailed blotting protocols see Tab. 3) using the Trans-Blot Turbo System (Bio-Rad; 1704150). In order to visualize the total amount of protein blotted, the fluorescence of the crosslinked trihalo-tryptophan components was imaged at UV-light with the ChemiDoc XRS+ Imager (Bio-Rad). The picture of the total lane protein served as an internal reference control during the analysis. To cover all non-specific binding sites, an appropriate blocking solution was applied to the membrane for 90min (for detailed conditions see Tab. 3). Next, the membrane was incubated over night with the diluted primary antibody under the conditions shown in Table 3, washed extensively in Tris-buffered saline containing 0.001% Tween-20 (TBST) to remove all unbound primary antibody and incubated with respective secondary antibodies conjugated with horseradish peroxidase (Tab. 3). Following a second washing step to remove all unbound secondary antibody, the membranes were incubated for 5min with developer solution (Bio-Rad; Tab.3) and the protein/antibody complexes were then visualized by capturing luminescence with the ChemiDoc XRS+ Imager. The images were analyzed with ImageLab software (Bio-Rad) that was specifically created for the ChemiDoc Imager.

In some cases the blots were stripped to remove bound antibody complexes (Re-Blot Plus Strong Solution 10x; Millipore, Darmstadt, Germany), blocked twice for 10min with the appropriate blocking solution and reprobed with fresh primary antibodies. Wash steps, incubation with secondary antibody and detection were carried out as described above.

Table 3. List of antibodies used in immunoblotting experiments with their respective application protocols.

Primary antibody	Secondary antibody	Blotting protocol	Blocking solution	Developer solution
pCREB (Ser133) Milipore 06519 1:5000 in 5% BSA	Anti-rabbit IgG, 7074S 1:5000 in 5% BSA	StandardSD (30min)	5% BSA	Clarity™ Western ECL Substrate (Bio-Rad)
pCamKII (Thr286) cs12716S 1:1000 in 5% BSA	Anti-rabbit IgG, 7074S 1:1000 in 5% BSA	StandardSD (30min)	5% BSA	Clarity™ Western ECL Substrate
Sp1 Milipore 07645 1:1000 in 5% BSA	Anti-rabbit IgG, 7074S 1:5000 in 5% MP	StandardSD (30min)	5% BSA	Clarity™ Western ECL Substrate
Cx43 cs3512S 1:1000 in 5% BSA	Anti-rabbit IgG, 7074S 1:1000 in TBS-T	StandardSD (30min)	5% BSA	Clarity™ Western ECL Substrate
pCx43 (Ser282) Thermo PA5-64641 1:500 in 5% BSA	Anti-rabbit IgG, 7074S 1:1000 in TBS-T	StandardSD (30min)	5% BSA	Super Signal™ West Dura Extended Duration Substrate (ThermoFisher)
pCx43 (Ser279) Thermo PA5-64777 1:500 in 5% BSA	Anti-rabbit IgG, 7074S 1:2000 in 2% BSA	StandardSD (30min)	5% BSA	Clarity Max™ Western ECL Substrate (Bio-Rad)
pCx43 (Ser368) cs3511S 1:1000 in 5% BSA	Anti-rabbit IgG, 7074S 1:1000 in TBS-T	StandardSD (30min)	5% BSA	Clarity™ Western ECL Substrate
Cx30 Thermo 71-2200 1:250 in 5% MP Samples heated to 70°C for 15min	Anti-rabbit IgG, 7074S 1:1000 in TBS-T	StandardSD (30min)	5% MP	Super Signal™ West Dura Extended Duration Substrate
MYPT1 cs2634S 1:1000 in 5% BSA	Anti-rabbit IgG, 7074S 1:1000 in TBS-T	StandardSD (30min)	5% BSA	Clarity Max™ Western ECL Substrate
pMYPT1 (Thr696) cs4563S 1:500 in 5% MP	Anti-rabbit IgG, 7074S 1:1000 in 3% MP	StandardSD (30min)	5% MP	Clarity Max™ Western ECL Substrate

pSAPK/JNK (Thr183/Tyr185) cs9251S 1:5000 in 5% BSA	Anti-rabbit IgG, 7074S 1:5000 in TBS-T	StandardSD (30min)	5% BSA	Super Signal™ West Dura Extended Duration Substrate
pAkt (Thr308) cs13038S 1:1000 in 5% MP	Anti-rabbit IgG, 7074S 1:5000 in 5% MP	StandardSD (30min)	5% MP	Clarity Max™ Western ECL Substrate
Gem A-3 sc-514497 1:2000 in 5% BSA	m-IgGκ BP-HRP sc-516102 1:2000 in TBS-T	Low MW (5min)	5% BSA	Clarity Max™ Western ECL Substrate
peEF2 (Thr56) cs2331 1:000 in 5% BSA	Anti-rabbit IgG, 7074S 1:1000 in TBS-T	StandardSD (30min)	5% MP	Clarity™ Western ECL Substrate
ROCK1 cs4035 1:2000 in 5% BSA	Anti-rabbit IgG, 7074S 1:2000 in TBS-T	StandardSD (30min)	5% BSA	Super Signal™ West Dura Extended Duration Substrate
pAMPK (Thr172) cs2535 1:2000 in 5% BSA	Anti-rabbit IgG, 7074S 1:2000 in TBS-T	StandardSD (30min)	5% BSA	Clarity™ Western ECL Substrate
EAAT1 sc515839 1:400 in 5% BSA	m-IgGκ BP-HRP sc-516102 1:1000 in TBS-T	StandardSD (30min)	5% BSA	Super Signal™ West Dura Extended Duration Substrate
EAAT2 sc365634 1:10000 in 5% BSA	m-IgGκ BP-HRP sc-516102 1:2000 in TBS-T	StandardSD (30min)	5% BSA	Clarity™ Western ECL Substrate
pp38 (Thr180/Tyr182) sc17852 1:1000 in 5% BSA	Anti-rabbit IgG, 7074S 1:1000 in TBS-T	Mixed MW (7min)	5% BSA	Clarity™ Western ECL Substrate
pERK1/2 cs9101 1:5000 in 5% BSA	Anti-rabbit IgG, 7074S 1:1000 in TBS-T	StandardSD (30min)	5% BSA	Clarity™ Western ECL Substrate
ERK1/2 cs9102 1:1000 in 5% BSA	Anti-rabbit IgG, 7074S 1:1000 in TBS-T	StandardSD (30min)	5% BSA	Clarity™ Western ECL Substrate
pERK5 (Thr218/Tyr220) Millipore 07-507 1:5000 in 3% MP	Anti-rabbit IgG, 7074S 1:5000 in 3% MP	StandardSD (30min)	3% MP	Clarity Max™ Western ECL Substrate
GFAP cs12389 1:5000 in 5% BSA	Anti-rabbit IgG, 7074S 1:2000 in TBS-T	StandardSD (30min)	5% BSA	Clarity™ Western ECL Substrate
Beta-Tubulin cs2146 1:1000 in 5% MP	Anti-rabbit IgG, 7074S 1:1000 in TBS-T	StandardSD (30min)	5% MP	Clarity™ Western ECL Substrate
pEzrin (Thr567) ab47293 1:1000 in 5%BSA	Anti-rabbit IgG, 1:1000 in 5%BSA	StandardSD (30min)	5% BSA	Super Signal™ West Dura Extended Duration Substrate

2.9 Immunocytochemistry

H32 cells or astrocytes (14d post-enrichment) were seeded in four-chamber glass slides ($7x10^5$ cells/chamber; Corning; 354104). After 1h of serum starvation, cells were stimulated with varying concentrations of OXT for 10min or 3h. For fixation, 4% PFA was added to the medium (1:1) for 2min, whereafter the medium was aspirated and 0.5ml of 4%PFA was added for 10min. Next, chambers were washed three times with PBS-T and consequently rinsed with PBS. After blocking for 30min (0.1% TritonX-100 (Sigma Aldrich), 1% FBS, 10% normal goat serum in PBS), cells were incubated with primary antibodies (Tab.4) diluted in PBS containing 0.5% TritonX-100 and 3.3% FBS for 2h at RT. Following a second blocking step in 3% BSA for 10min, appropriate secondary antibodies (Tab.3) were applied for 2h at RT in the dark to prevent photobleaching. Finally, the slides were covered with ProLong® Gold containing DAPI (Cell Signaling Technology, Princeton, USA; cs8961) and incubated overnight at RT in the dark. Images were taken with a Leica SP8 confocal laser scanning microscope and quantified as described in 2.12 with ImageJ software (Version 1.52e).

Table 4. List of primary antibodies with their respective dilutions and secondary antibodies used in immunocytochemistry experiments.

Primary antibody	**Secondary antibody** (All ThermoFisher)
GFAP cs12389 1:1000	goat-anti rabbit AlexaFluor488 1:1000
ZO1 ThermoFisher 1:100	goat anti-mouse AlexaFluor594 1:1000
Gem A-3 sc-514497 1:100	goat anti-mouse AlexaFluor594 1:1000
pMLC(Ser19) cs3671 1:50	goat anti-rabbit AlexaFluor594 1:1000
GFP ThermoFisher PA1-980A 1:200	goat-anti rabbit AlexaFluor488 1:1000
AlexaFluor488 Phalloidin cs8878 1:20	-
AlexaFluor594 Phalloidin cs8953 1:20	-

2.10 Immunohistochemistry

Ten or 20min after *icv* OXT administration rats were transcardially perfused with 4%PFA in PBS (see 2.3), and the brains were harvested and post-fixed in 4%PFA for 3h followed by cryo-protection in 30% sucrose for 2 days and consequent snap-freezing in isopentane. Frontal 40-µM sections were prepared with a cryostat, washed three times in PBS for 20min and blocked in PBS containing 2%goat serum and 1%TritonX-100 for 1h at RT. Consequently, slices were incubated with primary antibody solutions (Tab.5) at 4°C overnight. After three washing steps with PBS, appropriate secondary antibodies (Tab.5) diluted in blocking solution were added to the slices for 2h at RT. The sections were mounted on object slides using ProLong® Gold containing DAPI (Cell Signaling) and imaged using a Leica SP8 confocal laser scanning microscope.

Table 5. List of primary antibodies with their respective dilutions and secondary antibodies used in immunohistochemistry experiments.

Primary antibody	**Secondary antibody** (All ThermoFisher)
GFAP cs12389 1:500	goat-anti rabbit AlexaFluor488 1:1000
GFAP ab50738 1:500	goat-anti chicken AlexaFluor488 1:1000
Gem A-3 sc-514497 1:100	goat anti-mouse AlexaFluor594 1:1000
mCherry abcam 167453 1:800	goat anti-rabbit AlexaFluor594 1:1000
Homer1 SySy 160 003 1:250	donkey anti-rabbit AlexaFluor647 1:500
Vglut1 Sysy 135 311 1:250	goat anti-mouse AlexaFluor594 1:500
GFP Aves AB_2307313 1:500	goat-anti chicken AlexaFluor488 1:500
OXT-Neurophysin clone PS38 kindly provided by Dr. Harold Gainer 1:500	goat anti-mouse AlexaFluor555 1:1000
CNP1 SySy 355 004 1:500	goat anti-guinea pig AlexaFluor488 1:1000
MAP2 SySy 188 006 1:500	goat anti-chicken AlexaFluor647 1:1000
NeuN MAB377 1:500	goat anti-mouse AlexaFluor555 1:1000

2.11 Gap-junctional intercellular communication (GJIC)

In order to investigate the effects and mechanisms of OXT on the degree of astrocytic intercellular coupling, scrape loading dye transfer experiments were performed. To this end, $8x10^5$ primary astrocytes of different age (7d, 14d) were seeded in poly-D-lysine coated 35-mm TC dishes ($3x10^5$ cells/dish; Corning; CLS3294) 2d prior to the experiments. After 1h of serum starvation, OXT (1nM–1µM) or AVP (1nM-100nM) was added to the medium for various timepoints (5-180min). To investigate the underlying signaling cascades, cells were preincubated with one of various pharmacological inhibitors (1µM U0126; 10µM Gö6983; 1µM L368,889; 1µM Carbenoxolone, Sigma Aldrich; C4790) or Veh (Ringer's solution) 1h prior to stimulation. After the respective treatments, the medium was aspirated, and the dishes were rinsed three times with Ca^{2+}-free PBS to remove remaining stimulants and prevent uncoupling of the cells. Next, 1ml of pre-warmed (37°C) lucifer yellow (1mg/ml in Ca^{2+}-free PBS, Sigma Aldrich; L0259) or, in case of EGFP expressing cells, Biocytin (1mg/ml in Ca^{2+}-free PBS, Sigma Aldrich; B4261) was added to the dish, and three cuts were made through the cell layer with a rounded surgical blade, allowing the fluorescent solution to diffuse within the astrocytic network. After 10min of incubation at 37°C, cells were washed three times with PBS and fixed with 0.5ml 4% PFA. For Biocytin experiments, an AlexaFluor594-conjugated Streptavidin (ThermoFisher; S32356) was used to visualize Biocytin diffusion. The fluorescence signal was viewed using an epifluorescence microscope (Leica dm5000b) and images of each cut were taken. The fluorescent dye spread area was quantified with ImageJ software (Version 1.52e).

2.12 Bioimaging and Image Analysis

For all experiments, microscopy settings as well as image analysis settings were kept identical within one experiment. *In vitro* experiments were replicated at least three times.

Morphological analysis in vitro, in vivo and ex vivo

Astrocytes were stained for GFAP and DAPI as described above and images were taken with either a Leica SP8 (for *in vitro* and *in vivo*) or SP6 (for *ex vivo*) confocal laser scanning microscope. In case of cultured cells, five pictures throughout one culture chamber (1024x1024) were acquired per treatment condition and analyzed with ImageJ software (Version 1.52e) as depicted in Fig.6a. For *in vivo* and *ex vivo* analyses, three z-sections per animal (*in vivo*: 30µM, 0.5µM/z-section, 1024x1024, PVN and hippocampus (CA1 region); *ex vivo*: 30µM, 0.5µM/z-section, 1024x1024, hippocampus (CA1 region)) were acquired and analyzed with ImageJ software (Version 1.52e) as described in Fig.6b.

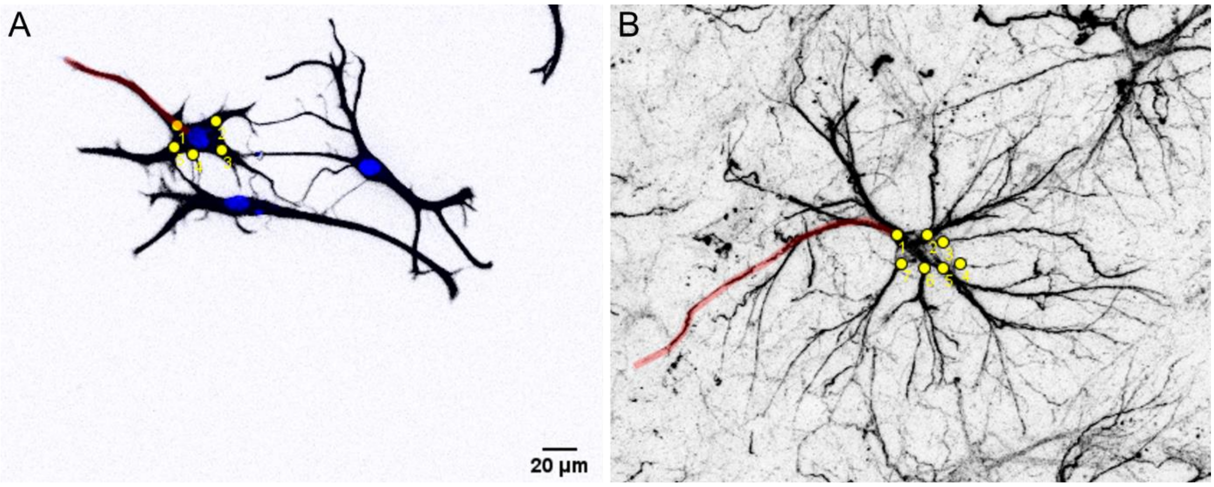

Figure 6. Quantification of length (red lines) and number (yellow dots) of primary GFAP+ processes of astrocytes *in vitro* and *in vivo* using ImageJ. **A)** Primary rat cortical astrocytes stained for GFAP/DAPI and analyzed for length of longest primary process, as well as number of primary processes. **B)** Rat hippocampal (CA1 region) astrocyte stained for GFAP and analyzed for length of longest primary process, as well as number of primary processes. Lengths were measured from the edge of the nucleus indicated by DAPI staining to the end of the process of interest.

3D-reconstruction of GFP-expressing astrocytes

In order to analyze OXT-induced changes to volume and surface area of astrocytes, animals received unilateral intrahippocampal (CA1 region) infusions of 1µl vector plasmid solution containing AAV2/5-GFAP-GFP in PBS (titer $1x10^{13}$ GC/ml, kindly provided by Dr. Nathalie Rouach). After 14 days, hippocampi were harvested and acute slices (350µM) were prepared as described under 2.4. 3D-reconstruction was accomplished using IMARIS software (Version 9.3, Bitplane AG, Zürich, Switzerland). In detail, two astrocytes per z-section were randomly selected (Fig.7a), and a region of interest (ROI) was created in 3D around each of these cells (Fig.7b-c). Next, a 3D object was generated within these ROIs (Fig.7d-e), allowing quantification of both cellular surface and volume.

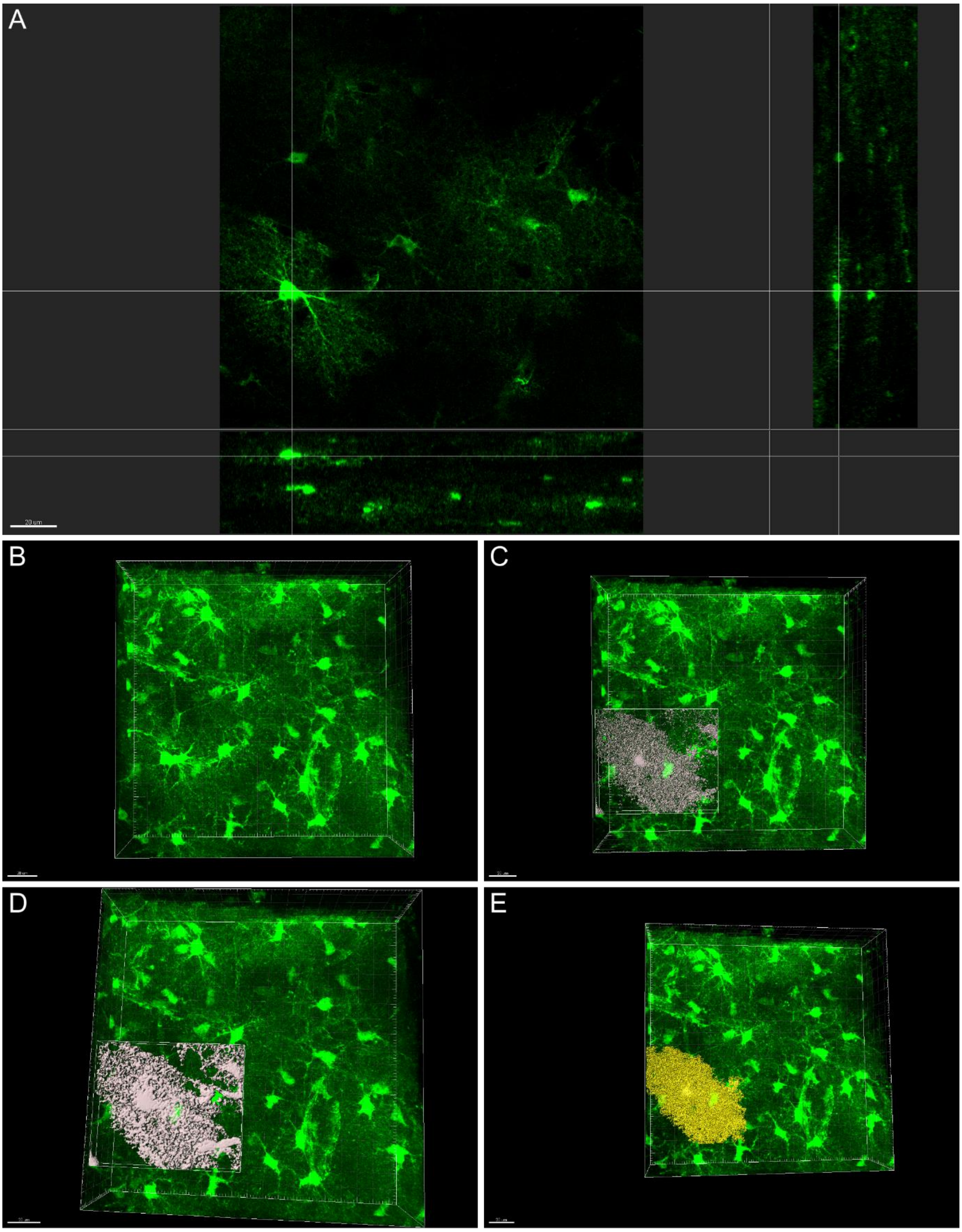

Figure 7. 3D reconstruction of GFP-expressing hippocampal astrocytes in acute *ex vivo* slice preparations using IMARIS. **A)** Astrocyte of interest depicted in a 2D image of the z-section. Lower/lateral panels show position of the cell in the context of the z-section. **B-C)** Generation of a 3D ROI around the cell of interest. **D-E)** Generation of a 3D object resembling the original shape of the astrocyte.

Determination of astrocyte-synapse spatial relationship by STED nanoscopy

STED nanoscopy was performed on acute *ex vivo* slice preparations (see 2.4) using a costum built STED-microscope (Abberrior/Scientifica). Synaptic distance to the closest astrocytic element was quantified with a Fiji-Plugin (provided by Philippe Mailly, CIRB imaging facility, College de France, Paris) only including synapses that a) showed no wider distance than 300nm between pre-and postsynaptic element and b) contained Homer1/VGlut1 fluorescence maxima in both, deconvolved confocal images and STED images.

Colocalization studies

To assess the degree of Cx43 localization at cell/cell-contacts, the tight-junction protein ZO1 was used as a marker for points of intercellular contact (Penes et al., 2005). The number of Cx43/ZO1-immunoreactive (ir) punctae was determined manually to ensure inclusion of points solely located at cellular contact zones.

Intensity measurements and determination of above threshold cells in vitro and in vivo

For immunofluorescence intensity measurements and maxima quantification, images were taken with a Leica SP8 confocal laser scanning microscope (63x Obj., 16-Bit, 1024x1024) and analyzed with ImageJ software (Version 1.52e). Following background subtraction, a ROI was manually generated around cells of interest and fluorescence intensity within the ROI was measured. Determination of above threshold cells was accomplished by use of the find maxima function of ImageJ on a background subtracted single image (*in vitro* experiments) or a sum z-projection (*in vivo* experiments; 30µM, 0.5µM/z-section, 1024x1024). Above threshold cells were defined as single cells marked by DAPI staining displaying at least one maximum of the fluorescence of interest.

2.13 Statistical Analysis

For statistical analysis, GraphPadPrism (V.8, GraphPad Software, San Diego, USA) was used. Data were first tested for normal distribution by Shapiro-Wilks-test. In case of normally distributed data, statistical hypothesis testing was carried out by two-tailed Student's *t*-test, one-way (factor: treatment) or two-way (factors: pre-treatment and treatment) ANOVA, followed by a Bonferroni post-hoc analysis, whenever appropriate. Data shown in graphs represent mean +/- SEM; significance was accepted at $p < 0.05$. For non-normally distributed data, statistical hypothesis testing was carried out by two-tailed Mann-Whitney-U-test or Kruskal-Wallis-test followed by Dunn-Bonferroni post-hoc analysis whenever appropriate.

Here, data shown in graphs represent median + min/max and significance was accepted at $p < 0.05$.

3 RESULTS

3.1 Establishment of primary rat cortical astrocyte cultures

To study OXTR-mediated signaling in astrocytes, primary rat cortical astrocytes were cultured (see 2.5) after a protocol adapted from (Schildge et al., 2013). As described for astrocytes cultured *in vitro* , numbers of primary processes ranged from one to seven, displaying a less complex cellular morphology compared to astrocytes *in vivo/ex vivo* (Fig.8a). Furthermore, 96% of cells within the cultures showed GFAP expression as assessed by immunocytochemistry, with the remaining 4% representing either microglial/oligodendrocytical remainders of the isolation process or astrocytes not expressing GFAP (Fig.8b; Morrison and de Vellis, 1981; Schildge et al., 2013). Endpoint PCR revealed expression of genes preferentially or exclusively expressed in astrocytes, including genes coding for the gap-junction proteins Cx43 (*Gja1*) and Cx26 (Gjb2) , as well as genes coding for the neurotransmitter transport proteins EAAT1/EAAT2 (*Slc1a3/Slc1a2*) and GAT1/GAT3 (*Gat1/Gat3*) (Fig.8c). As previously described for cultured astrocytes, *Oxtr* mRNA was detectable in RNA from six independent cultures (Fig.8c).

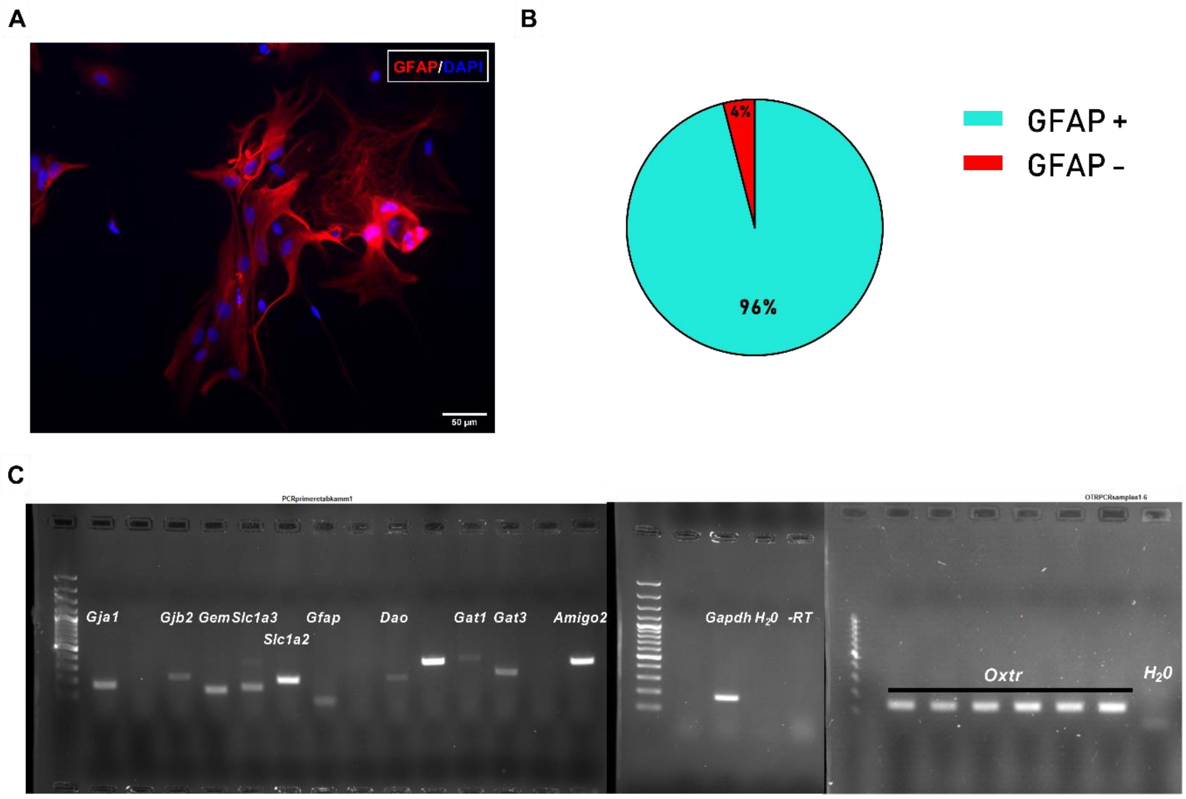

Figure 8. Characteristics of primary rat cortical astrocytes used for *in vitro* studies. **A)** Representative ICC image performed on an exemplary astrocyte culture 14d post-enrichment. Most cultured astrocytes displayed one to seven primary processes and an average process length of ~30-60µM. **B)** Quantification of the purity of five independent cultures assessed by GFAP staining. **C)** Agarose gel showing expression of various genes preferentially or exclusively expressed in astrocytes, as well as *Oxtr* expression in six independent cultures.

3.2 Characterization of the effects of OXT on astrocytes

Effects of OXT on astrocytic signaling cascades and proteins in vitro and in vivo

To elucidate the molecular consequences of astrocytic OXTR signaling, synthetic OXT was either applied to primary rat cortical astrocytes (500nM for 10min) or administered *icv* in male Wistar rats. Subsequent analyses of changes in protein levels/phosphorylation state focused on proteins preferentially or exclusively expressed in astrocytes, as well as targets and brain regions previously linked to OXTR activation in other contexts (Blume et al., 2008; Devost et al., 2008b; Jurek and Neumann, 2018; Martinetz et al., 2019). For a summary of all examined targets please see Fig.9a (*in vitro* experiments) and Fig.9b (*in vivo* experiments). In primary astrocytes, OXT induced increases in pCreb(Ser133; t_{15}=2.840, p=0.012), pAkt(Thr308; t_{15}=2.303, p=0.036), pERK5(Thr218/Tyr220; t_7=2.309, p=0.054), pCx43(Ser368; t_{14}=3.506 p=0.004), pCx43(Ser279; U=1, p=0.016), pCx43(P1; *U*=10, p=0.021), pCx43(P2; t_{15}=2.574 p=0.021), pEzrin(Thr567; t_{10}=2.536, p=0.030) and pERK1/2 phosphorylation levels (t_{10}=2.459, p=0.038 pERK1; t_{10}=4.702, p<0.001 pERK2), while decreasing peEF(Thr56; *U*=0, p=0.008) and pMYPT(Thr696; t_{15}=2.068, p=0.056) phosphorylation. No changes were observed for pp38, pJNK(Thr183/Thr185) and pcamKII(Thr286). Furthermore, OXT-exposure caused elevated levels of the cytoskeleton-related proteins beta-Tubulin (*U*=2, p=0.032), ROCK1 (t_7=2.758, p=0.028), Gem (t_{18}=2.203, p=0.041) and Sp1 (t_{12}=2.470, p=0.030), while reducing GFAP (t_8=2.718, p=0.026). The astrocytic glutamate transporter EAAT2 was unaffected by OXT stimulation. Attempts to detect OXT-induced changes in RhoA activity by means of a pull-down assay of GTP-bound (i.e. active) RhoA, failed due to below detection limit endogenous activity of RhoA (data not shown).

Within the PVN, *icv* OXT increased levels of the gap-junction protein Cx30 (t_{11}=3.361, p=0.006), pCx43(Ser368; t_{11}=2.244, p=0.046) and the endogenous ROCK-inhibitor Gem (*U*=2, p=0.005) 10min post-administration, while downregulating EAAT2 (t_{12}=2.799, p=0.016) and the gap-junction protein Cx43 (t_{11}=3.546, p=0.005). The changes to Cx30 (*U*=2, p=0.005), Gem (*U*=7, p=0.051) and pCx43(Ser368; t_{11}=2.029, p=0.067) remained observable after 20min, whereas EAAT2 and Cx43 levels recovered to control levels. Within the hippocampus, elevated quantities of Cx30 (*U*=4, p=0.014) and pCx43(Ser368; t_{10}=2.195, p=0.053), as well as decreased quantities of Cx43 (t_{12}=6.664, p<0.001) were detected 10min following OXT administration. Here, the decrease in Cx43 persisted 20min post-administration (t_{12}=2.707, p=0.019), while EAAT1 (t_{10}=2.972, p=0.014) was downregulated. Within the amygdala, OXT elicited acute increases of Cx30 (*U*=7, p=0.051) and EAAT1 (t_{11}=4.387, p=0.001), while decreasing Gem levels (t_{12}=2.818, p=0.016). None of these differences remained significant at 20min post-administration. However, OXT upregulated GFAP (*U*=4, p=0.014) and decreased quantities of EAAT2 (t_{12}=2.533, p=0.026) at this timepoint.

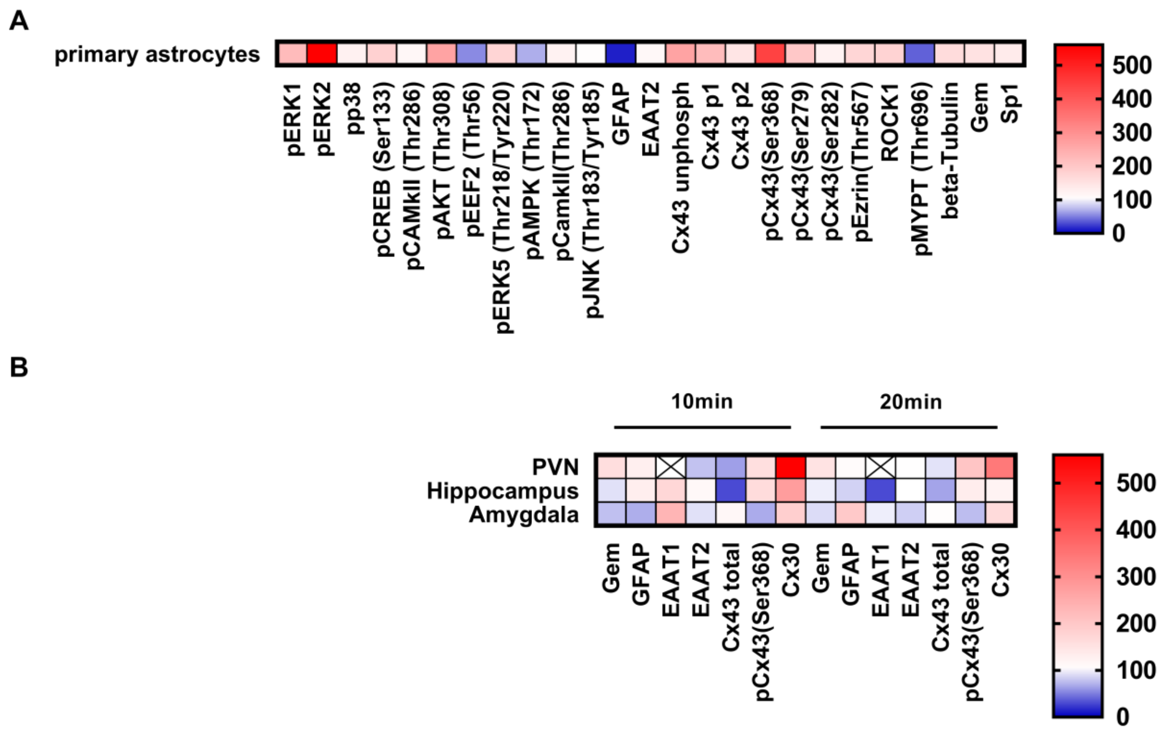

Figure 9. Effects of OXT on signaling pathways and proteins of astrocytes *in vitro* and *in vivo.* **A)** Heatmap of percentage changes in protein/phosphorylation levels following exposure of primary rat cortical astrocytes to 500nM OXT for 10min. **B)** Heatmap of percentage changes of protein/phosphorylation levels 10min or 20min after *icv* administration of OXT in punches derived from three different brain regions (PVN, hippocampus, amygdala). Downregulations are colored in blue, while upregulations are colored in red.

Effects of OXT on the expression of selected astrocytic genes

Based on the OXT-induced changes of astrocytic proteins, the expression of genes coding for these proteins was analyzed *in vitro* following OXT stimulation (500nM) for different timepoints. While there was no change in Cx43 (*Gja1)* expression, Cx30 (*Gjb6)* (independent t-test; t_9=2.134, p=0.062) and Cx26 (*Gjb2)* (Mann-Whitney *U*=4, p=0.052) expression both showed a trend to be decreased compared to the control group after 10min of exposure, but this difference did not reach statistical significance (Fig.10a). Thirty min after OXT application, an increase in *Gja1* (t_7=2.755, p=0.028) as well as *Gem* expression (t_7=2.373, p=0.049) was detected, while EAAT2 (*Slc1a2)* expression remained unchanged (Fig.10b). The observed trend of decreased *Gjb2* expression after 10min of stimulation became statistically significant at the 30min timepoint (t_7=4.427, p=0.003).

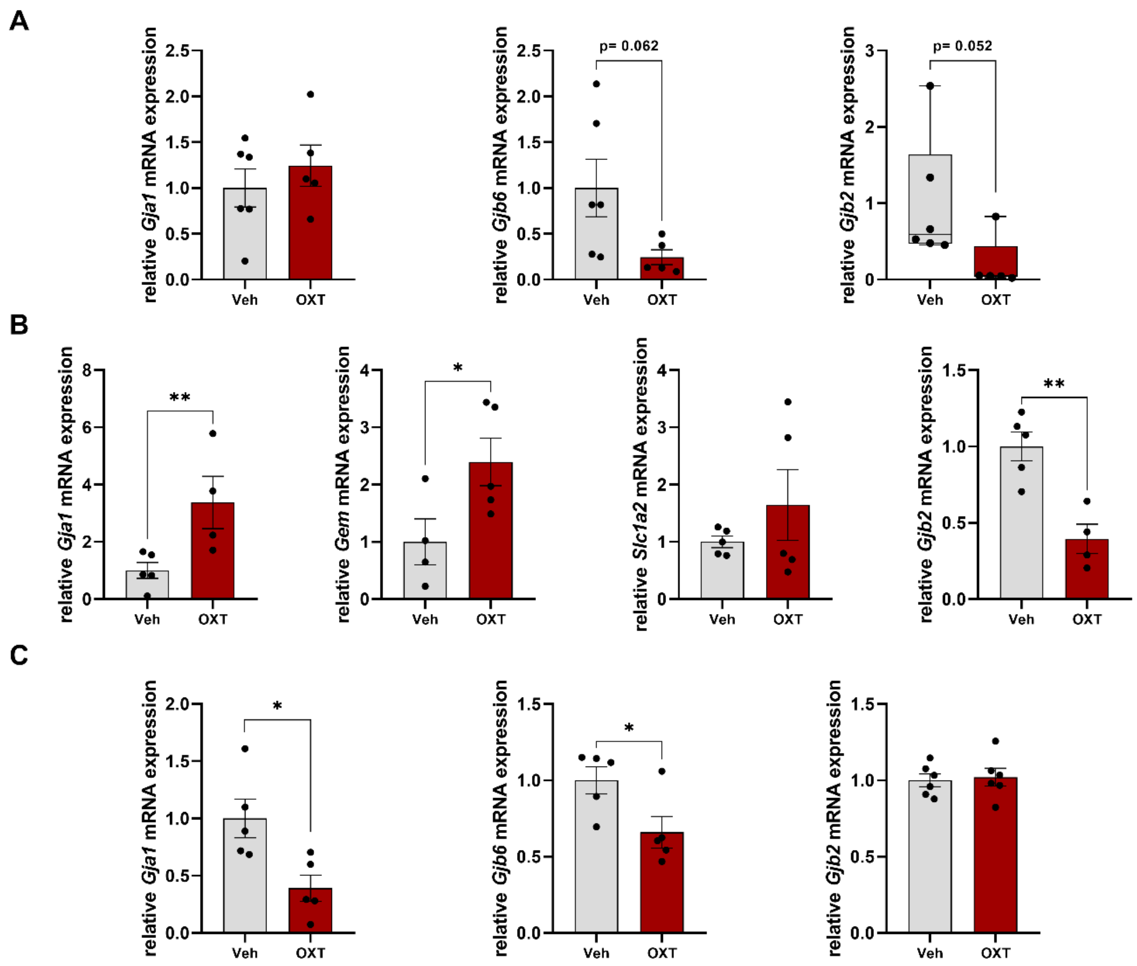

Figure 10. Expression of astrocytic genes following exposure to OXT for three differing timespans. **A)** *Gja1*, *Gjb6* and *Gjb2* mRNA levels after 10min of stimulation with 500nM OXT. **B)** *Gja1*, *Gem*, *Slc1a2* and *Gjb2* expression after 30 min of OXT exposure. **C)** *Gja1*, *Gjb6* and *Gjb2* mRNA levels following 180min of OXT application. Data represent mean relative expression +/- SEM for normally distributed data and median +/- min/max values for non-normally distributed data. * p<0.05, ** p <0.01.

Contrary to a shorter exposure, 180min of OXT stimulation caused a decrease in *Gja1* expression (Fig.10c; t_8=2.982, p=0.018), while *Gjb2* mRNA recovered to control levels. Following the tendency after 10min of exposure, *Gjb6* expression was lowered after 180min of OXT application compared to Veh-treated cells (t_8=2.486, p=0.039).

Effect of OXT on distribution of astrocytic gap-junctions and its impact on intercellular connectivity

Due to protein and mRNA analyses pointing towards a downregulation of astrocytic gap-junctions by OXT, I next tested, whether OXT affects gap-junctional intercellular communication (GJIC). To this end, dye-spread assays (Upham et al., 2016) were performed, in which the broad-range gap-junction inhibitor carbenoxolone (Rozental et al., 2001) served as a positive control (Fig.11a). In an initial dose-response experiment (Fig.11b), a treatment effect (one-way ANOVA; $F_{4,73}$=6.847, $p < 0.001$) was observable for doses of 10nM (p=0.001), 500nM (p=0.002), as well as 1µM (p=0.0004) of OXT with OXT acutely impairing GJIC. To investigate the underlying signaling mechanisms, cells were pre-treated with either 10µM of the MEK-inhibitor U0126, 1µM of the broad-range PKC-inhibitor Gö6983 or 1µM of the OXTR-antagonist L368,889 prior to exposure to 500nM OXT for 10min and subsequent GJIC assessment (Fig.11c). Differences were found depending on pre-treatment ($F_{3,62}$=5.919, p=0.001) and interaction ($F_{3,62}$=5.574, p=0.002), but not treatment ($F_{1,62}$=0.1290, p=0.7207). OXT treated cells showed impaired GJIC by around 20% (p=0.01), while this effect was blocked by each of the three pre-administered substances. Interestingly, the closely related sister-peptide AVP had no effect in these experiments (data not shown). Since the expression of gap-junctional genes varies over the time course of culture (Koulakoff et al., 2008; Li et al., 2019), an identical experiment was performed on cells cultured for 14 days (Fig.11d) after enrichment, yielding similar results (pre-treatment: $F_{2,39}$=5.609, p=0.007; interaction: $F_{2,39}$=7.117, p=0.002; treatment: $F_{1,39}$=1.862, p=0.1802; posthoc: p=0.002 Veh/OXT vs. Veh/Veh). Application of a positive control, i.e. the gap-junction blocker carbenoxolone, resulted in reduced GJIC by around 70% (t_{15}=14.75, $p < 0.0001$).

To visualize the impact of OXT on astrocytic gap-junctions on a single cell level, ICC of the most abundant astrocytic gap-junction protein Cx43 was carried out. Here, the tight-junction protein ZO1 was used as a marker for cell-cell contacts and Cx43/ZO1 colocalization (Fig.12a) was quantified following pre-treatments and treatments identical to GJIC experiments.

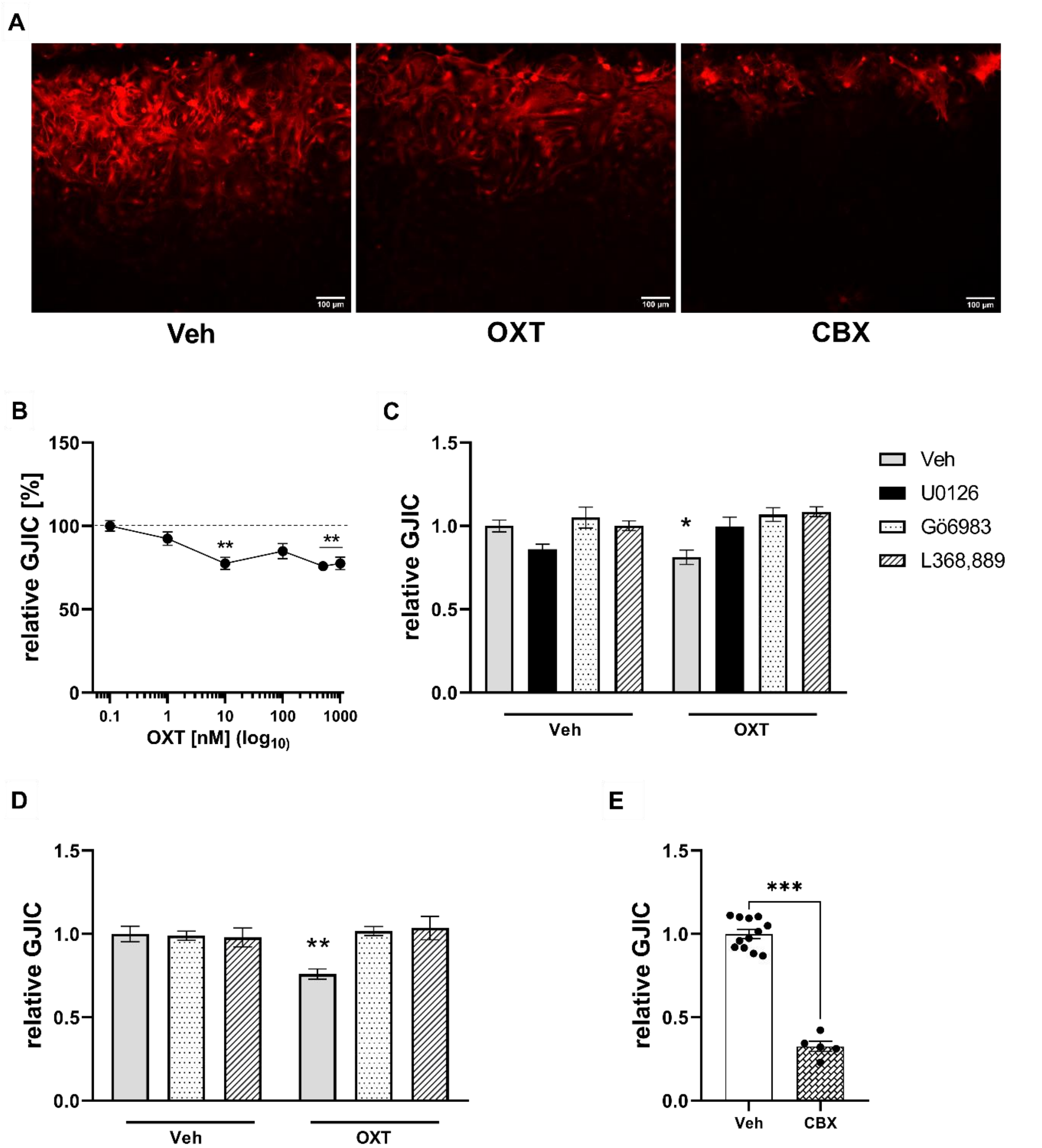

Figure 11. OXT impairs gap-junctional intercellular communication in a MEK, PKC and OXTR-dependent manner. **A)** Representative images of streptavidin staining visualizing the distance of biocytin diffusion within the astrocytic network. Middle and right panel show impaired GJIC by OXT and carbenoxolone treatment, respectively. **B)** Dose-response curve of acute OXT acting on GJIC. **C)** Impact of OXT on relative GJIC of astrocytes cultured for 7d following pre-treatment with either Veh (grey bars), U0126 (black bars), Gö6983 (dotted bars) or L368,889 (striped bars). **D)** Same as C), but performed on cells cultured for 14d. **E)** Quantification of GJIC after treatment with the gap-junction blocker carbenoxolone. Data represent mean relative GJIC+/- SEM. * p<0.05, ** p <0.01 *** p<0.001.

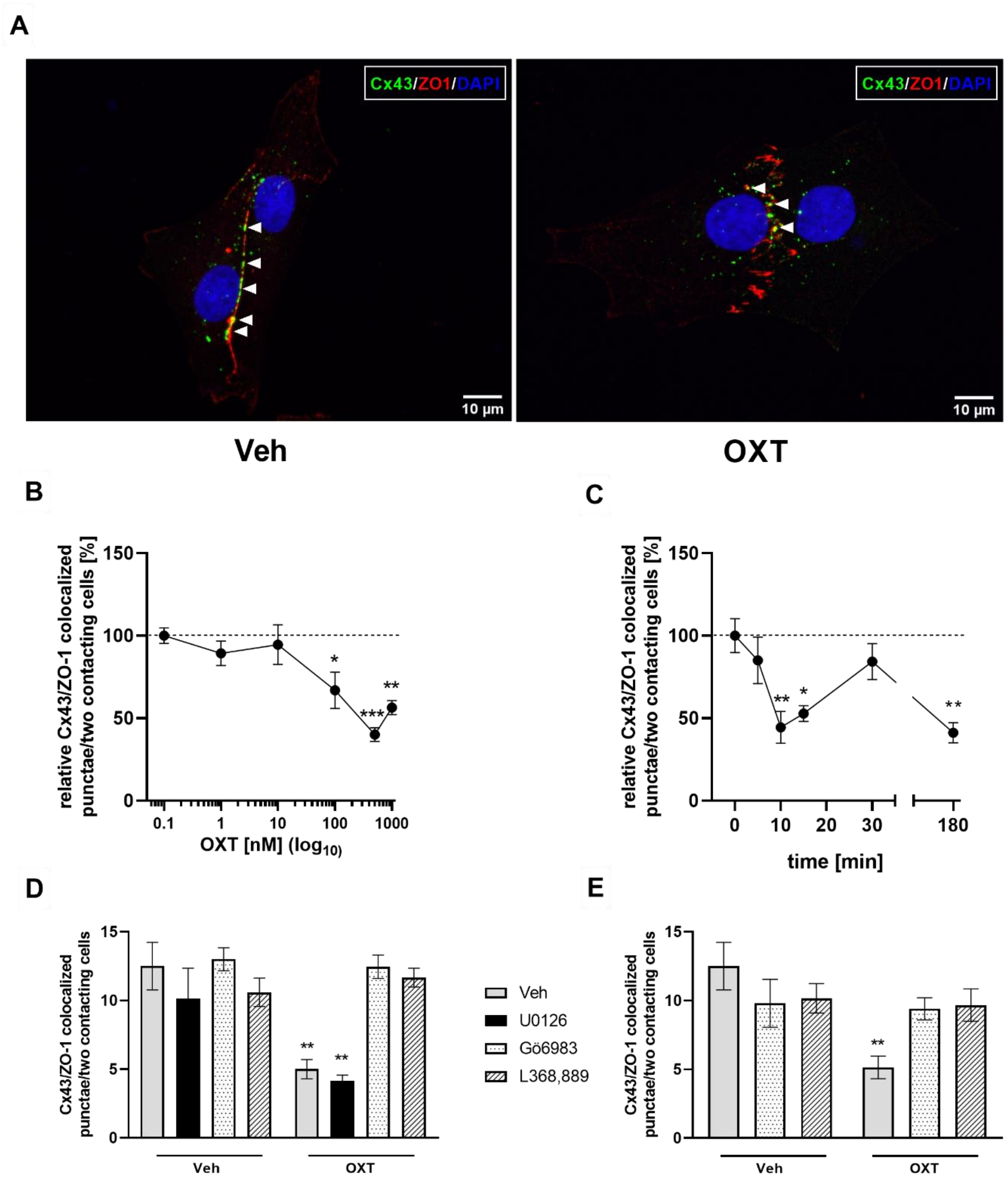

Figure 12. OXT reduces Cx43 localization at cell-cell contacts in a PKC and OXTR-dependent manner. **A)** Representative ICC images of cells stained for Cx43 (green), ZO1 (red) and DAPI (blue) displaying high levels of Cx43/ZO1 colocalization in the control group (left) and reduced colocalization in OXT treated cells (right). White arrows indicate points of Cx43/ZO1 colocalization. **B)** Dose-response curve of OXT affecting Cx43 localization at cell-cell contacts. **C)** Time-response curve of OXT (500nM) affecting Cx43 localization at cell-cell contacts.**D/E)** Impact of 15min (D) or 180min (E) of OXT exposure on Cx43/Zo1 colocalization following pre-treatment with either Veh (grey bars), U0126 (black bars), Gö6983 (dotted bars) or L368,889 (striped bars). Data represent mean absolute (D;E) or relative (B;C) Cx43/ZO1 colocalized punctae per two contacting cells +/- SEM. * p<0.05, ** p <0.01 *** p<0.001.

In a dose-response experiment (Fig.12b), a treatment effect ($F_{5,36}$=8.810, $p < 0.001$) was observable for OXT doses of 100nM (p=0.001), 500nM (p=0.002), as well as 1µM (p=0.0004) with OXT reducing Cx43 localization at cell-cell contacts by 35-60%. The effect first became significant at 10min and 15min post-stimulation (Fig.12c; p=0.005, p=0.024, respectively), while recovering to control levels at the 30min timepoint. After a longer exposure for 180min, a similar reduction as for the 10min timepoint was observable (p=0.003). To investigate the underlying signaling cascades, cells underwent identical pre-treatment conditions as described for GJIC experiments prior to stimulation with 500nM OXT for 15 min or 3h and subsequent Cx43 localization assessment (Fig.12d). After 15min of OXT stimulation, differences were found depending on treatment ($F_{1,46}$=13.16, p=0.001), pre-treatment ($F_{3,46}$=8.029, p=0.001), as well as interaction ($F_{3,46}$=5.267, p=0.003). OXT-treated cells displayed less Cx43 localization at cell-cell contacts (p=0.008), while this effect was PKC and OXTR-dependent, but not MEK-dependent (p=0.001). Similar to GJIC experiments, the closely related sister-peptide AVP had no effect (data not shown). A prolonged exposure with OXT for 180 min (Fig.12e), yielded similar results (pre-treatment: $F_{2,29}$=0.4274, p=0.656; interaction: $F_{2,29}$=5.237, p=0.011; treatment: $F_{1,29}$=7.061, p=0.013; p=0.002 Veh/OXT vs. Veh/Veh).

OXT-induced changes in astrocytic cytoskeletal dynamics and the impact on astrocyte-neuron spatial relationships

The modulation of neuronal communication by astrocytes highly depends on the spatial relationship of astrocytes and neuronal synapses, a relationship critically set by the astrocytic cytoskeleton. Since our studies revealed several changes of proteins associated with cytoskeletal dynamics, I opted to examine possible OXT- induced alterations of the cytoskeleton of astrocytes. In an initial dose-response experiment (Fig.13a/b) a treatment effect ($F_{4,539}$=2.760, p=0.0272) was observable with 500nM (p=0.016) of acute (10min) OXT causing a rapid elongation of astrocytic processes. To investigate the underlying signaling mechanisms, cells were pre-treated with either 10µM U0126, 1µM Gö6983 or 1µM L368,889 prior to exposure to 500nM OXT for 10min and subsequent analysis of primary process length and number. Differences in process length (Fig.13c) were found depending on pre-treatment ($F_{3,646}$=3.421, p=0.017) and interaction ($F_{3,646}$=4.480, p=0.004), but not treatment ($F_{1,646}$=2.024, p=0.1553). OXT-treated cells showed an increase in the length of primary processes by around 25% (p=0.008), while this effect was blocked by each of the three pre-administered substances. Additionally, differences in process number (Fig.13d) were found depending on treatment ($F_{1,414}$=4.220, p=0.041), pre-treatment ($F_{3,414}$=2.741, p=0.043) and interaction ($F_{3,414}$=6.179, p=0.0004) with OXT causing a ~30% increase in primary process number (p=0.002) that was MEK, PKC, as well as OXTR-dependent. Similar to gap-junction experiments, AVP had no effect in these experiments (data not shown).

To assess, whether prolonged exposure to OXT induces comparable effects with a similar underlying signaling profile, the above described experiments were repeated with 180min of OXT stimulation. In the corresponding dose-response experiment (Fig.13e), a similar treatment effect ($F_{5,554}$=3.738, p=0.002) was observable for a dose of 500nM (p=0.016). Differences in process length (Fig.13f) were found depending on treatment ($F_{1,515}$=9.444, p=0.002) and interaction ($F_{3,515}$=2.800, p=0.04), but not pre-treatment ($F_{3,515}$=2.402, p=0.067), while a significant treatment ($F_{1,450}$=7.111, p=0.008), pre-treatment ($F_{3,450}$=7.244, p<0.001) and interaction ($F_{3,450}$=11.97, p<0.001) effect was observed for the number of primary processes (Fig.13g). Stimulation for 180min increased both, the length (p=0.047) and number (p=0.018) of primary processes to a similar magnitude as 10min of OXT exposure.

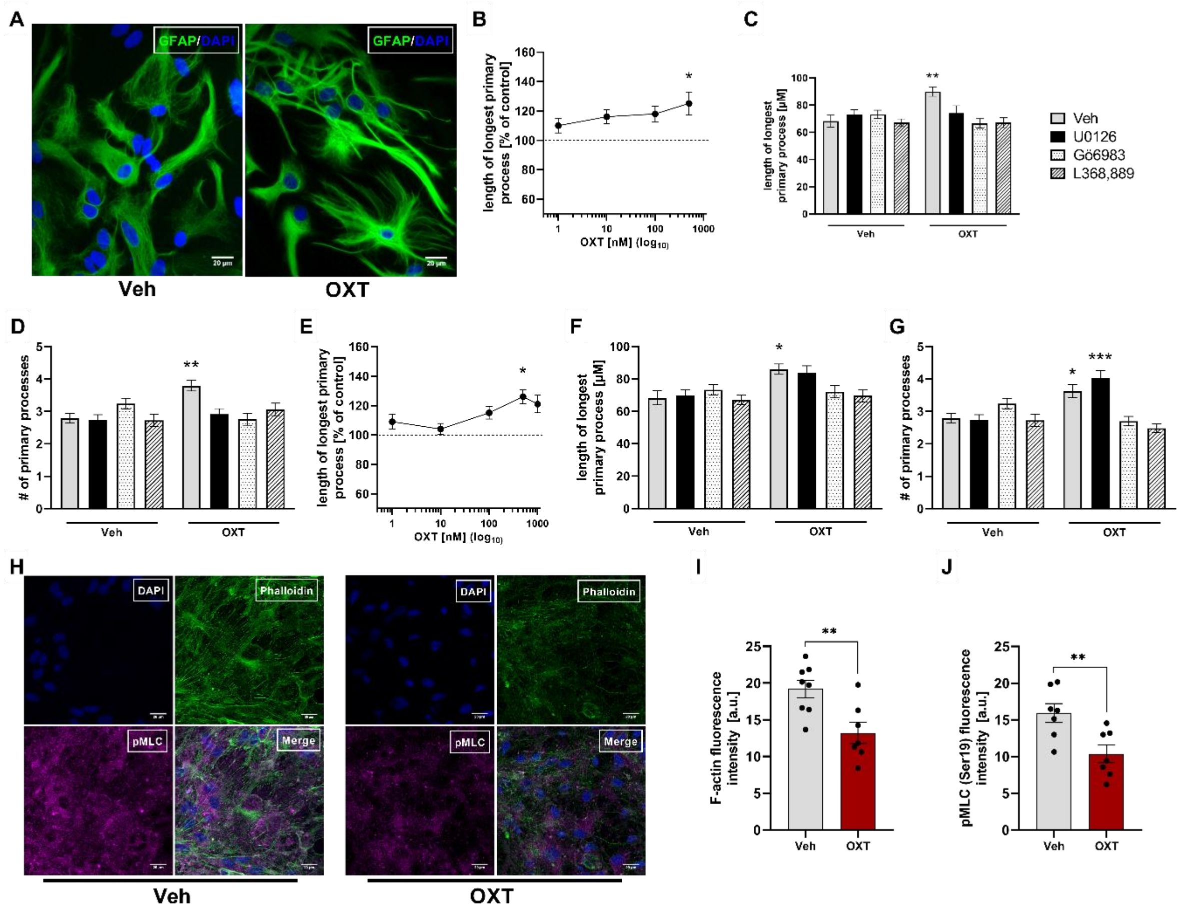

Figure 13. OXT induces elongation and formation of primary astrocytic processes in a PKC, MEK and OXTR-dependent manner. **A)** Representative ICC images of astrocytes stained for GFAP (green) and DAPI (blue). OXT treated cells display visible cytoskeletal changes. **B)** Dose-response curve of OXT affecting the length of the longest primary process. **C)** Effect of 10min OXT exposure on process length following pre-treatment with either Veh (grey bars), U0126 (black bars), Gö6983 (dotted bars) or L368,889 (striped bars). **D)** Effect of 10min OXT exposure on the number of primary processes following pre-treatment with either Veh, U0126, Gö6983 or L368,889. **e)** Same as B), but performed with 180min of OXT stimulation. **F)** Same as C), but performed with 180min of OXT stimulation. **G)** Same as D), but performed with 180min of OXT stimulation. **H)** Representative ICC staining of DAPI (blue), Phalloidin (green) and pMLC(Ser19) (magenta) in astrocytes treated with either Veh (left panel) or 500nM OXT for 3h (right panel). **I)** Quantification of Phalloidin immunofluorescence in OXT-treated cells compared to Veh-treated

cells. **J)** Quantification of pMLC(Ser19) immunofluorescence in OXT-treated cells compared to Veh-treated cells. Data represent mean absolute or relative values +/- SEM. * $p<0.05$, ** $p<0.01$ *** $p<0.001$.

Mechanistically, this effect was again dependent on PKC and OXTR activity, but in case of process numbers not dependent on MEK (Fig.13g; $p<0.001$ U0126/Veh vs. U0126/OXT). In line with this finding, OXT-treated cells pre-treated with U0126 displayed a similar tendency toward process elongation ($p=0.224$ Veh/Veh vs. U0126/OXT). Since cellular process formation and elongation are indicators of a dampened activity of the RhoA/ROCK pathway and protein analyses revealed an OXT-induced increase in the endogenous RhoA/ROCK inhibitor Gem, F-actin (Phalloidin) and phospho(Ser19)-myosin-light-chain-kinase fluorescent intensity measurements were used as indirect markers of RhoA/ROCK activity (Fig.13h; Totsukawa et al., 2000). OXT stimulation with 500nM OXT for 180min induced a decrease in F-actin stress fibres (Fig.13h/i; independent t-test; $t_{13}=3.225$, $p=0.007$) and pMLC (Ser19) levels (Fig.13h/j; $t_{12}=3.136$, $p=0.009$), both indicative of a dampened RhoA/ROCK activity. Taken together, these observations imply a rapid impact of OXT on the cytoskeleton of astrocytes *in vitro*.

To validate these effects *in vivo*, synthetic OXT was administered *icv* in male Wistar rats. PVN, as well as hippocampal (CA1 region) astrocytes were examined for OXT-induced changes in cellular morphology and possible changes in resulting neuron-astrocyte spatial relationships. Corroborating *in vitro* experiments, centrally administered OXT caused astrocytic process elongation (Fig.14a/b; $t_{10}=3.484$, $p=0.006$) and ramification (Fig.14a/c; $t_{10}=2.469$, $p=0.033$) within the PVN 10min post-administration, leading to an increased astrocytic coverage of OXT neurons (Fig.14a/d; $t_{10}=3.093$, $p=0.011$). The total amount of PVN GFAP+ cells remained unchanged (Fig.14e). Within the hippocampus (Fig.14f), a significant elongation of processes was not observable in an analysis with n=1 animal (Fig.14g; $t_{10}=1.510$, $p=0.162$). However, separate analysis of all acquired optical fields revealed a significant increase in process length (Fig.14a/d; $t_{29}=2.342$, $p=0.026$). The number of processes (Fig.14i), as well as the total number of GFAP+ cells (Fig.13j) were unaffected.

As GFAP is not expressed throughout the entity of an astrocyte, I next used a viral vector-based strategy to express GFP under the promoter of the *hGFAP* gene (Fig.15a). 3D-reconstruction (Fig.15b) revealed an increase in astrocyte surface (Fig.15c; $t_{20}=3.302$, $p=0.004$) and volume (Fig.15d; $t_{20}=2.155$, $p=0.046$) after OXT exposure. Co-staining with pre- / post-synaptic markers together with STED nanoscopy (Fig.15e-g) revealed an OXT-induced change in the spatial relationship between astrocytes and excitatory synapses 10min post-bath application in acute hippocampal slices (Fig.15h), suggesting an effect of OXT-induced cytoskeletal dynamics on neuronal communication.

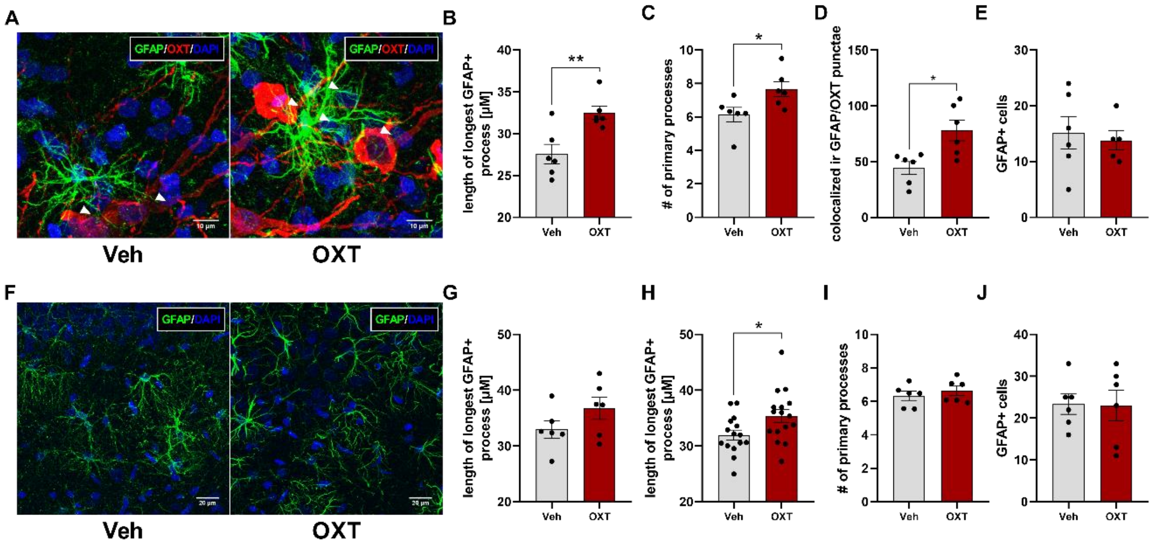

Figure 14. OXT affects the astrocytic cytoskeleton *in vivo*. **A)** Representative IHC images of PVN astrocytes (GFAP; green) co-stained with Neurophysin (OXT; red) and DAPI (blue) in animals that received either Veh (left panel) or OXT (right panel) *icv*. White arrows mark points of GFAP/Neurophysin (OXT) colocalization. **B-E)** Quantification of primary process length (B), primary process number (C), GFAP/OXT-colocalization (D) and number of GFAP+ cells (E) within the rat PVN 10min after OXT administration. **F)** Representative IHC images of hippocampal CA1 astrocytes (GFAP; green) co-stained with DAPI (blue) 10min post-*icv* administration of Veh or OXT. **G-J)** Quantification of primary process length for n=1 animal (G), Quantification of primary process length for n=1 optical field (H), primary process number (I) and number of GFAP+ cells (J) within the CA1 region of the rat hippocampus 10min after administration of *icv* OXT. Data represent mean absolute values +/- SEM. * p<0.05, ** p <0.01.

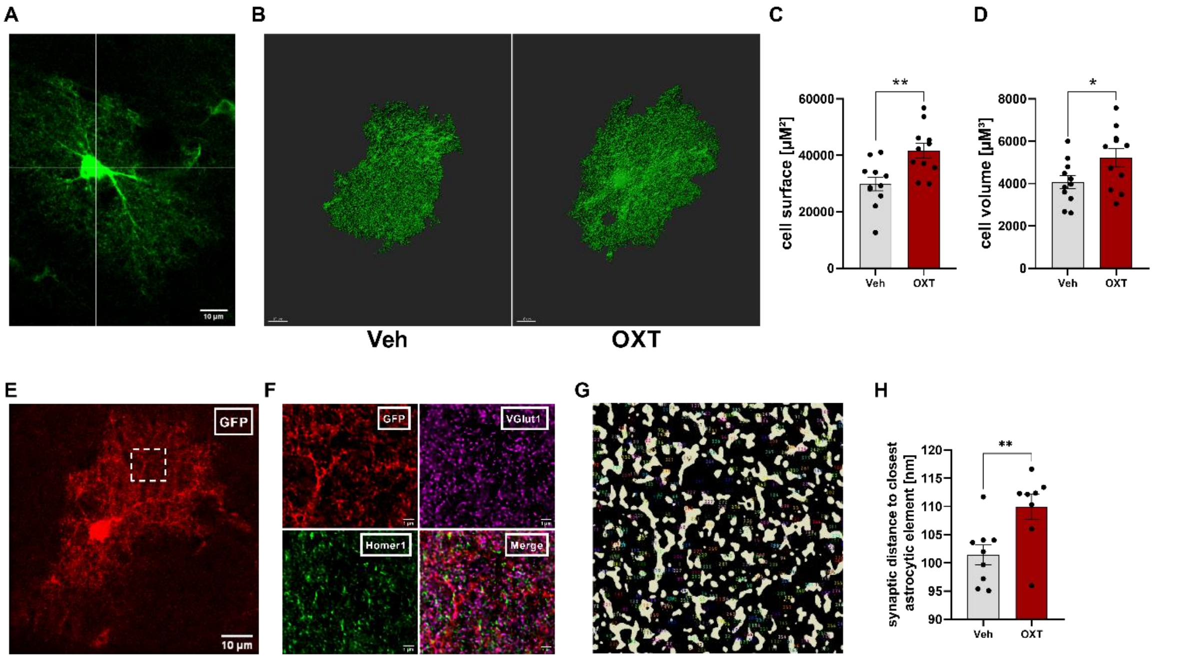

Figure 15. OXT alters three-dimensional features of astrocytes and neuron-astrocyte spatial relationships *ex vivo*. **A)** Representative confocal microscopy image of a GFP-expressing mouse hippocampal astrocyte. **B)** Representative 3D reconstructions of astrocytes created from Veh (left panel) or OXT (right panel) -treated acute hippocampal slices. **C)** Assessment of cellular surface area from 3D reconstructed astrocytes. **D)** Assessment of cellular volume from 3D reconstructed astrocytes. **E)** Representative confocal microscopy image of a GFP-expressing mouse hippocampal astrocyte. White dotted box indicates inlay for (F). **F)** Inlay of (E) including deconvolved confocal image of astrocytic element (GFP; red), as well as deconvolved STED-images of pre-synaptic (VGlut1; Magenta) and post-synaptic (Homer1; green) markers. **G)** ImageJ analysis plugin output displaying astrocytic elements in white and functional synapses as single colored dots. **H)** Quantification of average synapse/astrocyte distance per analyzed inlay. Data represent mean absolute values +/- SEM. * p<0.05, ** p <0.01.

3.3 Involvement of the Sp1 – Gem signaling axis

The involvement of the small GTPase Gem in the effects of OXT on astrocytes

Based on its OXT-induced *in vitro* and *in vivo* upregulation, as well as on the observed dampened activity of the RhoA/ROCK pathway, I hypothesized that the endogenous ROCK-inhibitor Gem plays an important role in conveying the effect of OXT on astrocytes. To test this hypothesis, I applied a siRNA-based knockdown approach *in vitro* (Fig.16a). Gem knockdown (pre-treatment: $F_{1,405}$=33.69, p<0.001; treatment: $F_{1,405}$=2.940, p=0.087; interaction: $F_{1,405}$=10.58, p=0.001) prevented OXT-induced process elongation (p=0.008), with siRNA/OXT-treated cells even displaying shortened processes compared to scrRNA/Veh-treated cells (Fig.16b; p=0.016). Although OXT did not induce significant ramification (pre-treatment: $F_{1,491}$=29.95, p<0.001; treatment: $F_{1,491}$=2.886, p=0.09; interaction: $F_{1,491}$=3.204, p=0.074) in cells transfected with scrRNA (p=0.092), cells transfected with *Gem* siRNA displayed significantly less primary processes than scrRNA/OXT-treated cells (Fig.16c; p<0.001). To exclude that the cytoskeleton of cells in which Gem had been knocked down is uncapable to respond to external stimuli, I applied the exogenous ROCK-inhibitor (1µM for 30min; Liao et al., 2007) to cells transfected with *Gem* siRNA as a positive control. Exposure to y-27632 induced significant process elongation in *Gem* siRNA/y-27632-treated cells compared to *Gem* siRNA/Veh-treated cells (Fig.16d; *U*=5936, p=0.009). Furthermore, the previously observed OXT-induced breakdown of F-actin stress-fibres is partially Gem-dependent, as knockdown of Gem blunted this effect (Fig.16e; pre-treatment: $F_{1,37}$=21.41, p<0.001; treatment: $F_{1,37}$=9.632, p=0.04; interaction: $F_{1,37}$=0.5877, p=0.448; p=0.003 scrRNA/Veh vs. scrRNA/OXT and p=0.063 siRNA/Veh vs. siRNA/OXT). Notably, OXT induced ROCK-activity solely in Gem knockdown astrocytes as assessed by pMYPT(Thr696) phosphorylation levels (Fig.16f; pre-treatment: $F_{1,12}$=19.86, p<0.001; treatment: $F_{1,12}$=15.42, p=0.002; interaction: $F_{1,12}$=15.42, p=0.006; p=0.003 for siRNA/Veh vs. siRNA/OXT). Similar to OXT effects on the cytoskeleton, I found OXT-induced effects on astrocytic gap-junctions to be Gem-dependent. Here, Gem knockdown prevented OXT-induced impairment of GJIC (Fig.16g; pre-treatment: $F_{1,59}$=6.837, p=0.011; treatment: $F_{1,59}$=0.5326, p=0.4684; interaction: $F_{1,59}$=9.424, p=0.003; p=0.0413 scrRNA/Veh vs. scrRNA/OXT), as well as reduction of Cx43 localization at cell-cell contacts by OXT (Fig.16h; pre-treatment: $F_{1,14}$=9.830, p=0.007; treatment: $F_{1,14}$=42.25, p<0.001; interaction: $F_{1,14}$=14.04, p=0.002; p<0.001 scrRNA/Veh vs. scrRNA/OXT and p=0.4316 siRNA/Veh vs. siRNA/OXT).

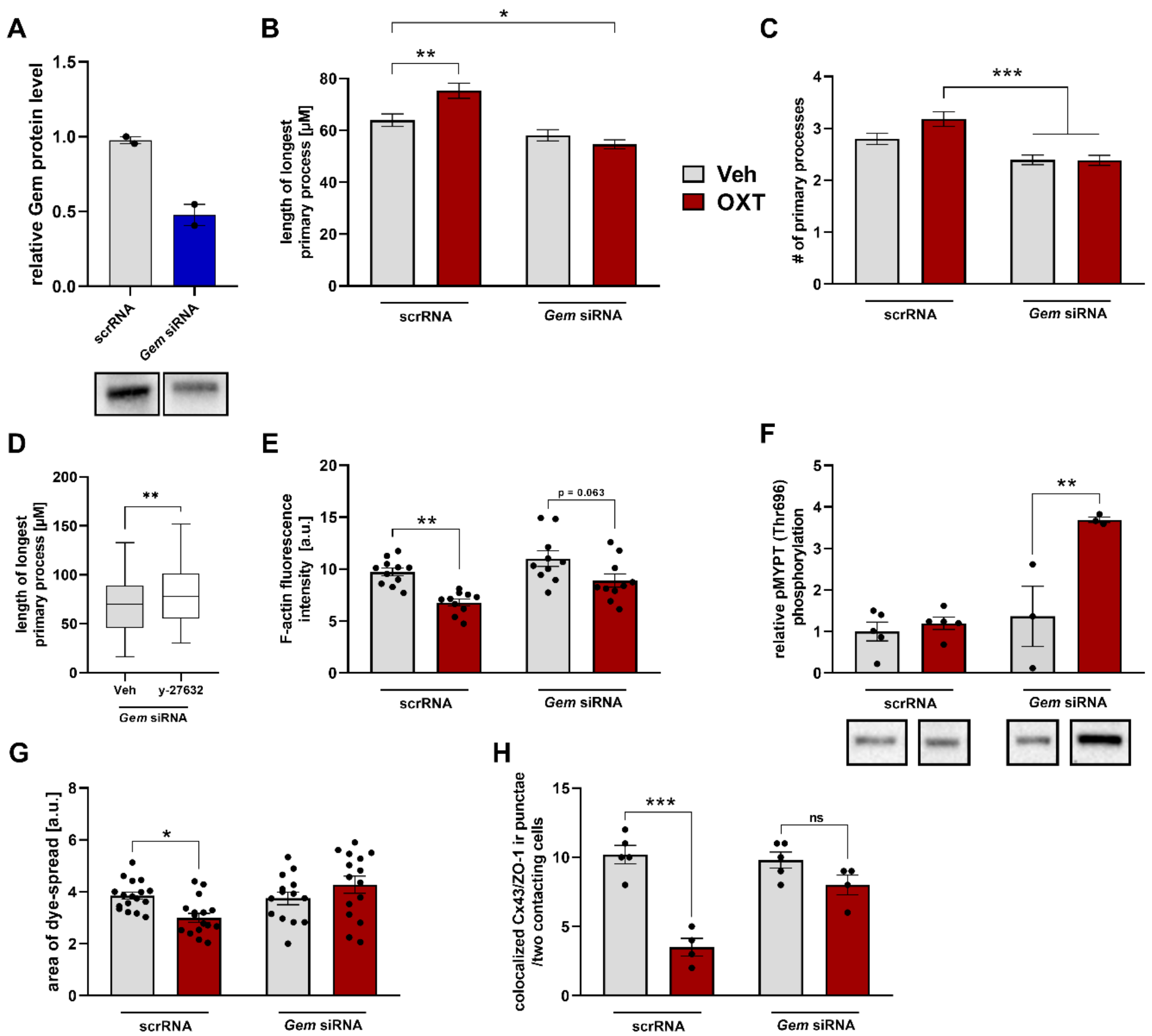

Figure 16. The *in vitro* effects of OXT on astrocytes are Gem-dependent. **A)** Validation of successful Gem knockdown by siRNA was performed by immunoblotting. Representative bands are shown below. **B-C)** Quantification of longest primary process (B) and primary process number (C) in cells transfected with either *Gem* siRNA or a control oligonucleotide (scrRNA) and subsequent administration of 500nM OXT for 10min. **D)** Length of longest primary process after exposure to 1µM y-27632 for 30min in cells transfected with *Gem* siRNA. **E)** Phalloidin immunofluorescence after Gem knockdown and subsequent OXT exposure. **F)** Relative phosphorylation of MYPT at Thr696 following Gem knockdown and subsequent OXT stimulation. Representative bands are shown below. **G)** Absolute area of lucifer yellow diffusion in dye spread experiments after Gem knockdown and subsequent OXT exposure. **H)** Impact of 15min OXT stimulation on Cx43/Zo1-colocalization following transfection with either Gem siRNA or a control oligonucleotide. Data represent mean relative or absolute values +/- SEM for normally distributed data and median +/- min/max values for non-normally distributed data. * p<0.05, ** p <0.01, *** p <0.001.

In a gain-of-function approach I next tested, whether overexpression of Gem (Gem OE) is able to mimic the effect of OXT on astrocytes. To this end, primary astrocytes were transfected with a plasmid expressing the ORF of the rat *Gem* mRNA under the control of the long promoter fragment of the *hGFAP* gene. First, successful overexpression was validated by immunofluorescence intensity measurements (Fig.17a/b; t_{14}=2.539, p=0.024), as well as immunoblotting (Fig.17c; t_8=3.137, p=0.014). qPCRs using primers binding in a region of the *Gem* mRNA not expressed by the Gem OE plasmid revealed a strong trend of decreased endogenous *Gem* mRNA (Fig.17d; t_{10}=2.172, p = 0.055), while increased mRNA levels were detected when using primers binding within the plasmid-expressed ORF of the *Gem* mRNA (Fig.17e; *U*=0, p = 0.002). In analyses of the cytoskeleton, Gem OE caused significant process elongation and ramification (Fig.17f-h; pre-treatment: $F_{1,354}$=4.552, p=0.037; treatment: $F_{1,354}$=1.832, p=0.1767; interaction: $F_{1,354}$=23.64, p<0.001; p<0.001 EGFP/Veh vs. EGFP/Gem OE) to a similar extent as OXT (p<0.001 EGFP/Veh vs. EGFP/OXT). Importantly, OXT had no add-on effect in Gem OE cells compared to EGFP expressing cells. Furthermore, Gem OE elicited significant stress fibre breakdown reminiscent of OXT treatment (Fig.17i/j; t_{14}=4.467, p < 0.001), as well as a strong reduction in ROCK-activity as assessed by quantification of pMYPT(Thr696) phosphorylation levels (Fig.17k; t_8=2.792, p=0.026).

In GJIC experiments, Gem OE impaired astrocyte network connectivity with no add-on effect of OXT (Fig.18a/b; pre-treatment: $F_{1,44}$=13.57, p<0.001; treatment: $F_{1,44}$=4.834, p=0.033; interaction: $F_{1,44}$=7.450, p=0.009; p<0.001 EGFP/Veh vs. EGFP/Gem OE; p= 0.018 EGFP/Veh vs. EGFP/OXT). On a molecular level, Gem OE altered Cx43 phosphorylation states (Fig.18c/d; t_8=2876, p=0.021 for P0 Cx43 t_7=4.090, p=0.005 for pCx43(Ser368)) and decreased Cx43 (*Gja1*) mRNA (Fig.18e; t_9=2.414, p=0.039) analogously to previous OXT stimulations.

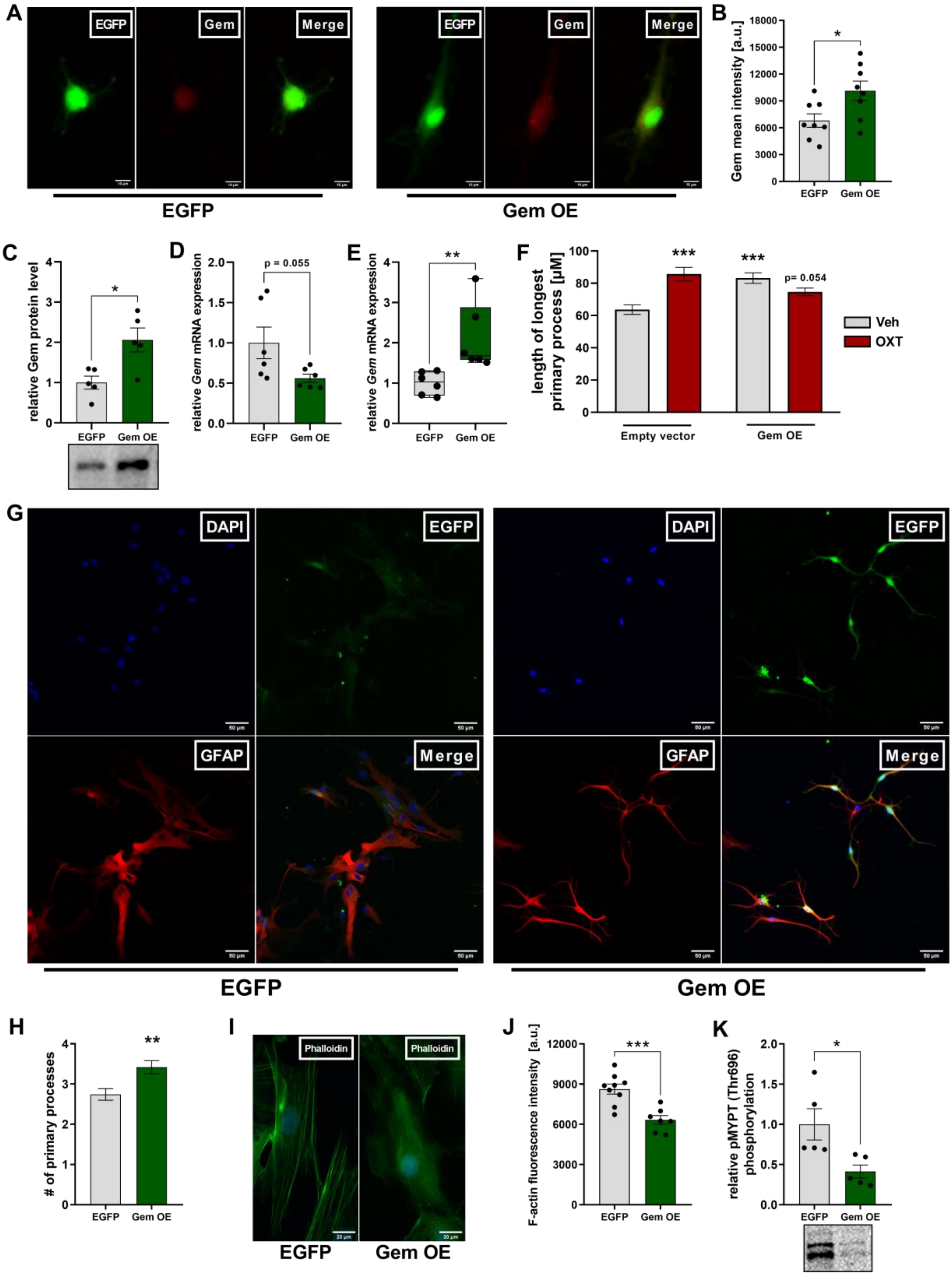

Figure 17. Overexpression of Gem is sufficient to mimic the effect of OXT on the cytoskeleton of astrocytes. **A)** Representative ICC images (EGFP, green; Gem, red) taken from cells transfected with an EGFP expressing control plasmid (left panel) or the ORF of the rat *Gem* mRNA (right panel) under the promoter of the *hGFAP* gene. **B)** Intensity of Gem-immunofluorescence in cells transfected with the EGFP control plasmid or the Gem OE plasmid. **C)** Validation of successful Gem OE on protein level. Representative bands are shown below. **D)** Assessment of potential compensatory effects of Gem OE on endogenous *Gem* mRNA by using primers binding within the 5'UTR. **E)** Validation of successful Gem OE on mRNA level by using primers binding within the ORF expressed by the transfected plasmid. **F-H)** Effects of Gem OE on the cytoskeleton of astrocytes assessed by means of quantification of process length (F) and process number (H). Representative ICC images taken from EGFP (left panel) or Gem

OE expressing cells (right panel) stained for DAPI (blue) and GFAP (red) (G). **I)** Representative ICC images of Phalloidin staining in EGFP or Gem OE transfected cells. **J)** Levels of Phalloidin immunofluorescence intensity in EGFP or Gem OE transfected cells. **K)** Assessment of ROCK activity by quantification of pMYPT (Thr696) phosphorylation levels in EGFP vs. Gem OE expressing cells. Data represent mean relative or absolute values +/- SEM for normally distributed data and median +/- min/max values for non-normally distributed data. * p<0.05, ** p <0.01, *** p <0.001.

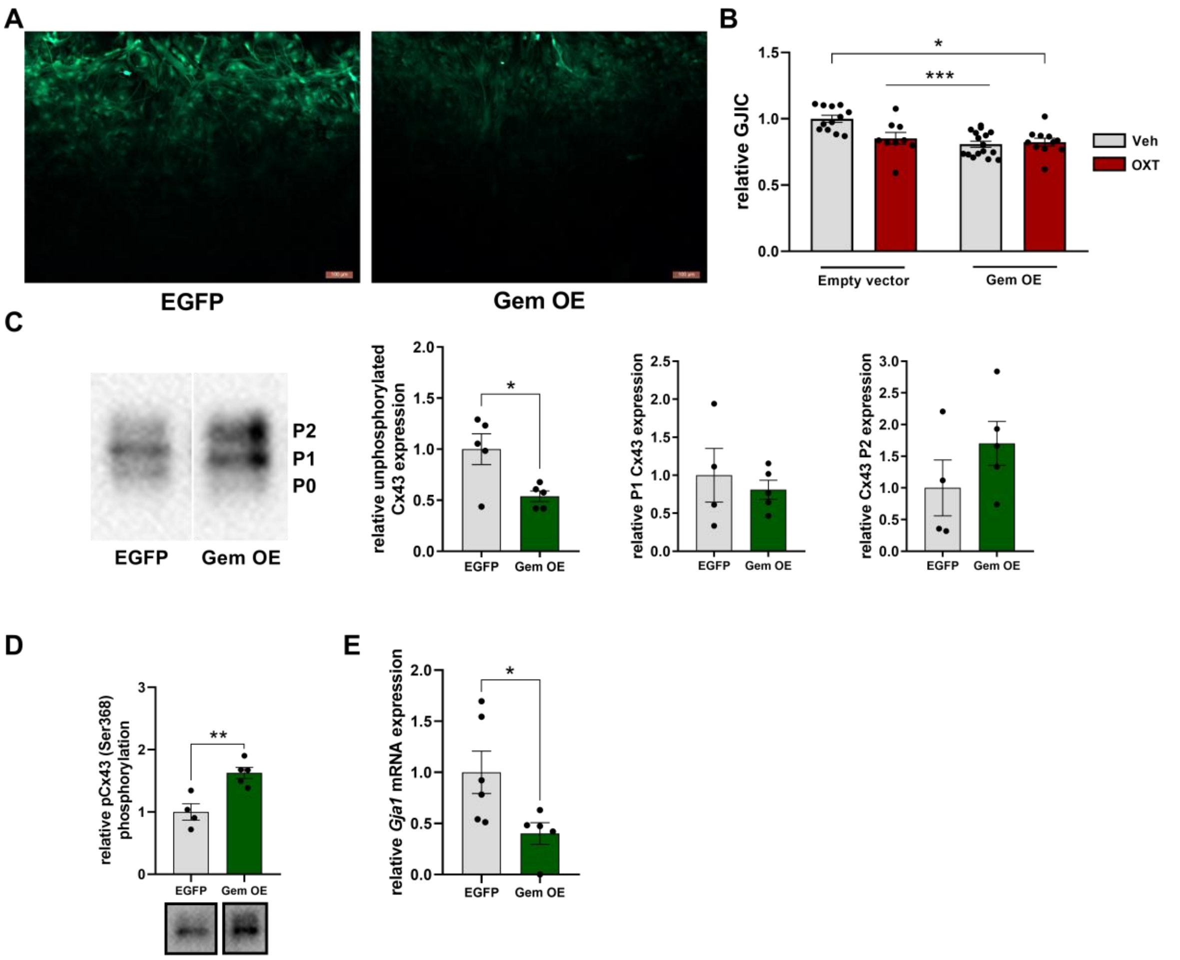

Figure 18. Overexpression of Gem is sufficient to mimic the effect of OXT on astrocytic gap-junctions. **A)** Representative ICC images of scrape-loading dye transfer experiments taken from cells transfected with a control plasmid (left panel) or the Gem OE plasmid (right panel). **B)** Degree of GJIC of cells transfected with either EGFP control plasmid or Gem OE plasmid following stimulation with 500nM OXT or Veh for 10min. **C)** Effect of Gem OE on the phosphorylation status of Cx43 with P0 representing the unphosphorylated form of Cx43 and P1/P2 representing two distinct phosphorylation sites. **D-E)** Impact of Gem OE on pCx43(Ser368) phosphorylation levels (D), as well as Cx43 (*Gja1*) mRNA (E). Data represent mean relative or absolute values +/- SEM. * p<0.05, ** p <0.01, *** p <0.001.

Potential involvement of astrocytic gap-junctions in OXT-induced cytoskeletal remodeling

To strengthen the link between OXT-induced regulation of astrocytic gap-junction proteins and altered cytoskeletal dynamics, acute hippocampal slices prepared from Cx30 or Cx43 knockout mice, as well as wildtype mice (C57BL/6) were treated with 500nM OXT for 10min. Similar to experiments in rats, OXT caused increases in domain area (Fig.19a-c; t_{14}=2.016, p=0.063 WT; t_{19}=3.900, p=0.001 Cx30KO), process length (*U*=6, p=0.020 WT; t_{22}=2.183, p=0.040 Cx30KO) and process number (t_{13}=2.321, p=0.037 WT; t_{19}=3.456, p=0.003 Cx30KO) in slices from WT and Cx30KO mice. In contrast, OXT did not alter these parameters of astrocytes in slices from Cx43KO mice (Fig.19d), suggesting an involvement of Cx43, but not Cx30 in OXT-induced cytoskeletal dynamics of astrocytes. To confirm these findings *in vitro* and subsequently study the involvement of Cx43 in OXT/Gem-induced alterations to the cytoskeleton of astrocytes, an siRNA-mediated knockdown of Cx43 was performed in rat primary cortical astrocytes (Fig. 19e; t_7=4.319, p=0.004). Corroborating *ex vivo* results, Cx43 knockdown prevented OXT-induced elongation of processes (Fig.19f; pre-treatment: $F_{1,680}$=4.074, p=0.044; treatment: $F_{1,680}$=3.572, p=0.059; interaction: $F_{1,680}$=3.617, p=0.058; p=0.010 scrRNA/Veh vs. scrRNA/OXT). To examine a potential regulation of Gem by reduced Cx43 levels, Gem protein levels in Cx43 knockdown cells were analyzed. Transfection with Cx43 siRNA did not affect the total amount of Gem (Fig.19g). However, Cx43 knockdown significantly increased the phosphorylated (i.e. active) amount of the Gem effector ezrin (Fig.19h; t_{11}=2.438, p=0.033). Here, Cx43 knockdown efficiency negatively correlated with the degree of ezrin phosphorylation, implying an increasing availability of active ezrin with falling Cx43 levels (Fig.19i; p=0.046, r^2=0.582).

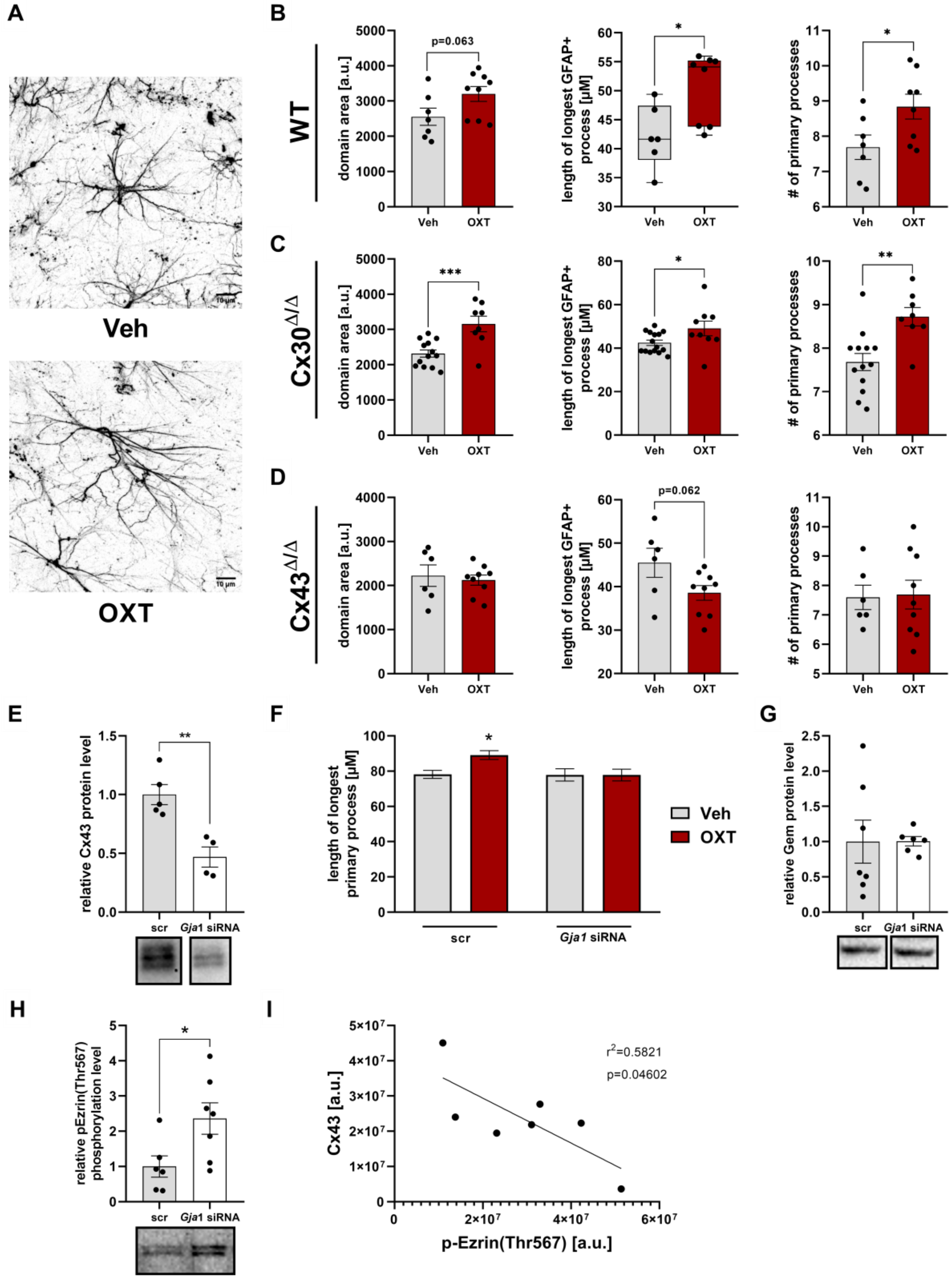

Figure 19. Cx43, but not Cx30 is involved in OXT-induced alterations of the cytoskeleton of astrocytes. **A)** Representative IHC images taken from mouse acute hippocampal slices treated with either 500nM OXT or Veh for 10min. **B-D)** Assessment of domain area, process length and process number in acute hippocampal slice preparations from either WT (B), Cx30 knockout (C) or Cx43 knockout (D) mice treated with 500nM OXT or Veh for 10min. **E)** Validation of successful Cx43 knockdown in rat primary astrocytes by means of immunoblotting. **F)** Quantification of longest primary process in cells transfected with either *Gja1* siRNA or a control oligonucleotide (scrRNA) and subsequent administration of 500nM OXT for 10min. **G)** Effect of Cx43 knockdown on Gem protein quantities. **H)** Effect of Cx43 knockdown on phosphorylation of ezrin on Thr576. **I)** Correlation of Cx43 level in Gja1 siRNA transfected cells with ezrin phosphorylation status. Data represent mean relative or absolute values +/- SEM. * p<0.05, ** p <0.01, *** p <0.001.

Regulation of Gem by OXT on a genomic level

In order to investigate by which transcription factor OXT upregulates Gem expression, I first used a publically available database (AliBaba 2.1; http://gene-regulation.com/pub/programs/alibaba2/index.html) for the prediction of transcription factor binding sites within the promoter region of the *Gem* gene (Tab.6). Here, the transcription factor Sp1 posed the highest quantity of binding sites (12 predicted binding sites vs. 1-2 binding sites for other transcription factors).

Table 6. List of predicted transcription factor binding sites within the promoter region of the rat *Gem* gene.

Transcription factor	**# of predicted binding sites within the promoter region of *Gem***
Sp1	12
NF-kappaB	2
AP-2alpha	2
AP-1	1
HNF-1C	1
CEPB-alpha	1
CEPB-beta	1
Pit-1b	1
NF-1	1
ETF	1
WT1	1
c-Fos	1
CREB	1
ATF	1
E1A 12S	1
RxR-beta	1
c-Jun	1
NF-kappa	1
CRE-BP1	1

Based on this *in silico* analysis and its OXT-induced upregulation (see 3.2), I hypothesized that the transcription factor Sp1 controls *Gem* expression and by this conveys OXT-induced Gem-dependent alterations to the cytoskeleton of astrocytes. To test this hypothesis, I applied a siRNA-based knockdown approach *in vitro* (Fig.20a/b; t_4=4.548, p=0.010 24h siRNA vs. scRNA and t_4=4.548, p=0.010 48h siRNA vs. scrRNA; *U*=2, p=0.065 qPCR). Sp1 knockdown prevented OXT-induced process elongation (Fig.20c; pre-treatment: $F_{1,1106}$=22.05, p<0.001; treatment: $F_{1,1106}$=0.027, p=0.871; interaction: $F_{1,1106}$=16.51, p<0.001; p=0.012 scrRNA/Veh vs. scrRNA/OXT), while reversing the effect of OXT in the Sp1 knockdown group (p=0.031 for siRNA/Veh vs. siRNA/OXT). Importantly, knockdown of Sp1 prevented the OXT-induced upregulation of Gem (Fig.20d/e; pre-treatment: $F_{1,832}$=5.285, p=0.022; treatment: $F_{1,832}$=15.89, p<0.001; interaction: $F_{1,832}$=22.32, p<0.001; p<0.001 scrRNA/Veh vs. scrRNA/OXT) and led to a decrease of *Gem* mRNA expression (t_9=2.818, p=0.020). To exclude that these observations are due to an insensitivity of OXTR-coupled pathways caused by secondary effects on *Oxtr* expression, I verified that Sp1 knockdown did not affect *Oxtr* mRNA levels (Fig.20g).

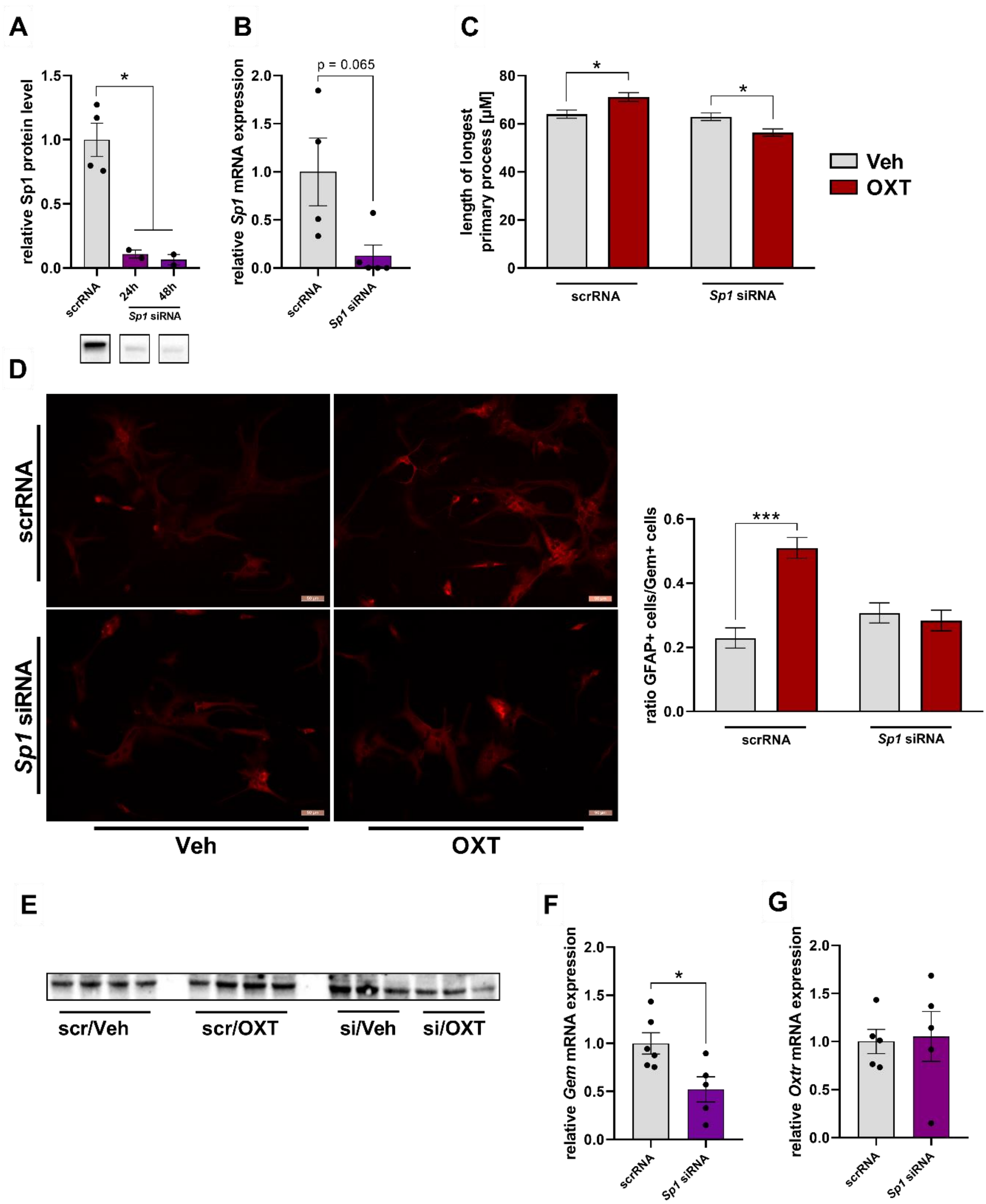

Figure 20. The transcription factor Sp1 conveys OXT-induced Gem expression. **A-B)** Validation of successful knockdown by immunoblotting (A) and qPCR (B). Representative bands are shown below. **C)** Quantification of longest primary process in cells transfected with either *Sp1* siRNA or a control oligonucleotide (scrRNA) and

subsequent administration of 500nM OXT for 10min. **D)** Representative ICC images taken from *Sp1* siRNA or scrRNA transfected cells subsequently exposed to OXT for 10min and stained for Gem. Quantification of above threshold (Gem+) cells was defined as single cells marked by DAPI/GFAP staining displaying at least one maximum of above threshold Gem fluorescence. **E)** Representative immunoblot of Gem showing noticeable OXT-induced increase of intensity solely in the scrRNA group. **F-G)** Effects of Sp1 knockdown on *Gem* (F) and *Oxtr* (G) mRNA expression. Data represent mean relative or absolute values +/- SEM, * p<0.05, ** p <0.01, *** p <0.001.

Differential regulation of the Sp1-Gem-ROCK axis in neuronal cells

Since OXT has contrary effects on the cytoskeleton of neuronal cells (Meyer et al., 2018), i.e. a retraction of neurites, I examined whether OXT differentially regulates the Sp1-Gem-ROCK signaling axis in neuronal cells compared to astrocytes. To this end, the neuronal cell line H32 was exposed to 100nM of OXT for 180min. Protein analyses revealed an OXT-induced increase in ROCK1 (t_{14}=3.744, p=0.002) and ROCK activity (t_{12}=3.244, p=0.007), as well as a decrease in Gem (t_{13}=3.700, p=0.003) and Sp1 (t_{12}=8.751, p<0.001) quantities (Fig.21a-d). To examine whether this activation of the ROCK pathway is required for OXT-induced neurite retraction, neuronal cells were pre-treated with either Veh or 1µM of the ROCK-inhibitor y-27632 and exposed to 100nM OXT for 180min. OXT caused a retraction of neurites which was prevented in cells pre-treated with y-27632, indicating that activation of ROCK is critical for OXT-induced neurite retraction (Fig.21e; pre-treatment: $F_{1,1884}$=15.18, p<0.001, treatment: $F_{1,1884}$=18.78, p<0.001, interaction: $F_{1,1884}$=7.396, p=0.007, p<0.001 Veh/Veh vs. Veh/OXT). To validate these findings *in vivo,* the cellular distribution of Gem was analyzed within the hippocampus of rats which were previously administered Veh or OXT *icv* (Fig.21f). In line with protein analyses (see 3.2), OXT did not alter the total amount of Gem (Fig.21g). However, an analysis of the distribution in astrocytes (GFAP+) vs. non-astrocytic cells (GFAP-) revealed an OXT-induced increase of Gem-positive (Gem+) astrocytes (t_{10}=2.771, p=0.020), as well as a simultaneous decrease of Gem-expressing non-astrocytic cells (t_{10}=2.606, p=0.029).

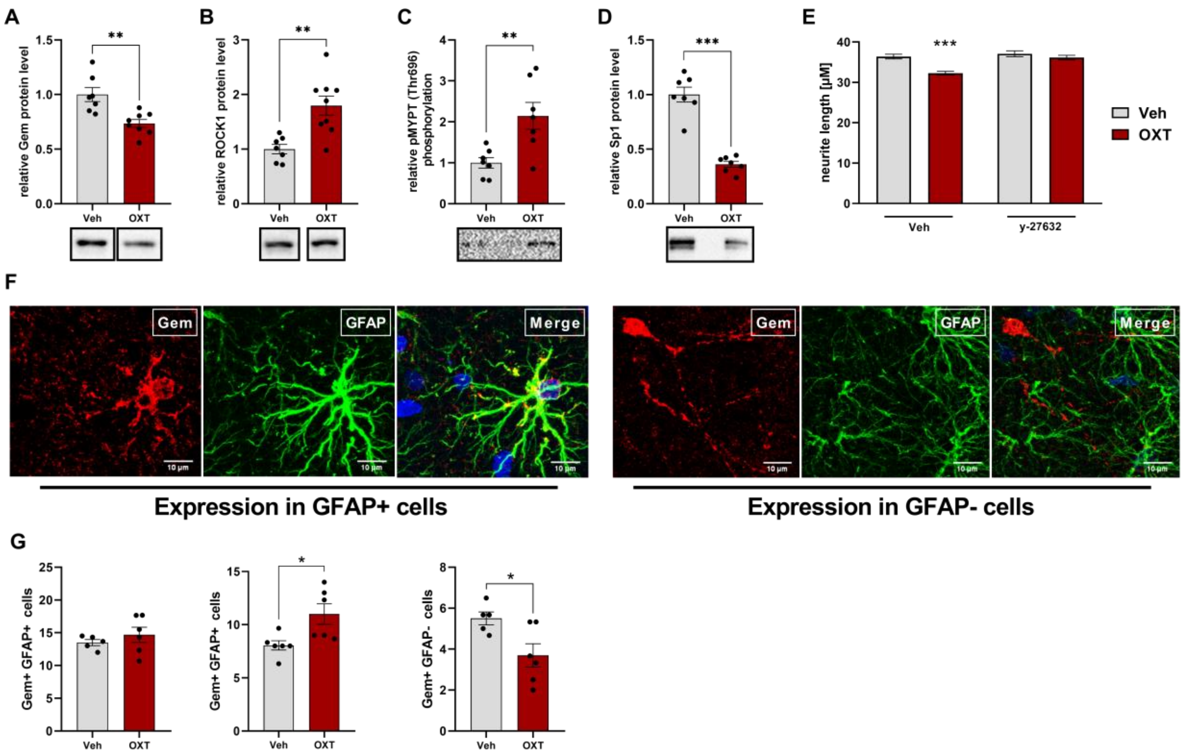

Figure 21. OXT polarizes Gem expression in neurons vs. astrocytes. **A-D)** Quantification of Gem (A), ROCK1 (B), pMYPT(Thr696, C) and Sp1 (D) protein levels in H32 cells by immunoblotting following exposure to 100nM OXT for 180min. Represenative bands are shown below. **E)** Neurite length of H32 cells following pre-treatment with either Veh or the ROCK-inhhibitor y-27632 and treatment with either Veh or 100nM OXT for 180min. **F/G)** Representative IHC images of hippocampal astrocytes (GFAP; green) co-stained with Gem (red) and DAPI (blue) in animals that received either Veh or OXT *icv*. Quantification of above threshold (Gem+) cells was defined as single cells marked by DAPI/GFAP (Gem+/GFAP+) or DAPI/absence of GFAP (Gem+/GFAP-) staining displaying at least one maximum of above threshold Gem fluorescence. Data represent mean relative or absolute values +/- SEM. * p<0.05, ** p <0.01, *** p <0.001**.**

3.4 Establishment of astrocyte-specific *Oxtr*/*Gem*-knockdown vectors

To study the physiological and behavioral relevance of astrocytic OXTR signaling and its downstream effector Gem, I aimed to establish viral vectors providing an astrocyte-specific knockdown of OXTR or Gem *in vivo*. First, shRNAs (see 2.5.1) were screened *in vitro* for knockdown efficiency. Unexpectedly, the *Oxtr*-shRNA expressing plasmid led to a significant increase in *Oxtr* mRNA expression 2d days post-transfection (Fig.22a; *U*=4, p=0.007). However, a significant downregulation of *Oxtr* mRNA was observed after more stable shRNA expression for 7d (Fig.22b; U=19, p=0.018).

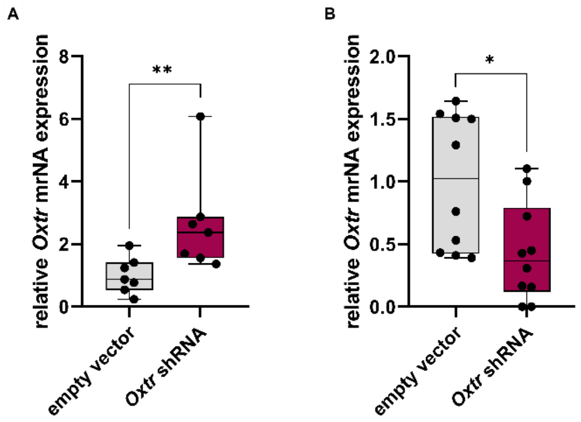

Figure 22. *In vitro* validation of successful shRNA-mediated knockdown of *Oxtr* mRNA. **A/B)** *Oxtr* mRNA levels analyzed by qPCR 2d (A) and 7d (B) after transfection of primary astrocytes with a plasmid expressing an shRNA targeted against *Oxtr* mRNA under the control of the long promoter fragment of the *hGFAP* gene. Data represent median +/- min/max values. * p<0.05, ** p <0.01.

Successful knockdown of Gem 7d post-transfection was validated by means of fluorescence intensity measurements (Fig.23a/b; t_{23}=3.723, p=0.001) and qPCR (Fig.23c; t_4=4.548, p=0.010 t_{10}=3.506, p=0.031). Notably, Gem knockdown caused a decrease in *Gja1* expression (Fig. 23d; t_{10}=2.443, p=0.035).

Since both shRNAs displayed sufficient knockdown efficiency, I designed AAV6-GFAP::shRNA vectors for the purpose of *in vivo* Gem or OXTR knockdown (see also 2.3 and Fig.4). In a preliminary experiment, I aimed to determine the optimal physical viral titer and volume for microinfusions of the PVN. The viral titers ranging from 10^8-10^{12} GC/ml, as well as the tested volumes (70/280/560nl) used in this experiment were chosen based on the literature of AAV-mediated transfections of the PVN (Garza et al., 2008; Koba et al., 2018; Zhang et al., 2013). Of the tested conditions, only a titer of 10^{12} GC/ml resulted in a detectable, but scattered, expression of the fluorescent reporter protein mCherry at the injection site (Fig.24). Thus, the ideal injection volume cannot be determined based on this experiment. The low rate of successful transfection indicates an insufficient amount of available viral particles. Nevertheless, all successfully transfected cells were mCherry+/GFAP+ double positive, indicating cell type-specificity for astrocytes.

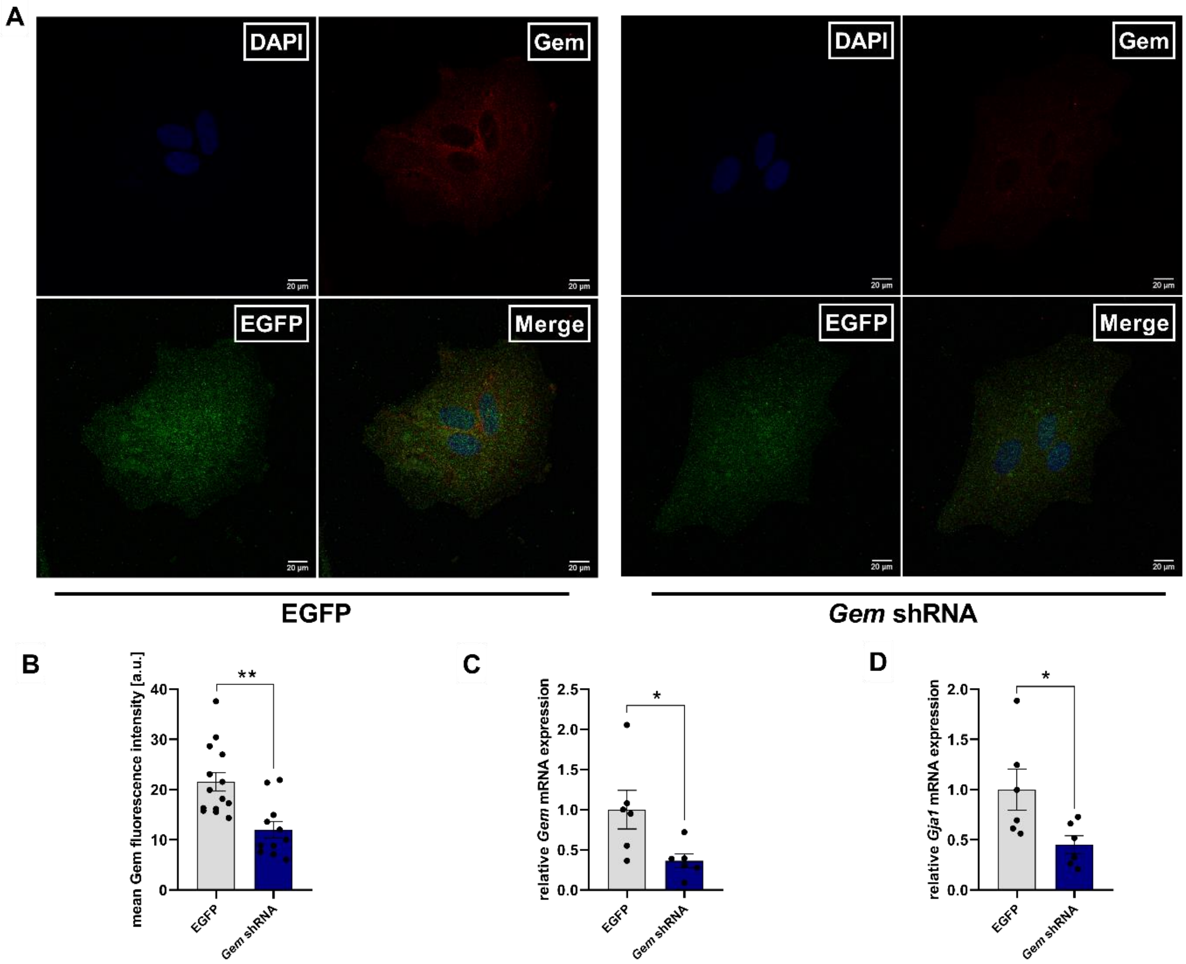

Figure 23. *In vitro* validation of shRNA-mediated knockdown of *Gem* mRNA. **A)** Representative ICC images of primary astrocytes transfected with a control plasmid (left panel) or an shRNA targeted against the *Gem* mRNA. **B/C)** Validation of successful Gem knockdown by quantification of immunofluorescence (A) and qPCR (B). **D)** Effect of Gem knockdown on *Gja1* mRNA levels. Data represent mean relative or absolute values +/- SEM. * p<0.05, ** p <0.01, *** p <0.001.

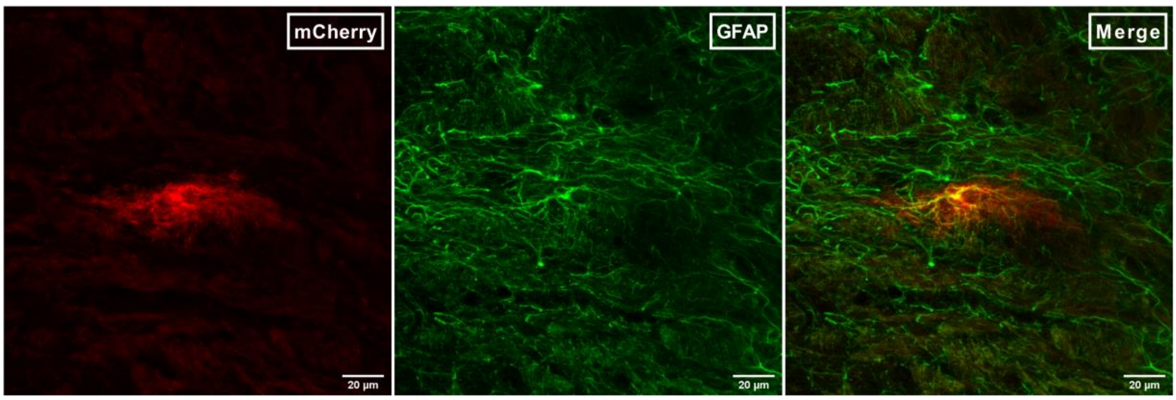

Figure 24. Cell type-specific targeting of PVN astrocytes with AAV6-GFAP::shRNA vectors. Representative IHC image taken from the PVN of animals that received unilateral microinfusions of 280nl OXTR knockdown vector at a physical viral titer of 10^{12} GC/ml. Successful transfection is indicated by the expression of the fluorescent reporter mCherry, while cell-type specificity is indicated by double positive immunostaining for mCherry and GFAP.

4 DISCUSSION

Especially in higher vertebrates, astrocytes are an indispensible part of signal processing within the brain. Thus, the mode of action of a neuroactive peptide such as OXT cannot be fully understood without this integral part of the CNS. The effects of OXT on neuronal cells have been well characterized, while its effects on astrocytic cells, specifically on OXTR-coupled signaling and its resulting cellular consequences, are poorly understood and might very well differ. To characterize the effect of OXT on astrocytic gene expression, intracellular signaling, as well as astrocyte-specific proteins, synthetic OXT was either administered *icv* in male Wistar rats or applied to cultured rat primary cortical astrocytes. Due to the results of this analysis implying an acute OXT-induced cytoskeletal remodeling and alterations to gap-junction coupling, I next examined the underlying molecular mechanisms and cellbiological consequences of these alterations. Here I found that OXT led to rapid elongation and formation of astrocytic processes *in vitro* and *in vivo*, while simultaneously impairing astrocytic intercellular connectivity. Mechanistically, both of these effects were OXTR-specific, conveyed via PKC and, to a lesser extent, MEK1/2 signaling. Notably, OXT-induced cytoskeletal remodeling and impairment of gap-junctions were characteristic for OXT, since its closely related sister-peptide AVP did not affect the examined parameters. CLSM and STED-microscopy following *icv* or *ex vivo* administration of OXT furthermore revealed changes to astrocyte-neuron spatial relationships in two brain regions associated with high responsiveness of astrocytic markers to OXT, i.e. PVN and hippocampus. In depth *in vitro* studies identified the previously undescribed Sp1-Gem signaling axis to be at the base of these effects. A combination of knockdown, knockout and overexpression experiments revealed that OXT drives *Gem* expression via the transcription factor Sp1 and that Gem is required and sufficient for the effects of OXT on astrocytes. The Sp1-Gem axis was differentially regulated by OXT in neuronal cells, identifying it as key driver in the cell type-specific response of astroglial cells to OXT. Based on these findings, I established astrocyte-specific AAV-mediated *Gem* or *Oxtr* shRNA knockdown vectors as tools for a targeted manipulation of astrocytic OXTR signaling and future assessment of astrocytic contribution to the physiological and behavioral effects of OXT. To this end, shRNA oligonucleotides were screened for knockdown efficiency *in vitro* and subsequently packaged into viral vectors providing astrocyte-specific expression via transcriptional control of shRNA expression under the *hGFAP* promoter.

4.1 Effects of OXT on astrocytic signaling cascades and proteins

To characterize the downstream effects of OXTR-coupled signaling on astrocytic phospho-cascades and proteins, I used cultured rat primary cortical astrocytes as a model sytem. Although cultured astrocytes have been shown to display a partially different gene expression profile as astrocytes under physiological conditions, the unique advantage of this model system is the absence of non-astrocytic OXTRs. Due to the exclusion of potential secondary effects via other OXTR expressing cells like neurons or microglia (Yuan et al., 2016), this allowed examination of exclusively astrocytic responses to OXT. Furthermore, administration of icv OXT provided, first, validation of the in vitro results and, in case of differing findings, a better understanding of which OXT-induced effects on astrocytes might involve other cell types.

The resulting pattern of rapid OXT-induced activation of CREB, various protein kinases, such as the MAPKs ERK1/2 and ERK5, PKB (Akt), as well as eEF2 dephosphorylation, compares well to OXT effects previously described in neuronal and myometrial cells (Blume et al., 2008; Devost et al., 2008b; Jurek and Neumann, 2018; Klein et al., 2013; Martinetz et al., 2019). The activation of astrocytic CREB is particularly intriguing, since OXT facilitates LTP formation and spatial memory in female mice via a CREB-dependent mechanism (Tomizawa et al., 2003). Since both cell types are required for LTP (Henneberger et al., 2010), it should be explored, whether this is due to neuronal and/or astrocytic CREB activity. Moreover, the absence of JNK activation as well is analogous to neuronal cells. However, astrocyte-specific differences consisted in a lack of OXT-triggered CamKII activation (van den Burg et al., 2015) and a decrease in the activity of Rho-associated protein kinase (ROCK). ROCK-conveyed signaling is involved in various cytoskeleton-associated cellular processes like contractility or migration and OXT activates myometrial ROCK to increase contractility during late pregnancy (Tahara et al., 2002). In contrast, I found OXT exposure to dampen the activity of the ROCK pathway as reflected by decreased phosphorylation of the downstream ROCK targets MLC and MYPT (for a detailed discussion of the role of ROCK please see 4.3).

In general, these findings point towards Ca^{2+} and EGFR as important upstream nodes of astrocytic OXTR signaling and underline the high responsiveness of astrocytes to OXT. This is in line with previous studies of Di Scala-Guenot et al. (1994) and (Wang and Hatton, 2007) in which OXT elicited rapid dose-dependent Ca^{2+} release from intracellular stores in cultured hypothalamic astrocytes or an increase of nuclear pERK1/2 in astrocytes of acute SON slice preparations, respectively. Moreover, identical to studies in SON slices of lactating, as well as virgin male rats (Wang et al., 2017; Wang and Hatton, 2009), I found a OXT-induced degradation of GFAP in cultured astrocytes. In contrast, icv OXT increased GFAP quantities of the amygdala 20min post-administration, while not affecting the intermediate filament in the

PVN or hippocampus. Since the exact amount of peptide reaching its target areas is hard to control in icv experiments, a possible explanation for the observed discrepancy between in vitro and in vivo experiments might be a dose-dependent differential regulation of GFAP by OXT. Indeed, dose-dependent differential coupling of downstream effectors has been described for the OXTR in HEK293 cells (Busnelli et al., 2012). However, since OXT-induced GFAP regulation was shown to be dose-dependent, but unidirectional (Wang and Hamilton, 2009), possible differences in the dose of OXT seem unsuitable to explain the observed differential regulation of GFAP. With previous work (Wang and Hamilton, 2009) and the *in vitro* results of the present thesis suggesting the regulation of GFAP by OXT to be independent of neurons, this discrepancy more likely reflects brain region-specific differences in the direct response of astrocytes to OXT. This demonstrates the differential responsiveness of astrocytes in distinct brain regions and mirrors their high degree of molecular heterogeneity (Chai et al., 2017). As major component of the astrocytic cytoskeleton, GFAP is responsible for the maintenance of astrocytic structure and shape (Li et al., 2020). Its OXT-induced regulation is in good agreement with its well described dynamic plasticity in response to an altered neurochemical environment (Camacho-Arroyo et al., 2011; Kumar et al., 2018) and highlights the rapid responsiveness of astrocytes to OXT (for further discussion on GFAP please see also 4.3).

Furthermore, central administration of OXT altered the levels of the astrocytic glutamate transporters EAAT1 and EAAT2. OXT transiently elevated EAAT1 in the amygdala 10min after the injection, while downregulating EAAT1 in the hippocampus after 20min. EAAT2 was reduced within the PVN and amygdala, but not the hippocampus. Since astrocytes clear ~90% of the available glutamate in the brain via EAAT1 and EAAT2 (Anderson and Swanson, 2000; Eulenburg and Gomeza, 2010), changes in the expression of these proteins can have profound effects on neuronal communication. EAAT2 expression positively correlates with the synaptic activity of glutamatergic neurons (Poitry-Yamate et al., 2002; Swanson et al., 1997), with glutamate acting as the main regulatory molecule for EAAT2 expression. Such an indirect, activity-dependent regulation of EAAT2 seems also likely in the case of OXT, since direct exposure of cultured astrocyted did not alter EAAT2 expression in the present thesis. OXT-induced downregulation of EAAT2 might therefore reflect an increase in GABAergic transmission, a condition that has been associated with OXT in multiple studies (Bulbul et al., 2011; Marlin et al., 2015). However, the concurrent upregulation of EAAT1 in the amygdala contradicts this idea. Notably, exposure of neuron-astrocyte co-cultures to excessive amounts of glutamate decreased EAAT2 expression, while simultaneously increasing EAAT1 levels (Schlag et al., 1998). In the light of this condition resulting in a similar EAAT regulatory profile as OXT, it might be that the exogenously applied amount of OXT elicited a supraphysiological degree of glutamatergic transmission. Therefore, the expression of astrocytic neurotransmitter transporters should be further explored under physiological conditions of elevated OXTergic activity, e.g. lactation or osmotic challenge. Indeed, EAAT2 expression is decreased within the SON of dehydrated rats (Boudaba et al., 2003). Similar to lactation, dehydration causes reduction of astroglial coverage and in turn increases glutamate availability, lending support to the idea of glutamate, not GABA, being the main driver of OXT-induced EAAT regulation.

4.2 Effect of OXT on expression and distribution of astrocytic gap-junctions and its impact on intercellular connectivity

A characteristic feature of astrocytes is their intercellular connectivity via homocellular gap-junctions composed of the connexin isoforms Cx26, Cx30 or Cx43. Cx43 is the major astrocytic isoform in the CNS, but is also widely expressed in the periphery in a variety of cell types (Andersen et al., 1993; Gros et al., 2004; Richard, 2000). So far, two studies have examined the regulation of Cx43 by OXT in peripheral contexts. In mouse embryonic stem cells, exposure to OXT for 3h induced Cx43 expression via a PKA-NF-κB/CREB/CBP signaling mechanism (Yun et al., 2012). A similar observation was made by Khan-Darwood et al. (1998), who found elevated Cx43 protein and phosphorylation levels after incubation of cultured baboon corpus luteum cells with OXT for two days (Khan-Dawood et al., 1998). Thus, I investigated the effect of OXT on astrocytic gap-junctions in vitro and in vivo. Central administration of OXT caused a strong and acute increase in Cx30 in all three examined brain regions, whereas it decreased Cx43 levels of the PVN and hippocampus. These changes were accompanied by an increase of Cx43 phosphorylation at Ser368. Notably, Cx43 quantities and phosphorylation were unaffected in the amygdala. Corroborating these results, OXT altered the phosphorylation of multiple sites of Cx43 in vitro. PKC-induced phosphorylation at Ser368 and MAPK-induced Ser279/Ser282 phosphorylation of Cx43 lead to altered permeability/selectivity, as well as internalization and possible subsequent degradation of the gap-junction (Fong et al., 2014; Nimlamool et al., 2015). Therefore, I hypothesized that OXT causes Cx43 internalization and consequent impairment of intercellular communication. In accordance with this idea, I found that OXT reduces GJIC in a PKC and MEK-dependent manner. Interestingly, the accompanying internalization of Cx43, as assessed by co-staining with ZO-1, was as well PKC, but not MEK-dependent. This suggests that OXT conveys the closure of Cx43 gap-junctions via the concerted activity of PKC and MAPK signaling, while it solely operates through PKC for the removal of Cx43 from cell/cell-contacts. The conducted dose-response experiments demonstrate that Cx43 internalization requires a higher dose of OXT, than impairment of GJIC. In comparison to the pharmacological gap-junction blocker carbenoxolone, the rather small degree of GJIC impairment exerted by OXT suggests more of a modulatory role in this process. While carbenoxolone inhibited GJIC by around 70%, the extent of OXT-induced inhibition did not surpass 25% even at a high dose of 1µM. The transient recovery of Cx43 localization at cell/cell contacts after 30min of OXT exposure might be due to the increase of Cx43 (Gja1) mRNA expression detected at this timepoint and likely reflects a compensatory feedback mechanism. However, prolonged stimulation with OXT mimicked the effect of acute exposure on GJIC and was at this timepoint accompanied by decreased Gja1 expression, indicating a manifestation of the inhibitory effect on gap-junctions. The expression pattern of connexin-coding genes (see 3.2) induced by OXT at varying timepoints demonstrates a highly dynamic and isoform-specific regulation of astrocytic gap-junctions by OXT that generally points towards inhibition of intercellular connectivity. However, if this is the case in vivo remains to be elucidated. The strong acute increase in Cx30 observed in vivo, but not in vitro, might compensate for the transient loss of GJIC caused by internalized/reduced Cx43 levels. Other than Cx43, Cx30 expression is generally induced by neurons via a contact dependent mechanism (Koulakoff et al., 2008) and is responsible for around 20% of astrocyte-astrocyte coupling (Gosejacob et al., 2011). Indeed, Cx30 has been shown to be upregulated in Cx43 deficient mice, in which it is able to partially compensate the decreased intercellular connectivity caused by the loss of Cx43 (Rouach et al., 2008; Wallraff et al., 2004). Thus, future studies should decipher the contribution of distinct connexin isoforms to the impact of OXT on astrocytic gap-junctional coupling. Here, dye-coupling experiments in ex vivo slice preparations of Cx43 and Cx30 knockout animals would provide a more detailed picture. Nevertheless, alterations in the interconnectivity of astroglial networks are able to produce profound effects on synaptic transmission and plasticity on multiple levels. First, metabolites required at sites of high neuronal activity are partially trafficked via astroglial gap-junctions, which have been shown to undergo activity-dependent reshaping to meet this demand (Gandhi et al., 2009; Rouach et al., 2008). Second, both potassium and glutamate reuptake efficiency are enhanced in areas of coupled astrocytes, pointing toward an inhibitory role of astroglial networks (Pannasch et al., 2011). In turn, disconnection of astrocytes by double genetic deletion of Cx43/Cx30 greatly improves excitatory transmission of CA1 pyramidal neurons due to an increased availability of potassium and glutamate at the synapses (Pannasch et al., 2011). Last, gliotransmission induced by neuronal activity can additionally be triggered at distal synapses by information spread via astroglial networks and thereby lead to secondary activation of neurons (Kang et al., 2005; Pannasch and Rouach, 2013; Serrano et al., 2006). However, due to a multitude of non-channel functions attributed to astrocytic connexins, the implications of their OXT-induced regulation might extend beyond the alteration of astrocyte-astrocyte coupling. In case of Cx30, its control of synapse invasion (Pannasch et al., 2014), synaptic glutamate clearance (Pannasch et al., 2019) and cellular migration/adhesion (Ghezali et al., 2018) has recently been demonstrated. Acute upregulation of Cx30 by OXT could thus cause a less efficient glutamate uptake akin to the implications of OXT-induced EAAT2 downregulation (as discussed in 4.1.). The idea of OXT additionally acting via connexin functions not involved in astrocytic interconnectivity is further supported by the regulation of Cx26 expression found in the present thesis. Cx26 is believed to not play a role in the coupling of astrocytes, and rather acts as a functional hemichannel (Huckstepp et al., 2010; Rouach et al., 2008).

Taken together, this thesis is the first to demonstrate the regulation of astrocytic gap-junctions and their forming proteins by OXT. The present findings indicate a rapid and dynamic remodeling of astroglial networks, potentially facilitating excitatory transmission in the affected brain areas. However, the consequences of OXT-elicited connexin regulation on neuronal communication should be addressed by work specifically targeted at this question.

4.3 OXT-induced changes in astrocytic cytoskeletal dynamics and the impact on astrocyte-neuron spatial relationships

Since astrocytes modulate and support neuronal function via mechanisms relying on diffusion of signaling molecules, ions or metabolites, the spatial arrangement and distance between astrocytic processes and neuronal structures are of functional importance (Reichenbach et al., 2010). This relationship is critically set by the astrocytic cytoskeleton (Heller and Rusakov, 2015; Zeug et al., 2018). Since my experiments had revealed several changes of proteins associated with cytoskeletal dynamics, such as beta-tubulin and the ROCK-pathway, I examined possible OXT-induced alterations of the cytoskeleton of astrocytes. Here, I found that OXT causes rapid process extension and ramification in vitro. Mechanistically, these effects were OXTR-specific, as well as PKC-dependent, while the acute induction, but not the maintenance, of these effects required MEK activity. These findings, for the first time, demonstrate an acute action of OXT on astroglial cytoskeletal remodeling that is directly mediated via the astrocytic OXTR and its downstream effectors. In vivo analyses confirmed the timepoint and directionality of these effects in the PVN and hippocampus. The dynamics of astrocytic processes under physiological conditions and in tissue culture are thought to be comparable in time, as both can elongate within a few minutes in acute slice preparations (Hirrlinger et al., 2004) or in cultured astrocytes (Cornell-Bell et al., 1990), respectively. Moreover, I found a tighter spatial relationship between PVN OXTergic neurons and GFAP-positive branches of astrocytes following central administration of OXT. Bath application of OXT to mouse hippocampal slice preparations further confirmed OXT-induced elongation and ramification of GFAP-positive processes.

The obtained results are in line with studies identifying OXT as a direct regulator of cellular morphology in different cell types (Lestanova et al., 2017; Meyer et al., 2018; Meyer et al., 2020; Ripamonti et al., 2017; Theodosis et al., 1986b). As outlined in the introduction, the directionality, i.e. retraction vs. elongation of processes, is cell type-dependent. However, the elongation and ramification generally observed in the present thesis seem to contradict the well-described retraction of terminal astroglial processes from SON OXT neurons during lactation (Theodosis et al., 1986a), a condition associated with high activity of the OXT system. A possible explanation might be a difference in the motility of the major astrocytic branches compared to their fine terminal processes. GFAP, used as one of the markers to visualize the astrocytic cytoskeleton in this thesis, solely stains the major somatic branches of astrocytes (Connor and Berkowitz, 1985). Since cultured astrocytes do not possess the same elaborate arborization as astrocytes in vivo, GFAP is suitable for the analysis of the astrocytic cytoskeleton in vitro, while it may not reveal a sufficiently precise picture of astrocytic morphology under physiological conditions (Reichenbach et al., 2010). In contrast, the subcellular distribution of fluorescent proteins, even to fine astrocytic processes, enables a more comprehensive analysis of the morphology of astrocytes and their spatial relationship to neighbouring cells. Indeed, I found a greater distance between synapses and GFP-expressing astrocytic elements in OXT treated hippocampal slices, which is consistent with the OXT-induced decreased astroglial coverage described in the SON (Theodosis et al., 1986b). In the same hippocampal slice preparations, I found GFAP positive processes to be increased in length and number (see also 4.5.) similar to in vitro experiments. It should thus be considered that GFAP might serve as a valuable marker of general cytoskeletal responsiveness, but may be unfit to determine the directionality of astrocytic cytoskeletal remodeling. For this purpose, targeted expression of fluorescent proteins (as used in the present thesis) or electron microscopy should be applied. As 3D reconstruction of GFP expressing astrocytes additionally revealed acute OXT-induced swelling, the increased astrocytic volume might drive PAPs away from synapses. Astrocytic swelling has been shown to be an indicator of neuronal activity (Guldner and Wolff, 1973) and is thought to result from an increased need of reuptake of neuronal K^+ and glutamate (Koyama et al., 1991). The consequent osmotic entry of water from the extracellular space through aquaporin channels in turn causes astrocytic hypertrophy that can affect PAP motility (Kimelberg, 2004; Nagelhus et al., 2004). In case of the SON, the neurobiological consequences of reduced astroglial synaptic coverage elicited by OXT are increased glutamate availability and release probability (Oliet et al., 2001), as well as an elevated glutamate spillover from uncovered to neighboring synapses (Piet et al., 2004). This lends further support to the idea of a transient facilitation of excitatory transmission discussed in the previous paragraphs (4.1 and 4.2).

Similar to findings in the SON (Theodosis et al., 1986b), I found no effect of AVP exposure on cytoskeletal dynamics in vitro, indicating a mode of action characteristic for OXT. Moreover, OXT-elicited astroglial uncovering of synapses within the SON is limited to OXTergic neurons

(Langle et al., 2003; Theodosis et al., 1986a). Eventhough the hippocampus does not contain OXT positive neurons, I found a similar effect in hippocampal slices ex vivo, marking this mode of action of OXT as more general and widespread than previously thought. Notably, Montagnese et al. (1990) showed that continuous icv administration of OXT for six days induces astrocytic cytoskeletal remodeling solely in pregnant/lactating rats or rats undergoing a prolonged diestrus. In animals with normal estrous cycles, the effect of OXT required concomitant intramuscular injections of progesterone and estradiol. The findings of the present thesis demonstrate that OXT alone is sufficient to induce astrocytic remodeling in male rodents, corroborating the concept of OXT, per se, being a general regulator of astrocytic plasticity.

4.4 The involvement of the small GTPase Gem in the effects of OXT on astrocytes

Based on its OXT-induced upregulation in vitro and in vivo, as well as on the observed dampened activity of the ROCK pathway, I hypothesized that the endogenous RhoA/ROCK-inhibitor Gem plays an important role in conveying the effect of OXT on astrocytes. To test this hypothesis, I applied a combinational approach of siRNA-based knockdown and overexpression experiments in vitro. Confirming my hypothesis, I found that Gem is required and sufficient for the effects of OXT on cytoskeletal dynamics and gap-junctional coupling of astrocytes. This identifies Gem as the common link between OXT-induced cytoskeletal remodeling and the regulation of astrocytic connexins.

Two main functions have been ascribed to Gem. First, the inhibition of L-VGCCs through interaction with the $Ca_{v1.2}$ subunit of the channel (Yang et al., 2012) and, second, regulation of cytoskeletal dynamics via inhibitory interaction with either RhoA or ROCK (Hatzoglou et al., 2007; Ward et al., 2002). Due to the lack of $Ca_{v1.2}$ expression in astrocytes (Zhang et al., 2014), it seems likely that Gem solely acts via the latter function in this cell type. The GTPase RhoA and its downstream effector ROCK are major cytoskeletal regulators in many cell types (Hall, 1998; Jaffe and Hall, 2005; Ponimaskin et al., 2007; Riento and Ridley, 2003), and as such have also been implicated in the control of astrocyte morphology (Holtje et al., 2005; John et al., 2004; Kalman et al., 1999). Hallmarks of astrocytic RhoA/ROCK activation are a retraction/loss of processes, whereas decreased RhoA/ROCK activity causes formation and outgrowth of processes, as well as a breakdown of F-actin stress-fibres. Our results show that in astrocytes Gem prevents the activation of RhoA/ROCK by OXT, which in other cell types, as well as in astrocytes with reduced levels of Gem, seems to be the default mode of OXT (see 4.6; Gogarten et al., 2001; Tahara et al., 2002). This unique feature, together with the general dependency of OXT effects on Gem, marks Gem as a key factor in the cell type-specific response of astroglial cells to OXT. Gem expression, as well as its function as cytoskeletal regulator are facilitated by PKC (Leone et al., 2001; Maguire et al., 1994; Ward et al., 2004). This is well in line with the observed PKC dependency of the effects of OXT on astrocytic cytoskeletal parameters and suggests that OXT regulates Gem expression and function via PKC signaling.

In addition to OXT-induced cytoskeletal remodeling, Gem directly governed gap-junctional coupling, as well as Cx43 localization and phosphorylation status. The link between the cytoskeleton and GJIC is still a matter of debate in the literature. While some studies report that disruption of the cytoskeleton impairs Cx43 trafficking to the membrane, and consequently GJIC (Butkevich et al., 2004; Derangeon et al., 2008; Smyth et al., 2012; Theiss and Meller, 2002), other work suggests no such relation (Giepmans et al., 2001; Johnson et al., 2002; Rouach et al., 2006). Adding to this complexity, pharmacological inhibition of ROCK caused Cx43 degradation in rat renal cells (Gomez et al., 2019), while other work has found no effect of decreased ROCK activity on GJIC in ZW13-2 cells (Kim et al., 2020), or even reported increased GJIC following ROCK-inihibition in corneal epithelial cells (Anderson et al., 2002). Specifically in cultured astrocytes, ROCK-inhibition alone did not reduce GJIC (Rouach et al., 2006). Since, in contrast, overexpression of Gem was sufficient to impair GJIC, Gem might thus exert its control of Cx43 via inhibition of RhoA, but not ROCK. In support of this idea, direct activation of RhoA was reported to impair GJIC in cardiac myocytes (Derangeon et al., 2008) and Gem has been shown to inhibit RhoA independently of ROCK (Hatzoglou et al., 2007). To support this hypothesis, future work should examine whether direct activation of RhoA is able to rescue Gem OE-induced effects on astrocytic gap-junctions. Attempts to directly detect OXT-induced inhibition of RhoA activity by means of a pull-down assay of GTP-bound (i.e. active) RhoA, failed due to below detection limit endogenous activity of RhoA (data not shown). In situ hybridization for RhoA in the rat spinal cord has shown very low levels in astrocytes (Erschbamer et al., 2005). Nevertheless, evidence that even below detection limit Rho GTPase expression levels are relevant for physiological processes in astrocytes come from functional studies demonstrating that introduction of constitutively active or dominant-negative RhoA or Rac1 can clearly affect astrocyte morphology in situ (Kalman et al., 1999; Nishida and Okabe, 2007).

Notably, Langle et al. (2003) found OXT-induced astroglial remodeling within the SON to be dependent on newly synthesized proteins, as the protein-sythesis inhibitor anismoycin prevented this effect. However, the identity of these proteins remained elusive. Therefore, the potential involvement of Gem in astroglial plasticity of the SON should be examined.

4.5 Involvement of astrocytic gap-junctions in OXT-induced cytoskeletal remodeling

To explore the possibility of an involvement of astrocytic connexins in OXT-induced cytoskeletal remodeling, hippocampal slices of WT, Cx30 or Cx43 knockout mice were treated with OXT. Similar to experiments in rats, OXT caused acute increases in domain area, process length and process number in slices from WT and Cx30KO mice. In contrast, OXT did not alter process length and number of Cx43 knockout astrocytes. Moreover, it showed a trend to decrease astrocytic domain area in slices from Cx43KO mice, overall suggesting an involvement of Cx43, but not Cx30, in OXT-induced cytoskeletal dynamics of astrocytes. Both Cx43 and Cx30 have been implicated in the regulation of cytoskeletal processes (Ghezali et al., 2018) via C-terminal interactions with components of the cytoskeleton such as tubulin and actin (Ambrosi et al., 2016; Qu et al., 2009; Wall et al., 2007). Cx30 not being required for OXT-induced cytoskeletal remodeling renders its upregulation by OXT more likely to play a role in glutamate clearance and/or compensate for the loss of Cx43-based gap-junctional coupling (as discussed under 4.2). However, the involvement of Cx43 is in good agreement with a large body of literature (reviewed in Kameritsch et al., 2012; Matsuuchi and Naus, 2013), identifying Cx43 to play an important role in cytoskeletal dynamics in a variety of cell types. For this purpose, Cx43 is providing a membrane-bound 'nexus' for proteins that subsequently induce cytoskeletal rearrangements required for the extension of processes or directed migration (Olk et al., 2010; Olk et al., 2009). These actions, which are independent of Cx43 channel functions, are characterized by dynamic disassembly and reassembly of cytoskeletal components. Besides their interaction with components of the cytoskeleton, Cx43 signaling hubs additionally contain transcription factors enabling them to exert downstream transcriptional control (Matsuuchi and Naus, 2013). Since I found both, upregulation of Gem, as well as decreased levels of Cx43, to be required for OXT-induced cytoskeletal remodeling, I investiged whether Gem levels are under regulatory control of Cx43. However, there was no direct regulation of Gem by reduced Cx43 levels in vitro. Notably, the ability of Gem to affect cytoskeletal dynamics requires the activated (i.e. phosphorylated) form of ezrin, which recruits Gem to the cell membrane and enables its inhibition of RhoA via the Rho-GAP Gmip (Hatzoglou et al., 2007). Adapter proteins like ezrin and drebrin (Butkevich et al., 2004; Dukic et al., 2017; Pidoux et al., 2014), which connect Cx43 to the cytoskeleton of its harboring cell, are part of Cx43 signaling scaffolds. While not affecting Gem levels directly, Cx43 knockdown significantly increased the phosphorylated amount of ezrin and negatively correlated with the degree of ezrin phosphorylation, implying an increasing availability of active ezrin with decreasing Cx43 levels. Due to its preferential expression in astrocytes within the CNS (Derouiche and Frotscher, 2001), as well as its direct interactions with Cx43 and Gem, ezrin might thus be the common link between Gem and Cx43-mediated cytoskeletal dynamics elicited by OXT. The phosphorylation of ezrin at Thr567, which is critical for its interaction with Gem, is induced by

PKC (Ng et al., 2001). The critical involvement of PKC-signaling in the effects of OXT further supports such a link. To strengthen this hypothesis, future work should address whether manipulation of ezrin is able to alter the effects of OXT on astrocytes. Furthermore, it would be of interest whether the OXT-induced increase in astrocytic volume is related to the downregulation of Cx43. Since astrocytic gap-junctions gate the distribution of ions and small molecules within astrocytic networks, their disconnection can lead to swelling due to the unability to equilibrate osmotically active substances (Quist et al., 2000). The resulting reduction in extracellular space has been shown to result in altered diffusional properties of neuroactive substances (Piet et al., 2004). Notably, this regulation of cell volume is characteristic for Cx43, since Cx43 knockout animals, in contrast to Cx30 deficient animals (Pannasch et al., 2014), show astrocytic swelling (Chever et al., 2014).

Taken together, OXT-induced cytoskeletal remodeling of astrocytes specifically involves the connexin isoform Cx43. This is likely mediated via C-terminal interactions of Cx43 that provide a link to the cytoskeleton and do not involve its channel function. Loss of Cx43 increases the available amount of active ezrin, a protein required the regulatory function of Gem on the cytoskeleton.

4.6 Transcriptional regulation of Gem by OXT

Since I had identified OXT-induced expression of *Gem* to play a critical role in the effect of OXT on astrocytes, I explored how OXT controls Gem on a transcriptional level. An initial *in silico* analysis suggested the transcription factor Sp1 as a promising candidate. *In vitro* experiments confirmed that Sp1 is required for the OXT-induced upregulation of Gem on the protein level and, in accordance with its regulation of Gem, for cytoskeletal remodeling by OXT. Moreover, Sp1 knockdown decreased *Gem* mRNA quantities, further supporting direct transcriptional control.

Sp1 was the first mammalian transcription factor to be cloned and characterized and as such is the founding member of the Specificity protein/Krüppel-like factor (Sp/KLF) family of transcription factors (Dynan and Tjian, 1983; Kadonaga et al., 1987; Philipsen and Suske, 1999). The DNA-binding of Sp1 is accomplished by three adjacent zinc finger domains that recognize GC-rich motifs (Suske et al., 2005). Due to its involvement in a wide variety of cellular processes, as well as its relatively stable and ubiquitous expression, Sp1 was once thought to serve as a constitutive activator of housekeeping genes (Tan and Khachigian, 2009). However, recent studies revealed a highly dynamic activity profile of Sp1, regulated by multiple post-translational modifications (Li and Davie, 2010) and Sp1 abundance itself (Li et al., 2004). In this context, both PKC and ERK1/2 have been shown to regulate Sp1 activity through multiple phosphorylations (Chu, 2012).

Notably, within the brain, several studies found Sp1 to be predominantly expressed by astrocytes (Hung et al., 2020; Mao et al., 2009). Astrocyte-specific inducible knockout of Sp1 in mice caused impaired outgrowth or death of hippocampal and cortical neurons and resulted in lower performances in object recognition and motor ability tasks (Hung et al., 2020). Moreover, loss of Sp1 severely altered astrocyte morphology into a less ramified and retracted state through unknown mechanisms (Hung et al., 2020). In contrast, I did not observe an effect of Sp1 knockdown alone, which might be due to remaining Sp1 activity in siRNA-transfected cells. However, contrary to its effect on control cells, OXT-stimulation resulted in retraction of processes in Sp1 knockdown cells. Since Sp1 knockdown reduced *Gem* levels and additionally prevented OXT-induced upregulation of Gem, a subsequent activation of the ROCK pathway by OXT, similar to observations in Gem knockdown cells, might explain this finding.

Specifically in astrocytes, Sp1 has been shown to positively regulate *P2rx7* (Garcia-Huerta et al., 2012), *Slc1a2* (Bradford et al., 2009), *Ccnd1* (Michinaga et al., 2013), *Cryab* (Hong et al., 2017), *Sod2* (Mao et al., 2006), as well as multiple genes of the complement system (Hung et al., 2020). As Sp1 controls the transcription of the *Oxtr* gene in ovine and mouse cell lines (Fleming et al., 2006; Mamrut et al., 2013), I excluded the possibility of astrocytic OXTR signaling being desensitized by Sp1 knockdown.

In line with Sp1-dependent upregulation of Gem, astrocytic Sp1 is generally understood as an activator of expression (Mao et al., 2009), although several lines of evidence demonstrate its ability to function as transcriptional repressor (Dabrowska and Zielinska, 2019; Hung et al., 2020). Transcriptional regulation of the *Gem* gene was so far only studied in blood T cells, in which Gem expression is driven by the transcription factors Tax and CREB (Chevalier et al., 2014). Since I found that OXT activates CREB in astrocytes and Sp1 interacts with CREB and other transcription factors (Safe and Kim, 2004), an indirect regulation of *Gem* via such an interaction cannot be excluded. Thus, future work should validate direct binding of Sp1 to the promoter region of *Gem* by means of chromatin immunoprecipitation. Moreover, it should be explored, to which extent Sp1 is involved in the regulation of astrocytic gap-junctions. This is of particular interest, as Sp1 exerts positive transcriptional control over the genes coding for Cx43 and Cx30 in different cell types (Essenfelder et al., 2005; Fernandez-Cobo et al., 2001; Hernandez et al., 2006; Teunissen et al., 2003; Villares et al., 2009; Vine et al., 2005). Whether this is the case in astrocytes remains to be elucidated.

Overall, this is the first work to link Sp1 to OXTR-coupled signaling in general and, by means of its regulation of Gem, identifies the previously undescribed OXTR-Sp1-Gem signaling axis as primary driver of OXT actions on astrocytes.

4.7 Differential regulation of the Sp1-Gem axis in neuronal cells

Since OXT has contrary effects on the cytoskeleton of neuronal cells (Meyer et al., 2018; Meyer et al., 2020; Ripamonti et al., 2017), i.e. a retraction of neurites, I examined whether OXT differentially regulates the Sp1-Gem signaling axis in neuronal cells compared to astrocytes. In contrast to astrocytes, OXT stimulation resulted in downregulation of Sp1 and Gem, which was accompanied by an increase in ROCK activity. To validate these findings *in vivo,* the cellular distribution of Gem was analyzed within the hippocampus of rats following central administration of OXT. This revealed an OXT-induced increase of Gem-positive astrocytes, as well as a simultaneous decrease of Gem-expressing non-astrocytic cells. In general, two-thirds of Gem-positive cells were of astrocytic identity, which is in accordance with its preferential expression in this cell type. Even though the Gem-positive non-astrocytic cells resembled neurons in their appearence, their exact identity is focus of ongoing work and thus remains to be elucidated.

Differential and even contrary responses to identical manipulations are well documented between neurons and astrocytes and might explain the observed polarization of Gem expression by OXT. For example, while G_q-coupled GPCR signaling activated both neurons and astrocytes, $G_{i/o}$-coupled GPCR signaling inhibited neurons, but activated astrocytes (Durkee et al., 2019). This is especially relevant in the context of OXT, since the OXTR couples to G_q and $G_{i/o}$ proteins alike (Busnelli et al., 2012; Ku et al., 1995). Moreover, activation of the GPCR effector PKC increased OXTR binding activity in neurons, while it had the opposite effect in astrocytes (Strosser et al., 2001). Further examples are found on the transcriptional level, where the same transcription factor can regulate vastly different gene networks in neurons or astrocytes with minimal overlap (Pardo et al., 2017). In the case of Sp/KLF transcription factors, the exertion of transcriptional control is characterized by the cell type-specific expression of their isoforms. While Sp1 is preferentially found in astrocytes, Sp4 is the dominant Sp transcription factor in mature neurons (Mao et al., 2006; Mao et al., 2009). Other than Sp1, Sp4 is often acting as a transcriptional repressor, particularly when expressed in the presence of Sp3 (Hagen et al., 1995; Mao et al., 2002; Wong et al., 2001). As shown for the *Sod2* gene, this can result in a contrary regulation of the same target gene through binding of different Sp isoforms to the same binding site (Mao et al., 2006). Therefore, future work should investigate a potential role of Sp4 in the downregulation of neuronal Gem by OXT.

Notably, I found OXT-induced neurite retraction of H32 cells to be dependent on ROCK activity. Previous studies showed that the transcription factor MEF-2A is required for the effect of OXT on the cytoskeleton of these cells (Meyer et al., 2018). Moreover, MEF-2A expression seems to define the morphological response of some cell types to OXT. In absence of MEF-2A, OXT caused process elongation, while it induced the opposite effect in MEF-2A expressing cells (Meyer et al., 2020). Indeed, we did not detect MEF-2A expression in astrocytes in a preliminary analysis (data not shown). Since I found activation of the ROCK pathway to be involved in OXT-elicited neurite retraction of H32 cells, it should be explored whether knockout of MEF-2A decreases the responsiveness of the ROCK pathway to OXT. A possible underlying mechanism is posed by the observed downregulation of Gem in H32 cells, which should result in a loss of Gem-exerted inhibition of ROCK. As Gem is not degraded via the proteasome pathway in H32 cells (Nerb, 2020), MEF-2A might regulate a protease that degrades Gem upon OXT stimulation and consequently disinhibits ROCK. Alternatively, MEF-2A may induce expression of a transcriptional repressor of Sp1 and by this cause reduced Gem expression.

Taken together, these findings further identify Gem as a defining factor in the cell type-specific response of astroglial cells to OXT.

4.8 Establishment of astrocyte-specific Oxtr/Gem-knockdown vectors

Based on my previous findings demonstrating that OXT acts directly on astrocytes and that these actions are conveyed by Gem, I aimed to establish astrocyte-specific *Gem* or *Oxtr* knockdown vectors as tools for a targeted manipulation of astrocytic OXTR signaling *in vivo*. This would enable future work to assess a potential astrocytic contribution to the physiological and behavioral effects of OXT.

To this end, shRNA oligonucleotides were screened for knockdown efficiency *in vitro.* Despite a compensatory effect on *Oxtr* expression 2d post-transfection, both shRNA plasmids caused a significant knockdown of their target mRNAs after a prolonged post-transfection period of one week and thus were chosen for the design of AAV-based vectors. In order to accomplish cell type specificity, first, an AAV6 capsid was selected for viral packaging. Among available adenoviral capsids, AAV6 packaged vectors show the highest tropism for astrocytes compared to other cell types of the CNS (Schober et al., 2016), while simultaneously providing good perturbance (Ellis et al., 2013). Second, transcriptional control of shRNA expression is exerted by the *hGFAP* promoter. Using a viral knockdown strategy provides several advantages over the creation of traditional knockout animal, e.g. via the Cre/loxP system. First, it enables brain region-specific assessment of the involvement of astrocytic OXTR-signaling. This is of particular relevance in the light of brain region-dependent heterogeneity of astrocytes, as well as due to brain region-specific differences in physiological/behavioral effects of OXT. Second, it permits manipulation of astrocytic gene expression in rats, for which the creation of transgenic animals is cost-ineffecient and of particular technical difficulty. It should, however, be mentioned that the target sequences of both used shRNAs are found in the mouse *Gem*/*Oxtr* mRNA sequences as well and might therefore prove suitable for an application in this species.

In a preliminary experiment, I aimed to determine the optimal physical viral titer and volume for microinfusions of the rat PVN. Of the tested conditions, only the highest physical viral titer resulted in a detectable, but scattered, expression of the fluorescent reporter protein mCherry at the injection site. The physical viral titers ranging from 10^8-10^{12} GC/ml used in this experiment were chosen based on the literature of AAV-mediated transfections of the PVN (Garza et al., 2008; Koba et al., 2018; Zhang et al., 2013). However, the low rate of successful transfection indicates an insufficient amount of available viral particles. Therefore, future microinfusions should be assessed with a viral titer of 10^{13} GC/ml.

4.9 Conclusion and future perspectives

Astrocytes are increasingly appreciated as indispensable components of the CNS that actively shape information processing. Thus, the biology of a neuroactive signaling peptide like OXT cannot be fully understood without taking its interactions with non-neuronal cell types into account. Therefore, the present thesis aimed to provide a better understanding of the effects and underlying mechanisms of direct OXT actions on astrocytes. Its findings demonstrate a rapid OXT-induced cytoskeletal remodeling and alterations to gap-junction coupling. Mechanistically, both of these effects were OXTR-specific, conveyed via PKC and, to a lesser extent, MEK1/2 signaling. Moreover, this mode of action was characteristic for OXT, since its closely related sister-peptide AVP did not affect the examined parameters. In depth *in vitro* analyses identified the previously undescribed Sp1-Gem signaling axis to be at the base of these effects. A combination of knockdown, knockout and overexpression experiments revealed that OXT drives *Gem* expression via the transcription factor Sp1 and that Gem is required and sufficient for the effects of OXT on astrocytes. The Sp1-Gem axis was differentially regulated by OXT in neuronal cells, identifying it as key driver in the cell type-specific response of astroglial cells to OXT. The intracellular events defining the effect of OXT on astrocytes are summarized in Fig.25. Their potential ramifications on the synaptic level, which point towards potentiation of excitatory neurotransmission by reducing astroglial governance over the synaptic environment, are illustrated in Fig.26.

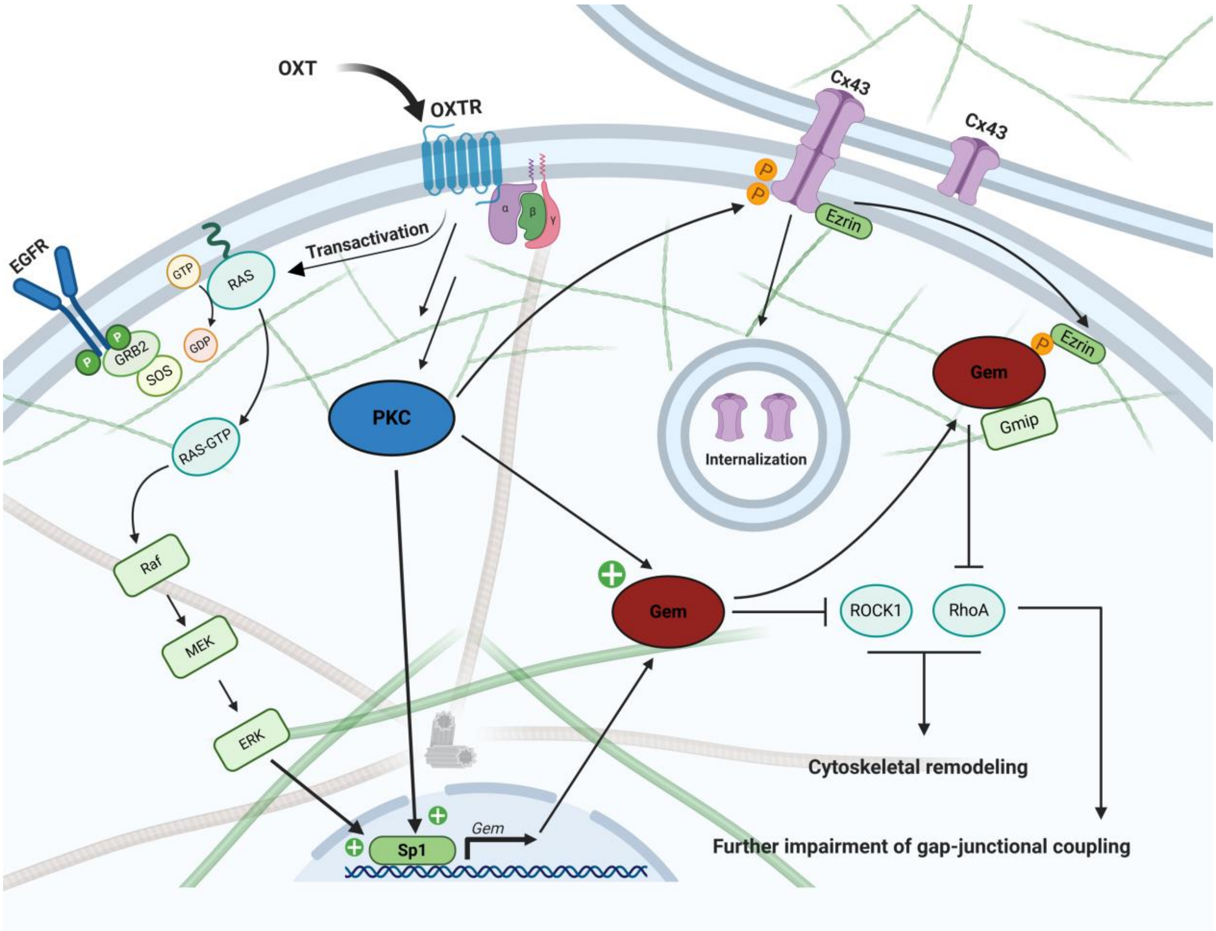

Figure 25. Schematic overview of OXTR-mediated signaling and its cellbiological consequences in astrocytes. Binding of OXT to its receptor induces activation of the MAPK-pathway and PKC signaling. Concerted action of ERK1/2 and PKC is required for induction of cytoskeletal remodeling and closure of gap-junctions. Concomitant PKC-induced Cx43 phosphorylation causes internalization of Cx43-based gap-junctions and increases the available amount of active, i.e. phosphorylated ezrin. PKC and ERK signaling converge at the transcription factor Sp1, which drives expression of *Gem*. Within the cytoplasm, PKC-activated Gem initiates cytoskeletal remodeling via direct inhibition of ROCK and, in complex with phosphorylated ezrin and Gmip, RhoA. Inhibition of RhoA might potentiate the impairment of gap-junctional intercellular connectivity. Illustration created with BioRender.com.

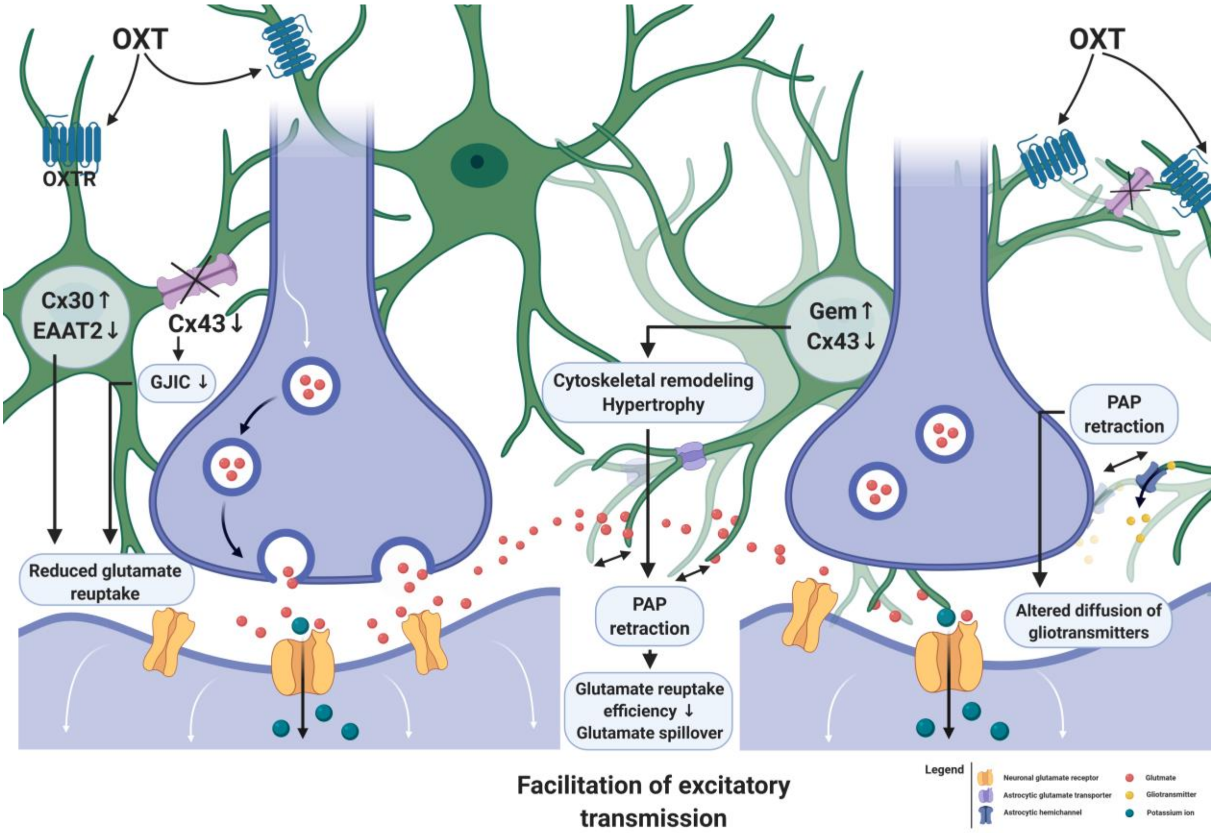

Figure 26. Schematic overview of OXT actions on astrocytes and their potential ramifications on the synaptic level. As shown in the present thesis, OXT acutely upregulates Cx30 and Gem in astrocytes, while downregulating Cx43 and EAAT2. In consequence, K^+ buffering via astrocytic networks and reuptake of glutamate are less efficient. Simultaneous astroglial cytoskeletal remodeling and swelling cause retraction of PAPs from the synaptic clefts, furthering the decrease in astrocytic glutamate reuptake and permitting spillover to neighbouring synapses. Thus, oxytocin might potentiate excitatory neurotransmission by reducing astroglial governance over the synaptic environment. Illustration created with BioRender.com.

The present thesis provides the first overview of astrocytic OXTR-coupled signaling and its cellbiological consequences. By identifying cell type-specific mediators that define the outcome of this signaling, this work furthers our understanding of how the OXT system is able to bring about physiological and behavioral responses, which are diverse and highly specific at the same time. The astrocyte-specific *Gem*/*Oxtr*-shRNA vectors derived from this thesis might provide tools for a targeted manipulation of astrocytic OXTR signaling and future assessment of astrocytic contribution to the physiological and behavioral effects of OXT. In this way, this thesis might serve as a base for future studies pursuing a more integrative and holistic approach in OXT research.

Finally, a number of important limitations need to be considered. Even though key findings were constantly validated *in vivo*, the majority of experiments were performed in cultured astrocytes. The use of this model system naturally results in the possibility of findings lacking biological relevance. Future work should therefore aim to further validate the described findings *in vivo/ex vivo* and demonstrate their involvement in physiological and cognitive processes.

Second, in all experiments OXT was applied exogenously, which might have resulted in supraphysiological stimulation of target cells. The described mechanisms should thus be further explored under physiological conditions of elevated OXTergic activity, e.g. lactation or osmotic challenge. In addition, their involvement in processes depending on endogenous release of OXT should be demonstrated.

References

Acher, R., Chauvet, J., and Chauvet, M.T. (1995). Man and the chimaera. Selective versus neutral oxytocin evolution. Adv Exp Med Biol *395*, 615-627.
Adan, R.A., Cox, J.J., Beischlag, T.V., and Burbach, J.P. (1993). A composite hormone response element mediates the transactivation of the rat oxytocin gene by different classes of nuclear hormone receptors. Mol Endocrinol *7*, 47-57.
Akerlund, M., Bossmar, T., Brouard, R., Kostrzewska, A., Laudanski, T., Lemancewicz, A., Serradeil-Le Gal, C., and Steinwall, M. (1999). Receptor binding of oxytocin and vasopressin antagonists and inhibitory effects on isolated myometrium from preterm and term pregnant women. Br J Obstet Gynaecol *106*, 1047-1053.
Altevogt, B.M., and Paul, D.L. (2004). Four classes of intercellular channels between glial cells in the CNS. J Neurosci *24*, 4313-4323.
Altstein, M., and Gainer, H. (1988). Differential biosynthesis and posttranslational processing of vasopressin and oxytocin in rat brain during embryonic and postnatal development. J Neurosci *8*, 3967-3977.
Alvarez-Maubecin, V., Garcia-Hernandez, F., Williams, J.T., and Van Bockstaele, E.J. (2000). Functional coupling between neurons and glia. J Neurosci *20*, 4091-4098.
Ambrosi, C., Ren, C., Spagnol, G., Cavin, G., Cone, A., Grintsevich, E.E., Sosinsky, G.E., and Sorgen, P.L. (2016). Connexin43 Forms Supramolecular Complexes through Non-Overlapping Binding Sites for Drebrin, Tubulin, and ZO-1. PLoS One *11*, e0157073.
Andersen, J., Grine, E., Eng, C.L., Zhao, K., Barbieri, R.L., Chumas, J.C., and Brink, P.R. (1993). Expression of connexin-43 in human myometrium and leiomyoma. Am J Obstet Gynecol *169*, 1266-1276.
Anderson, C.M., and Swanson, R.A. (2000). Astrocyte glutamate transport: review of properties, regulation, and physiological functions. Glia *32*, 1-14.
Anderson, S.C., Stone, C., Tkach, L., and SundarRaj, N. (2002). Rho and Rho-kinase (ROCK) signaling in adherens and gap junction assembly in corneal epithelium. Invest Ophthalmol Vis Sci *43*, 978-986.
Anlauf, E., and Derouiche, A. (2013). Glutamine synthetase as an astrocytic marker: its cell type and vesicle localization. Front Endocrinol (Lausanne) *4*, 144.
Araque, A., Carmignoto, G., Haydon, P.G., Oliet, S.H., Robitaille, R., and Volterra, A. (2014). Gliotransmitters travel in time and space. Neuron *81*, 728-739.
Araque, A., Parpura, V., Sanzgiri, R.P., and Haydon, P.G. (1999). Tripartite synapses: glia, the unacknowledged partner. Trends Neurosci *22*, 208-215.
Ayar, A., Ozcan, M., Alcin, E., Serhatlioglu, I., Ozcan, S., Kutlu, S., and Kelestimur, H. (2014). Oxytocin activates calcium signaling in rat sensory neurons through a protein kinase C-dependent mechanism. J Physiol Biochem *70*, 43-48.
Bakermans-Kranenburg, M.J., and van Ijzendoorn, M.H. (2014). A sociability gene? Meta-analysis of oxytocin receptor genotype effects in humans. Psychiatr Genet *24*, 45-51.
Bandeira, F., Lent, R., and Herculano-Houzel, S. (2009). Changing numbers of neuronal and non-neuronal cells underlie postnatal brain growth in the rat. Proc Natl Acad Sci U S A *106*, 14108-14113.
Beery, A.K., McEwen, L.M., MacIsaac, J.L., Francis, D.D., and Kobor, M.S. (2016). Natural variation in maternal care and cross-tissue patterns of oxytocin receptor gene methylation in rats. Horm Behav *77*, 42-52.
Beguin, P., Mahalakshmi, R.N., Nagashima, K., Cher, D.H., Takahashi, A., Yamada, Y., Seino, Y., and Hunziker, W. (2005). 14-3-3 and calmodulin control subcellular distribution of Kir/Gem and its regulation of cell shape and calcium channel activity. J Cell Sci *118*, 1923-1934.
Beguin, P., Nagashima, K., Gonoi, T., Shibasaki, T., Takahashi, K., Kashima, Y., Ozaki, N., Geering, K., Iwanaga, T., and Seino, S. (2001). Regulation of Ca2+ channel expression at the cell surface by the small G-protein kir/Gem. Nature *411*, 701-706.

Bellesi, M., de Vivo, L., Tononi, G., and Cirelli, C. (2015). Effects of sleep and wake on astrocytes: clues from molecular and ultrastructural studies. BMC Biol *13*, 66.
Bergmann, K. (1857). Notiz über einige Strukturverhältnisse des Cerebellums und Rückenmarks. Z Med *8*, 360-363.
Bignami, A., Eng, L.F., Dahl, D., and Uyeda, C.T. (1972). Localization of the glial fibrillary acidic protein in astrocytes by immunofluorescence. Brain Res *43*, 429-435.
Blanks, A.M., Shmygol, A., and Thornton, S. (2007). Regulation of oxytocin receptors and oxytocin receptor signaling. Semin Reprod Med *25*, 52-59.
Blume, A., Bosch, O.J., Miklos, S., Torner, L., Wales, L., Waldherr, M., and Neumann, I.D. (2008). Oxytocin reduces anxiety via ERK1/2 activation: local effect within the rat hypothalamic paraventricular nucleus. Eur J Neurosci *27*, 1947-1956.
Boudaba, C., Linn, D.M., Halmos, K.C., and Tasker, J.G. (2003). Increased tonic activation of presynaptic metabotropic glutamate receptors in the rat supraoptic nucleus following chronic dehydration. J Physiol *551*, 815-823.
Bradford, J., Shin, J.Y., Roberts, M., Wang, C.E., Li, X.J., and Li, S. (2009). Expression of mutant huntingtin in mouse brain astrocytes causes age-dependent neurological symptoms. Proc Natl Acad Sci U S A *106*, 22480-22485.
Brighton, P.J., Rana, S., Challiss, R.J., Konje, J.C., and Willets, J.M. (2011). Arrestins differentially regulate histamine- and oxytocin-evoked phospholipase C and mitogen-activated protein kinase signalling in myometrial cells. Br J Pharmacol *162*, 1603-1617.
Brizzee, K.R., and Jacobs, L.A. (1959). The glia/neuron index in the submolecular layers of the motor cortex in the cat. Anat Rec *134*, 97-105.
Bulbul, M., Babygirija, R., Cerjak, D., Yoshimoto, S., Ludwig, K., and Takahashi, T. (2011). Hypothalamic oxytocin attenuates CRF expression via GABA(A) receptors in rats. Brain Res *1387*, 39-45.
Bushong, E.A., Martone, M.E., Jones, Y.Z., and Ellisman, M.H. (2002). Protoplasmic astrocytes in CA1 stratum radiatum occupy separate anatomical domains. J Neurosci *22*, 183-192.
Busnelli, M., Kleinau, G., Muttenthaler, M., Stoev, S., Manning, M., Bibic, L., Howell, L.A., McCormick, P.J., Di Lascio, S., Braida, D., *et al.* (2016). Design and Characterization of Superpotent Bivalent Ligands Targeting Oxytocin Receptor Dimers via a Channel-Like Structure. J Med Chem *59*, 7152-7166.
Busnelli, M., Sauliere, A., Manning, M., Bouvier, M., Gales, C., and Chini, B. (2012). Functional selective oxytocin-derived agonists discriminate between individual G protein family subtypes. J Biol Chem *287*, 3617-3629.
Butkevich, E., Hulsmann, S., Wenzel, D., Shirao, T., Duden, R., and Majoul, I. (2004). Drebrin is a novel connexin-43 binding partner that links gap junctions to the submembrane cytoskeleton. Curr Biol *14*, 650-658.
Cahoy, J.D., Emery, B., Kaushal, A., Foo, L.C., Zamanian, J.L., Christopherson, K.S., Xing, Y., Lubischer, J.L., Krieg, P.A., Krupenko, S.A., *et al.* (2008). A transcriptome database for astrocytes, neurons, and oligodendrocytes: a new resource for understanding brain development and function. J Neurosci *28*, 264-278.
Camacho-Arroyo, I., Gonzalez-Arenas, A., Espinosa-Raya, J., Pina-Medina, A.G., and Picazo, O. (2011). Short- and long-term treatment with estradiol or progesterone modifies the expression of GFAP, MAP2 and Tau in prefrontal cortex and hippocampus. Life Sci *89*, 123-128.
Chai, H., Diaz-Castro, B., Shigetomi, E., Monte, E., Octeau, J.C., Yu, X., Cohn, W., Rajendran, P.S., Vondriska, T.M., Whitelegge, J.P., *et al.* (2017). Neural Circuit-Specialized Astrocytes: Transcriptomic, Proteomic, Morphological, and Functional Evidence. Neuron *95*, 531-549.e539.
Chevalier, S.A., Turpin, J., Cachat, A., Afonso, P.V., Gessain, A., Brady, J.N., Pise-Masison, C.A., and Mahieux, R. (2014). Gem-induced cytoskeleton remodeling increases cellular migration of HTLV-1-infected cells, formation of infected-to-target T-cell conjugates and viral transmission. PLoS Pathog *10*, e1003917.
Chever, O., Pannasch, U., Ezan, P., and Rouach, N. (2014). Astroglial connexin 43 sustains glutamatergic synaptic efficacy. Philos Trans R Soc Lond B Biol Sci *369*, 20130596.

Choi, J.W., Kang, S.M., Lee, Y., Hong, S.H., Sanek, N.A., Young, W.S., and Lee, H.J. (2013). MicroRNA profiling in the mouse hypothalamus reveals oxytocin-regulating microRNA. J Neurochem *126*, 331-337.
Chu, S. (2012). Transcriptional regulation by post-transcriptional modification--role of phosphorylation in Sp1 transcriptional activity. Gene *508*, 1-8.
Chung, D., Kim, Y.S., Phillips, J.N., Ulloa, A., Ku, C.Y., Galan, H.L., and Sanborn, B.M. (2010). Attenuation of canonical transient receptor potential-like channel 6 expression specifically reduces the diacylglycerol-mediated increase in intracellular calcium in human myometrial cells. Endocrinology *151*, 406-416.
Chung, W.S., Clarke, L.E., Wang, G.X., Stafford, B.K., Sher, A., Chakraborty, C., Joung, J., Foo, L.C., Thompson, A., Chen, C.*, et al.* (2013). Astrocytes mediate synapse elimination through MEGF10 and MERTK pathways. Nature *504*, 394-400.
Chvatal, A., Pastor, A., Mauch, M., Sykova, E., and Kettenmann, H. (1995). Distinct populations of identified glial cells in the developing rat spinal cord slice: ion channel properties and cell morphology. Eur J Neurosci *7*, 129-142.
Cohen, L., Mohr, R., Chen, Y.Y., Huang, M., Kato, R., Dorin, D., Tamanoi, F., Goga, A., Afar, D., Rosenberg, N.*, et al.* (1994). Transcriptional activation of a ras-like gene (kir) by oncogenic tyrosine kinases. Proc Natl Acad Sci U S A *91*, 12448-12452.
Colaianni, G., Tamma, R., Di Benedetto, A., Yuen, T., Sun, L., Zaidi, M., and Zallone, A. (2014). The oxytocin-bone axis. J Neuroendocrinol *26*, 53-57.
Connor, J.R., and Berkowitz, E.M. (1985). A demonstration of glial filament distribution in astrocytes isolated from rat cerebral cortex. Neuroscience *16*, 33-44.
Conti, F., Sertic, S., Reversi, A., and Chini, B. (2009). Intracellular trafficking of the human oxytocin receptor: evidence of receptor recycling via a Rab4/Rab5 "short cycle". Am J Physiol Endocrinol Metab *296*, E532-542.
Cornell-Bell, A.H., Finkbeiner, S.M., Cooper, M.S., and Smith, S.J. (1990). Glutamate induces calcium waves in cultured astrocytes: long-range glial signaling. Science *247*, 470-473.
Correll, R.N., Pang, C., Niedowicz, D.M., Finlin, B.S., and Andres, D.A. (2008). The RGK family of GTP-binding proteins: regulators of voltage-dependent calcium channels and cytoskeleton remodeling. Cell Signal *20*, 292-300.
Dabrowska, J., Hazra, R., Guo, J.D., Dewitt, S., and Rainnie, D.G. (2013). Central CRF neurons are not created equal: phenotypic differences in CRF-containing neurons of the rat paraventricular hypothalamus and the bed nucleus of the stria terminalis. Front Neurosci *7*, 156.
Dabrowska, K., and Zielinska, M. (2019). Silencing of Transcription Factor Sp1 Promotes SN1 Transporter Regulation by Ammonia in Mouse Cortical Astrocytes. Int J Mol Sci *20*.
Dallerac, G., Chever, O., and Rouach, N. (2013). How do astrocytes shape synaptic transmission? Insights from electrophysiology. Front Cell Neurosci *7*, 159.
De Vries, G.J., and Buijs, R.M. (1983). The origin of the vasopressinergic and oxytocinergic innervation of the rat brain with special reference to the lateral septum. Brain Res *273*, 307-317.
Deing, V., Roggenkamp, D., Kuhnl, J., Gruschka, A., Stab, F., Wenck, H., Burkle, A., and Neufang, G. (2013). Oxytocin modulates proliferation and stress responses of human skin cells: implications for atopic dermatitis. Exp Dermatol *22*, 399-405.
Deneen, B., Ho, R., Lukaszewicz, A., Hochstim, C.J., Gronostajski, R.M., and Anderson, D.J. (2006). The transcription factor NFIA controls the onset of gliogenesis in the developing spinal cord. Neuron *52*, 953-968.
Derangeon, M., Bourmeyster, N., Plaisance, I., Pinet-Charvet, C., Chen, Q., Duthe, F., Popoff, M.R., Sarrouilhe, D., and Herve, J.C. (2008). RhoA GTPase and F-actin dynamically regulate the permeability of Cx43-made channels in rat cardiac myocytes. J Biol Chem *283*, 30754-30765.
Dermietzel, R., Hertberg, E.L., Kessler, J.A., and Spray, D.C. (1991). Gap junctions between cultured astrocytes: immunocytochemical, molecular, and electrophysiological analysis. J Neurosci *11*, 1421-1432.
Dermietzel, R., Hwang, T.K., and Spray, D.S. (1990). The gap junction family: structure, function and chemistry. Anat Embryol (Berl) *182*, 517-528.

Derouiche, A., and Frotscher, M. (2001). Peripheral astrocyte processes: monitoring by selective immunostaining for the actin-binding ERM proteins. Glia *36*, 330-341.
Devost, D., Carrier, M.E., and Zingg, H.H. (2008a). Oxytocin-induced activation of eukaryotic elongation factor 2 in myometrial cells is mediated by protein kinase C. Endocrinology *149*, 131-138.
Devost, D., Wrzal, P., and Zingg, H.H. (2008b). Oxytocin receptor signalling. Prog Brain Res *170*, 167-176.
Di Benedetto, A., Sun, L., Zambonin, C.G., Tamma, R., Nico, B., Calvano, C.D., Colaianni, G., Ji, Y., Mori, G., Grano, M.*, et al.* (2014). Osteoblast regulation via ligand-activated nuclear trafficking of the oxytocin receptor. Proc Natl Acad Sci U S A *111*, 16502-16507.
Di Scala-Guenot, D., Mouginot, D., and Strosser, M.T. (1994). Increase of intracellular calcium induced by oxytocin in hypothalamic cultured astrocytes. Glia *11*, 269-276.
Di Scala-Guenot, D., and Strosser, M.T. (1992a). Oxytocin receptors on cultured astroglial cells. Kinetic and pharmacological characterization of oxytocin-binding sites on intact hypothalamic and hippocampic cells from foetal rat brain. Biochem J *284 (Pt 2)*, 491-497.
Di Scala-Guenot, D., and Strosser, M.T. (1992b). Oxytocin receptors on cultured astroglial cells. Regulation by a guanine-nucleotide-binding protein and effect of Mg2+. Biochem J *284 (Pt 2)*, 499-505.
Dityatev, A., and Rusakov, D.A. (2011). Molecular signals of plasticity at the tetrapartite synapse. Curr Opin Neurobiol *21*, 353-359.
Dolen, G., Darvishzadeh, A., Huang, K.W., and Malenka, R.C. (2013). Social reward requires coordinated activity of nucleus accumbens oxytocin and serotonin. Nature *501*, 179-184.
Donaldson, Z.R., and Young, L.J. (2008). Oxytocin, vasopressin, and the neurogenetics of sociality. Science *322*, 900-904.
Du, Y., Kiyoshi, C.M., Wang, Q., Wang, W., Ma, B., Alford, C.C., Zhong, S., Wan, Q., Chen, H., Lloyd, E.E.*, et al.* (2016). Genetic Deletion of TREK-1 or TWIK-1/TREK-1 Potassium Channels does not Alter the Basic Electrophysiological Properties of Mature Hippocampal Astrocytes In Situ. Front Cell Neurosci *10*, 13.
Dukic, A.R., Haugen, L.H., Pidoux, G., Leithe, E., Bakke, O., and Tasken, K. (2017). A protein kinase A-ezrin complex regulates connexin 43 gap junction communication in liver epithelial cells. Cell Signal *32*, 1-11.
Durkee, C.A., Covelo, A., Lines, J., Kofuji, P., Aguilar, J., and Araque, A. (2019). Gi/o protein-coupled receptors inhibit neurons but activate astrocytes and stimulate gliotransmission. Glia *67*, 1076-1093.
Dynan, W.S., and Tjian, R. (1983). Isolation of transcription factors that discriminate between different promoters recognized by RNA polymerase II. Cell *32*, 669-680.
Eckertova, M., Ondrejcakova, M., Krskova, K., Zorad, S., and Jezova, D. (2011). Subchronic treatment of rats with oxytocin results in improved adipocyte differentiation and increased gene expression of factors involved in adipogenesis. Br J Pharmacol *162*, 452-463.
Ek-Vitorin, J.F., King, T.J., Heyman, N.S., Lampe, P.D., and Burt, J.M. (2006). Selectivity of connexin 43 channels is regulated through protein kinase C-dependent phosphorylation. Circ Res *98*, 1498-1505.
Eliava, M., Melchior, M., Knobloch-Bollmann, H.S., Wahis, J., da Silva Gouveia, M., Tang, Y., Ciobanu, A.C., Triana Del Rio, R., Roth, L.C., Althammer, F.*, et al.* (2016). A New Population of Parvocellular Oxytocin Neurons Controlling Magnocellular Neuron Activity and Inflammatory Pain Processing. Neuron *89*, 1291-1304.
Ellis, B.L., Hirsch, M.L., Barker, J.C., Connelly, J.P., Steininger, R.J., 3rd, and Porteus, M.H. (2013). A survey of ex vivo/in vitro transduction efficiency of mammalian primary cells and cell lines with Nine natural adeno-associated virus (AAV1-9) and one engineered adeno-associated virus serotype. Virol J *10*, 74.
Erschbamer, M.K., Hofstetter, C.P., and Olson, L. (2005). RhoA, RhoB, RhoC, Rac1, Cdc42, and Tc10 mRNA levels in spinal cord, sensory ganglia, and corticospinal tract neurons and long-lasting specific changes following spinal cord injury. J Comp Neurol *484*, 224-233.
Esseltine, J.L., and Laird, D.W. (2016). Next-Generation Connexin and Pannexin Cell Biology. Trends Cell Biol *26*, 944-955.

Essenfelder, G.M., Larderet, G., Waksman, G., and Lamartine, J. (2005). Gene structure and promoter analysis of the human GJB6 gene encoding connexin 30. Gene *350*, 33-40.
Eulenburg, V., and Gomeza, J. (2010). Neurotransmitter transporters expressed in glial cells as regulators of synapse function. Brain Res Rev *63*, 103-112.
Evans, W.H., and Martin, P.E. (2002). Gap junctions: structure and function (Review). Mol Membr Biol *19*, 121-136.
Feng, J., Ito, M., Ichikawa, K., Isaka, N., Nishikawa, M., Hartshorne, D.J., and Nakano, T. (1999). Inhibitory phosphorylation site for Rho-associated kinase on smooth muscle myosin phosphatase. J Biol Chem *274*, 37385-37390.
Fernandez-Cobo, M., Stewart, D., Drujan, D., and De Maio, A. (2001). Promoter activity of the rat connexin 43 gene in NRK cells. J Cell Biochem *81*, 514-522.
Fischmann, T.O., Smith, C.K., Mayhood, T.W., Myers, J.E., Reichert, P., Mannarino, A., Carr, D., Zhu, H., Wong, J., Yang, R.S.*, et al.* (2009). Crystal structures of MEK1 binary and ternary complexes with nucleotides and inhibitors. Biochemistry *48*, 2661-2674.
Fleming, J.G., Spencer, T.E., Safe, S.H., and Bazer, F.W. (2006). Estrogen regulates transcription of the ovine oxytocin receptor gene through GC-rich SP1 promoter elements. Endocrinology *147*, 899-911.
Fong, J.T., Nimlamool, W., and Falk, M.M. (2014). EGF induces efficient Cx43 gap junction endocytosis in mouse embryonic stem cell colonies via phosphorylation of Ser262, Ser279/282, and Ser368. FEBS Lett *588*, 836-844.
Freeman, M.R. (2010). Specification and morphogenesis of astrocytes. Science *330*, 774-778.
Frey, W.D., Sharma, K., Cain, T.L., Nishimori, K., Teruyama, R., and Kim, J. (2018). Oxytocin receptor is regulated by Peg3. PLoS One *13*, e0202476.
Friede, R. (1954). [Quantitative share of the glia in development of the cortex]. Acta Anat (Basel) *20*, 290-296.
Frommann, C. (1867). Untersuchungen über die normale und pathologische Anatomie des Rückenmarks. Jena: Verlag Friedrisch Frommann.
G Paxinos, C.W. (2008). The Rat Brain in Stereotaxic Coordinates. Academic Press *6*.
Gainer, H., Sarne, Y., and Brownstein, M.J. (1977). Neurophysin biosynthesis: conversion of a putative precursor during axonal transport. Science *195*, 1354-1356.
Gandhi, G.K., Cruz, N.F., Ball, K.K., Theus, S.A., and Dienel, G.A. (2009). Selective astrocytic gap junctional trafficking of molecules involved in the glycolytic pathway: impact on cellular brain imaging. J Neurochem *110*, 857-869.
Gao, P., Postiglione, M.P., Krieger, T.G., Hernandez, L., Wang, C., Han, Z., Streicher, C., Papusheva, E., Insolera, R., Chugh, K.*, et al.* (2014). Deterministic progenitor behavior and unitary production of neurons in the neocortex. Cell *159*, 775-788.
Garcia-Huerta, P., Diaz-Hernandez, M., Delicado, E.G., Pimentel-Santillana, M., Miras-Portugal, M.T., and Gomez-Villafuertes, R. (2012). The specificity protein factor Sp1 mediates transcriptional regulation of P2X7 receptors in the nervous system. J Biol Chem *287*, 44628-44644.
Garcia-Marin, V., Garcia-Lopez, P., and Freire, M. (2007). Cajal's contributions to glia research. Trends Neurosci *30*, 479-487.
Garza, J.C., Kim, C.S., Liu, J., Zhang, W., and Lu, X.Y. (2008). Adeno-associated virus-mediated knockdown of melanocortin-4 receptor in the paraventricular nucleus of the hypothalamus promotes high-fat diet-induced hyperphagia and obesity. J Endocrinol *197*, 471-482.
Ge, W.P., and Jia, J.M. (2016). Local production of astrocytes in the cerebral cortex. Neuroscience *323*, 3-9.
Ghezali, G., Calvo, C.F., Pillet, L.E., Llense, F., Ezan, P., Pannasch, U., Bemelmans, A.P., Etienne Manneville, S., and Rouach, N. (2018). Connexin 30 controls astroglial polarization during postnatal brain development. Development *145*.
Giaume, C., Fromaget, C., el Aoumari, A., Cordier, J., Glowinski, J., and Gros, D. (1991). Gap junctions in cultured astrocytes: single-channel currents and characterization of channel-forming protein. Neuron *6*, 133-143.
Giaume, C., Koulakoff, A., Roux, L., Holcman, D., and Rouach, N. (2010). Astroglial networks: a step further in neuroglial and gliovascular interactions. Nat Rev Neurosci *11*, 87-99.

Giaume, C., Leybaert, L., Naus, C.C., and Saez, J.C. (2013). Connexin and pannexin hemichannels in brain glial cells: properties, pharmacology, and roles. Front Pharmacol *4*, 88.
Giepmans, B.N., Verlaan, I., Hengeveld, T., Janssen, H., Calafat, J., Falk, M.M., and Moolenaar, W.H. (2001). Gap junction protein connexin-43 interacts directly with microtubules. Curr Biol *11*, 1364-1368.
Gimpl, G., and Fahrenholz, F. (2001). The oxytocin receptor system: structure, function, and regulation. Physiol Rev *81*, 629-683.
Gogarten, W., Emala, C.W., Lindeman, K.S., and Hirshman, C.A. (2001). Oxytocin and lysophosphatidic acid induce stress fiber formation in human myometrial cells via a pathway involving Rho-kinase. Biol Reprod *65*, 401-406.
Golubev, A. (1988). Glia and neuroglia relationships in the cerebral nervous system of the

Turbellaria (electron microscopy data). Fortschr Zool *36*, 31-37.
Gomez, G.I., Velarde, V., and Saez, J.C. (2019). Role of a RhoA/ROCK-Dependent Pathway on Renal Connexin43 Regulation in the Angiotensin II-Induced Renal Damage. Int J Mol Sci *20*.
Goodman, O.B., Jr., Krupnick, J.G., Santini, F., Gurevich, V.V., Penn, R.B., Gagnon, A.W., Keen, J.H., and Benovic, J.L. (1996). Beta-arrestin acts as a clathrin adaptor in endocytosis of the beta2-adrenergic receptor. Nature *383*, 447-450.
Gosejacob, D., Dublin, P., Bedner, P., Huttmann, K., Zhang, J., Tress, O., Willecke, K., Pfrieger, F., Steinhauser, C., and Theis, M. (2011). Role of astroglial connexin30 in hippocampal gap junction coupling. Glia *59*, 511-519.
Grinevich, V., Knobloch-Bollmann, H.S., Eliava, M., Busnelli, M., and Chini, B. (2016). Assembling the Puzzle: Pathways of Oxytocin Signaling in the Brain. Biol Psychiatry *79*, 155-164.
Gros, D., Dupays, L., Alcolea, S., Meysen, S., Miquerol, L., and Theveniau-Ruissy, M. (2004). Genetically modified mice: tools to decode the functions of connexins in the heart-new models for cardiovascular research. Cardiovasc Res *62*, 299-308.
Grosche, J., Kettenmann, H., and Reichenbach, A. (2002). Bergmann glial cells form distinct morphological structures to interact with cerebellar neurons. J Neurosci Res *68*, 138-149.
Guldner, F.H., and Wolff, J.R. (1973). Multi-lamellar astroglial wrapping of neuronal elements in the hypothalamus of rat. Experientia *29*, 1355-1356.
Gunton, J.E., Sisavanh, M., Stokes, R.A., Satin, J., Satin, L.S., Zhang, M., Liu, S.M., Cai, W., Cheng, K., Cooney, G.J.*, et al.* (2012). Mice deficient in GEM GTPase show abnormal glucose homeostasis due to defects in beta-cell calcium handling. PLoS One *7*, e39462.
Gutkowska, J., and Jankowski, M. (2012). Oxytocin revisited: its role in cardiovascular regulation. J Neuroendocrinol *24*, 599-608.
Hagen, G., Dennig, J., Preiss, A., Beato, M., and Suske, G. (1995). Functional analyses of the transcription factor Sp4 reveal properties distinct from Sp1 and Sp3. J Biol Chem *270*, 24989-24994.
Halassa, M.M., Fellin, T., and Haydon, P.G. (2007a). The tripartite synapse: roles for gliotransmission in health and disease. Trends Mol Med *13*, 54-63.
Halassa, M.M., Fellin, T., Takano, H., Dong, J.H., and Haydon, P.G. (2007b). Synaptic islands defined by the territory of a single astrocyte. J Neurosci *27*, 6473-6477.
Halbach, P., Pillers, D.A., York, N., Asuma, M.P., Chiu, M.A., Luo, W., Tokarz, S., Bird, I.M., and Pattnaik, B.R. (2015). Oxytocin expression and function in the posterior retina: a novel signaling pathway. Invest Ophthalmol Vis Sci *56*, 751-760.
Hall, A. (1998). Rho GTPases and the actin cytoskeleton. Science *279*, 509-514.
Han, X., Chen, M., Wang, F., Windrem, M., Wang, S., Shanz, S., Xu, Q., Oberheim, N.A., Bekar, L., Betstadt, S.*, et al.* (2013). Forebrain engraftment by human glial progenitor cells enhances synaptic plasticity and learning in adult mice. Cell Stem Cell *12*, 342-353.
Harris, A.L. (2007). Connexin channel permeability to cytoplasmic molecules. Prog Biophys Mol Biol *94*, 120-143.
Hartline, D.K. (2011). The evolutionary origins of glia. Glia *59*, 1215-1236.
Hasbi, A., Devost, D., Laporte, S.A., and Zingg, H.H. (2004). Real-time detection of interactions between the human oxytocin receptor and G protein-coupled receptor kinase-2. Mol Endocrinol *18*, 1277-1286.

Hatton, G.I. (1990). Emerging concepts of structure-function dynamics in adult brain: the hypothalamo-neurohypophysial system. Prog Neurobiol *34*, 437-504.
Hatzoglou, A., Ader, I., Splingard, A., Flanders, J., Saade, E., Leroy, I., Traver, S., Aresta, S., and de Gunzburg, J. (2007). Gem associates with Ezrin and acts via the Rho-GAP protein Gmip to down-regulate the Rho pathway. Mol Biol Cell *18*, 1242-1252.
Heller, J.P., and Rusakov, D.A. (2015). Morphological plasticity of astroglia: Understanding synaptic microenvironment. Glia *63*, 2133-2151.
Henneberger, C., Papouin, T., Oliet, S.H., and Rusakov, D.A. (2010). Long-term potentiation depends on release of D-serine from astrocytes. Nature *463*, 232-236.
Hernandez, M., Shao, Q., Yang, X.J., Luh, S.P., Kandouz, M., Batist, G., Laird, D.W., and Alaoui-Jamali, M.A. (2006). A histone deacetylation-dependent mechanism for transcriptional repression of the gap junction gene cx43 in prostate cancer cells. Prostate *66*, 1151-1161.
Hertz, L. (1965). Possible role of neuroglia: a potassium-mediated neuronal--neuroglial--neuronal impulse transmission system. Nature *206*, 1091-1094.
Herve, J.C., and Derangeon, M. (2013). Gap-junction-mediated cell-to-cell communication. Cell Tissue Res *352*, 21-31.
Hild, W., Chang, J.J., and Tasaki, I. (1958). Electrical responses of astrocytic glia from the mammalian central nervous system cultivated in vitro. Experientia *14*, 220-221.
Hirrlinger, J., Hulsmann, S., and Kirchhoff, F. (2004). Astroglial processes show spontaneous motility at active synaptic terminals in situ. Eur J Neurosci *20*, 2235-2239.
Hol, E.M., and Pekny, M. (2015). Glial fibrillary acidic protein (GFAP) and the astrocyte intermediate filament system in diseases of the central nervous system. Curr Opin Cell Biol *32*, 121-130.
Holtje, M., Hoffmann, A., Hofmann, F., Mucke, C., Grosse, G., Van Rooijen, N., Kettenmann, H., Just, I., and Ahnert-Hilger, G. (2005). Role of Rho GTPase in astrocyte morphology and migratory response during in vitro wound healing. J Neurochem *95*, 1237-1248.
Hong, Y., Zhao, T., Li, X.J., and Li, S. (2017). Mutant Huntingtin Inhibits alphaB-Crystallin Expression and Impairs Exosome Secretion from Astrocytes. J Neurosci *37*, 9550-9563.
Houades, V., Rouach, N., Ezan, P., Kirchhoff, F., Koulakoff, A., and Giaume, C. (2006). Shapes of astrocyte networks in the juvenile brain. Neuron Glia Biol *2*, 3-14.
Hoyle, C.H. (1999). Neuropeptide families and their receptors: evolutionary perspectives. Brain Res *848*, 1-25.
Huang, H., Michetti, C., Busnelli, M., Manago, F., Sannino, S., Scheggia, D., Giancardo, L., Sona, D., Murino, V., Chini, B.*, et al.* (2014). Chronic and acute intranasal oxytocin produce divergent social effects in mice. Neuropsychopharmacology *39*, 1102-1114.
Huckstepp, R.T., id Bihi, R., Eason, R., Spyer, K.M., Dicke, N., Willecke, K., Marina, N., Gourine, A.V., and Dale, N. (2010). Connexin hemichannel-mediated CO2-dependent release of ATP in the medulla oblongata contributes to central respiratory chemosensitivity. J Physiol *588*, 3901-3920.
Hung, C.Y., Hsu, T.I., Chuang, J.Y., Su, T.P., Chang, W.C., and Hung, J.J. (2020). Sp1 in Astrocyte Is Important for Neurite Outgrowth and Synaptogenesis. Mol Neurobiol *57*, 261-277.
Ivell, R., and Richter, D. (1984). Structure and comparison of the oxytocin and vasopressin genes from rat. Proc Natl Acad Sci U S A *81*, 2006-2010.
Jaffe, A.B., and Hall, A. (2005). Rho GTPases: biochemistry and biology. Annu Rev Cell Dev Biol *21*, 247-269.
John, G.R., Chen, L., Rivieccio, M.A., Melendez-Vasquez, C.V., Hartley, A., and Brosnan, C.F. (2004). Interleukin-1beta induces a reactive astroglial phenotype via deactivation of the Rho GTPase-Rock axis. J Neurosci *24*, 2837-2845.
Johnson, J.L., Monfregola, J., Napolitano, G., Kiosses, W.B., and Catz, S.D. (2012). Vesicular trafficking through cortical actin during exocytosis is regulated by the Rab27a effector JFC1/Slp1 and the RhoA-GTPase-activating protein Gem-interacting protein. Mol Biol Cell *23*, 1902-1916.
Johnson, R.G., Meyer, R.A., Li, X.R., Preus, D.M., Tan, L., Grunenwald, H., Paulson, A.F., Laird, D.W., and Sheridan, J.D. (2002). Gap junctions assemble in the presence of cytoskeletal inhibitors, but enhanced assembly requires microtubules. Exp Cell Res *275*, 67-80.

Jungblut, M., Tiveron, M.C., Barral, S., Abrahamsen, B., Knobel, S., Pennartz, S., Schmitz, J., Perraut, M., Pfrieger, F.W., Stoffel, W., *et al.* (2012). Isolation and characterization of living primary astroglial cells using the new GLAST-specific monoclonal antibody ACSA-1. Glia *60*, 894-907.
Jurek, B., and Neumann, I.D. (2018). The Oxytocin Receptor: From Intracellular Signaling to Behavior. Physiol Rev *98*, 1805-1908.
Jurek, B., Slattery, D.A., Hiraoka, Y., Liu, Y., Nishimori, K., Aguilera, G., Neumann, I.D., and van den Burg, E.H. (2015). Oxytocin Regulates Stress-Induced Crf Gene Transcription through CREB-Regulated Transcription Coactivator 3. J Neurosci *35*, 12248-12260.
Jurek, B., Slattery, D.A., Maloumby, R., Hillerer, K., Koszinowski, S., Neumann, I.D., and van den Burg, E.H. (2012). Differential contribution of hypothalamic MAPK activity to anxiety-like behaviour in virgin and lactating rats. PLoS One *7*, e37060.
Kadonaga, J.T., Carner, K.R., Masiarz, F.R., and Tjian, R. (1987). Isolation of cDNA encoding transcription factor Sp1 and functional analysis of the DNA binding domain. Cell *51*, 1079-1090.
Kalman, D., Gomperts, S.N., Hardy, S., Kitamura, M., and Bishop, J.M. (1999). Ras family GTPases control growth of astrocyte processes. Mol Biol Cell *10*, 1665-1683.
Kameritsch, P., Pogoda, K., and Pohl, U. (2012). Channel-independent influence of connexin 43 on cell migration. Biochim Biophys Acta *1818*, 1993-2001.
Kang, N., Xu, J., Xu, Q., Nedergaard, M., and Kang, J. (2005). Astrocytic glutamate release-induced transient depolarization and epileptiform discharges in hippocampal CA1 pyramidal neurons. J Neurophysiol *94*, 4121-4130.
Kawano, Y., Fukata, Y., Oshiro, N., Amano, M., Nakamura, T., Ito, M., Matsumura, F., Inagaki, M., and Kaibuchi, K. (1999). Phosphorylation of myosin-binding subunit (MBS) of myosin phosphatase by Rho-kinase in vivo. J Cell Biol *147*, 1023-1038.
Khan-Dawood, F.S., Yang, J., and Dawood, M.Y. (1998). Hormonal regulation of connexin-43 in baboon corpora lutea. J Endocrinol *157*, 405-414.
Kim, H.J., Kim, M.J., Mostafa, M.N., Park, J.H., Choi, H.S., Kim, Y.S., and Choi, E.K. (2020). RhoA/ROCK Regulates Prion Pathogenesis by Controlling Connexin 43 Activity. Int J Mol Sci *21*.
Kim, S.H., MacIntyre, D.A., Firmino Da Silva, M., Blanks, A.M., Lee, Y.S., Thornton, S., Bennett, P.R., and Terzidou, V. (2015). Oxytocin activates NF-kappaB-mediated inflammatory pathways in human gestational tissues. Mol Cell Endocrinol *403*, 64-77.
Kim, S.H., Pohl, O., Chollet, A., Gotteland, J.P., Fairhurst, A.D., Bennett, P.R., and Terzidou, V. (2017). Differential Effects of Oxytocin Receptor Antagonists, Atosiban and Nolasiban, on Oxytocin Receptor-Mediated Signaling in Human Amnion and Myometrium. Mol Pharmacol *91*, 403-415.
Kimelberg, H.K. (2004). Water homeostasis in the brain: basic concepts. Neuroscience *129*, 851-860.
Kimura, T., Tanizawa, O., Mori, K., Brownstein, M.J., and Okayama, H. (1992). Structure and expression of a human oxytocin receptor. Nature *356*, 526-529.
Kjenseth, A., Fykerud, T., Rivedal, E., and Leithe, E. (2010). Regulation of gap junction intercellular communication by the ubiquitin system. Cell Signal *22*, 1267-1273.
Klein, B.Y., Tamir, H., Hirschberg, D.L., Glickstein, S.B., and Welch, M.G. (2013). Oxytocin modulates mTORC1 pathway in the gut. Biochem Biophys Res Commun *432*, 466-471.
Knobloch, H.S., Charlet, A., Hoffmann, L.C., Eliava, M., Khrulev, S., Cetin, A.H., Osten, P., Schwarz, M.K., Seeburg, P.H., Stoop, R., *et al.* (2012). Evoked axonal oxytocin release in the central amygdala attenuates fear response. Neuron *73*, 553-566.
Knobloch, H.S., and Grinevich, V. (2014). Evolution of oxytocin pathways in the brain of vertebrates. Front Behav Neurosci *8*, 31.
Koba, S., Hanai, E., Kumada, N., Kataoka, N., Nakamura, K., and Watanabe, T. (2018). Sympathoexcitation by hypothalamic paraventricular nucleus neurons projecting to the rostral ventrolateral medulla. J Physiol *596*, 4581-4595.
Koulakoff, A., Ezan, P., and Giaume, C. (2008). Neurons control the expression of connexin 30 and connexin 43 in mouse cortical astrocytes. Glia *56*, 1299-1311.
Koyama, Y., Baba, A., and Iwata, H. (1991). L-glutamate-induced swelling of cultured astrocytes is dependent on extracellular Ca2+. Neurosci Lett *122*, 210-212.

Krey, J.F., Pasca, S.P., Shcheglovitov, A., Yazawa, M., Schwemberger, R., Rasmusson, R., and Dolmetsch, R.E. (2013). Timothy syndrome is associated with activity-dependent dendritic retraction in rodent and human neurons. Nat Neurosci *16*, 201-209.
Kriegstein, A., and Alvarez-Buylla, A. (2009). The glial nature of embryonic and adult neural stem cells. Annu Rev Neurosci *32*, 149-184.
Ku, C.Y., Qian, A., Wen, Y., Anwer, K., and Sanborn, B.M. (1995). Oxytocin stimulates myometrial guanosine triphosphatase and phospholipase-C activities via coupling to G alpha q/11. Endocrinology *136*, 1509-1515.
Kumar, P., Godbole, N.M., Chaturvedi, C.P., Singh, R.S., George, N., Upadhyay, A., Anjum, B., Godbole, M.M., and Sinha, R.A. (2018). Mechanisms involved in epigenetic down-regulation of Gfap under maternal hypothyroidism. Biochem Biophys Res Commun *502*, 375-381.
Kunzelmann, P., Schroder, W., Traub, O., Steinhauser, C., Dermietzel, R., and Willecke, K. (1999). Late onset and increasing expression of the gap junction protein connexin30 in adult murine brain and long-term cultured astrocytes. Glia *25*, 111-119.
Labuschagne, I., Phan, K.L., Wood, A., Angstadt, M., Chua, P., Heinrichs, M., Stout, J.C., and Nathan, P.J. (2010). Oxytocin attenuates amygdala reactivity to fear in generalized social anxiety disorder. Neuropsychopharmacology *35*, 2403-2413.
Landgraf, R., and Neumann, I.D. (2004). Vasopressin and oxytocin release within the brain: a dynamic concept of multiple and variable modes of neuropeptide communication. Front Neuroendocrinol *25*, 150-176.
Langle, S.L., Poulain, D.A., and Theodosis, D.T. (2003). Induction of rapid, activity-dependent neuronal-glial remodelling in the adult rat hypothalamus in vitro. Eur J Neurosci *18*, 206-214.
Lavialle, M., Aumann, G., Anlauf, E., Prols, F., Arpin, M., and Derouiche, A. (2011). Structural plasticity of perisynaptic astrocyte processes involves ezrin and metabotropic glutamate receptors. Proc Natl Acad Sci U S A *108*, 12915-12919.
Lema, S.C., Sanders, K.E., and Walti, K.A. (2015). Arginine vasotocin, isotocin and nonapeptide receptor gene expression link to social status and aggression in sex-dependent patterns. J Neuroendocrinol *27*, 142-157.
Leng, G., and Ludwig, M. (2008). Neurotransmitters and peptides: whispered secrets and public announcements. J Physiol *586*, 5625-5632.
Lenhossék, M. (1895). Der feinere Bau des Nervsensystems im Lichte neuester Forschung. Berlin: Fischer’s Medicinische Buchhandlung H Kornfield.
Leone, A., Mitsiades, N., Ward, Y., Spinelli, B., Poulaki, V., Tsokos, M., and Kelly, K. (2001). The Gem GTP-binding protein promotes morphological differentiation in neuroblastoma. Oncogene *20*, 3217-3225.
Lestanova, Z., Bacova, Z., Kiss, A., Havranek, T., Strbak, V., and Bakos, J. (2016). Oxytocin Increases Neurite Length and Expression of Cytoskeletal Proteins Associated with Neuronal Growth. J Mol Neurosci *59*, 184-192.
Lestanova, Z., Puerta, F., Alanazi, M., Bacova, Z., Kiss, A., Castejon, A.M., and Bakos, J. (2017). Downregulation of Oxytocin Receptor Decreases the Length of Projections Stimulated by Retinoic Acid in the U-87MG Cells. Neurochem Res *42*, 1006-1014.
Li, D., Liu, X., Liu, T., Liu, H., Tong, L., Jia, S., and Wang, Y.F. (2020). Neurochemical regulation of the expression and function of glial fibrillary acidic protein in astrocytes. Glia *68*, 878-897.
Li, J., Khankan, R.R., Caneda, C., Godoy, M.I., Haney, M.S., Krawczyk, M.C., Bassik, M.C., Sloan, S.A., and Zhang, Y. (2019). Astrocyte-to-astrocyte contact and a positive feedback loop of growth factor signaling regulate astrocyte maturation. Glia *67*, 1571-1597.
Li, L., and Davie, J.R. (2010). The role of Sp1 and Sp3 in normal and cancer cell biology. Ann Anat *192*, 275-283.
Li, L., He, S., Sun, J.M., and Davie, J.R. (2004). Gene regulation by Sp1 and Sp3. Biochem Cell Biol *82*, 460-471.
Liao, J.K., Seto, M., and Noma, K. (2007). Rho kinase (ROCK) inhibitors. J Cardiovasc Pharmacol *50*, 17-24.

Lin, Y.T., Huang, C.C., and Hsu, K.S. (2012). Oxytocin promotes long-term potentiation by enhancing epidermal growth factor receptor-mediated local translation of protein kinase Mzeta. J Neurosci *32*, 15476-15488.
Lippman Bell, J.J., Lordkipanidze, T., Cobb, N., and Dunaevsky, A. (2010). Bergmann glial ensheathment of dendritic spines regulates synapse number without affecting spine motility. Neuron Glia Biol *6*, 193-200.
Lovatt, D., Sonnewald, U., Waagepetersen, H.S., Schousboe, A., He, W., Lin, J.H., Han, X., Takano, T., Wang, S., Sim, F.J.*, et al.* (2007). The transcriptome and metabolic gene signature of protoplasmic astrocytes in the adult murine cortex. J Neurosci *27*, 12255-12266.
Ludwin, S.K., Kosek, J.C., and Eng, L.F. (1976). The topographical distribution of S-100 and GFA proteins in the adult rat brain: an immunohistochemical study using horseradish peroxidase-labelled antibodies. J Comp Neurol *165*, 197-207.
Lundgaard, I., Osorio, M.J., Kress, B.T., Sanggaard, S., and Nedergaard, M. (2014). White matter astrocytes in health and disease. Neuroscience *276*, 161-173.
MacDonald, K., and Feifel, D. (2014). Oxytocin's role in anxiety: a critical appraisal. Brain Res *1580*, 22-56.
Magavi, S., Friedmann, D., Banks, G., Stolfi, A., and Lois, C. (2012). Coincident generation of pyramidal neurons and protoplasmic astrocytes in neocortical columns. J Neurosci *32*, 4762-4772.
Maguire, J., Santoro, T., Jensen, P., Siebenlist, U., Yewdell, J., and Kelly, K. (1994). Gem: an induced, immediate early protein belonging to the Ras family. Science *265*, 241-244.
Mahalakshmi, R.N., Nagashima, K., Ng, M.Y., Inagaki, N., Hunziker, W., and Beguin, P. (2007a). Nuclear transport of Kir/Gem requires specific signals and importin alpha5 and is regulated by calmodulin and predicted serine phosphorylations. Traffic *8*, 1150-1163.
Mahalakshmi, R.N., Ng, M.Y., Guo, K., Qi, Z., Hunziker, W., and Beguin, P. (2007b). Nuclear localization of endogenous RGK proteins and modulation of cell shape remodeling by regulated nuclear transport. Traffic *8*, 1164-1178.
Mamrut, S., Harony, H., Sood, R., Shahar-Gold, H., Gainer, H., Shi, Y.J., Barki-Harrington, L., and Wagner, S. (2013). DNA methylation of specific CpG sites in the promoter region regulates the transcription of the mouse oxytocin receptor. PLoS One *8*, e56869.
Mao, X., Moerman-Herzog, A.M., Wang, W., and Barger, S.W. (2006). Differential transcriptional control of the superoxide dismutase-2 kappaB element in neurons and astrocytes. J Biol Chem *281*, 35863-35872.
Mao, X., Moerman, A.M., and Barger, S.W. (2002). Neuronal kappa B-binding factors consist of Sp1-related proteins. Functional implications for autoregulation of N-methyl-D-aspartate receptor-1 expression. J Biol Chem *277*, 44911-44919.
Mao, X.R., Moerman-Herzog, A.M., Chen, Y., and Barger, S.W. (2009). Unique aspects of transcriptional regulation in neurons--nuances in NFkappaB and Sp1-related factors. J Neuroinflammation *6*, 16.
Marlin, B.J., Mitre, M., D'Amour J, A., Chao, M.V., and Froemke, R.C. (2015). Oxytocin enables maternal behaviour by balancing cortical inhibition. Nature *520*, 499-504.
Martin, R., Bajo-Graneras, R., Moratalla, R., Perea, G., and Araque, A. (2015). Circuit-specific signaling in astrocyte-neuron networks in basal ganglia pathways. Science *349*, 730-734.
Martinetz, S., Meinung, C.P., Jurek, B., von Schack, D., van den Burg, E.H., Slattery, D.A., and Neumann, I.D. (2019). De Novo Protein Synthesis Mediated by the Eukaryotic Elongation Factor 2 Is Required for the Anxiolytic Effect of Oxytocin. Biol Psychiatry *85*, 802-811.
Matsuuchi, L., and Naus, C.C. (2013). Gap junction proteins on the move: connexins, the cytoskeleton and migration. Biochim Biophys Acta *1828*, 94-108.
Meme, W., Vandecasteele, M., Giaume, C., and Venance, L. (2009). Electrical coupling between hippocampal astrocytes in rat brain slices. Neurosci Res *63*, 236-243.
Meyer, M., Berger, I., Winter, J., and Jurek, B. (2018). Oxytocin alters the morphology of hypothalamic neurons via the transcription factor myocyte enhancer factor 2A (MEF-2A). Mol Cell Endocrinol *477*, 156-162.

Meyer, M., Kuffner, K., Winter, J., Neumann, I.D., Wetzel, C.H., and Jurek, B. (2020). Myocyte Enhancer Factor 2A (MEF2A) Defines Oxytocin-Induced Morphological Effects and Regulates Mitochondrial Function in Neurons. Int J Mol Sci *21*.
Michinaga, S., Ishida, A., Takeuchi, R., and Koyama, Y. (2013). Endothelin-1 stimulates cyclin D1 expression in rat cultured astrocytes via activation of Sp1. Neurochem Int *63*, 25-34.
Mikoshiba, K. (2007). IP3 receptor/Ca2+ channel: from discovery to new signaling concepts. J Neurochem *102*, 1426-1446.
Mishima, T., and Hirase, H. (2010). In vivo intracellular recording suggests that gray matter astrocytes in mature cerebral cortex and hippocampus are electrophysiologically homogeneous. J Neurosci *30*, 3093-3100.
Mittaud, P., Labourdette, G., Zingg, H., and Guenot-Di Scala, D. (2002). Neurons modulate oxytocin receptor expression in rat cultured astrocytes: involvement of TGF-beta and membrane components. Glia *37*, 169-177.
Mittelbronn, M., Dietz, K., Schluesener, H.J., and Meyermann, R. (2001). Local distribution of microglia in the normal adult human central nervous system differs by up to one order of magnitude. Acta Neuropathol *101*, 249-255.
Mohr, E., Bahnsen, U., Kiessling, C., and Richter, D. (1988). Expression of the vasopressin and oxytocin genes in rats occurs in mutually exclusive sets of hypothalamic neurons. FEBS Lett *242*, 144-148.
Mohr, E., and Richter, D. (2003). Local synthesis of the rat Vasopressin precursor in dendrites of in vitro cultured nerve cells. Brain Res Mol Brain Res *114*, 115-122.
Montagnese, C., Poulain, D.A., and Theodosis, D.T. (1990). Influence of ovarian steroids on the ultrastructural plasticity of the adult rat supraoptic nucleus induced by central administration of oxytocin. J Neuroendocrinol *2*, 225-231.
Morris, J.F., and Pow, D.V. (1991). Widespread release of peptides in the central nervous system: quantitation of tannic acid-captured exocytoses. Anat Rec *231*, 437-445.
Morrison, R.S., and de Vellis, J. (1981). Growth of purified astrocytes in a chemically defined medium. Proc Natl Acad Sci U S A *78*, 7205-7209.
Mugele, K., Kugler, H., and Spiess, J. (1993). Immortalization of a fetal rat brain cell line that expresses corticotropin-releasing factor mRNA. DNA Cell Biol *12*, 119-126.
Mugnaini, E. (1986). Cell junctions of astrocytes, ependymal and related cells in the mammal central nervous system, with emphasis on the hypothesis of a generalized syncytium of supporting cells. In: *Astrocytes*, edited by Federoff S, Vernadakis A New York: Academic, 329-371.
Müller, H. (1851). Zur Histologie der Netzhaut. Z Wiss Zool, 234-237.
Murtazina, D.A., Chung, D., Ulloa, A., Bryan, E., Galan, H.L., and Sanborn, B.M. (2011). TRPC1, STIM1, and ORAI influence signal-regulated intracellular and endoplasmic reticulum calcium dynamics in human myometrial cells. Biol Reprod *85*, 315-326.
Nagelhus, E.A., Mathiisen, T.M., and Ottersen, O.P. (2004). Aquaporin-4 in the central nervous system: cellular and subcellular distribution and coexpression with KIR4.1. Neuroscience *129*, 905-913.
Nagy, J.I., Dudek, F.E., and Rash, J.E. (2004). Update on connexins and gap junctions in neurons and glia in the mammalian nervous system. Brain Res Brain Res Rev *47*, 191-215.
Nagy, J.I., Lynn, B.D., Tress, O., Willecke, K., and Rash, J.E. (2011). Connexin26 expression in brain parenchymal cells demonstrated by targeted connexin ablation in transgenic mice. Eur J Neurosci *34*, 263-271.
Nagy, J.I., Patel, D., Ochalski, P.A., and Stelmack, G.L. (1999). Connexin30 in rodent, cat and human brain: selective expression in gray matter astrocytes, co-localization with connexin43 at gap junctions and late developmental appearance. Neuroscience *88*, 447-468.
Neary, J.T., Kang, Y., and Shi, Y.F. (2004). Signaling from nucleotide receptors to protein kinase cascades in astrocytes. Neurochem Res *29*, 2037-2042.

Nerb, J. (2020). Oxytocin receptor mediated signaling pathways in astrocytes and neuronal cells. Bachelor Thesis.
Ng, T., Parsons, M., Hughes, W.E., Monypenny, J., Zicha, D., Gautreau, A., Arpin, M., Gschmeissner, S., Verveer, P.J., Bastiaens, P.I., *et al.* (2001). Ezrin is a downstream effector of trafficking PKC-integrin complexes involved in the control of cell motility. Embo j *20*, 2723-2741.
Nielsen, S., Nagelhus, E.A., Amiry-Moghaddam, M., Bourque, C., Agre, P., and Ottersen, O.P. (1997). Specialized membrane domains for water transport in glial cells: high-resolution immunogold cytochemistry of aquaporin-4 in rat brain. J Neurosci *17*, 171-180.
Nimlamool, W., Andrews, R.M., and Falk, M.M. (2015). Connexin43 phosphorylation by PKC and MAPK signals VEGF-mediated gap junction internalization. Mol Biol Cell *26*, 2755-2768.
Nishida, H., and Okabe, S. (2007). Direct astrocytic contacts regulate local maturation of dendritic spines. J Neurosci *27*, 331-340.
Nolte, C., Matyash, M., Pivneva, T., Schipke, C.G., Ohlemeyer, C., Hanisch, U.K., Kirchhoff, F., and Kettenmann, H. (2001). GFAP promoter-controlled EGFP-expressing transgenic mice: a tool to visualize astrocytes and astrogliosis in living brain tissue. Glia *33*, 72-86.
Ogata, K., and Kosaka, T. (2002). Structural and quantitative analysis of astrocytes in the mouse hippocampus. Neuroscience *113*, 221-233.
Oikonomou, G., and Shaham, S. (2011). The glia of Caenorhabditis elegans. Glia *59*, 1253-1263.
Oliet, S.H., Piet, R., and Poulain, D.A. (2001). Control of glutamate clearance and synaptic efficacy by glial coverage of neurons. Science *292*, 923-926.
Olk, S., Turchinovich, A., Grzendowski, M., Stuhler, K., Meyer, H.E., Zoidl, G., and Dermietzel, R. (2010). Proteomic analysis of astroglial connexin43 silencing uncovers a cytoskeletal platform involved in process formation and migration. Glia *58*, 494-505.
Olk, S., Zoidl, G., and Dermietzel, R. (2009). Connexins, cell motility, and the cytoskeleton. Cell Motil Cytoskeleton *66*, 1000-1016.
Opatowsky, Y., Sasson, Y., Shaked, I., Ward, Y., Chomsky-Hecht, O., Litvak, Y., Selinger, Z., Kelly, K., and Hirsch, J.A. (2006). Structure-function studies of the G-domain from human gem, a novel small G-protein. FEBS Lett *580*, 5959-5964.
Orellana, J.A., Saez, P.J., Cortes-Campos, C., Elizondo, R.J., Shoji, K.F., Contreras-Duarte, S., Figueroa, V., Velarde, V., Jiang, J.X., Nualart, F., *et al.* (2012). Glucose increases intracellular free Ca(2+) in tanycytes via ATP released through connexin 43 hemichannels. Glia *60*, 53-68.
Orellana, J.A., Saez, P.J., Shoji, K.F., Schalper, K.A., Palacios-Prado, N., Velarde, V., Giaume, C., Bennett, M.V., and Saez, J.C. (2009). Modulation of brain hemichannels and gap junction channels by pro-inflammatory agents and their possible role in neurodegeneration. Antioxid Redox Signal *11*, 369-399.
Orkand, R.K., Nicholls, J.G., and Kuffler, S.W. (1966). Effect of nerve impulses on the membrane potential of glial cells in the central nervous system of amphibia. J Neurophysiol *29*, 788-806.
Ostroff, L.E., Manzur, M.K., Cain, C.K., and Ledoux, J.E. (2014). Synapses lacking astrocyte appear in the amygdala during consolidation of Pavlovian threat conditioning. J Comp Neurol *522*, 2152-2163.
Ostrowski, N.L., Young, W.S., 3rd, and Lolait, S.J. (1995). Estrogen increases renal oxytocin receptor gene expression. Endocrinology *136*, 1801-1804.
Palanisamy, A., Kannappan, R., Xu, Z., Martino, A., Friese, M.B., Boyd, J.D., Crosby, G., and Culley, D.J. (2018). Oxytocin alters cell fate selection of rat neural progenitor cells in vitro. PLoS One *13*, e0191160.
Panatier, A., Theodosis, D.T., Mothet, J.P., Touquet, B., Pollegioni, L., Poulain, D.A., and Oliet, S.H. (2006). Glia-derived D-serine controls NMDA receptor activity and synaptic memory. Cell *125*, 775-784.
Pannasch, U., Dossi, E., Ezan, P., and Rouach, N. (2019). Astroglial Cx30 sustains neuronal population bursts independently of gap-junction mediated biochemical coupling. Glia *67*, 1104-1112.
Pannasch, U., Freche, D., Dallerac, G., Ghezali, G., Escartin, C., Ezan, P., Cohen-Salmon, M., Benchenane, K., Abudara, V., Dufour, A., *et al.* (2014). Connexin 30 sets synaptic strength by controlling astroglial synapse invasion. Nat Neurosci *17*, 549-558.
Pannasch, U., and Rouach, N. (2013). Emerging role for astroglial networks in information processing: from synapse to behavior. Trends Neurosci *36*, 405-417.

Pannasch, U., Vargova, L., Reingruber, J., Ezan, P., Holcman, D., Giaume, C., Sykova, E., and Rouach, N. (2011). Astroglial networks scale synaptic activity and plasticity. Proc Natl Acad Sci U S A *108*, 8467-8472.
Pardo, L., Valor, L.M., Eraso-Pichot, A., Barco, A., Golbano, A., Hardingham, G.E., Masgrau, R., and Galea, E. (2017). CREB Regulates Distinct Adaptive Transcriptional Programs in Astrocytes and Neurons. Sci Rep *7*, 6390.
Pekny, M., Johansson, C.B., Eliasson, C., Stakeberg, J., Wallen, A., Perlmann, T., Lendahl, U., Betsholtz, C., Berthold, C.H., and Frisen, J. (1999). Abnormal reaction to central nervous system injury in mice lacking glial fibrillary acidic protein and vimentin. J Cell Biol *145*, 503-514.
Pelvig, D.P., Pakkenberg, H., Stark, A.K., and Pakkenberg, B. (2008). Neocortical glial cell numbers in human brains. Neurobiol Aging *29*, 1754-1762.
Penes, M.C., Li, X., and Nagy, J.I. (2005). Expression of zonula occludens-1 (ZO-1) and the transcription factor ZO-1-associated nucleic acid-binding protein (ZONAB)-MsY3 in glial cells and colocalization at oligodendrocyte and astrocyte gap junctions in mouse brain. Eur J Neurosci *22*, 404-418.
Peters, S., Slattery, D.A., Uschold-Schmidt, N., Reber, S.O., and Neumann, I.D. (2014). Dose-dependent effects of chronic central infusion of oxytocin on anxiety, oxytocin receptor binding and stress-related parameters in mice. Psychoneuroendocrinology *42*, 225-236.
Philipsen, S., and Suske, G. (1999). A tale of three fingers: the family of mammalian Sp/XKLF transcription factors. Nucleic Acids Res *27*, 2991-3000.
Piddini, E., Schmid, J.A., de Martin, R., and Dotti, C.G. (2001). The Ras-like GTPase Gem is involved in cell shape remodelling and interacts with the novel kinesin-like protein KIF9. Embo j *20*, 4076-4087.
Pidoux, G., Gerbaud, P., Dompierre, J., Lygren, B., Solstad, T., Evain-Brion, D., and Tasken, K. (2014). A PKA-ezrin-Cx43 signaling complex controls gap junction communication and thereby trophoblast cell fusion. J Cell Sci *127*, 4172-4185.
Piet, R., Vargova, L., Sykova, E., Poulain, D.A., and Oliet, S.H. (2004). Physiological contribution of the astrocytic environment of neurons to intersynaptic crosstalk. Proc Natl Acad Sci U S A *101*, 2151-2155.
Poitry-Yamate, C.L., Vutskits, L., and Rauen, T. (2002). Neuronal-induced and glutamate-dependent activation of glial glutamate transporter function. J Neurochem *82*, 987-997.
Ponimaskin, E., Voyno-Yasenetskaya, T., Richter, D.W., Schachner, M., and Dityatev, A. (2007). Morphogenic signaling in neurons via neurotransmitter receptors and small GTPases. Mol Neurobiol *35*, 278-287.
Pont, J.N., McArdle, C.A., and Lopez Bernal, A. (2012). Oxytocin-stimulated NFAT transcriptional activation in human myometrial cells. Mol Endocrinol *26*, 1743-1756.
Postina, R., Kojro, E., and Fahrenholz, F. (1996). Separate agonist and peptide antagonist binding sites of the oxytocin receptor defined by their transfer into the V2 vasopressin receptor. J Biol Chem *271*, 31593-31601.
Pow, D.V., and Morris, J.F. (1989). Dendrites of hypothalamic magnocellular neurons release neurohypophysial peptides by exocytosis. Neuroscience *32*, 435-439.
Qu, C., Gardner, P., and Schrijver, I. (2009). The role of the cytoskeleton in the formation of gap junctions by Connexin 30. Exp Cell Res *315*, 1683-1692.
Quinones-Jenab, V., Jenab, S., Ogawa, S., Adan, R.A., Burbach, J.P., and Pfaff, D.W. (1997). Effects of estrogen on oxytocin receptor messenger ribonucleic acid expression in the uterus, pituitary, and forebrain of the female rat. Neuroendocrinology *65*, 9-17.
Quist, A.P., Rhee, S.K., Lin, H., and Lal, R. (2000). Physiological role of gap-junctional hemichannels. Extracellular calcium-dependent isosmotic volume regulation. J Cell Biol *148*, 1063-1074.
Reichenbach, A. (1989). Glia:neuron index: review and hypothesis to account for different values in various mammals. Glia *2*, 71-77.
Reichenbach, A., Derouiche, A., and Kirchhoff, F. (2010). Morphology and dynamics of perisynaptic glia. Brain Res Rev *63*, 11-25.
Reversi, A., Rimoldi, V., Brambillasca, S., and Chini, B. (2006). Effects of cholesterol manipulation on the signaling of the human oxytocin receptor. Am J Physiol Regul Integr Comp Physiol *291*, R861-869.

Rhodes, C.H., Morrell, J.I., and Pfaff, D.W. (1981). Immunohistochemical analysis of magnocellular elements in rat hypothalamus: distribution and numbers of cells containing neurophysin, oxytocin, and vasopressin. J Comp Neurol *198*, 45-64.
Richard, G. (2000). Connexins: a connection with the skin. Exp Dermatol *9*, 77-96.
Richard, S., and Zingg, H.H. (1990). The human oxytocin gene promoter is regulated by estrogens. J Biol Chem *265*, 6098-6103.
Riento, K., and Ridley, A.J. (2003). Rocks: multifunctional kinases in cell behaviour. Nat Rev Mol Cell Biol *4*, 446-456.
Ripamonti, S., Ambrozkiewicz, M.C., Guzzi, F., Gravati, M., Biella, G., Bormuth, I., Hammer, M., Tuffy, L.P., Sigler, A., Kawabe, H., *et al.* (2017). Transient oxytocin signaling primes the development and function of excitatory hippocampal neurons. Elife *6*.
Romero-Fernandez, W., Borroto-Escuela, D.O., Agnati, L.F., and Fuxe, K. (2013). Evidence for the existence of dopamine D2-oxytocin receptor heteromers in the ventral and dorsal striatum with facilitatory receptor-receptor interactions. Mol Psychiatry *18*, 849-850.
Rouach, N., Koulakoff, A., Abudara, V., Willecke, K., and Giaume, C. (2008). Astroglial metabolic networks sustain hippocampal synaptic transmission. Science *322*, 1551-1555.
Rouach, N., Pebay, A., Meme, W., Cordier, J., Ezan, P., Etienne, E., Giaume, C., and Tence, M. (2006). S1P inhibits gap junctions in astrocytes: involvement of G and Rho GTPase/ROCK. Eur J Neurosci *23*, 1453-1464.
Roux, L., Benchenane, K., Rothstein, J.D., Bonvento, G., and Giaume, C. (2011). Plasticity of astroglial networks in olfactory glomeruli. Proc Natl Acad Sci U S A *108*, 18442-18446.
Rozen, F., Russo, C., Banville, D., and Zingg, H.H. (1995). Structure, characterization, and expression of the rat oxytocin receptor gene. Proc Natl Acad Sci U S A *92*, 200-204.
Rozental, R., Srinivas, M., and Spray, D.C. (2001). How to close a gap junction channel. Efficacies and potencies of uncoupling agents. Methods Mol Biol *154*, 447-476.
Sabatier, N., Caquineau, C., Dayanithi, G., Bull, P., Douglas, A.J., Guan, X.M., Jiang, M., Van der Ploeg, L., and Leng, G. (2003). Alpha-melanocyte-stimulating hormone stimulates oxytocin release from the dendrites of hypothalamic neurons while inhibiting oxytocin release from their terminals in the neurohypophysis. J Neurosci *23*, 10351-10358.
Saez, J.C., Berthoud, V.M., Branes, M.C., Martinez, A.D., and Beyer, E.C. (2003). Plasma membrane channels formed by connexins: their regulation and functions. Physiol Rev *83*, 1359-1400.
Safe, S., and Kim, K. (2004). Nuclear receptor-mediated transactivation through interaction with Sp proteins. Prog Nucleic Acid Res Mol Biol *77*, 1-36.
Sanborn, B.M. (2007). Hormonal signaling and signal pathway crosstalk in the control of myometrial calcium dynamics. Semin Cell Dev Biol *18*, 305-314.
Sasson, Y., Navon-Perry, L., Huppert, D., and Hirsch, J.A. (2011). RGK family G-domain:GTP analog complex structures and nucleotide-binding properties. J Mol Biol *413*, 372-389.
Savchenko, V.L., McKanna, J.A., Nikonenko, I.R., and Skibo, G.G. (2000). Microglia and astrocytes in the adult rat brain: comparative immunocytochemical analysis demonstrates the efficacy of lipocortin 1 immunoreactivity. Neuroscience *96*, 195-203.
Schildge, S., Bohrer, C., Beck, K., and Schachtrup, C. (2013). Isolation and culture of mouse cortical astrocytes. J Vis Exp.
Schlag, B.D., Vondrasek, J.R., Munir, M., Kalandadze, A., Zelenaia, O.A., Rothstein, J.D., and Robinson, M.B. (1998). Regulation of the glial Na+-dependent glutamate transporters by cyclic AMP analogs and neurons. Mol Pharmacol *53*, 355-369.
Schober, A.L., Gagarkin, D.A., Chen, Y., Gao, G., Jacobson, L., and Mongin, A.A. (2016). Recombinant Adeno-Associated Virus Serotype 6 (rAAV6) Potently and Preferentially Transduces Rat Astrocytes In vitro and In vivo. Front Cell Neurosci *10*, 262.
Schumacher, M., Coirini, H., Pfaff, D.W., and McEwen, B.S. (1990). Behavioral effects of progesterone associated with rapid modulation of oxytocin receptors. Science *250*, 691-694.
Serrano, A., Haddjeri, N., Lacaille, J.C., and Robitaille, R. (2006). GABAergic network activation of glial cells underlies hippocampal heterosynaptic depression. J Neurosci *26*, 5370-5382.

Sharma, D., Handa, R.J., and Uht, R.M. (2012). The ERbeta ligand 5alpha-androstane, 3beta,17beta-diol (3beta-diol) regulates hypothalamic oxytocin (Oxt) gene expression. Endocrinology *153*, 2353-2361.
Sherwood, C.C., Stimpson, C.D., Raghanti, M.A., Wildman, D.E., Uddin, M., Grossman, L.I., Goodman, M., Redmond, J.C., Bonar, C.J., Erwin, J.M.*, et al.* (2006). Evolution of increased glia-neuron ratios in the human frontal cortex. Proc Natl Acad Sci U S A *103*, 13606-13611.
Shlykov, S.G., Yang, M., Alcorn, J.L., and Sanborn, B.M. (2003). Capacitative cation entry in human myometrial cells and augmentation by hTrpC3 overexpression. Biol Reprod *69*, 647-655.
Sierra, A., Tremblay, M.E., and Wake, H. (2014). Never-resting microglia: physiological roles in the healthy brain and pathological implications. Front Cell Neurosci *8*, 240.
Sladek, C.D., and Somponpun, S.J. (2004). Oestrogen receptor beta: role in neurohypophyseal neurones. J Neuroendocrinol *16*, 365-371.
Smith, M.P., Ayad, V.J., Mundell, S.J., McArdle, C.A., Kelly, E., and Lopez Bernal, A. (2006). Internalization and desensitization of the oxytocin receptor is inhibited by Dynamin and clathrin mutants in human embryonic kidney 293 cells. Mol Endocrinol *20*, 379-388.
Smyth, J.W., Vogan, J.M., Buch, P.J., Zhang, S.S., Fong, T.S., Hong, T.T., and Shaw, R.M. (2012). Actin cytoskeleton rest stops regulate anterograde traffic of connexin 43 vesicles to the plasma membrane. Circ Res *110*, 978-989.
Soares, M.C., Bshary, R., Mendonca, R., Grutter, A.S., and Oliveira, R.F. (2012). Arginine vasotocin regulation of interspecific cooperative behaviour in a cleaner fish. PLoS One *7*, e39583.
Sofroniew, M.V. (1980). Projections from vasopressin, oxytocin, and neurophysin neurons to neural targets in the rat and human. J Histochem Cytochem *28*, 475-478.
Sofroniew, M.V. (1983). Morphology of vasopressin and oxytocin neurones and their central and vascular projections. Prog Brain Res *60*, 101-114.
Sohl, G., Odermatt, B., Maxeiner, S., Degen, J., and Willecke, K. (2004). New insights into the expression and function of neural connexins with transgenic mouse mutants. Brain Res Brain Res Rev *47*, 245-259.
Splingard, A., Menetrey, J., Perderiset, M., Cicolari, J., Regazzoni, K., Hamoudi, F., Cabanie, L., El Marjou, A., Wells, A., Houdusse, A.*, et al.* (2007). Biochemical and structural characterization of the gem GTPase. J Biol Chem *282*, 1905-1915.
Strosser, M.T., Evrard, M.E., Breton, C., and Guenot-Di Scala, D. (2001). Phorbol ester differentially regulates oxytocin receptor binding activity in hypothalamic cultured neurons and astrocytes. Peptides *22*, 677-683.
Sun, W., Cornwell, A., Li, J., Peng, S., Osorio, M.J., Aalling, N., Wang, S., Benraiss, A., Lou, N., Goldman, S.A*., et al.* (2017). SOX9 Is an Astrocyte-Specific Nuclear Marker in the Adult Brain Outside the Neurogenic Regions. J Neurosci *37*, 4493-4507.
Suske, G., Bruford, E., and Philipsen, S. (2005). Mammalian SP/KLF transcription factors: bring in the family. Genomics *85*, 551-556.
Swanson, L.W., Sawchenko, P.E., Wiegand, S.J., and Price, J.L. (1980). Separate neurons in the paraventricular nucleus project to the median eminence and to the medulla or spinal cord. Brain Res *198*, 190-195.
Swanson, R.A., Liu, J., Miller, J.W., Rothstein, J.D., Farrell, K., Stein, B.A., and Longuemare, M.C. (1997). Neuronal regulation of glutamate transporter subtype expression in astrocytes. J Neurosci *17*, 932-940.
Tabernero, A., Medina, J.M., and Giaume, C. (2006). Glucose metabolism and proliferation in glia: role of astrocytic gap junctions. J Neurochem *99*, 1049-1061.
Tahara, M., Morishige, K., Sawada, K., Ikebuchi, Y., Kawagishi, R., Tasaka, K., and Murata, Y. (2002). RhoA/Rho-kinase cascade is involved in oxytocin-induced rat uterine contraction. Endocrinology *143*, 920-929.
Tan, N.Y., and Khachigian, L.M. (2009). Sp1 phosphorylation and its regulation of gene transcription. Mol Cell Biol *29*, 2483-2488.
Taylor, A.H., Whitley, G.S., and Nussey, S.S. (1989). The interaction of arginine vasopressin and oxytocin with bovine adrenal medulla cells. J Endocrinol *121*, 133-139.

Terzidou, V., Blanks, A.M., Kim, S.H., Thornton, S., and Bennett, P.R. (2011). Labor and inflammation increase the expression of oxytocin receptor in human amnion. Biol Reprod *84*, 546-552.
Terzidou, V., Lee, Y., Lindstrom, T., Johnson, M., Thornton, S., and Bennett, P.R. (2006). Regulation of the human oxytocin receptor by nuclear factor-kappaB and CCAAT/enhancer-binding protein-beta. J Clin Endocrinol Metab *91*, 2317-2326.
Terzidou, V., Sooranna, S.R., Kim, L.U., Thornton, S., Bennett, P.R., and Johnson, M.R. (2005). Mechanical stretch up-regulates the human oxytocin receptor in primary human uterine myocytes. J Clin Endocrinol Metab *90*, 237-246.
Teunissen, B.E., Jansen, A.T., van Amersfoorth, S.C., O'Brien, T.X., Jongsma, H.J., and Bierhuizen, M.F. (2003). Analysis of the rat connexin 43 proximal promoter in neonatal cardiomyocytes. Gene *322*, 123-136.
Theiss, C., and Meller, K. (2002). Microinjected anti-actin antibodies decrease gap junctional intercellular commmunication in cultured astrocytes. Exp Cell Res *281*, 197-204.
Theodosis, D.T. (1985). Oxytocin-immunoreactive terminals synapse on oxytocin neurones in the supraoptic nucleus. Nature *313*, 682-684.
Theodosis, D.T., Chapman, D.B., Montagnese, C., Poulain, D.A., and Morris, J.F. (1986a). Structural plasticity in the hypothalamic supraoptic nucleus at lactation affects oxytocin-, but not vasopressin-secreting neurones. Neuroscience *17*, 661-678.
Theodosis, D.T., Montagnese, C., Rodriguez, F., Vincent, J.D., and Poulain, D.A. (1986b). Oxytocin induces morphological plasticity in the adult hypothalamo-neurohypophysial system. Nature *322*, 738-740.
Thrane, A.S., Rangroo Thrane, V., Zeppenfeld, D., Lou, N., Xu, Q., Nagelhus, E.A., and Nedergaard, M. (2012). General anesthesia selectively disrupts astrocyte calcium signaling in the awake mouse cortex. Proc Natl Acad Sci U S A *109*, 18974-18979.
Tomizawa, K., Iga, N., Lu, Y.F., Moriwaki, A., Matsushita, M., Li, S.T., Miyamoto, O., Itano, T., and Matsui, H. (2003). Oxytocin improves long-lasting spatial memory during motherhood through MAP kinase cascade. Nat Neurosci *6*, 384-390.
Tooze, S.A. (1998). Biogenesis of secretory granules in the trans-Golgi network of neuroendocrine and endocrine cells. Biochim Biophys Acta *1404*, 231-244.
Totsukawa, G., Yamakita, Y., Yamashiro, S., Hartshorne, D.J., Sasaki, Y., and Matsumura, F. (2000). Distinct roles of ROCK (Rho-kinase) and MLCK in spatial regulation of MLC phosphorylation for assembly of stress fibers and focal adhesions in 3T3 fibroblasts. J Cell Biol *150*, 797-806.
Ulloa, A., Gonzales, A.L., Zhong, M., Kim, Y.S., Cantlon, J., Clay, C., Ku, C.Y., Earley, S., and Sanborn, B.M. (2009). Reduction in TRPC4 expression specifically attenuates G-protein coupled receptor-stimulated increases in intracellular calcium in human myometrial cells. Cell Calcium *46*, 73-84.
Upham, B.L., Sovadinova, I., and Babica, P. (2016). Gap Junctional Intercellular Communication: A Functional Biomarker to Assess Adverse Effects of Toxicants and Toxins, and Health Benefits of Natural Products. J Vis Exp.
Valiunas, V., Polosina, Y.Y., Miller, H., Potapova, I.A., Valiuniene, L., Doronin, S., Mathias, R.T., Robinson, R.B., Rosen, M.R., Cohen, I.S., *et al.* (2005). Connexin-specific cell-to-cell transfer of short interfering RNA by gap junctions. J Physiol *568*, 459-468.
Van Aelst, L., and D'Souza-Schorey, C. (1997). Rho GTPases and signaling networks. Genes Dev *11*, 2295-2322.
van den Burg, E.H., Stindl, J., Grund, T., Neumann, I.D., and Strauss, O. (2015). Oxytocin Stimulates Extracellular Ca2+ Influx Through TRPV2 Channels in Hypothalamic Neurons to Exert Its Anxiolytic Effects. Neuropsychopharmacology *40*, 2938-2947.
Van Kesteren, R.E., Smit, A.B., De Lange, R.P., Kits, K.S., Van Golen, F.A., Van Der Schors, R.C., De With, N.D., Burke, J.F., and Geraerts, W.P. (1995). Structural and functional evolution of the vasopressin/oxytocin superfamily: vasopressin-related conopressin is the only member present in Lymnaea, and is involved in the control of sexual behavior. J Neurosci *15*, 5989-5998.
Vanhove, B., Hofer-Warbinek, R., Kapetanopoulos, A., Hofer, E., Bach, F.H., and de Martin, R. (1997). Gem, a GTP-binding protein from mitogen-stimulated T cells, is induced in endothelial cells upon activation by inflammatory cytokines. Endothelium *5*, 51-61.

Vargas-Pinilla, P., Paixao-Cortes, V.R., Pare, P., Tovo-Rodrigues, L., Vieira, C.M., Xavier, A., Comas, D., Pissinatti, A., Sinigaglia, M., Rigo, M.M., *et al.* (2015). Evolutionary pattern in the OXT-OXTR system in primates: coevolution and positive selection footprints. Proc Natl Acad Sci U S A *112*, 88-93.
Venkatachalam, K., Zheng, F., and Gill, D.L. (2003). Regulation of canonical transient receptor potential (TRPC) channel function by diacylglycerol and protein kinase C. J Biol Chem *278*, 29031-29040.
Verkhratsky, A., and Nedergaard, M. (2018). Physiology of Astroglia. Physiol Rev *98*, 239-389.
Villares, G.J., Dobroff, A.S., Wang, H., Zigler, M., Melnikova, V.O., Huang, L., and Bar-Eli, M. (2009). Overexpression of protease-activated receptor-1 contributes to melanoma metastasis via regulation of connexin 43. Cancer Res *69*, 6730-6737.
Vine, A.L., Leung, Y.M., and Bertram, J.S. (2005). Transcriptional regulation of connexin 43 expression by retinoids and carotenoids: similarities and differences. Mol Carcinog *43*, 75-85.
Wall, M.E., Otey, C., Qi, J., and Banes, A.J. (2007). Connexin 43 is localized with actin in tenocytes. Cell Motil Cytoskeleton *64*, 121-130.
Wallraff, A., Odermatt, B., Willecke, K., and Steinhauser, C. (2004). Distinct types of astroglial cells in the hippocampus differ in gap junction coupling. Glia *48*, 36-43.
Walz, W. (2000). Controversy surrounding the existence of discrete functional classes of astrocytes in adult gray matter. Glia *31*, 95-103.
Walz, W., and Lang, M.K. (1998). Immunocytochemical evidence for a distinct GFAP-negative subpopulation of astrocytes in the adult rat hippocampus. Neurosci Lett *257*, 127-130.
Wang, P., Qin, D., and Wang, Y.F. (2017). Oxytocin Rapidly Changes Astrocytic GFAP Plasticity by Differentially Modulating the Expressions of pERK 1/2 and Protein Kinase A. Front Mol Neurosci *10*, 262.
Wang, Y.F., and Hamilton, K. (2009). Chronic vs. acute interactions between supraoptic oxytocin neurons and astrocytes during lactation: role of glial fibrillary acidic protein plasticity. ScientificWorldJournal *9*, 1308-1320.
Wang, Y.F., and Hatton, G.I. (2007). Interaction of extracellular signal-regulated protein kinase 1/2 with actin cytoskeleton in supraoptic oxytocin neurons and astrocytes: role in burst firing. J Neurosci *27*, 13822-13834.
Wang, Y.F., and Hatton, G.I. (2009). Astrocytic plasticity and patterned oxytocin neuronal activity: dynamic interactions. J Neurosci *29*, 1743-1754.
Ward, Y., Spinelli, B., Quon, M.J., Chen, H., Ikeda, S.R., and Kelly, K. (2004). Phosphorylation of critical serine residues in Gem separates cytoskeletal reorganization from down-regulation of calcium channel activity. Mol Cell Biol *24*, 651-661.
Ward, Y., Yap, S.F., Ravichandran, V., Matsumura, F., Ito, M., Spinelli, B., and Kelly, K. (2002). The GTP binding proteins Gem and Rad are negative regulators of the Rho-Rho kinase pathway. J Cell Biol *157*, 291-302.
Wiegand, V., and Gimpl, G. (2012). Specification of the cholesterol interaction with the oxytocin receptor using a chimeric receptor approach. Eur J Pharmacol *676*, 12-19.
Wong, W.K., Chen, K., and Shih, J.C. (2001). Regulation of human monoamine oxidase B gene by Sp1 and Sp3. Mol Pharmacol *59*, 852-859.
Wrzal, P.K., Devost, D., Petrin, D., Goupil, E., Iorio-Morin, C., Laporte, S.A., Zingg, H.H., and Hebert, T.E. (2012). Allosteric interactions between the oxytocin receptor and the beta2-adrenergic receptor in the modulation of ERK1/2 activation are mediated by heterodimerization. Cell Signal *24*, 342-350.
Yang, T., Puckerin, A., and Colecraft, H.M. (2012). Distinct RGK GTPases differentially use alpha1- and auxiliary beta-binding-dependent mechanisms to inhibit CaV1.2/CaV2.2 channels. PLoS One *7*, e37079.
Yeh, C.Y., Verkhratsky, A., Terzieva, S., and Rodriguez, J.J. (2013). Glutamine synthetase in astrocytes from entorhinal cortex of the triple transgenic animal model of Alzheimer's disease is not affected by pathological progression. Biogerontology *14*, 777-787.
Ying, L., Becard, M., Lyell, D., Han, X., Shortliffe, L., Husted, C.I., Alvira, C.M., and Cornfield, D.N. (2015). The transient receptor potential vanilloid 4 channel modulates uterine tone during pregnancy. Sci Transl Med *7*, 319ra204.

Yuan, L., Liu, S., Bai, X., Gao, Y., Liu, G., Wang, X., Liu, D., Li, T., Hao, A., and Wang, Z. (2016). Oxytocin inhibits lipopolysaccharide-induced inflammation in microglial cells and attenuates microglial activation in lipopolysaccharide-treated mice. J Neuroinflammation *13*, 77.
Yun, S.P., Park, S.S., Ryu, J.M., Park, J.H., Kim, M.O., Lee, J.H., and Han, H.J. (2012). Mechanism of PKA-dependent and lipid-raft independent stimulation of Connexin43 expression by oxytoxin in mouse embryonic stem cells. Mol Endocrinol *26*, 1144-1157.
Zamanian, J.L., Xu, L., Foo, L.C., Nouri, N., Zhou, L., Giffard, R.G., and Barres, B.A. (2012). Genomic analysis of reactive astrogliosis. J Neurosci *32*, 6391-6410.
Zeug, A., Muller, F.E., Anders, S., Herde, M.K., Minge, D., Ponimaskin, E., and Henneberger, C. (2018). Control of astrocyte morphology by Rho GTPases. Brain Res Bull *136*, 44-53.
Zhang, Y., Chen, K., Sloan, S.A., Bennett, M.L., Scholze, A.R., O'Keeffe, S., Phatnani, H.P., Guarnieri, P., Caneda, C., Ruderisch, N., *et al.* (2014). An RNA-sequencing transcriptome and splicing database of glia, neurons, and vascular cells of the cerebral cortex. J Neurosci *34*, 11929-11947.
Zhang, Y., Gao, Y., Speth, R.C., Jiang, N., Mao, Y., Sumners, C., and Li, H. (2013). Adenoviral and adeno-associated viral vectors-mediated neuronal gene transfer to cardiovascular control regions of the rat brain. Int J Med Sci *10*, 607-616.
Zhong, M., Yang, M., and Sanborn, B.M. (2003). Extracellular signal-regulated kinase 1/2 activation by myometrial oxytocin receptor involves Galpha(q)Gbetagamma and epidermal growth factor receptor tyrosine kinase activation. Endocrinology *144*, 2947-2956.
Zhou, X.B., Lutz, S., Steffens, F., Korth, M., and Wieland, T. (2007). Oxytocin receptors differentially signal via Gq and Gi proteins in pregnant and nonpregnant rat uterine myocytes: implications for myometrial contractility. Mol Endocrinol *21*, 740-752.

Appendix 1

a) AAV6-GFAP *Gem* shRNA vector

Vector Summary

Vector ID	VB191205-1113khu
Vector Name	pAAV[miR30]-GFAP_long>mCherry:{sh-rGem}:WPRE
Date Created (Pacific Time)	2019-12-04
Vector Size	7040 bp
Viral Genome Size	4443 bp
Vector Type	Mammalian miR30-shRNA Knockdown AAV Vector
Inserted Promoter	GFAP_long
Inserted ORF	mCherry
Inserted shRNA	{sh-rGem}
Target Sequence	AGACAGAAGACATTCCTATAAT
Plasmid Copy Number	High
Antibiotic Resistance	Ampicillin
Cloning Host	VB UltraStable (or alternative strain)

Vector Components

Name	Position	Size (bp)	Type	Description	Application notes
5' ITR	1-141	141	ITR	AAV 5' inverted terminal repeat (functional equivalent of wild-type 5' ITR)	Allows replication of the viral genome and its packaging into virus.
GFAP_long	169-2346	2178	Promoter	Human glial fibrillary acidic protein promoter (2.1 kb)	Tissue specificity: Brain. Cell type specificity: Astrocytes.
Kozak	2371-2376	6	Miscellaneous	Kozak translation initiation sequence	Facilitates translation initiation of ATG start codon downstream of the Kozak sequence.
mCherry	2377-3087	711	ORF	Variant of mRFP1 generated by mutagenesis	Commonly used red fluorescent protein; fast maturation compared to its predecessor, mRFP1.
5' miR-30E	3112-3239	128	Miscellaneous	Human miR30 5' context with several bases mutation	Allows to form mature shRNA and trigger knockdown.
{sh-rGem}	3240-3302	63	shRNA	*None*	*None*
3' miR-30E	3303-3432	130	Miscellaneous	Human miR30 3' context with several bases mutation	Allows to form mature shRNA and trigger knockdown.
WPRE	3460-4057	598	Miscellaneous	Woodchuck hepatitis virus posttranscriptional regulatory element	Enhances virus stability in packaging cells, leading to higher titer of packaged virus; enhances higher expression of transgenes.
BGH pA	4088-4295	208	PolyA_signal	Bovine growth hormone polyadenylation signal	Allows transcription termination and polyadenylation of mRNA transcribed by Pol II RNA polymerase.
3' ITR	complement (4303-4443)	141	ITR	AAV 3' inverted terminal repeat	Allows replication of the viral genome and its packaging into virus.
Ampicillin	5360-6220	861	ORF	Ampicillin resistance gene	Allows E. coli to be resistant to ampicillin.

Name	Position	Size (bp)	Type	Description	Application notes
pUC ori	6391-6979	589	Rep_origin	pUC origin of replication	Facilitates plasmid replication in E. coli; regulates high-copy plasmid number (500-700).

Note: Components added by user are listed in **bold red** text.

Vector Sequence

```
1 CCTGCAGGCA GCTGCGCGCT CGCTCGCTCA CTGAGGCCGC CCGGGCAAAG CCCGGGCGTC GGGCGACCTT TGGTCGCCCG
81 GCCTCAGTGA GCGAGCGAGC GCGCAGAGAG GGAGTGGCCA ACTCCATCAC TAGGGGTTCC TTCTAGACAA CTTTGTATAG
161 AAAAGTTGGA GCTCCCACCT CCCTCTCTGT GCTGGGACTC ACAGAGGGAG ACCTCAGGAG GCAGTCTGTC CATCACATGT
241 CCAAATGCAG AGCATACCCT GGGCTGGGCG CAGTGGCGCA CAACTGTAAT TCCAGCACTT TGGGAGGCTG ATGTGGAAGG
321 ATCACTTGAG CCCAGAAGTT CTAGACCAGC CTGGGCAACA TGGCAAGACC CTATCTCTAC AAAAAAAGTT AAAAAATCAG
401 CCACGTGTGG TGACACACAC CTGTAGTCCC AGCTATTCAG GAGGCTGAGG TGAGGGGATC ACTTAAGGCT GGGAGGTTGA
481 GGCTGCAGTG AGTCGTGGTT GCGCCACTGC ACTCCAGCCT GGGCAACAGT GAGACCCTGT CTCAAAAGAC AAAAAAAAAA
561 AAAAAAAAAA AAGAACATAT CCTGGTGTGG AGTAGGGGAC GCTGCTCTGA CAGAGGCTCG GGGGCCTGAG CTGGCTCTGT
641 GAGCTGGGGA GGAGGCAGAC AGCCAGGCCT TGTCTGCAAG CAGACCTGGC AGCATTGGGC TGGCCGCCCC CCAGGGCCTC
721 CTCTTCATGC CCAGTGAATG ACTCACCTTG GCACAGACAC AATGTTCGGG GTGGGCACAG TGCCTGCTTC CCGCCGCACC
801 CCAGCCCCCC TCAAATGCCT TCCGAGAAGC CCATTGAGCA GGGGGCTTGC ATTGCACCCC AGCCTGACAG CCTGGCATCT
881 TGGGATAAAA GCAGCACAGC CCCCTAGGGG CTGCCCTTGC TGTGTGGCGC CACCGGCGGT GGAGAACAAG GCTCTATTCA
961 GCCTGTGCCC AGGAAAGGGG ATCAGGGGAT GCCCAGGCAT GGACAGTGGG TGGCAGGGGG GGAGAGGAGG GCTGTCTGCT
1041 TCCCAGAAGT CCAAGGACAC AAATGGGTGA GGGGACTGGG CAGGGTTCTG ACCCTGTGGG ACCAGAGTGG AGGGCGTAGA
1121 TGGACCTGAA GTCTCCAGGG ACAACAGGGC CCAGGTCTCA GGCTCCTAGT TGGGCCCAGT GGCTCCAGCG TTTCCAAACC
1201 CATCCATCCC CAGAGGTTCT TCCCATCTCT CCAGGCTGAT GTGTGGGAAC TCGAGGAAAT AAATCTCCAG TGGGAGACGG
1281 AGGGGTGGCC AGGGAAACGG GGCGCTGCAG GAATAAAGAC GAGCCAGCAC AGCCAGCTCA TGCGTAACGG CTTTGTGGAG
1361 CTGTCAAGGC CTGGTCTCTG GGAGAGAGGC ACAGGGAGGC CAGACAAGGA AGGGGTGACC TGGAGGGACA GATCCAGGGG
1441 CTAAAGTCCT GATAAGGCAA GAGAGTGCCG GCCCCCTCTT GCCCTATCAG GACCTCCACT GCCACATAGA GGCCATGATT
1521 GACCCTTAGA CAAAGGGCTG GTGTCCAATC CCAGCCCCCA GCCCCAGAAC TCCAGGGAAT GAATGGGCAG AGAGCAGGAA
1601 TGTGGGACAT CTGTGTTCAA GGGAAGGACT CCAGGAGTCT GCTGGGAATG AGGCCTAGTA GGAAATGAGG TGGCCCTTGA
1681 GGGTACAGAA CAGGTTCATT CTTCGCCAAA TTCCCAGCAC CTTGCAGGCA CTTACAGCTG AGTGAGATAA TGCCTGGGTT
1761 ATGAAATCAA AAAGTTGGAA AGCAGGTCAG AGGTCATCTG GTACAGCCCT TCCTTCCCTT TTTTTTTTTT TTTTTTTTTG
1841 TGAGACAAGG TCTCTCTCTG TTGCCCAGGC TGGAGTGGCG CAAACACAGC TCACTGCAGC CTCAACCTAC TGGGCTCAAG
1921 CAATCCTCCA GCCTCAGCCT CCCAAAGTGC TGGGATTACA AGCATGAGCC ACCCCACTCA GCCCTTTCCT TCCTTTTTAA
2001 TTGATGCATA ATAATTGTAA GTATTCATCA TGGTCCAACC AACCCTTTCT TGACCCACCT TCCTAGAGAG AGGGTCCTCT
2081 TGCTTCAGCG GTCAGGGCCC CAGACCCATG GTCTGGCTCC AGGTACCACC TGCCTCATGC AGGAGTTGGC GTGCCCAGGA
2161 AGCTCTGCCT CTGGGCACAG TGACCTCAGT GGGGTGAGGG GAGCTCTCCC CATAGCTGGG CTGCGGCCCA ACCCCACCCC
2241 CTCAGGCTAT GCCAGGGGGT GTTGCCAGGG GCACCCGGGC ATCGCCAGTC TAGCCCACTC CTTCATAAAG CCCTCGCATC
2321 CCAGGAGCGA GCAGAGCCAG AGCAGGCAAG TTTGTACAAA AAAGCAGGCT GCCACCATGG TGAGCAAGGG CGAGGAGGAT
2401 AACATGGCCA TCATCAAGGA GTTCATGCGC TTCAAGGTGC ACATGGAGGG CTCCGTGAAC GGCCACGAGT TCGAGATCGA
2481 GGGCGAGGGC GAGGGCCGCC CCTACGAGGG CACCCAGACC GCCAAGCTGA AGGTGACCAA GGGTGGCCCC CTGCCCTTCG
2561 CCTGGGACAT CCTGTCCCCT CAGTTCATGT ACGGCTCCAA GGCCTACGTG AAGCACCCCG CCGACATCCC CGACTACTTG
2641 AAGCTGTCCT TCCCCGAGGG CTTCAAGTGG GAGCGCGTGA TGAACTTCGA GGACGGCGGC GTGGTGACCG TGACCCAGGA
2721 CTCCTCCCTG CAGGACGGCG AGTTCATCTA CAAGGTGAAG CTGCGCGGCA CCAACTTCCC CTCCGACGGC CCCGTAATGC
2801 AGAAGAAGAC CATGGGCTGG GAGGCCTCCT CCGAGCGGAT GTACCCCGAG GACGGCGCCC TGAAGGGCGA GATCAAGCAG
2881 AGGCTGAAGC TGAAGGACGG CGGCCACTAC GACGCTGAGG TCAAGACCAC CTACAAGGCC AAGAAGCCCG TGCAGCTGCC
```

Vector Sequence

```
   1 CCTGCAGGCA GCTGCGCGCT CGCTCGCTCA CTGAGGCCGC CCGGGCAAAG CCCGGGCGTC GGGCGACCTT TGGTCGCCCG
  81 GCCTCAGTGA GCGAGCGAGC GCGCAGAGAG GGAGTGGCCA ACTCCATCAC TAGGGGTTCC TTCTAGACAA CTTTGTATAG
 161 AAAAGTTGGA GCTCCCACCT CCCTCTCTGT GCTGGGACTC ACAGAGGGAG ACCTCAGGAG GCAGTCTGTC CATCACATGT
 241 CCAAATGCAG AGCATACCCT GGGCTGGGCG CAGTGGCGCA CAACTGTAAT TCCAGCACTT TGGGAGGCTG ATGTGGAAGG
 321 ATCACTTGAG CCCAGAAGTT CTAGACCAGC CTGGGCAACA TGGCAAGACC CTATCTCTAC AAAAAAAGTT AAAAAATCAG
 401 CCACGTGTGG TGACACACAC CTGTAGTCCC AGCTATTCAG GAGGCTGAGG TGAGGGGATC ACTTAAGGCT GGGAGGTTGA
 481 GGCTGCAGTG AGTCGTGGTT GCGCCACTGC ACTCCAGCCT GGGCAACAGT GAGACCCTGT CTCAAAAGAC AAAAAAAAAA
 561 AAAAAAAAAA AAGAACATAT CCTGGTGTGG AGTAGGGGAC GCTGCTCTGA CAGAGGCTCG GGGGCCTGAG CTGGCTCTGT
 641 GAGCTGGGGA GGAGGCAGAC AGCCAGGCCT TGTCTGCAAG CAGACCTGGC AGCATTGGGC TGGCCGCCCC CCAGGGCCTC
 721 CTCTTCATGC CCAGTGAATG ACTCACCTTG GCACAGACAC AATGTTCGGG GTGGGCACAG TGCCTGCTTC CCGCCGCACC
 801 CCAGCCCCCC TCAAATGCCT TCCGAGAAGC CCATTGAGCA GGGGGCTTGC ATTGCACCCC AGCCTGACAG CCTGGCATCT
 881 TGGGATAAAA GCAGCACAGC CCCCTAGGGG CTGCCCTTGC TGTGTGGCGC CACCGGCGGT GGAGAACAAG GCTCTATTCA
 961 GCCTGTGCCC AGGAAAGGGG ATCAGGGGAT GCCCAGGCAT GGACAGTGGG TGGCAGGGGG GGAGAGGAGG GCTGTCTGCT
1041 TCCCAGAAGT CCAAGGACAC AAATGGGTGA GGGGACTGGG CAGGGTTCTG ACCCTGTGGG ACCAGAGTGG AGGGCGTAGA
1121 TGGACCTGAA GTCTCCAGGG ACAACAGGGC CCAGGTCTCA GGCTCCTAGT TGGGCCCAGT GGCTCCAGCG TTTCCAAACC
1201 CATCCATCCC CAGAGGTTCT TCCCATCTCT CCAGGCTGAT GTGTGGGAAC TCGAGGAAAT AAATCTCCAG TGGGAGACGG
1281 AGGGGTGGCC AGGGAAACGG GGCGCTGCAG GAATAAAGAC GAGCCAGCAC AGCCAGCTCA TGCGTAACGG CTTTGTGGAG
1361 CTGTCAAGGC CTGGTCTCTG GGAGAGAGGC ACAGGGAGGC CAGACAAGGA AGGGGTGACC TGGAGGGACA GATCCAGGGG
1441 CTAAAGTCCT GATAAGGCAA GAGAGTGCCG GCCCCCTCTT GCCCTATCAG GACCTCCACT GCCACATAGA GGCCATGATT
1521 GACCCTTAGA CAAAGGGCTG GTGTCCAATC CCAGCCCCCA GCCCCAGAAC TCCAGGGAAT GAATGGGCAG AGAGCAGGAA
1601 TGTGGGACAT CTGTGTTCAA GGGAAGGACT CCAGGAGTCT GCTGGGAATG AGGCCTAGTA GGAAATGAGG TGGCCCTTGA
1681 GGGTACAGAA CAGGTTCATT CTTCGCCAAA TTCCCAGCAC CTTGCAGGCA CTTACAGCTG AGTGAGATAA TGCCTGGGTT
1761 ATGAAATCAA AAAGTTGGAA AGCAGGTCAG AGGTCATCTG GTACAGCCCT TCCTTCCCTT TTTTTTTTTT TTTTTTTTTG
1841 TGAGACAAGG TCTCTCTCTG TTGCCCAGGC TGGAGTGGCG CAAACACAGC TCACTGCAGC CTCAACCTAC TGGGCTCAAG
1921 CAATCCTCCA GCCTCAGCCT CCCAAAGTGC TGGGATTACA AGCATGAGCC ACCCCACTCA GCCCTTTCCT TCCTTTTTAA
2001 TTGATGCATA ATAATTGTAA GTATTCATCA TGGTCCAACC AACCCTTTCT TGACCCACCT TCCTAGAGAG AGGGTCCTCT
2081 TGCTTCAGCG GTCAGGGCCC CAGACCCATG GTCTGGCTCC AGGTACCACC TGCCTCATGC AGGAGTTGGC GTGCCCAGGA
2161 AGCTCTGCCT CTGGGCACAG TGACCTCAGT GGGGTGAGGG GAGCTCTCCC CATAGCTGGG CTGCGGCCCA ACCCCACCCC
2241 CTCAGGCTAT GCCAGGGGGT GTTGCCAGGG GCACCCGGGC ATCGCCAGTC TAGCCCACTC CTTCATAAAG CCCTCGCATC
2321 CCAGGAGCGA GCAGAGCCAG AGCAGGCAAG TTTGTACAAA AAAGCAGGCT GCCACCATGG TGAGCAAGGG CGAGGAGGAT
2401 AACATGGCCA TCATCAAGGA GTTCATGCGC TTCAAGGTGC ACATGGAGGG CTCCGTGAAC GGCCACGAGT TCGAGATCGA
2481 GGGCGAGGGC GAGGGCCGCC CCTACGAGGG CACCCAGACC GCCAAGCTGA AGGTGACCAA GGGTGGCCCC CTGCCCTTCG
2561 CCTGGGACAT CCTGTCCCCT CAGTTCATGT ACGGCTCCAA GGCCTACGTG AAGCACCCCG CCGACATCCC CGACTACTTG
2641 AAGCTGTCCT TCCCCGAGGG CTTCAAGTGG GAGCGCGTGA TGAACTTCGA GGACGGCGGC GTGGTGACCG TGACCCAGGA
2721 CTCCTCCCTG CAGGACGGCG AGTTCATCTA CAAGGTGAAG CTGCGCGGCA CCAACTTCCC CTCCGACGGC CCCGTAATGC
2801 AGAAGAAGAC CATGGGCTGG GAGGCCTCCT CCGAGCGGAT GTACCCCGAG GACGGCGCCC TGAAGGGCGA GATCAAGCAG
2881 AGGCTGAAGC TGAAGGACGG CGGCCACTAC GACGCTGAGG TCAAGACCAC CTACAAGGCC AAGAAGCCCG TGCAGCTGCC
```

2961 CGGCGCCTAC AACGTCAACA TCAAGTTGGA CATCACCTCC CACAACGAGG ACTACACCAT CGTGGAACAG TACGAACGCG
3041 CCGAGGGCCG CCACTCCACC GGCGGCATGG ACGAGCTGTA CAAGTAAACC CAGCTTTCTT GTACAAAGTG GTGTTTGAAT
3121 GAGGCTTCAG TACTTTACAG AATCGTTGCC TGCACATCTT GGAAACACTT GCTGGGATTA CTTCGACTTC TTAACCCAAC
3201 AGAAGGCTCG AGAAGGTATA TTGCTGTTGA CAGTGAGCGC GACAGAAGAC ATTCCTATAA TTAGTGAAGC CACAGATGTA
3281 ATTATAGGAA TGTCTTCTGT CTTGCCTACT GCCTCGGACT TCAAGGGGCT AGAATTCGAG CAATTATCTT GTTTACTAAA
3361 ACTGAATACC TTGCTATCTC TTTGATACAT TTTTACAAAG CTGAATTAAA ATGGTATAAA TTAAATCACT TTCAACTTTA
3441 TTATACATAG TTGGAATTCC GATAATCAAC CTCTGGATTA CAAAATTTGT GAAAGATTGA CTGGTATTCT TAACTATGTT
3521 GCTCCTTTTA CGCTATGTGG ATACGCTGCT TTAATGCCTT TGTATCATGC TATTGCTTCC CGTATGGCTT TCATTTTCTC
3601 CTCCTTGTAT AAATCCTGGT TGCTGTCTCT TTATGAGGAG TTGTGGCCCG TTGTCAGGCA ACGTGGCGTG GTGTGCACTG
3681 TGTTTGCTGA CGCAACCCCC ACTGGTTGGG GCATTGCCAC CACCTGTCAG CTCCTTTCCG GGACTTTCGC TTTCCCCCTC
3761 CCTATTGCCA CGGCGGAACT CATCGCCGCC TGCCTTGCCC GCTGCTGGAC AGGGGCTCGG CTGTTGGGCA CTGACAATTC
3841 CGTGGTGTTG TCGGGGAAGC TGACGTCCTT TCCATGGCTG CTCGCCTGTG TTGCCACCTG GATTCTGCGC GGGACGTCCT
3921 TCTGCTACGT CCCTTCGGCC CTCAATCCAG CGGACCTTCC TTCCCGCGGC CTGCTGCCGG CTCTGCGGCC TCTTCCGCGT
4001 CTTCGCCTTC GCCCTCAGAC GAGTCGGATC TCCCTTTGGG CCGCCTCCCC GCATCGGGAA TTCCTAGAGC TCGCTGATCA
4081 GCCTCGACTG TGCCTTCTAG TTGCCAGCCA TCTGTTGTTT GCCCCTCCCC CGTGCCTTCC TTGACCCTGG AAGGTGCCAC
4161 TCCCACTGTC CTTTCCTAAT AAAATGAGGA AATTGCATCG CATTGTCTGA GTAGGTGTCA TTCTATTCTG GGGGGTGGGG
4241 TGGGGCAGGA CAGCAAGGGG GAGGATTGGG AAGAGAATAG CAGGCATGCT GGGGAGGGCC GCAGGAACCC CTAGTGATGG
4321 AGTTGGCCAC TCCCTCTCTG CGCGCTCGCT CGCTCACTGA GGCCGGGCGA CCAAAGGTCG CCCGACGCCC GGGCTTTGCC
4401 CGGGCGGCCT CAGTGAGCGA GCGAGCGCGC AGCTGCCTGC AGGGGCGCCT GATGCGGTAT TTTCTCCTTA CGCATCTGTG
4481 CGGTATTTCA CACCGCATAC GTCAAAGCAA CCATAGTACG CGCCCTGTAG CGGCGCATTA AGCGCGGCGG GGGTGGTGGT
4561 TACGCGCAGC GTGACCGCTA CACTTGCCAG CGCCTTAGCG CCCGCTCCTT TCGCTTTCTT CCCTTCCTTT CTCGCCACGT
4641 TCGCCGGCTT TCCCCGTCAA GCTCTAAATC GGGGGCTCCC TTTAGGGTTC CGATTTAGTG CTTTACGGCA CCTCGACCCC
4721 AAAAAACTTG ATTTGGGTGA TGGTTCACGT AGTGGGCCAT CGCCCTGATA GACGGTTTTT CGCCCTTTGA CGTTGGAGTC
4801 CACGTTCTTT AATAGTGGAC TCTTGTTCCA AACTGGAACA ACACTCAACT CTATCTCGGG CTATTCTTTT GATTTATAAG
4881 GGATTTTGCC GATTTCGGTC TATTGGTTAA AAAATGAGCT GATTTAACAA AAATTTAACG CGAATTTTAA CAAAATATTA
4961 ACGTTTACAA TTTTATGGTG CACTCTCAGT ACAATCTGCT CTGATGCCGC ATAGTTAAGC CAGCCCCGAC ACCCGCCAAC
5041 ACCCGCTGAC GCGCCCTGAC GGGCTTGTCT GCTCCCGGCA TCCGCTTACA GACAAGCTGT GACCGTCTCC GGGAGCTGCA
5121 TGTGTCAGAG GTTTTCACCG TCATCACCGA AACGCGCGAG ACGAAAGGGC CTCGTGATAC GCCTATTTTT ATAGGTTAAT
5201 GTCATGATAA TAATGGTTTC TTAGACGTCA GGTGGCACTT TTCGGGGAAA TGTGCGCGGA ACCCCTATTT GTTTATTTTT
5281 CTAAATACAT TCAAATATGT ATCCGCTCAT GAGACAATAA CCCTGATAAA TGCTTCAATA ATATTGAAAA AGGAAGAGTA
5361 TGAGTATTCA ACATTTCCGT GTCGCCCTTA TTCCCTTTTT TGCGGCATTT TGCCTTCCTG TTTTTGCTCA CCCAGAAACG
5441 CTGGTGAAAG TAAAAGATGC TGAAGATCAG TTGGGTGCAC GAGTGGGTTA CATCGAACTG GATCTCAACA GCGGTAAGAT
5521 CCTTGAGAGT TTTCGCCCCG AAGAACGTTT TCCAATGATG AGCACTTTTA AAGTTCTGCT ATGTGGCGCG GTATTATCCC
5601 GTATTGACGC CGGGCAAGAG CAACTCGGTC GCCGCATACA CTATTCTCAG AATGACTTGG TTGAGTACTC ACCAGTCACA
5681 GAAAAGCATC TTACGGATGG CATGACAGTA AGAGAATTAT GCAGTGCTGC CATAACCATG AGTGATAACA CTGCGGCCAA
5761 CTTACTTCTG ACAACGATCG GAGGACCGAA GGAGCTAACC GCTTTTTTGC ACAACATGGG GGATCATGTA ACTCGCCTTG
5841 ATCGTTGGGA ACCGGAGCTG AATGAAGCCA TACCAAACGA CGAGCGTGAC ACCACGATGC CTGTAGCAAT GGCAACAACG
5921 TTGCGCAAAC TATTAACTGG CGAACTACTT ACTCTAGCTT CCCGGCAACA ATTAATAGAC TGGATGGAGG CGGATAAAGT
6001 TGCAGGACCA CTTCTGCGCT CGGCCCTTCC GGCTGGCTGG TTTATTGCTG ATAAATCTGG AGCCGGTGAG CGTGGAAGCC
6081 GCGGTATCAT TGCAGCACTG GGGCCAGATG GTAAGCCCTC CCGTATCGTA GTTATCTACA CGACGGGGAG TCAGGCAACT
6161 ATGGATGAAC GAAATAGACA GATCGCTGAG ATAGGTGCCT CACTGATTAA GCATTGGTAA CTGTCAGACC AAGTTTACTC
6241 ATATATACTT TAGATTGATT TAAAACTTCA TTTTTAATTT AAAAGGATCT AGGTGAAGAT CCTTTTTGAT AATCTCATGA
6321 CCAAAATCCC TTAACGTGAG TTTTCGTTCC ACTGAGCGTC AGACCCCGTA GAAAAGATCA AAGGATCTTC TTGAGATCCT
6401 TTTTTTCTGC GCGTAATCTG CTGCTTGCAA ACAAAAAAAC CACCGCTACC AGCGGTGGTT TGTTTGCCGG ATCAAGAGCT
6481 ACCAACTCTT TTTCCGAAGG TAACTGGCTT CAGCAGAGCG CAGATACCAA ATACTGTTCT TCTAGTGTAG CCGTAGTTAG
6561 GCCACCACTT CAAGAACTCT GTAGCACCGC CTACATACCT CGCTCTGCTA ATCCTGTTAC CAGTGGCTGC TGCCAGTGGC
6641 GATAAGTCGT GTCTTACCGG GTTGGACTCA AGACGATAGT TACCGGATAA GGCGCAGCGG TCGGGCTGAA CGGGGGGTTC
6721 GTGCACACAG CCCAGCTTGG AGCGAACGAC CTACACCGAA CTGAGATACC TACAGCGTGA GCTATGAGAA AGCGCCACGC

6801 TTCCCGAAGG GAGAAAGGCG GACAGGTATC CGGTAAGCGG CAGGGTCGGA ACAGGAGAGC GCACGAGGGA GCTTCCAGGG
6881 GGAAACGCCT GGTATCTTTA TAGTCCTGTC GGGTTTCGCC ACCTCTGACT TGAGCGTCGA TTTTTGTGAT GCTCGTCAGG
6961 GGGGCGGAGC CTATGGAAAA ACGCCAGCAA CGCGGCCTTT TTACGGTTCC TGGCCTTTTG CTGGCCTTTT GCTCACATGT

Validation by Restriction Enzyme Digestion

Restriction Enzymes	Cutting Sites	DNA Fragments (bp)
NcoI	2107, 2376, 2811, 3873	269, 435, 1062, 5274
ApaLI	2438, 3674, 4979, 5476, 6722	1236, 1305, 497, 1246, 2756
ApaLI+NcoI	2107, 2376, 2438, 2811, 3674, 3873, 4979, 5476, 6722	269, 62, 373, 863, 199, 1106, 497, 1246, 2425

b) AAV6-GFAP *Oxtr* shRNA vector

Vector Summary

Vector ID	VB191205-1084svn
Vector Name	pAAV[miR30]-GFAP_long>mCherry:{sh-rOXTR}:WPRE
Date Created (Pacific Time)	2019-12-04
Vector Size	7040 bp
Viral Genome Size	4443 bp
Vector Type	Mammalian miR30-shRNA Knockdown AAV Vector
Inserted Promoter	GFAP_long
Inserted ORF	mCherry
Inserted shRNA	{sh-rOXTR}
Target Sequence	CTGCTGTGTCGTCTGGTCAAAT
Plasmid Copy Number	High
Antibiotic Resistance	Ampicillin
Cloning Host	VB UltraStable (or alternative strain)

Vector Components

Name	Position	Size (bp)	Type	Description	Application notes
5' ITR	1-141	141	ITR	AAV 5' inverted terminal repeat (functional equivalent of wild-type 5' ITR)	Allows replication of the viral genome and its packaging into virus.
GFAP_long	169-2346	2178	Promoter	Human glial fibrillary acidic protein promoter (2.1 kb)	Tissue specificity: Brain. Cell type specificity: Astrocytes.
Kozak	2371-2376	6	Miscellaneous	Kozak translation initiation sequence	Facilitates translation initiation of ATG start codon downstream of the Kozak sequence.
mCherry	2377-3087	711	ORF	Variant of mRFP1 generated by mutagenesis	Commonly used red fluorescent protein; fast maturation compared to its predecessor, mRFP1.
5' miR-30E	3112-3239	128	Miscellaneous	Human miR30 5' context with several bases mutation	Allows to form mature shRNA and trigger knockdown.
{sh-rOXTR}	3240-3302	63	shRNA	*None*	*None*
3' miR-30E	3303-3432	130	Miscellaneous	Human miR30 3' context with several bases mutation	Allows to form mature shRNA and trigger knockdown.
WPRE	3460-4057	598	Miscellaneous	Woodchuck hepatitis virus posttranscriptional regulatory element	Enhances virus stability in packaging cells, leading to higher titer of packaged virus; enhances higher expression of transgenes.
BGH pA	4088-4295	208	PolyA_signal	Bovine growth hormone polyadenylation signal	Allows transcription termination and polyadenylation of mRNA transcribed by Pol II RNA polymerase.
3' ITR	complement (4303-4443)	141	ITR	AAV 3' inverted terminal repeat	Allows replication of the viral genome and its packaging into virus.
Ampicillin	5360-6220	861	ORF	Ampicillin resistance gene	Allows E. coli to be resistant to ampicillin.

Name	Position	Size (bp)	Type	Description	Application notes
pUC ori	6391-6979	589	Rep_origin	pUC origin of replication	Facilitates plasmid replication in E. coli; regulates high-copy plasmid number (500-700).

Note: Components added by user are listed in **bold red** text.

Vector Sequence

```
   1 CCTGCAGGCA GCTGCGCGCT CGCTCGCTCA CTGAGGCCGC CCGGGCAAAG CCCGGGCGTC GGGCGACCTT TGGTCGCCCG
  81 GCCTCAGTGA GCGAGCGAGC GCGCAGAGAG GGAGTGGCCA ACTCCATCAC TAGGGGTTCC TTCTAGACAA CTTTGTATAG
 161 AAAAGTTGGA GCTCCCACCT CCCTCTCTGT GCTGGGACTC ACAGAGGGAG ACCTCAGGAG GCAGTCTGTC CATCACATGT
 241 CCAAATGCAG AGCATACCCT GGGCTGGGCG CAGTGGCGCA CAACTGTAAT TCCAGCACTT TGGGAGGCTG ATGTGGAAGG
 321 ATCACTTGAG CCCAGAAGTT CTAGACCAGC CTGGGCAACA TGGCAAGACC CTATCTCTAC AAAAAAAGTT AAAAAATCAG
 401 CCACGTGTGG TGACACACAC CTGTAGTCCC AGCTATTCAG GAGGCTGAGG TGAGGGGATC ACTTAAGGCT GGGAGGTTGA
 481 GGCTGCAGTG AGTCGTGGTT GCGCCACTGC ACTCCAGCCT GGGCAACAGT GAGACCCTGT CTCAAAAGAC AAAAAAAAAA
 561 AAAAAAAAAA AAGAACATAT CCTGGTGTGG AGTAGGGGAC GCTGCTCTGA CAGAGGCTCG GGGGCCTGAG CTGGCTCTGT
 641 GAGCTGGGGA GGAGGCAGAC AGCCAGGCCT TGTCTGCAAG CAGACCTGGC AGCATTGGGC TGGCCGCCCC CCAGGGCCTC
 721 CTCTTCATGC CCAGTGAATG ACTCACCTTG GCACAGACAC AATGTTCGGG GTGGGCACAG TGCCTGCTTC CCGCCGCACC
 801 CCAGCCCCCC TCAAATGCCT TCCGAGAAGC CCATTGAGCA GGGGGCTTGC ATTGCACCCC AGCCTGACAG CCTGGCATCT
 881 TGGGATAAAA GCAGCACAGC CCCCTAGGGG CTGCCCTTGC TGTGTGGCGC CACCGGCGGT GGAGAACAAG GCTCTATTCA
 961 GCCTGTGCCC AGGAAAGGGG ATCAGGGGAT GCCCAGGCAT GGACAGTGGG TGGCAGGGGG GGAGAGGAGG GCTGTCTGCT
1041 TCCCAGAAGT CCAAGGACAC AAATGGGTGA GGGGACTGGG CAGGGTTCTG ACCCTGTGGG ACCAGAGTGG AGGGCGTAGA
1121 TGGACCTGAA GTCTCCAGGG ACAACAGGGC CCAGGTCTCA GGCTCCTAGT TGGGCCCAGT GGCTCCAGCG TTTCCAAACC
1201 CATCCATCCC CAGAGGTTCT TCCCATCTCT CCAGGCTGAT GTGTGGGAAC TCGAGGAAAT AAATCTCCAG TGGGAGACGG
1281 AGGGGTGGCC AGGGAAACGG GGCGCTGCAG GAATAAAGAC GAGCCAGCAC AGCCAGCTCA TGCGTAACGG CTTTGTGGAG
1361 CTGTCAAGGC CTGGTCTCTG GGAGAGAGGC ACAGGGAGGC CAGACAAGGA AGGGGTGACC TGGAGGGACA GATCCAGGGG
1441 CTAAAGTCCT GATAAGGCAA GAGAGTGCCG GCCCCCTCTT GCCCTATCAG GACCTCCACT GCCACATAGA GGCCATGATT
1521 GACCCTTAGA CAAAGGGCTG GTGTCCAATC CCAGCCCCCA GCCCCAGAAC TCCAGGGAAT GAATGGGCAG AGAGCAGGAA
1601 TGTGGGACAT CTGTGTTCAA GGGAAGGACT CCAGGAGTCT GCTGGGAATG AGGCCTAGTA GGAAATGAGG TGGCCCTTGA
1681 GGGTACAGAA CAGGTTCATT CTTCGCCAAA TTCCCAGCAC CTTGCAGGCA CTTACAGCTG AGTGAGATAA TGCCTGGGTT
1761 ATGAAATCAA AAAGTTGGAA AGCAGGTCAG AGGTCATCTG GTACAGCCCT TCCTTCCCTT TTTTTTTTTT TTTTTTTTTG
1841 TGAGACAAGG TCTCTCTCTG TTGCCCAGGC TGGAGTGGCG CAAACACAGC TCACTGCAGC CTCAACCTAC TGGGCTCAAG
1921 CAATCCTCCA GCCTCAGCCT CCCAAAGTGC TGGGATTACA AGCATGAGCC ACCCCACTCA GCCCTTTCCT TCCTTTTTAA
2001 TTGATGCATA ATAATTGTAA GTATTCATCA TGGTCCAACC AACCCTTTCT TGACCCACCT TCCTAGAGAG AGGGTCCTCT
2081 TGCTTCAGCG GTCAGGGCCC CAGACCCATG GTCTGGCTCC AGGTACCACC TGCCTCATGC AGGAGTTGGC GTGCCCAGGA
2161 AGCTCTGCCT CTGGGCACAG TGACCTCAGT GGGGTGAGGG GAGCTCTCCC CATAGCTGGG CTGCGGCCCA ACCCCACCCC
2241 CTCAGGCTAT GCCAGGGGGT GTTGCCAGGG GCACCCGGGC ATCGCCAGTC TAGCCCACTC CTTCATAAAG CCCTCGCATC
2321 CCAGGAGCGA GCAGAGCCAG AGCAGGCAAG TTTGTACAAA AAAGCAGGCT GCCACCATGG TGAGCAAGGG CGAGGAGGAT
2401 AACATGGCCA TCATCAAGGA GTTCATGCGC TTCAAGGTGC ACATGGAGGG CTCCGTGAAC GGCCACGAGT TCGAGATCGA
2481 GGGCGAGGGC GAGGGCCGCC CCTACGAGGG CACCCAGACC GCCAAGCTGA AGGTGACCAA GGGTGGCCCC CTGCCCTTCG
2561 CCTGGGACAT CCTGTCCCCT CAGTTCATGT ACGGCTCCAA GGCCTACGTG AAGCACCCCG CCGACATCCC CGACTACTTG
2641 AAGCTGTCCT TCCCCGAGGG CTTCAAGTGG GAGCGCGTGA TGAACTTCGA GGACGGCGGC GTGGTGACCG TGACCCAGGA
2721 CTCCTCCCTG CAGGACGGCG AGTTCATCTA CAAGGTGAAG CTGCGCGGCA CCAACTTCCC CTCCGACGGC CCCGTAATGC
2801 AGAAGAAGAC CATGGGCTGG GAGGCCTCCT CCGAGCGGAT GTACCCCGAG GACGGCGCCC TGAAGGGCGA GATCAAGCAG
2881 AGGCTGAAGC TGAAGGACGG CGGCCACTAC GACGCTGAGG TCAAGACCAC CTACAAGGCC AAGAAGCCCG TGCAGCTGCC
```

2961 CGGCGCCTAC AACGTCAACA TCAAGTTGGA CATCACCTCC CACAACGAGG ACTACACCAT CGTGGAACAG TACGAACGCG
3041 CCGAGGGCCG CCACTCCACC GGCGGCATGG ACGAGCTGTA CAAGTAAACC CAGCTTTCTT GTACAAAGTG GTGTTTGAAT
3121 GAGGCTTCAG TACTTTACAG AATCGTTGCC TGCACATCTT GGAAACACTT GCTGGGATTA CTTCGACTTC TTAACCCAAC
3201 AGAAGGCTCG AGAAGGTATA TTGCTGTTGA CAGTGAGCGA TGCTGTGTCG TCTGGTCAAA TTAGTGAAGC CACAGATGTA
3281 ATTTGACCAG ACGACACAGC AGTGCCTACT GCCTCGGACT TCAAGGGGCT AGAATTCGAG CAATTATCTT GTTTACTAAA
3361 ACTGAATACC TTGCTATCTC TTTGATACAT TTTTACAAAG CTGAATTAAA ATGGTATAAA TTAAATCACT TTCAACTTTA
3441 TTATACATAG TTGGAATTCC GATAATCAAC CTCTGGATTA CAAAATTTGT GAAAGATTGA CTGGTATTCT TAACTATGTT
3521 GCTCCTTTTA CGCTATGTGG ATACGCTGCT TTAATGCCTT TGTATCATGC TATTGCTTCC CGTATGGCTT TCATTTTCTC
3601 CTCCTTGTAT AAATCCTGGT TGCTGTCTCT TTATGAGGAG TTGTGGCCCG TTGTCAGGCA ACGTGGCGTG GTGTGCACTG
3681 TGTTTGCTGA CGCAACCCCC ACTGGTTGGG GCATTGCCAC CACCTGTCAG CTCCTTTCCG GGACTTTCGC TTTCCCCCTC
3761 CCTATTGCCA CGGCGGAACT CATCGCCGCC TGCCTTGCCC GCTGCTGGAC AGGGGCTCGG CTGTTGGGCA CTGACAATTC
3841 CGTGGTGTTG TCGGGGAAGC TGACGTCCTT TCCATGGCTG CTCGCCTGTG TTGCCACCTG GATTCTGCGC GGGACGTCCT
3921 TCTGCTACGT CCCTTCGGCC CTCAATCCAG CGGACCTTCC TTCCCGCGGC CTGCTGCCGG CTCTGCGGCC TCTTCCGCGT
4001 CTTCGCCTTC GCCCTCAGAC GAGTCGGATC TCCCTTTGGG CCGCCTCCCC GCATCGGGAA TTCCTAGAGC TCGCTGATCA
4081 GCCTCGACTG TGCCTTCTAG TTGCCAGCCA TCTGTTGTTT GCCCCTCCCC CGTGCCTTCC TTGACCCTGG AAGGTGCCAC
4161 TCCCACTGTC CTTTCCTAAT AAAATGAGGA AATTGCATCG CATTGTCTGA GTAGGTGTCA TTCTATTCTG GGGGGTGGGG
4241 TGGGGCAGGA CAGCAAGGGG GAGGATTGGG AAGAGAATAG CAGGCATGCT GGGGAGGGCC GCAGGAACCC CTAGTGATGG
4321 AGTTGGCCAC TCCCTCTCTG CGCGCTCGCT CGCTCACTGA GGCCGGGCGA CCAAAGGTCG CCCGACGCCC GGGCTTTGCC
4401 CGGGCGGCCT CAGTGAGCGA GCGAGCGCGC AGCTGCCTGC AGGGGCGCCT GATGCGGTAT TTTCTCCTTA CGCATCTGTG
4481 CGGTATTTCA CACCGCATAC GTCAAAGCAA CCATAGTACG CGCCCTGTAG CGGCGCATTA AGCGCGGCGG GGGTGGTGGT
4561 TACGCGCAGC GTGACCGCTA CACTTGCCAG CGCCTTAGCG CCCGCTCCTT TCGCTTTCTT CCCTTCCTTT CTCGCCACGT
4641 TCGCCGGCTT TCCCCGTCAA GCTCTAAATC GGGGGCTCCC TTTAGGGTTC CGATTTAGTG CTTTACGGCA CCTCGACCCC
4721 AAAAAACTTG ATTTGGGTGA TGGTTCACGT AGTGGGCCAT CGCCCTGATA GACGGTTTTT CGCCCTTTGA CGTTGGAGTC
4801 CACGTTCTTT AATAGTGGAC TCTTGTTCCA AACTGGAACA ACACTCAACT CTATCTCGGG CTATTCTTTT GATTTATAAG
4881 GGATTTTGCC GATTTCGGTC TATTGGTTAA AAAATGAGCT GATTTAACAA AAATTTAACG CGAATTTTAA CAAAATATTA
4961 ACGTTTACAA TTTTATGGTG CACTCTCAGT ACAATCTGCT CTGATGCCGC ATAGTTAAGC CAGCCCCGAC ACCCGCCAAC
5041 ACCCGCTGAC GCGCCCTGAC GGGCTTGTCT GCTCCCGGCA TCCGCTTACA GACAAGCTGT GACCGTCTCC GGGAGCTGCA
5121 TGTGTCAGAG GTTTTCACCG TCATCACCGA AACGCGCGAG ACGAAAGGGC CTCGTGATAC GCCTATTTTT ATAGGTTAAT
5201 GTCATGATAA TAATGGTTTC TTAGACGTCA GGTGGCACTT TTCGGGGAAA TGTGCGCGGA ACCCCTATTT GTTTATTTTT
5281 CTAAATACAT TCAAATATGT ATCCGCTCAT GAGACAATAA CCCTGATAAA TGCTTCAATA ATATTGAAAA AGGAAGAGTA
5361 TGAGTATTCA ACATTTCCGT GTCGCCCTTA TTCCCTTTTT TGCGGCATTT TGCCTTCCTG TTTTTGCTCA CCCAGAAACG
5441 CTGGTGAAAG TAAAAGATGC TGAAGATCAG TTGGGTGCAC GAGTGGGTTA CATCGAACTG GATCTCAACA GCGGTAAGAT
5521 CCTTGAGAGT TTTCGCCCCG AAGAACGTTT TCCAATGATG AGCACTTTTA AAGTTCTGCT ATGTGGCGCG GTATTATCCC
5601 GTATTGACGC CGGGCAAGAG CAACTCGGTC GCCGCATACA CTATTCTCAG AATGACTTGG TTGAGTACTC ACCAGTCACA
5681 GAAAAGCATC TTACGGATGG CATGACAGTA AGAGAATTAT GCAGTGCTGC CATAACCATG AGTGATAACA CTGCGGCCAA
5761 CTTACTTCTG ACAACGATCG GAGGACCGAA GGAGCTAACC GCTTTTTTGC ACAACATGGG GGATCATGTA ACTCGCCTTG
5841 ATCGTTGGGA ACCGGAGCTG AATGAAGCCA TACCAAACGA CGAGCGTGAC ACCACGATGC CTGTAGCAAT GGCAACAACG
5921 TTGCGCAAAC TATTAACTGG CGAACTACTT ACTCTAGCTT CCCGGCAACA ATTAATAGAC TGGATGGAGG CGGATAAAGT
6001 TGCAGGACCA CTTCTGCGCT CGGCCCTTCC GGCTGGCTGG TTTATTGCTG ATAAATCTGG AGCCGGTGAG CGTGGAAGCC
6081 GCGGTATCAT TGCAGCACTG GGGCCAGATG GTAAGCCCTC CCGTATCGTA GTTATCTACA CGACGGGGAG TCAGGCAACT
6161 ATGGATGAAC GAAATAGACA GATCGCTGAG ATAGGTGCCT CACTGATTAA GCATTGGTAA CTGTCAGACC AAGTTTACTC
6241 ATATATACTT TAGATTGATT TAAAACTTCA TTTTTAATTT AAAAGGATCT AGGTGAAGAT CCTTTTTGAT AATCTCATGA
6321 CCAAAATCCC TTAACGTGAG TTTTCGTTCC ACTGAGCGTC AGACCCCGTA GAAAAGATCA AAGGATCTTC TTGAGATCCT
6401 TTTTTTCTGC GCGTAATCTG CTGCTTGCAA ACAAAAAAAC CACCGCTACC AGCGGTGGTT TGTTTGCCGG ATCAAGAGCT
6481 ACCAACTCTT TTTCCGAAGG TAACTGGCTT CAGCAGAGCG CAGATACCAA ATACTGTTCT TCTAGTGTAG CCGTAGTTAG
6561 GCCACCACTT CAAGAACTCT GTAGCACCGC CTACATACCT CGCTCTGCTA ATCCTGTTAC CAGTGGCTGC TGCCAGTGGC
6641 GATAAGTCGT GTCTTACCGG GTTGGACTCA AGACGATAGT TACCGGATAA GGCGCAGCGG TCGGGCTGAA CGGGGGGTTC
6721 GTGCACACAG CCCAGCTTGG AGCGAACGAC CTACACCGAA CTGAGATACC TACAGCGTGA GCTATGAGAA AGCGCCACGC

```
6801 TTCCCGAAGG GAGAAAGGCG GACAGGTATC CGGTAAGCGG CAGGGTCGGA ACAGGAGAGC GCACGAGGGA GCTTCCAGGG
6881 GGAAACGCCT GGTATCTTTA TAGTCCTGTC GGGTTTCGCC ACCTCTGACT TGAGCGTCGA TTTTTGTGAT GCTCGTCAGG
6961 GGGGCGGAGC CTATGGAAAA ACGCCAGCAA CGCGGCCTTT TTACGGTTCC TGGCCTTTTG CTGGCCTTTT GCTCACATGT
```

Validation by Restriction Enzyme Digestion

Restriction Enzymes	Cutting Sites	DNA Fragments (bp)
NcoI	2107, 2376, 2811, 3873	269, 435, 1062, 5274
ApaLI	2438, 3674, 4979, 5476, 6722	1236, 1305, 497, 1246, 2756
ApaLI+NcoI	2107, 2376, 2438, 2811, 3674, 3873, 4979, 5476, 6722	269, 62, 373, 863, 199, 1106, 497, 1246, 2425

Appendix 2

a) CMV-EGFP control plasmid

Vector Summary

Vector ID	VB181226-1397jaz
Vector Name	pRP[Exp]-EGFP/Puro-CAG>Stuffer300
Date Created (Pacific Time)	2018-12-26
Vector Size	6582 bp
Vector Type	Mammalian Gene Expression Vector
Plasmid Copy Number	High
Antibiotic Resistance	Ampicillin
Cloning Host	Stbl3 (or alternative strain)

Vector Components

Name	Position	Size (bp)	Type	Description	Application notes
CAG	22-1754	1733	misc_feature	*None*	note=CAG

Name	Position	Size (bp)	Type	Description	Application notes
Stuffer_300bp	1779-2078	300	ORF	*None*	note=Unknown feature type:ORF color: #0ed8aa; direction: RIGHT
SV40 late pA	2123-2344	222	PolyA_signal	Simian virus 40 late polyadenylation signal	note=Unknown feature type:PolyA_signal color: #5566f5; direction: RIGHT
CMV promoter	2348-2935	588	Promoter	Human cytomegalovirus immediate early enhancer/promoter	note=Unknown feature type:Promoter color: #ef6cdf; direction: RIGHT full_name=Human cytomegalovirus immediate early promoter
EGFP/Puro	2967-4283	1317	ORF	EGFP fused with Puro	note=Unknown feature type:Marker color: #c54b7c; direction: RIGHT full_name=EGFP and puromycin dual reporter gene
BGH pA	4327-4551	225	PolyA_signal	Bovine growth hormone polyadenylation signal	note=Unknown feature type:PolyA_signal color: #d05c0a; direction: RIGHT full_name=Bovine growth hormone polyadenylation
pUC ori	complement (4747-5335)	589	Rep_origin	pUC origin of replication	note=Unknown feature type:Rep_origin color: #fd3434; direction: LEFT full_name=pUC origin of replication
Ampicillin	complement (5506-6366)	861	ORF	Ampicillin resistance gene	note=Unknown feature type:ORF color: #46c6ef; direction: LEFT full_name=Ampicillin resistance gene

Note: Components added by user are listed in **bold red** text.

Vector Sequence

```
  1 CAACTTTGTA TAGAAAAGTT GCTCGACATT GATTATTGAC TAGTTATTAA TAGTAATCAA TTACGGGGTC ATTAGTTCAT
 81 AGCCCATATA TGGAGTTCCG CGTTACATAA CTTACGGTAA ATGGCCCGCC TGGCTGACCG CCCAACGACC CCCGCCCATT
161 GACGTCAATA ATGACGTATG TTCCCATAGT AACGCCAATA GGGACTTTCC ATTGACGTCA ATGGGTGGAG TATTTACGGT
241 AAACTGCCCA CTTGGCAGTA CATCAAGTGT ATCATATGCC AAGTACGCCC CCTATTGACG TCAATGACGG TAAATGGCCC
321 GCCTGGCATT ATGCCCAGTA CATGACCTTA TGGGACTTTC CTACTTGGCA GTACATCTAC GTATTAGTCA TCGCTATTAC
```

401 CATGGTCGAG GTGAGCCCCA CGTTCTGCTT CACTCTCCCC ATCTCCCCCC CCTCCCCACC CCCAATTTTG TATTTATTTA
481 TTTTTTAATT ATTTTGTGCA GCGATGGGGG CGGGGGGGGG GGGGGGGCGC GCGCCAGGCG GGGCGGGGCG GGGCGAGGGG
561 CGGGGCGGGG CGAGGCGGAG AGGTGCGGCG GCAGCCAATC AGAGCGGCGC GCTCCGAAAG TTTCCTTTTA TGGCGAGGCG
641 GCGGCGGCGG CGGCCCTATA AAAAGCGAAG CGCGCGGCGG GCGGGAGTCG CTGCGCGCTG CCTTCGCCCC GTGCCCCGCT
721 CCGCCGCCGC CTCGCGCCGC CCGCCCCGGC TCTGACTGAC CGCGTTACTC CCACAGGTGA GCGGGCGGGA CGGCCCTTCT
801 CCTCCGGGCT GTAATTAGCG CTTGGTTTAA TGACGGCTTG TTTCTTTTCT GTGGCTGCGT GAAAGCCTTG AGGGGCTCCG
881 GGAGGGCCCT TTGTGCGGGG GGAGCGGCTC GGGGGGTGCG TGCGTGTGTG TGTGCGTGGG GAGCGCCGCG TGCGGCTCCG
961 CGCTGCCCGG CGGCTGTGAG CGCTGCGGGC GCGGCGCGGG GCTTTGTGCG CTCCGCAGTG TGCGCGAGGG GAGCGCGGCC
1041 GGGGGCGGTG CCCCGCGGTG CGGGGGGGGC TGCGAGGGGA ACAAAGGCTG CGTGCGGGGT GTGTGCGTGG GGGGGTGAGC
1121 AGGGGGTGTG GGCGCGTCGG TCGGGCTGCA ACCCCCCCTG CACCCCCCTC CCCGAGTTGC TGAGCACGGC CCGGCTTCGG
1201 GTGCGGGGCT CCGTACGGGG CGTGGCGCGG GGCTCGCCGT GCCGGGCGGG GGGTGGCGGC AGGTGGGGGT GCCGGGCGGG
1281 GCGGGGCCGC CTCGGGCCGG GGAGGGCTCG GGGGAGGGGC GCGGCGGCCC CCGGAGCGCC GGCGGCTGTC GAGGCGCGGC
1361 GAGCCGCAGC CATTGCCTTT TATGGTAATC GTGCGAGAGG GCGCAGGGAC TTCCTTTGTC CCAAATCTGT GCGGAGCCGA
1441 AATCTGGGAG GCGCCGCCGC ACCCCCTCTA GCGGGCGCGG GGCGAAGCGG TGCGGCGCCG GCAGGAAGGA AATGGGCGGG
1521 GAGGGCCTTC GTGCGTCGCC GCGCCGCCGT CCCCTTCTCC CTCTCCAGCC TCGGGGCTGT CCGCGGGGGG ACGGCTGCCT
1601 TCGGGGGGGA CGGGGCAGGG CGGGGTTCGG CTTCTGGCGT GTGACCGGCG GCTCTAGAGC CTCTGCTAAC CATGTTCATG
1681 CCTTCTTCTT TTTCCTACAG CTCCTGGGCA ACGTGCTGGT TATTGTGCTG TCTCATCATT TTGGCAAAGA ATTGCAAGTT
1761 TGTACAAAAA AGCAGGCTGT CGTTTTACAA CGTCGTGACT GGGAAAACCC TGGCGTTACC CAACTTAATC GCCTTGCAGC
1841 ACATCCCCCT TTCGCCAGCT GGCGTAATAG CGAAGAGGCC CGCACCGATC GCCCTTCCCA ACAGTTGCGC AGCCTGAATG
1921 GCGAATGGCG CTTTGCCTGG TTTCCGGCAC CAGAAGCGGT GCCGGAAAGC TGGCTGGAGT GCGATCTTCC TGAGGCCGAT
2001 ACTGTCGTCG TCCCCTCAAA CTGGCAGATG CACGGTTACG ATGCGCCCAT CTACACCAAC GTAACCTATC CCATTACGAC
2081 CCAGCTTTCT TGTACAAAGT GGTGATGGCC GGCCGCTTCG AGCAGACATG ATAAGATACA TTGATGAGTT TGGACAAACC
2161 ACAACTAGAA TGCAGTGAAA AAAATGCTTT ATTTGTGAAA TTTGTGATGC TATTGCTTTA TTTGTAACCA TTATAAGCTG
2241 CAATAAACAA GTTAACAACA ACAATTGCAT TCATTTTATG TTTCAGGTTC AGGGGGAGGT GTGGGAGGTT TTTTAAAGCA
2321 AGTAAAACCT CTACAAATGT GGTACGCGTT GACATTGATT ATTGACTAGT TATTAATAGT AATCAATTAC GGGGTCATTA
2401 GTTCATAGCC CATATATGGA GTTCCGCGTT ACATAACTTA CGGTAAATGG CCCGCCTGGC TGACCGCCCA ACGACCCCCG
2481 CCCATTGACG TCAATAATGA CGTATGTTCC CATAGTAACG CCAATAGGGA CTTTCCATTG ACGTCAATGG GTGGAGTATT
2561 TACGGTAAAC TGCCCACTTG GCAGTACATC AAGTGTATCA TATGCCAAGT ACGCCCCCTA TTGACGTCAA TGACGGTAAA
2641 TGGCCCGCCT GGCATTATGC CCAGTACATG ACCTTATGGG ACTTTCCTAC TTGGCAGTAC ATCTACGTAT TAGTCATCGC
2721 TATTACCATG GTGATGCGGT TTTGGCAGTA CATCAATGGG CGTGGATAGC GGTTTGACTC ACGGGGATTT CCAAGTCTCC
2801 ACCCCATTGA CGTCAATGGG AGTTTGTTTT GGCACCAAAA TCAACGGGAC TTTCCAAAAT GTCGTAACAA CTCCGCCCCA
2881 TTGACGCAAA TGGGCGGTAG GCGTGTACGG TGGGAGGTCT ATATAAGCAG AGCTCTCTGG CTAACTAGAG AACCCACTGC
2961 GCCACCATGG TGAGCAAGGG CGAGGAGCTG TTCACCGGGG TGGTGCCCAT CCTGGTCGAG CTGGACGGCG ACGTAAACGG
3041 CCACAAGTTC AGCGTGTCCG GCGAGGGCGA GGGCGATGCC ACCTACGGCA AGCTGACCCT GAAGTTCATC TGCACCACCG
3121 GCAAGCTGCC CGTGCCCTGG CCCACCCTCG TGACCACCCT GACCTACGGC GTGCAGTGCT TCAGCCGCTA CCCCGACCAC
3201 ATGAAGCAGC ACGACTTCTT CAAGTCCGCC ATGCCCGAAG GCTACGTCCA GGAGCGCACC ATCTTCTTCA AGGACGACGG
3281 CAACTACAAG ACCCGCGCCG AGGTGAAGTT CGAGGGCGAC ACCCTGGTGA ACCGCATCGA GCTGAAGGGC ATCGACTTCA
3361 AGGAGGACGG CAACATCCTG GGGCACAAGC TGGAGTACAA CTACAACAGC CACAACGTCT ATATCATGGC CGACAAGCAG
3441 AAGAACGGCA TCAAGGTGAA CTTCAAGATC CGCCACAACA TCGAGGACGG CAGCGTGCAG CTCGCCGACC ACTACCAGCA
3521 GAACACCCCC ATCGGCGACG GCCCCGTGCT GCTGCCCGAC AACCACTACC TGAGCACCCA GTCCGCCCTG AGCAAAGACC
3601 CCAACGAGAA GCGCGATCAC ATGGTCCTGC TGGAGTTCGT GACCGCCGCC GGGATCACTC TCGGCATGGA CGAGCTGTAC
3681 AAGATGACCG AGTACAAGCC CACGGTGCGC CTCGCCACCC GCGACGACGT CCCCAGGGCC GTACGCACCC TCGCCGCCGC
3761 GTTCGCCGAC TACCCCGCCA CGCGCCACAC CGTCGATCCG GACCGCCACA TCGAGCGGGT CACCGAGCTG CAAGAACTCT
3841 TCCTCACGCG CGTCGGGCTC GACATCGGCA AGGTGTGGGT CGCGGACGAC GGCGCCGCGG TGGCGGTCTG GACCACGCCG
3921 GAGAGCGTCG AAGCGGGGGC GGTGTTCGCC GAGATCGGCC CGCGCATGGC CGAGTTGAGC GGTTCCCGGC TGGCCGCGCA
4001 GCAACAGATG GAAGGCCTCC TGGCGCCGCA CCGGCCCAAG GAGCCCGCGT GGTTCCTGGC CACCGTCGGC GTCTCGCCCG
4081 ACCACCAGGG CAAGGGTCTG GGCAGCGCCG TCGTGCTCCC CGGAGTGGAG GCGGCCGAGC GCGCCGGGGT GCCCGCCTTC
4161 CTGGAGACCT CCGCGCCCCG CAACCTCCCC TTCTACGAGC GGCTCGGCTT CACCGTCACC GCCGACGTCG AGGTGCCCGA

```
4241 AGGACCGCGC ACCTGGTGCA TGACCCGCAA GCCCGGTGCC TGACTCGAGT CTAGAGGGCC CGTTTAAACC CGCTGATCAG
4321 CCTCGACTGT GCCTTCTAGT TGCCAGCCAT CTGTTGTTTG CCCCTCCCCC GTGCCTTCCT TGACCCTGGA AGGTGCCACT
4401 CCCACTGTCC TTTCCTAATA AAATGAGGAA ATTGCATCGC ATTGTCTGAG TAGGTGTCAT TCTATTCTGG GGGGTGGGGT
4481 GGGGCAGGAC AGCAAGGGGG AGGATTGGGA AGACAATAGC AGGCATGCTG GGGATGCGGT GGGCTCTATG GGCGGCCGCG
4561 GCGCTCTTCC GCTTCCTCGC TCACTGACTC GCTGCGCTCG GTCGTTCGGC TGCGGCGAGC GGTATCAGCT CACTCAAAGG
4641 CGGTAATACG GTTATCCACA GAATCAGGGG ATAACGCAGG AAAGAACATG TGAGCAAAAG GCCAGCAAAA GGCCAGGAAC
4721 CGTAAAAAGG CCGCGTTGCT GGCGTTTTTC CATAGGCTCC GCCCCCCTGA CGAGCATCAC AAAAATCGAC GCTCAAGTCA
4801 GAGGTGGCGA AACCCGACAG GACTATAAAG ATACCAGGCG TTTCCCCCTG GAAGCTCCCT CGTGCGCTCT CCTGTTCCGA
4881 CCCTGCCGCT TACCGGATAC CTGTCCGCCT TTCTCTCTTC GGGAAGCGTG GCGCTTTCTC ATAGCTCACG CTGTAGGTAT
4961 CTCAGTTCGG TGTAGGTCGT TCGCTCCAAG CTGGGCTGTG TGCACGAACC CCCCGTTCAG CCCGACCGCT GCGCCTTATC
5041 CGGTAACTAT CGTCTTGAGT CCAACCCGGT AAGACACGAC TTATCGCCAC TGGCAGCAGC CACTGGTAAC AGGATTAGCA
5121 GAGCGAGGTA TGTAGGCGGT GCTACAGAGT TCTTGAAGTG GTGGCCTAAC TACGGCTACA CTAGAAGAAC AGTATTTGGT
5201 ATCTGCGCTC TGCTGAAGCC AGTTACCTTC GGAAAAAGAG TTGGTAGCTC TTGATCCGGC AAACAAACCA CCGCTGGTAG
5281 CGGTGGTTTT TTTGTTTGCA AGCAGCAGAT TACGCGCAGA AAAAAAGGAT CTCAAGAAGA TCCTTTGATC TTTTCTACGG
5361 GGTCTGACGC TCAGTGGAAC GAAAACTCAC GTTAAGGGAT TTTGGTCATG AGATTATCAA AAAGGATCTT CACCTAGATC
5441 CTTTTAAATT AAAAATGAAG TTTTAAATCA ATCTAAAGTA TATATGAGTA AACTTGGTCT GACAGTTACC AATGCTTAAT
5521 CAGTGAGGCA CCTATCTCAG CGATCTGTCT ATTTCGTTCA TCCATAGTTG CCTGACTCCC CGTCGTGTAG ATAACTACGA
5601 TACGGGAGGG CTTACCATCT GGCCCCAGTG CTGCAATGAT ACCGCGAGAC CCACGCTCAC CGGCTCCAGA TTTATCAGCA
5681 ATAAACCAGC CAGCCGGAAG GGCCGAGCGC AGAAGTGGTC CTGCAACTTT ATCCGCCTCC ATCCAGTCTA TTAATTGTTG
5761 CCGGGAAGCT AGAGTAAGTA GTTCGCCAGT TAATAGTTTG CGCAACGTTG TTGCCATTGC TACAGGCATC GTGGTGTCAC
5841 GCTCGTCGTT TGGTATGGCT TCATTCAGCT CCGGTTCCCA ACGATCAAGG CGAGTTACAT GATCCCCCAT GTTGTGCAAA
5921 AAAGCGGTTA GCTCCTTCGG TCCTCCGATC GTTGTCAGAA GTAAGTTGGC CGCAGTGTTA TCACTCATGG TTATGGCAGC
6001 ACTGCATAAT TCTCTTACTG TCATGCCATC CGTAAGATGC TTTTCTGTGA CTGGTGAGTA CTCAACCAAG TCATTCTGAG
6081 AATAGTGTAT GCGGCGACCG AGTTGCTCTT GCCCGGCGTC AATACGGGAT AATACCGCGC CACATAGCAG AACTTTAAAA
6161 GTGCTCATCA TTGGAAAACG TTCTTCGGGG CGAAAACTCT CAAGGATCTT ACCGCTGTTG AGATCCAGTT CGATGTAACC
6241 CACTCGTGCA CCCAACTGAT CTTCAGCATC TTTTACTTTC ACCAGCGTTT CTGGGTGAGC AAAAACAGGA AGGCAAAATG
6321 CCGCAAAAAA GGGAATAAGG GCGACACGGA AATGTTGAAT ACTCATACTC TTCCTTTTTC AATATTATTG AAGCATTTAT
6401 CAGGGTTATT GTCTCATGAG CGGATACATA TTTGAATGTA TTTAGAAAAA TAAACAAATA GGGGTTCCGC GCACATTTCC
6481 CCGAAAAGTG CCACCTGACG TCTAAGAAAC CATTATTATC ATGACATTAA CCTATAAAAA TAGGCGTATC ACGAGGCCCT
6561 TTCGTCGGCG CGCCGCGGCC GC
```

Validation by Restriction Enzyme Digestion

Restriction Enzymes	Cutting Sites	DNA Fragments (bp)
NaeI	1341, 1500, 2111	159, 611, 5812
FspI	1909, 5802	3893, 2689
SpeI	40, 2366	2326, 4256
ApaLI	5001, 6247	1246, 5336
ApaLI+FspI	1909, 5001, 5802, 6247	3092, 801, 445, 2244
ApaLI+SpeI	40, 2366, 5001, 6247	2326, 2635, 1246, 375
ApaLI+NaeI	1341, 1500, 2111, 5001, 6247	159, 611, 2890, 1246, 1676

b) GFAP-*Gem* overexpression plasmid

Vector Summary

Vector ID	VB190514-1022kfc
Vector Name	pRP[Exp]-EGFP-GFAP_long>rGem[NM_001106637.1]
Date Created (Pacific Time)	2019-05-13
Vector Size	7024 bp
Vector Type	Mammalian Gene Expression Vector
Inserted Promoter	GFAP_long
Inserted ORF	rGem[NM_001106637.1]
Inserted Marker	EGFP
Plasmid Copy Number	High
Antibiotic Resistance	Ampicillin
Cloning Host	Stbl3 (or alternative strain)

Name	Position	Size (bp)	Type	Description	Application notes
GFAP_long	22-2199	2178	Promoter	Human glial fibrillary acidic protein promoter (2.1 kb)	Tissue specificity: Brain. Cell type specificity: Astrocytes.
Kozak	2224-2229	6	Miscellaneous	Kozak translation initiation sequence	Facilitates translation initiation of ATG start codon downstream of the Kozak sequence.
rGem[NM_001106637.1]	2230-3117	888	ORF	*None*	*None*
SV40 late pA	3162-3383	222	PolyA_signal	Simian virus 40 late polyadenylation signal	Allows transcription termination and polyadenylation of mRNA transcribed by Pol II RNA polymerase.
CMV promoter	3387-3974	588	Promoter	Human cytomegalovirus immediate early enhancer/promoter	Strong promoter; may have variable strength in some cell types.
EGFP	4006-4725	720	ORF	Enhanced green fluorescent protein; codon optimized based on a variant of wild type GFP from the jellyfish Aequorea victoria	Commonly used green fluorescent protein; ranked high in brightness, photostability and pH stability among all fluorescent proteins.
BGH pA	4769-4993	225	PolyA_signal	Bovine growth hormone polyadenylation signal	Allows transcription termination and polyadenylation of mRNA transcribed by Pol II RNA polymerase.
pUC ori	complement (5189-5777)	589	Rep_origin	pUC origin of replication	Facilitates plasmid replication in E. coli; regulates high-copy plasmid number (500-700).
Ampicillin	complement (5948-6808)	861	ORF	Ampicillin resistance gene	Allows E. coli to be resistant to ampicillin.

Vector Sequence

```
   1 CAACTTTGTA TAGAAAAGTT GGAGCTCCCA CCTCCCTCTC TGTGCTGGGA CTCACAGAGG GAGACCTCAG GAGGCAGTCT
  81 GTCCATCACA TGTCCAAATG CAGAGCATAC CCTGGGCTGG GCGCAGTGGC GCACAACTGT AATTCCAGCA CTTTGGGAGG
 161 CTGATGTGGA AGGATCACTT GAGCCCAGAA GTTCTAGACC AGCCTGGGCA ACATGGCAAG ACCCTATCTC TACAAAAAAA
 241 GTTAAAAAAT CAGCCACGTG TGGTGACACA CACCTGTAGT CCCAGCTATT CAGGAGGCTG AGGTGAGGGG ATCACTTAAG
 321 GCTGGGAGGT TGAGGCTGCA GTGAGTCGTG GTTGCGCCAC TGCACTCCAG CCTGGGCAAC AGTGAGACCC TGTCTCAAAA
 401 GACAAAAAAA AAAAAAAAAA AAAAAGAACA TATCCTGGTG TGGAGTAGGG GACGCTGCTC TGACAGAGGC TCGGGGGCCT
 481 GAGCTGGCTC TGTGAGCTGG GGAGGAGGCA GACAGCCAGG CCTTGTCTGC AAGCAGACCT GGCAGCATTG GGCTGGCCGC
 561 CCCCCAGGGC CTCCTCTTCA TGCCCAGTGA ATGACTCACC TTGGCACAGA CACAATGTTC GGGGTGGGCA CAGTGCCTGC
 641 TTCCCGCCGC ACCCCAGCCC CCCTCAAATG CCTTCCGAGA AGCCCATTGA GCAGGGGGCT TGCATTGCAC CCCAGCCTGA
 721 CAGCCTGGCA TCTTGGGATA AAAGCAGCAC AGCCCCCTAG GGGCTGCCCT TGCTGTGTGG CGCCACCGGC GGTGGAGAAC
 801 AAGGCTCTAT TCAGCCTGTG CCCAGGAAAG GGGATCAGGG GATGCCCAGG CATGGACAGT GGGTGGCAGG GGGGGAGAGG
 881 AGGGCTGTCT GCTTCCCAGA AGTCCAAGGA CACAAATGGG TGAGGGGACT GGGCAGGGTT CTGACCCTGT GGGACCAGAG
 961 TGGAGGGCGT AGATGGACCT GAAGTCTCCA GGGACAACAG GGCCCAGGTC TCAGGCTCCT AGTTGGGCCC AGTGGCTCCA
1041 GCGTTTCCAA ACCCATCCAT CCCCAGAGGT TCTTCCCATC TCTCCAGGCT GATGTGTGGG AACTCGAGGA AATAAATCTC
1121 CAGTGGGAGA CGGAGGGGTG GCCAGGGAAA CGGGGCGCTG CAGGAATAAA GACGAGCCAG CACAGCCAGC TCATGCGTAA
1201 CGGCTTTGTG GAGCTGTCAA GGCCTGGTCT CTGGGAGAGA GGCACAGGGA GGCCAGACAA GGAAGGGGTG ACCTGGAGGG
1281 ACAGATCCAG GGGCTAAAGT CCTGATAAGG CAAGAGAGTG CCGGCCCCCT CTTGCCCTAT CAGGACCTCC ACTGCCACAT
1361 AGAGGCCATG ATTGACCCTT AGACAAAGGG CTGGTGTCCA ATCCCAGCCC CCAGCCCCAG AACTCCAGGG AATGAATGGG
1441 CAGAGAGCAG GAATGTGGGA CATCTGTGTT CAAGGGAAGG ACTCCAGGAG TCTGCTGGGA ATGAGGCCTA GTAGGAAATG
1521 AGGTGGCCCT TGAGGGTACA GAACAGGTTC ATTCTTCGCC AAATTCCCAG CACCTTGCAG GCACTTACAG CTGAGTGAGA
1601 TAATGCCTGG GTTATGAAAT CAAAAAGTTG GAAAGCAGGT CAGAGGTCAT CTGGTACAGC CCTTCCTTCC CTTTTTTTTT
1681 TTTTTTTTTT TTGTGAGACA AGGTCTCTCT CTGTTGCCCA GGCTGGAGTG GCGCAAACAC AGCTCACTGC AGCCTCAACC
1761 TACTGGGCTC AAGCAATCCT CCAGCCTCAG CCTCCCAAAG TGCTGGGATT ACAAGCATGA GCCACCCCAC TCAGCCCTTT
1841 CCTTCCTTTT TAATTGATGC ATAATAATTG TAAGTATTCA TCATGGTCCA ACCAACCCTT TCTTGACCCA CCTTCCTAGA
1921 GAGAGGGTCC TCTTGCTTCA GCGGTCAGGG CCCCAGACCC ATGGTCTGGC TCCAGGTACC ACCTGCCTCA TGCAGGAGTT
2001 GGCGTGCCCA GGAAGCTCTG CCTCTGGGCA CAGTGACCTC AGTGGGGTGA GGGGAGCTCT CCCCATAGCT GGGCTGCGGC
2081 CCAACCCCAC CCCCTCAGGC TATGCCAGGG GGTGTTGCCA GGGGCACCCG GGCATCGCCA GTCTAGCCCA CTCCTTCATA
2161 AAGCCCTCGC ATCCCAGGAG CGAGCAGAGC CAGAGCAGGC AAGTTTGTAC AAAAAAGCAG GCTGCCACCA TGACTCTGAA
2241 TAACGTCACC ATGCGCCAAG GCACTGTGGG CATGCAGCCA CAGCAACGCT GGAGCATCCC TGCTGATGGC AGGCATCTGA
2321 TGGTCCAGAA GGATCCCCAC CCCTGCAACC CCCACAACCA CCACTCCACT GCTCCCGATG ACCACTGCCG GCGGAGCTGG
2401 TCCTCCGAGT CCACAGACTC GGTTATCTCT TCCGAGTCAG GAAACACCTA CTACCGAGTG GTGCTTATTG GGGAGCAAGG
2481 AGTGGGCAAG TCCACCCTGG CCAACATCTT TGCAGGTGTA CATGACAGCA TGGACAGCGA CTGTGAGGTC TTGGGAGAAG
2561 ATACATATGA GCGTACCCTG GTCGTTGATG GAGAGAGTGC AACCATTATC CTACTGGACA TGTGGGAAAA TAAGGGGGAG
2641 AATGAATGGC TCCACGACCA CTGCATGCAG GTCGGGGACG CCTACCTGAT CGTCTACTCC ATCACAGACC GGGCGAGCTT
2721 TGAGAAGGCG TCTGAGCTGA GGATCCAGCT CCGCAGGGCC CGGCAGACAG AAGACATTCC TATAATTTTG GTTGGCAACA
2801 AAAGCGACTT AGTGCGGTGT CGAGAAGTGT CTGTGTCAGA AGGGAGAGCT TGTGCCGTGG TGTTCGACTG CAAATTCATC
2881 GAGACCTCTG CAGCCGTGCA GCACAACGTG AAGGAACTGT TTGAGGGCAT TGTGCGGCAG GTCCGTCTGC GTCGGGACAG
2961 CAAGGAAAAG AACGAGAGGA GGCTGGCCTA CCAGAAGAGG CGGGAGAGTA TCCCCAGGAA AGCCAGACGC TTCTGGGGCA
3041 AAATTGTAGC CAAAAACAAC AAGAACATGG CTTTCAAGCT CAAGTCAAAA TCCTGCCATG ACCTGTCTGT GCTCTAGACC
3121 CAGCTTTCTT GTACAAAGTG GTGATGGCCG GCCGCTTCGA GCAGACATGA TAAGATACAT TGATGAGTTT GGACAAACCA
3201 CAACTAGAAT GCAGTGAAAA AAATGCTTTA TTTGTGAAAT TTGTGATGCT ATTGCTTTAT TTGTAACCAT TATAAGCTGC
3281 AATAAACAAG TTAACAACAA CAATTGCATT CATTTTATGT TTCAGGTTCA GGGGGAGGTG TGGGAGGTTT TTTAAAGCAA
3361 GTAAAACCTC TACAAATGTG GTACGCGTTG ACATTGATTA TTGACTAGTT ATTAATAGTA ATCAATTACG GGGTCATTAG
```

3441 TTCATAGCCC ATATATGGAG TTCCGCGTTA CATAACTTAC GGTAAATGGC CCGCCTGGCT GACCGCCCAA CGACCCCCGC
3521 CCATTGACGT CAATAATGAC GTATGTTCCC ATAGTAACGC CAATAGGGAC TTTCCATTGA CGTCAATGGG TGGAGTATTT
3601 ACGGTAAACT GCCCACTTGG CAGTACATCA AGTGTATCAT ATGCCAAGTA CGCCCCCTAT TGACGTCAAT GACGGTAAAT
3681 GGCCCGCCTG GCATTATGCC CAGTACATGA CCTTATGGGA CTTTCCTACT TGGCAGTACA TCTACGTATT AGTCATCGCT
3761 ATTACCATGG TGATGCGGTT TTGGCAGTAC ATCAATGGGC GTGGATAGCG GTTTGACTCA CGGGGATTTC CAAGTCTCCA
3841 CCCCATTGAC GTCAATGGGA GTTTGTTTTG GCACCAAAAT CAACGGGACT TTCCAAAATG TCGTAACAAC TCCGCCCCAT
3921 TGACGCAAAT GGGCGGTAGG CGTGTACGGT GGGAGGTCTA TATAAGCAGA GCTCTCTGGC TAACTAGAGA ACCCACTGCG
4001 CCACCATGGT GAGCAAGGGC GAGGAGCTGT TCACCGGGGT GGTGCCCATC CTGGTCGAGC TGGACGGCGA CGTAAACGGC
4081 CACAAGTTCA GCGTGTCCGG CGAGGGCGAG GGCGATGCCA CCTACGGCAA GCTGACCCTG AAGTTCATCT GCACCACCGG
4161 CAAGCTGCCC GTGCCCTGGC CCACCCTCGT GACCACCCTG ACCTACGGCG TGCAGTGCTT CAGCCGCTAC CCCGACCACA
4241 TGAAGCAGCA CGACTTCTTC AAGTCCGCCA TGCCCGAAGG CTACGTCCAG GAGCGCACCA TCTTCTTCAA GGACGACGGC
4321 AACTACAAGA CCCGCGCCGA GGTGAAGTTC GAGGGCGACA CCCTGGTGAA CCGCATCGAG CTGAAGGGCA TCGACTTCAA
4401 GGAGGACGGC AACATCCTGG GGCACAAGCT GGAGTACAAC TACAACAGCC ACAACGTCTA TATCATGGCC GACAAGCAGA
4481 AGAACGGCAT CAAGGTGAAC TTCAAGATCC GCCACAACAT CGAGGACGGC AGCGTGCAGC TCGCCGACCA CTACCAGCAG
4561 AACACCCCCA TCGGCGACGG CCCCGTGCTG CTGCCCGACA ACCACTACCT GAGCACCCAG TCCGCCCTGA GCAAAGACCC
4641 CAACGAGAAG CGCGATCACA TGGTCCTGCT GGAGTTCGTG ACCGCCGCCG GGATCACTCT CGGCATGGAC GAGCTGTACA
4721 AGTAACTCGA GTCTAGAGGG CCCGTTTAAA CCCGCTGATC AGCCTCGACT GTGCCTTCTA GTTGCCAGCC ATCTGTTGTT
4801 TGCCCCTCCC CCGTGCCTTC CTTGACCCTG GAAGGTGCCA CTCCCACTGT CCTTTCCTAA TAAAATGAGG AAATTGCATC
4881 GCATTGTCTG AGTAGGTGTC ATTCTATTCT GGGGGGTGGG GTGGGGCAGG ACAGCAAGGG GGAGGATTGG GAAGACAATA
4961 GCAGGCATGC TGGGGATGCG GTGGGCTCTA TGGGCGGCCG CGGCGCTCTT CCGCTTCCTC GCTCACTGAC TCGCTGCGCT
5041 CGGTCGTTCG GCTGCGGCGA GCGGTATCAG CTCACTCAAA GGCGGTAATA CGGTTATCCA CAGAATCAGG GGATAACGCA
5121 GGAAAGAACA TGTGAGCAAA AGGCCAGCAA AAGGCCAGGA ACCGTAAAAA GGCCGCGTTG CTGGCGTTTT TCCATAGGCT
5201 CCGCCCCCCT GACGAGCATC ACAAAAATCG ACGCTCAAGT CAGAGGTGGC GAAACCCGAC AGGACTATAA AGATACCAGG
5281 CGTTTCCCCC TGGAAGCTCC CTCGTGCGCT CTCCTGTTCC GACCCTGCCG CTTACCGGAT ACCTGTCCGC CTTTCTCTCT
5361 TCGGGAAGCG TGGCGCTTTC TCATAGCTCA CGCTGTAGGT ATCTCAGTTC GGTGTAGGTC GTTCGCTCCA AGCTGGGCTG
5441 TGTGCACGAA CCCCCCGTTC AGCCCGACCG CTGCGCCTTA TCCGGTAACT ATCGTCTTGA GTCCAACCCG GTAAGACACG
5521 ACTTATCGCC ACTGGCAGCA GCCACTGGTA ACAGGATTAG CAGAGCGAGG TATGTAGGCG GTGCTACAGA GTTCTTGAAG
5601 TGGTGGCCTA ACTACGGCTA CACTAGAAGA ACAGTATTTG GTATCTGCGC TCTGCTGAAG CCAGTTACCT TCGGAAAAAG
5681 AGTTGGTAGC TCTTGATCCG GCAAACAAAC CACCGCTGGT AGCGGTGGTT TTTTTGTTTG CAAGCAGCAG ATTACGCGCA
5761 GAAAAAAAGG ATCTCAAGAA GATCCTTTGA TCTTTTCTAC GGGGTCTGAC GCTCAGTGGA ACGAAAACTC ACGTTAAGGG
5841 ATTTTGGTCA TGAGATTATC AAAAAGGATC TTCACCTAGA TCCTTTTAAA TTAAAAATGA AGTTTTAAAT CAATCTAAAG
5921 TATATATGAG TAAACTTGGT CTGACAGTTA CCAATGCTTA ATCAGTGAGG CACCTATCTC AGCGATCTGT CTATTTCGTT
6001 CATCCATAGT TGCCTGACTC CCCGTCGTGT AGATAACTAC GATACGGGAG GGCTTACCAT CTGGCCCCAG TGCTGCAATG
6081 ATACCGCGAG ACCCACGCTC ACCGGCTCCA GATTTATCAG CAATAAACCA GCCAGCCGGA AGGGCCGAGC GCAGAAGTGG
6161 TCCTGCAACT TTATCCGCCT CCATCCAGTC TATTAATTGT TGCCGGGAAG CTAGAGTAAG TAGTTCGCCA GTTAATAGTT
6241 TGCGCAACGT TGTTGCCATT GCTACAGGCA TCGTGGTGTC ACGCTCGTCG TTTGGTATGG CTTCATTCAG CTCCGGTTCC
6321 CAACGATCAA GGCGAGTTAC ATGATCCCCC ATGTTGTGCA AAAAAGCGGT TAGCTCCTTC GGTCCTCCGA TCGTTGTCAG
6401 AAGTAAGTTG GCCGCAGTGT TATCACTCAT GGTTATGGCA GCACTGCATA ATTCTCTTAC TGTCATGCCA TCCGTAAGAT
6481 GCTTTTCTGT GACTGGTGAG TACTCAACCA AGTCATTCTG AGAATAGTGT ATGCGGCGAC CGAGTTGCTC TTGCCCGGCG
6561 TCAATACGGG ATAATACCGC GCCACATAGC AGAACTTTAA AAGTGCTCAT CATTGGAAAA CGTTCTTCGG GGCGAAAACT
6641 CTCAAGGATC TTACCGCTGT TGAGATCCAG TTCGATGTAA CCCACTCGTG CACCCAACTG ATCTTCAGCA TCTTTTACTT
6721 TCACCAGCGT TTCTGGGTGA GCAAAAACAG GAAGGCAAAA TGCCGCAAAA AAGGGAATAA GGGCGACACG GAAATGTTGA
6801 ATACTCATAC TCTTCCTTTT TCAATATTAT TGAAGCATTT ATCAGGGTTA TTGTCTCATG AGCGGATACA TATTTGAATG
6881 TATTTAGAAA AATAAACAAA TAGGGGTTCC GCGCACATTT CCCCGAAAAG TGCCACCTGA CGTCTAAGAA ACCATTATTA
6961 TCATGACATT AACCTATAAA AATAGGCGTA TCACGAGGCC CTTTCGTCGG CGCGCCGCGG CCGC

Restriction Enzymes	Cutting Sites	DNA Fragments (bp)
NaeI	1323, 2390, 3150	1067, 760, 5197
SmaI	2130	7024
XmaI	2128	7024
ApaLI	5443, 6689	1246, 5778
DraIII	2908	7024
ApaLI+XmaI	2128, 5443, 6689	3315, 1246, 2463
ApaLI+SmaI	2130, 5443, 6689	3313, 1246, 2465
ApaLI+NaeI	1323, 2390, 3150, 5443, 6689	1067, 760, 2293, 1246, 1658
ApaLI+DraIII	2908, 5443, 6689	2535, 1246, 3243

c) GFAP-*Gem* shRNA knockdown plasmid

Vector Summary

Vector ID	VB190507-1061xgu
Vector Name	pRP[miR30]-GFAP_long>EGFP:{rGem}
Date Created (Pacific Time)	2019-05-06
Vector Size	5586 bp
Vector Type	Mammalian miR30-shRNA Knockdown Vector
Inserted Promoter	GFAP_long
Inserted ORF	EGFP
Inserted shRNA	{rGem}
Target Sequence	AGACAGAAGACATTCCTATAAT
Plasmid Copy Number	High
Antibiotic Resistance	Ampicillin
Cloning Host	Stbl3 (or alternative strain)

Vector Components

Name	Position	Size (bp)	Type	Description	Application notes
GFAP_long	22-2199	2178	Promoter	Human glial fibrillary acidic protein promoter (2.1 kb)	Tissue specificity: Brain. Cell type specificity: Astrocytes.
Kozak	2224-2229	6	Miscellaneous	Kozak translation initiation sequence	Facilitates translation initiation of ATG start codon downstream of the Kozak sequence.
EGFP	2230-2949	720	ORF	Enhanced green fluorescent protein; codon optimized based on a variant of wild type GFP from the jellyfish Aequorea victoria	Commonly used green fluorescent protein; ranked high in brightness, photostability and pH stability among all fluorescent proteins.
5' miR-30E	2974-3101	128	Miscellaneous	Human miR30 5' context with several bases mutation	Allows to form mature shRNA and trigger knockdown.
{rGem}	3102-3164	63	shRNA	*None*	*None*
3' miR-30E	3165-3294	130	Miscellaneous	Human miR30 3' context with several bases mutation	Allows to form mature shRNA and trigger knockdown.
SV40 late pA	3334-3555	222	PolyA_signal	Simian virus 40 late polyadenylation signal	Allows transcription termination and polyadenylation of mRNA transcribed by Pol II RNA polymerase.
pUC ori	complement (3751-4339)	589	Rep_origin	pUC origin of replication	Facilitates plasmid replication in E. coli; regulates high-copy plasmid number (500-700).
Ampicillin	complement (4510-5370)	861	ORF	Ampicillin resistance gene	Allows E. coli to be resistant to ampicillin.

Note: Components added by user are listed in **bold red** text.

Vector Sequence

1 CAACTTTGTA TAGAAAAGTT GGAGCTCCCA CCTCCCTCTC TGTGCTGGGA CTCACAGAGG GAGACCTCAG GAGGCAGTCT
81 GTCCATCACA TGTCCAAATG CAGAGCATAC CCTGGGCTGG GCGCAGTGGC GCACAACTGT AATTCCAGCA CTTTGGGAGG
161 CTGATGTGGA AGGATCACTT GAGCCCAGAA GTTCTAGACC AGCCTGGGCA ACATGGCAAG ACCCTATCTC TACAAAAAAA
241 GTTAAAAAAT CAGCCACGTG TGGTGACACA CACCTGTAGT CCCAGCTATT CAGGAGGCTG AGGTGAGGGG ATCACTTAAG
321 GCTGGGAGGT TGAGGCTGCA GTGAGTCGTG GTTGCGCCAC TGCACTCCAG CCTGGGCAAC AGTGAGACCC TGTCTCAAAA
401 GACAAAAAAA AAAAAAAAAA AAAAAGAACA TATCCTGGTG TGGAGTAGGG GACGCTGCTC TGACAGAGGC TCGGGGGCCT
481 GAGCTGGCTC TGTGAGCTGG GGAGGAGGCA GACAGCCAGG CCTTGTCTGC AAGCAGACCT GGCAGCATTG GGCTGGCCGC
561 CCCCCAGGGC CTCCTCTTCA TGCCCAGTGA ATGACTCACC TTGGCACAGA CACAATGTTC GGGGTGGGCA CAGTGCCTGC
641 TTCCCGCCGC ACCCCAGCCC CCCTCAAATG CCTTCCGAGA AGCCCATTGA GCAGGGGGCT TGCATTGCAC CCCAGCCTGA
721 CAGCCTGGCA TCTTGGGATA AAAGCAGCAC AGCCCCCTAG GGGCTGCCCT TGCTGTGTGG CGCCACCGGC GGTGGAGAAC
801 AAGGCTCTAT TCAGCCTGTG CCCAGGAAAG GGGATCAGGG GATGCCCAGG CATGGACAGT GGGTGGCAGG GGGGGAGAGG
881 AGGGCTGTCT GCTTCCCAGA AGTCCAAGGA CACAAATGGG TGAGGGGACT GGGCAGGGTT CTGACCCTGT GGGACCAGAG
961 TGGAGGGCGT AGATGGACCT GAAGTCTCCA GGGACAACAG GGCCCAGGTC TCAGGCTCCT AGTTGGGCCC AGTGGCTCCA
1041 GCGTTTCCAA ACCCATCCAT CCCCAGAGGT TCTTCCCATC TCTCCAGGCT GATGTGTGGG AACTCGAGGA AATAAATCTC
1121 CAGTGGGAGA CGGAGGGGTG GCCAGGGAAA CGGGGCGCTG CAGGAATAAA GACGAGCCAG CACAGCCAGC TCATGCGTAA
1201 CGGCTTTGTG GAGCTGTCAA GGCCTGGTCT CTGGGAGAGA GGCACAGGGA GGCCAGACAA GGAAGGGGTG ACCTGGAGGG
1281 ACAGATCCAG GGGCTAAAGT CCTGATAAGG CAAGAGAGTG CCGGCCCCCT CTTGCCCTAT CAGGACCTCC ACTGCCACAT
1361 AGAGGCCATG ATTGACCCTT AGACAAAGGG CTGGTGTCCA ATCCCAGCCC CCAGCCCCAG AACTCCAGGG AATGAATGGG
1441 CAGAGAGCAG GAATGTGGGA CATCTGTGTT CAAGGGAAGG ACTCCAGGAG TCTGCTGGGA ATGAGGCCTA GTAGGAAATG
1521 AGGTGGCCCT TGAGGGTACA GAACAGGTTC ATTCTTCGCC AAATTCCCAG CACCTTGCAG GCACTTACAG CTGAGTGAGA
1601 TAATGCCTGG GTTATGAAAT CAAAAAGTTG GAAAGCAGGT CAGAGGTCAT CTGGTACAGC CCTTCCTTCC CTTTTTTTTT
1681 TTTTTTTTTT TTGTGAGACA AGGTCTCTCT CTGTTGCCCA GGCTGGAGTG GCGCAAACAC AGCTCACTGC AGCCTCAACC
1761 TACTGGGCTC AAGCAATCCT CCAGCCTCAG CCTCCCAAAG TGCTGGGATT ACAAGCATGA GCCACCCCAC TCAGCCCTTT
1841 CCTTCCTTTT TAATTGATGC ATAATAATTG TAAGTATTCA TCATGGTCCA ACCAACCCTT TCTTGACCCA CCTTCCTAGA
1921 GAGAGGGTCC TCTTGCTTCA GCGGTCAGGG CCCCAGACCC ATGGTCTGGC TCCAGGTACC ACCTGCCTCA TGCAGGAGTT
2001 GGCGTGCCCA GGAAGCTCTG CCTCTGGGCA CAGTGACCTC AGTGGGGTGA GGGGAGCTCT CCCCATAGCT GGGCTGCGGC
2081 CCAACCCCAC CCCCTCAGGC TATGCCAGGG GGTGTTGCCA GGGGCACCCG GGCATCGCCA GTCTAGCCCA CTCCTTCATA
2161 AAGCCCTCGC ATCCCAGGAG CGAGCAGAGC CAGAGCAGGC AAGTTTGTAC AAAAAAGCAG GCTGCCACCA TGGTGAGCAA
2241 GGGCGAGGAG CTGTTCACCG GGGTGGTGCC CATCCTGGTC GAGCTGGACG GCGACGTAAA CGGCCACAAG TTCAGCGTGT
2321 CCGGCGAGGG CGAGGGCGAT GCCACCTACG GCAAGCTGAC CCTGAAGTTC ATCTGCACCA CCGGCAAGCT GCCCGTGCCC
2401 TGGCCCACCC TCGTGACCAC CCTGACCTAC GGCGTGCAGT GCTTCAGCCG CTACCCCGAC CACATGAAGC AGCACGACTT
2481 CTTCAAGTCC GCCATGCCCG AAGGCTACGT CCAGGAGCGC ACCATCTTCT TCAAGGACGA CGGCAACTAC AAGACCCGCG
2561 CCGAGGTGAA GTTCGAGGGC GACACCCTGG TGAACCGCAT CGAGCTGAAG GGCATCGACT TCAAGGAGGA CGGCAACATC
2641 CTGGGGCACA AGCTGGAGTA CAACTACAAC AGCCACAACG TCTATATCAT GGCCGACAAG CAGAAGAACG GCATCAAGGT
2721 GAACTTCAAG ATCCGCCACA ACATCGAGGA CGGCAGCGTG CAGCTCGCCG ACCACTACCA GCAGAACACC CCCATCGGCG
2801 ACGGCCCCGT GCTGCTGCCC GACAACCACT ACCTGAGCAC CCAGTCCGCC CTGAGCAAAG ACCCCAACGA GAAGCGCGAT
2881 CACATGGTCC TGCTGGAGTT CGTGACCGCC GCCGGGATCA CTCTCGGCAT GGACGAGCTG TACAAGTAAA CCCAGCTTTC
2961 TTGTACAAAG TGGTGTTTGA ATGAGGCTTC AGTACTTTAC AGAATCGTTG CCTGCACATC TTGGAAACAC TTGCTGGGAT
3041 TACTTCGACT TCTTAACCCA ACAGAAGGCT CGAGAAGGTA TATTGCTGTT GACAGTGAGC GCGACAGAAG ACATTCCTAT
3121 AATTAGTGAA GCCACAGATG TAATTATAGG AATGTCTTCT GTCTTGCCTA CTGCCTCGGA CTTCAAGGGG CTAGAATTCG
3201 AGCAATTATC TTGTTTACTA AAACTGAATA CCTTGCTATC TCTTTGATAC ATTTTTACAA AGCTGAATTA AAATGGTATA
3281 AATTAAATCA CTTTCAACTT TATTATACAT AGTTGATGGC CGGCCGCTTC GAGCAGACAT GATAAGATAC ATTGATGAGT
3361 TTGGACAAAC CACAACTAGA ATGCAGTGAA AAAAATGCTT TATTTGTGAA ATTTGTGATG CTATTGCTTT ATTTGTAACC
3441 ATTATAAGCT GCAATAAACA AGTTAACAAC AACAATTGCA TTCATTTTAT GTTTCAGGTT CAGGGGGAGG TGTGGGAGGT
3521 TTTTTAAAGC AAGTAAAACC TCTACAAATG TGGTAGCGGC CGCGGCGCTC TTCCGCTTCC TCGCTCACTG ACTCGCTGCG
3601 CTCGGTCGTT CGGCTGCGGC GAGCGGTATC AGCTCACTCA AAGGCGGTAA TACGGTTATC CACAGAATCA GGGGATAACG
3681 CAGGAAAGAA CATGTGAGCA AAAGGCCAGC AAAAGGCCAG GAACCGTAAA AAGGCCGCGT TGCTGGCGTT TTTCCATAGG
3761 CTCCGCCCCC CTGACGAGCA TCACAAAAAT CGACGCTCAA GTCAGAGGTG GCGAAACCCG ACAGGACTAT AAAGATACCA
3841 GGCGTTTCCC CCTGGAAGCT CCCTCGTGCG CTCTCCTGTT CCGACCCTGC CGCTTACCGG ATACCTGTCC GCCTTTCTCT

```
3921 CTTCGGGAAG CGTGGCGCTT TCTCATAGCT CACGCTGTAG GTATCTCAGT TCGGTGTAGG TCGTTCGCTC CAAGCTGGGC
4001 TGTGTGCACG AACCCCCCGT TCAGCCCGAC CGCTGCGCCT TATCCGGTAA CTATCGTCTT GAGTCCAACC CGGTAAGACA
4081 CGACTTATCG CCACTGGCAG CAGCCACTGG TAACAGGATT AGCAGAGCGA GGTATGTAGG CGGTGCTACA GAGTTCTTGA
4161 AGTGGTGGCC TAACTACGGC TACACTAGAA GAACAGTATT TGGTATCTGC GCTCTGCTGA AGCCAGTTAC CTTCGGAAAA
4241 AGAGTTGGTA GCTCTTGATC CGGCAAACAA ACCACCGCTG GTAGCGGTGG TTTTTTTGTT TGCAAGCAGC AGATTACGCG
4321 CAGAAAAAAA GGATCTCAAG AAGATCCTTT GATCTTTTCT ACGGGGTCTG ACGCTCAGTG GAACGAAAAC TCACGTTAAG
4401 GGATTTTGGT CATGAGATTA TCAAAAAGGA TCTTCACCTA GATCCTTTTA AATTAAAAAT GAAGTTTTAA ATCAATCTAA
4481 AGTATATATG AGTAAACTTG GTCTGACAGT TACCAATGCT TAATCAGTGA GGCACCTATC TCAGCGATCT GTCTATTTCG
4561 TTCATCCATA GTTGCCTGAC TCCCCGTCGT GTAGATAACT ACGATACGGG AGGGCTTACC ATCTGGCCCC AGTGCTGCAA
4641 TGATACCGCG AGACCCACGC TCACCGGCTC CAGATTTATC AGCAATAAAC CAGCCAGCCG GAAGGGCCGA GCGCAGAAGT
4721 GGTCCTGCAA CTTTATCCGC CTCCATCCAG TCTATTAATT GTTGCCGGGA AGCTAGAGTA AGTAGTTCGC CAGTTAATAG
4801 TTTGCGCAAC GTTGTTGCCA TTGCTACAGG CATCGTGGTG TCACGCTCGT CGTTTGGTAT GGCTTCATTC AGCTCCGGTT
4881 CCCAACGATC AAGGCGAGTT ACATGATCCC CCATGTTGTG CAAAAAAGCG GTTAGCTCCT TCGGTCCTCC GATCGTTGTC
4961 AGAAGTAAGT TGGCCGCAGT GTTATCACTC ATGGTTATGG CAGCACTGCA TAATTCTCTT ACTGTCATGC CATCCGTAAG
5041 ATGCTTTTCT GTGACTGGTG AGTACTCAAC CAAGTCATTC TGAGAATAGT GTATGCGGCG ACCGAGTTGC TCTTGCCCGG
5121 CGTCAATACG GGATAATACC GCGCCACATA GCAGAACTTT AAAAGTGCTC ATCATTGGAA AACGTTCTTC GGGGCGAAAA
5201 CTCTCAAGGA TCTTACCGCT GTTGAGATCC AGTTCGATGT AACCCACTCG TGCACCCAAC TGATCTTCAG CATCTTTTAC
5281 TTTCACCAGC GTTTCTGGGT GAGCAAAAAC AGGAAGGCAA AATGCCGCAA AAAAGGGAAT AAGGGCGACA CGGAAATGTT
5361 GAATACTCAT ACTCTTCCTT TTTCAATATT ATTGAAGCAT TTATCAGGGT TATTGTCTCA TGAGCGGATA CATATTTGAA
5441 TGTATTTAGA AAAATAAACA AATAGGGGTT CCGCGCACAT TTCCCCGAAA AGTGCCACCT GACGTCTAAG AAACCATTAT
5521 TATCATGACA TTAACCTATA AAAATAGGCG TATCACGAGG CCCTTTCGTC GGCGCGCCGC GGCCGC
```

Validation by Restriction Enzyme Digestion

Restriction Enzymes	Cutting Sites	DNA Fragments (bp)
NcoI	1960, 2229	269, 5317
ApaLI	4005, 5251	1246, 4340
ApaLI+NcoI	1960, 2229, 4005, 5251	269, 1776, 1246, 2295

d) GFAP-*Oxtr* shRNA knockdown plasmid

Vector Summary

Vector ID	VB190808-1095zxy
Vector Name	pRP[miR30]-GFAP_long>EGFP:{rOXTR}
Date Created (Pacific Time)	2019-08-07
Vector Size	5586 bp
Vector Type	Mammalian miR30-shRNA Knockdown Vector
Inserted Promoter	GFAP_long
Inserted ORF	EGFP
Inserted shRNA	{rOXTR}
Target Sequence	GGACGCAGAGTGGTGCTAATTT
Plasmid Copy Number	High
Antibiotic Resistance	Ampicillin
Cloning Host	VB UltraStable (or alternative strain)

Vector Components

Name	Position	Size (bp)	Type	Description	Application notes
GFAP_long	22-2199	2178	Promoter	Human glial fibrillary acidic protein promoter (2.1 kb)	Tissue specificity: Brain. Cell type specificity: Astrocytes.
Kozak	2224-2229	6	Miscellaneous	Kozak translation initiation sequence	Facilitates translation initiation of ATG start codon downstream of the Kozak sequence.
EGFP	2230-2949	720	ORF	Enhanced green fluorescent protein; codon optimized based on a variant of wild type GFP from the jellyfish Aequorea victoria	Commonly used green fluorescent protein; ranked high in brightness, photostability and pH stability among all fluorescent proteins.
5' miR-30E	2974-3101	128	Miscellaneous	Human miR30 5' context with several bases mutation	Allows to form mature shRNA and trigger knockdown.
{rOXTR}	3102-3164	63	shRNA	*None*	*None*
3' miR-30E	3165-3294	130	Miscellaneous	Human miR30 3' context with several bases mutation	Allows to form mature shRNA and trigger knockdown.
SV40 late pA	3334-3555	222	PolyA_signal	Simian virus 40 late polyadenylation signal	Allows transcription termination and polyadenylation of mRNA transcribed by Pol II RNA polymerase.
pUC ori	complement (3751-4339)	589	Rep_origin	pUC origin of replication	Facilitates plasmid replication in E. coli; regulates high-copy plasmid number (500-700).
Ampicillin	complement (4510-5370)	861	ORF	Ampicillin resistance gene	Allows E. coli to be resistant to ampicillin.

Note: Components added by user are listed in **bold red** text.

Vector Sequence

```
   1 CAACTTTGTA TAGAAAAGTT GGAGCTCCCA CCTCCCTCTC TGTGCTGGGA CTCACAGAGG GAGACCTCAG GAGGCAGTCT

  81 GTCCATCACA TGTCCAAATG CAGAGCATAC CCTGGGCTGG GCGCAGTGGC GCACAACTGT AATTCCAGCA CTTTGGGAGG
 161 CTGATGTGGA AGGATCACTT GAGCCCAGAA GTTCTAGACC AGCCTGGGCA ACATGGCAAG ACCCTATCTC TACAAAAAAA
 241 GTTAAAAAAT CAGCCACGTG TGGTGACACA CACCTGTAGT CCCAGCTATT CAGGAGGCTG AGGTGAGGGG ATCACTTAAG
 321 GCTGGGAGGT TGAGGCTGCA GTGAGTCGTG GTTGCGCCAC TGCACTCCAG CCTGGGCAAC AGTGAGACCC TGTCTCAAAA
 401 GACAAAAAAA AAAAAAAAAA AAAAAGAACA TATCCTGGTG TGGAGTAGGG GACGCTGCTC TGACAGAGGC TCGGGGGCCT
 481 GAGCTGGCTC TGTGAGCTGG GGAGGAGGCA GACAGCCAGG CCTTGTCTGC AAGCAGACCT GGCAGCATTG GGCTGGCCGC
 561 CCCCCAGGGC CTCCTCTTCA TGCCCAGTGA ATGACTCACC TTGGCACAGA CACAATGTTC GGGGTGGGCA CAGTGCCTGC
 641 TTCCCGCCGC ACCCCAGCCC CCCTCAAATG CCTTCCGAGA AGCCCATTGA GCAGGGGGCT TGCATTGCAC CCCAGCCTGA
 721 CAGCCTGGCA TCTTGGGATA AAAGCAGCAC AGCCCCCTAG GGGCTGCCCT TGCTGTGTGG CGCCACCGGC GGTGGAGAAC
 801 AAGGCTCTAT TCAGCCTGTG CCCAGGAAAG GGGATCAGGG GATGCCCAGG CATGGACAGT GGGTGGCAGG GGGGGAGAGG
 881 AGGGCTGTCT GCTTCCCAGA AGTCCAAGGA CACAAATGGG TGAGGGGACT GGGCAGGGTT CTGACCCTGT GGGACCAGAG
 961 TGGAGGGCGT AGATGGACCT GAAGTCTCCA GGGACAACAG GGCCCAGGTC TCAGGCTCCT AGTTGGGCCC AGTGGCTCCA
1041 GCGTTTCCAA ACCCATCCAT CCCCAGAGGT TCTTCCCATC TCTCCAGGCT GATGTGTGGG AACTCGAGGA AATAAATCTC
1121 CAGTGGGAGA CGGAGGGGTG GCCAGGGAAA CGGGGCGCTG CAGGAATAAA GACGAGCCAG CACAGCCAGC TCATGCGTAA
1201 CGGCTTTGTG GAGCTGTCAA GGCCTGGTCT CTGGGAGAGA GGCACAGGGA GGCCAGACAA GGAAGGGGTG ACCTGGAGGG
1281 ACAGATCCAG GGGCTAAAGT CCTGATAAGG CAAGAGAGTG CCGGCCCCCT CTTGCCCTAT CAGGACCTCC ACTGCCACAT
1361 AGAGGCCATG ATTGACCCTT AGACAAAGGG CTGGTGTCCA ATCCCAGCCC CCAGCCCCAG AACTCCAGGG AATGAATGGG
1441 CAGAGAGCAG GAATGTGGGA CATCTGTGTT CAAGGGAAGG ACTCCAGGAG TCTGCTGGGA ATGAGGCCTA GTAGGAAATG
1521 AGGTGGCCCT TGAGGGTACA GAACAGGTTC ATTCTTCGCC AAATTCCCAG CACCTTGCAG GCACTTACAG CTGAGTGAGA
1601 TAATGCCTGG GTTATGAAAT CAAAAAGTTG GAAAGCAGGT CAGAGGTCAT CTGGTACAGC CCTTCCTTCC CTTTTTTTTT
1681 TTTTTTTTTT TTGTGAGACA AGGTCTCTCT CTGTTGCCCA GGCTGGAGTG GCGCAAACAC AGCTCACTGC AGCCTCAACC
1761 TACTGGGCTC AAGCAATCCT CCAGCCTCAG CCTCCCAAAG TGCTGGGATT ACAAGCATGA GCCACCCCAC TCAGCCCTTT
1841 CCTTCCTTTT TAATTGATGC ATAATAATTG TAAGTATTCA TCATGGTCCA ACCAACCCTT TCTTGACCCA CCTTCCTAGA
1921 GAGAGGGTCC TCTTGCTTCA GCGGTCAGGG CCCCAGACCC ATGGTCTGGC TCCAGGTACC ACCTGCCTCA TGCAGGAGTT
2001 GGCGTGCCCA GGAAGCTCTG CCTCTGGGCA CAGTGACCTC AGTGGGGTGA GGGGAGCTCT CCCCATAGCT GGGCTGCGGC
2081 CCAACCCCAC CCCCTCAGGC TATGCCAGGG GGTGTTGCCA GGGGCACCCG GGCATCGCCA GTCTAGCCCA CTCCTTCATA
2161 AAGCCCTCGC ATCCCAGGAG CGAGCAGAGC CAGAGCAGGC AAGTTTGTAC AAAAAAGCAG GCTGCCACCA TGGTGAGCAA
2241 GGGCGAGGAG CTGTTCACCG GGGTGGTGCC CATCCTGGTC GAGCTGGACG GCGACGTAAA CGGCCACAAG TTCAGCGTGT
2321 CCGGCGAGGG CGAGGGCGAT GCCACCTACG GCAAGCTGAC CCTGAAGTTC ATCTGCACCA CCGGCAAGCT GCCCGTGCCC
2401 TGGCCCACCC TCGTGACCAC CCTGACCTAC GGCGTGCAGT GCTTCAGCCG CTACCCCGAC CACATGAAGC AGCACGACTT
2481 CTTCAAGTCC GCCATGCCCG AAGGCTACGT CCAGGAGCGC ACCATCTTCT TCAAGGACGA CGGCAACTAC AAGACCCGCG
2561 CCGAGGTGAA GTTCGAGGGC GACACCCTGG TGAACCGCAT CGAGCTGAAG GGCATCGACT TCAAGGAGGA CGGCAACATC
2641 CTGGGGCACA AGCTGGAGTA CAACTACAAC AGCCACAACG TCTATATCAT GGCCGACAAG CAGAAGAACG GCATCAAGGT
2721 GAACTTCAAG ATCCGCCACA ACATCGAGGA CGGCAGCGTG CAGCTCGCCG ACCACTACCA GCAGAACACC CCCATCGGCG
2801 ACGGCCCCGT GCTGCTGCCC GACAACCACT ACCTGAGCAC CCAGTCCGCC CTGAGCAAAG ACCCCAACGA GAAGCGCGAT
2881 CACATGGTCC TGCTGGAGTT CGTGACCGCC GCCGGGATCA CTCTCGGCAT GGACGAGCTG TACAAGTAAA CCCAGCTTTC
2961 TTGTACAAAG TGGTGTTTGA ATGAGGCTTC AGTACTTTAC AGAATCGTTG CCTGCACATC TTGGAAACAC TTGCTGGGAT
3041 TACTTCGACT TCTTAACCCA ACAGAAGGCT CGAGAAGGTA TATTGCTGTT GACAGTGAGC GAGACGCAGA GTGGTGCTAA
3121 TTTTAGTGAA GCCACAGATG TAAAATTAGC ACCACTCTGC GTCCTGCCTA CTGCCTCGGA CTTCAAGGGG CTAGAATTCG
3201 AGCAATTATC TTGTTTACTA AAACTGAATA CCTTGCTATC TCTTTGATAC ATTTTTACAA AGCTGAATTA AAATGGTATA
3281 AATTAAATCA CTTTCAACTT TATTATACAT AGTTGATGGC CGGCCGCTTC GAGCAGACAT GATAAGATAC ATTGATGAGT
3361 TTGGACAAAC CACAACTAGA ATGCAGTGAA AAAAATGCTT TATTTGTGAA ATTTGTGATG CTATTGCTTT ATTTGTAACC
3441 ATTATAAGCT GCAATAAACA AGTTAACAAC AACAATTGCA TTCATTTTAT GTTTCAGGTT CAGGGGGAGG TGTGGGAGGT
3521 TTTTTAAAGC AAGTAAAACC TCTACAAATG TGGTAGCGGC CGCGGCGCTC TTCCGCTTCC TCGCTCACTG ACTCGCTGCG
3601 CTCGGTCGTT CGGCTGCGGC GAGCGGTATC AGCTCACTCA AAGGCGGTAA TACGGTTATC CACAGAATCA GGGGATAACG
3681 CAGGAAAGAA CATGTGAGCA AAAGGCCAGC AAAAGGCCAG GAACCGTAAA AAGGCCGCGT TGCTGGCGTT TTTCCATAGG
3761 CTCCGCCCCC CTGACGAGCA TCACAAAAAT CGACGCTCAA GTCAGAGGTG GCGAAACCCG ACAGGACTAT AAAGATACCA
3841 GGCGTTTCCC CCTGGAAGCT CCCTCGTGCG CTCTCCTGTT CCGACCCTGC CGCTTACCGG ATACCTGTCC GCCTTTCTCT
```

```
3921 CTTCGGGAAG CGTGGCGCTT TCTCATAGCT CACGCTGTAG GTATCTCAGT TCGGTGTAGG TCGTTCGCTC CAAGCTGGGC
4001 TGTGTGCACG AACCCCCCGT TCAGCCCGAC CGCTGCGCCT TATCCGGTAA CTATCGTCTT GAGTCCAACC CGGTAAGACA
4081 CGACTTATCG CCACTGGCAG CAGCCACTGG TAACAGGATT AGCAGAGCGA GGTATGTAGG CGGTGCTACA GAGTTCTTGA
4161 AGTGGTGGCC TAACTACGGC TACACTAGAA GAACAGTATT TGGTATCTGC GCTCTGCTGA AGCCAGTTAC CTTCGGAAAA
4241 AGAGTTGGTA GCTCTTGATC CGGCAAACAA ACCACCGCTG GTAGCGGTGG TTTTTTTGTT TGCAAGCAGC AGATTACGCG
4321 CAGAAAAAAA GGATCTCAAG AAGATCCTTT GATCTTTTCT ACGGGGTCTG ACGCTCAGTG GAACGAAAAC TCACGTTAAG
4401 GGATTTTGGT CATGAGATTA TCAAAAAGGA TCTTCACCTA GATCCTTTTA AATTAAAAAT GAAGTTTTAA ATCAATCTAA
4481 AGTATATATG AGTAAACTTG GTCTGACAGT TACCAATGCT TAATCAGTGA GGCACCTATC TCAGCGATCT GTCTATTTCG
4561 TTCATCCATA GTTGCCTGAC TCCCCGTCGT GTAGATAACT ACGATACGGG AGGGCTTACC ATCTGGCCCC AGTGCTGCAA
4641 TGATACCGCG AGACCCACGC TCACCGGCTC CAGATTTATC AGCAATAAAC CAGCCAGCCG GAAGGGCCGA GCGCAGAAGT
4721 GGTCCTGCAA CTTTATCCGC CTCCATCCAG TCTATTAATT GTTGCCGGGA AGCTAGAGTA AGTAGTTCGC CAGTTAATAG
4801 TTTGCGCAAC GTTGTTGCCA TTGCTACAGG CATCGTGGTG TCACGCTCGT CGTTTGGTAT GGCTTCATTC AGCTCCGGTT
4881 CCCAACGATC AAGGCGAGTT ACATGATCCC CCATGTTGTG CAAAAAAGCG GTTAGCTCCT TCGGTCCTCC GATCGTTGTC
4961 AGAAGTAAGT TGGCCGCAGT GTTATCACTC ATGGTTATGG CAGCACTGCA TAATTCTCTT ACTGTCATGC CATCCGTAAG
5041 ATGCTTTTCT GTGACTGGTG AGTACTCAAC CAAGTCATTC TGAGAATAGT GTATGCGGCG ACCGAGTTGC TCTTGCCCGG
5121 CGTCAATACG GGATAATACC GCGCCACATA GCAGAACTTT AAAAGTGCTC ATCATTGGAA AACGTTCTTC GGGGCGAAAA
5201 CTCTCAAGGA TCTTACCGCT GTTGAGATCC AGTTCGATGT AACCCACTCG TGCACCCAAC TGATCTTCAG CATCTTTTAC
5281 TTTCACCAGC GTTTCTGGGT GAGCAAAAAC AGGAAGGCAA AATGCCGCAA AAAAGGGAAT AAGGGCGACA CGGAAATGTT
5361 GAATACTCAT ACTCTTCCTT TTTCAATATT ATTGAAGCAT TTATCAGGGT TATTGTCTCA TGAGCGGATA CATATTTGAA
5441 TGTATTTAGA AAAATAAACA AATAGGGGTT CCGCGCACAT TTCCCCGAAA AGTGCCACCT GACGTCTAAG AAACCATTAT
5521 TATCATGACA TTAACCTATA AAAATAGGCG TATCACGAGG CCCTTTCGTC GGCGCGCCGC GGCCGC
```

Validation by Restriction Enzyme Digestion

Restriction Enzymes	Cutting Sites	DNA Fragments (bp)
NcoI	1960, 2229	269, 5317
ApaLI	4005, 5251	1246, 4340
ApaLI+NcoI	1960, 2229, 4005, 5251	269, 1776, 1246, 2295

Appendix 3

Laemmli Sample Buffer (4×)

Tris (1.0M, pH 6.8)	10 mL
SDS	4.0 g
Glycerol	20 mL
β-Mercaptoethanol	10 mL
Bromophenol blue	0.1 g
dH_2O	to 50 mL

Danksagung

Zuallererst geht großer Dank an meine Betreuerin Prof. Inga Neumann, vor allem für ihre Bereitschaft und ihr Vertrauen, mir von Anfang an große wissenschaftliche Freiheit zu geben. Es hat mir ermöglicht, meine eigenen Ideen zu verfolgen und mich enorm weiterzuentwickeln. Das ist in dieser frühen Phase der wissenschaftlichen Laufbahn alles andere als selbstverständlich und war eine meiner größten Antriebsfedern. Nichtsdestotrotz hat sie mich stets unterstützt, wenn das nötig oder möglich war; egal ob es um den Aufbau einer Kollaboration, das Korrekturlesen oder den Publikationsprozess des ersten Papers ging. Danke!

Großer Dank gilt auch Dr. Nathalie Rouach, die mir einen Forschungsaufenthalt in ihrer Gruppe ermöglicht hat. Sie und ihre Gruppe haben mir dabei eine enorme persönliche und wissenschaftliche Gastfreundschaft entgegengebracht, die ich als prägend empfunden habe. Dank gilt auch Dr. Gregory Ghezali, Pascal Ezan und Dr. Davide Mazaud, die immer bereit waren, sich den nervigen Bedürfnissen des deutschen Gastes zu widmen.

Ben, dir möchte ich für alles danken, was du in diesem Labor etabliert hast. Es hat mir enorm geholfen, meine Arbeit methodisch zu bewältigen. Deine stete Hilfsbereitschaft wird für mich immer vorbildhaft sein. Ich wünsche dir alles Gute für deinen weiteren Werdegang und hoffe, noch das ein oder andere Bier mit dir zu trinken. In the end, it did matter!

I want to thank Dr. Sareh Pandamooz, who suddenly joined our group in the time I needed help the most. Thank you for never getting tired of doing all these transfections with me, this project would not be as progressed without you! I am in your debt.

Auch nie müde geworden sind meine Bachelorstudentinnen Jana Nurgatina und Judith Nerb, sowie meine Praktikant*innen Nora Jahnen, Benedikt Nerb, Jessica Manchen, Felix Lützenkirchen, Ramona Pawlak, Michael Schletter und Muriel Zanicolo. Danke für das Waschen endloser Membranen und das geduldige Ertragen der ein oder anderen experimentellen Sackgasse.

Tobi, Julia, Magdalena und Vini, in euch habe ich nicht nur gute Kollegen, sondern auch Freunde gefunden. Das ist in unserem Alter gar nicht mehr so einfach. ;) Danke für all die Lachanfälle im Büro, die leeren Weinflaschen und Maßkrüge, die Nester, die Fressorgien, die langen Feiern, aber auch die wissenschaftlichen Diskussionen und Ratschläge.

Meiner Mutter möchte ich danken, für das bedingungslose Unterstützen meiner Interessen. Du hast von Anfang an meine Selbstständigkeit gefördert, eine Eigenschaft die mir in dieser Arbeit von allergrößtem Nutzen war. Es war ein langer Weg, seitdem ein Artikel auf unserem Wohnzimmertisch mein Interesse für Endokrinologie geweckt hat. Ihn zu gehen wäre ohne dich nicht möglich gewesen. Ich freue mich auf noch viele Jahre unserer vertrauten Gespräche.

Mein größter Dank gilt meiner wunderbaren Partnerin Anna. Du hast trotz unserer Wochenendbeziehung immer Verständnis gezeigt, wenn ich sonntags wieder ins Labor gefahren bin und mich stets aufgebaut, wenn ich frustriert war. Auch in den drei Monaten, in denen ich komplett weg war, hast du mir nichts als Unterstützung gezeigt. Du warst und bist mein Zuhause und Zufluchtsort.